

Cooperative effects on functionalised vesicles



DISSERTATION ZUR ERLANGUNG DES DOKTORGRADES DER NATURWISSENSCHAFTEN
(DR. RER. NAT.) DER FAKULTÄT CHEMIE UND PHARMAZIE
DER UNIVERSITÄT REGENSBURG

Vorgelegt von

Michal Poznik

aus Bratislava, Slowakei

Regensburg 2016

The experimental work was carried out between October 2012 and May 2016 at the University of Regensburg, Institute of Organic Chemistry under the supervision of Prof. Dr. Burkhard König.

The PhD-thesis was submitted on: 31.05.2016

Date of colloquium: 1.07.2016

Board of Examiners

PD. Dr. Sabine Amslinger (Chairman)

Prof. Dr. Burkhard König (1st Referee)

Prof. Dr. Olga Garcia Mancheño (2nd Referee)

PD. Dr. Rainer Müller (Examiner)

*„You should get to the point where anyone else would quit
and you're NOT GOING TO STOP THERE.“*

Shia LaBeouf

Table of Contents

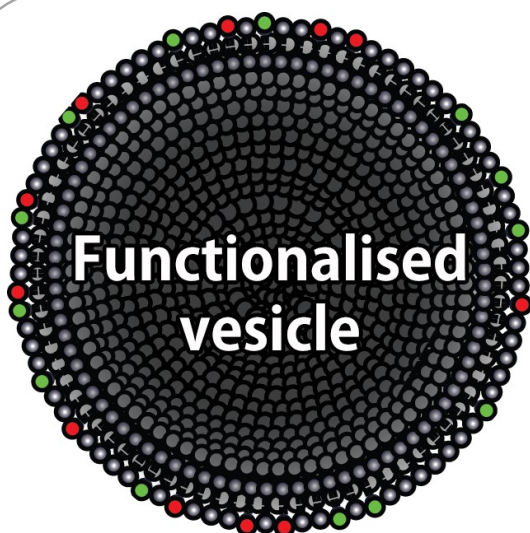
1 Introduction – short overview	1
1.1 Functionalised vesicles	2
1.2 Rapid screening of photocatalytic reactions	4
1.3 References	6
2 Cooperative hydrolysis of aryl esters on functionalized membrane surfaces and in micellar solutions	9
2.1 Introduction	10
2.2 Results and discussion.....	14
2.2.1 Vesicular hydrolysis	14
2.2.2 Micellar hydrolysis	16
2.2.3 Mechanism and kinetics	17
2.2.4 Comparison with hydrolytic enzymes.....	20
2.3 Conclusions.....	22
2.4 Experimental Part.....	23
2.4.1 General Methods and Material.....	23
2.4.2 Synthesis of membrane additives used as membrane additives.....	23
2.4.3 Synthesis of fluorescein esters.....	26
2.4.4 Preparation and characterization of the membrane.....	30
2.4.5 Determination of cmc value for cyclen 1	31
2.4.6 Calibration curves for fluorescein concentration	31
2.4.7 Estimated pKa values of membrane additives	32
2.4.8 Kinetic measurements	32
2.4.9 Processing of the kinetic data	36
2.5 References	41

3	Enantioselective ester hydrolysis by an achiral catalyst co-embedded with chiral amphiphiles into a vesicle membrane	45
3.1	Introduction.....	46
3.2	Results and discussion.....	48
3.2.1	Kinetic effects	49
3.2.2	Enantiodiscrimination in ester hydrolysis.....	49
3.3	Conclusions.....	52
3.4	Experimental part.....	53
3.4.1	General methods and materials.....	53
3.4.2	Synthesis	53
3.4.3	Synthesis of the membrane additives.....	57
3.4.4	Preparation and characterization of the vesicles	61
3.5	References	63
4	The interface makes a difference: Lanthanide ion coated vesicles hydrolyse phosphodiester	67
4.1	Introduction.....	68
4.2	Results and discussion.....	69
4.2.1	Interaction of metal cations with DOPC vesicles.....	69
4.2.2	Hydrolysis of BNPP with different metal ions.....	71
4.2.3	Different lipids	71
4.2.4	Comparison of the hydrolytic properties.....	72
4.3	Conclusions.....	73
4.4	Experimental part.....	74
4.5	General methods and materials	74
4.5.1	Preparation and characterization of the vesicles	74
4.5.2	Detection of metal binding by carboxyfluorescein	75
4.5.3	Europium phosphorescence in the presence of the DOPC membrane.....	76
4.5.4	Sensitisation of europium emission by pyrene	77
4.5.5	Kinetic measurements.....	78
4.6	References	84

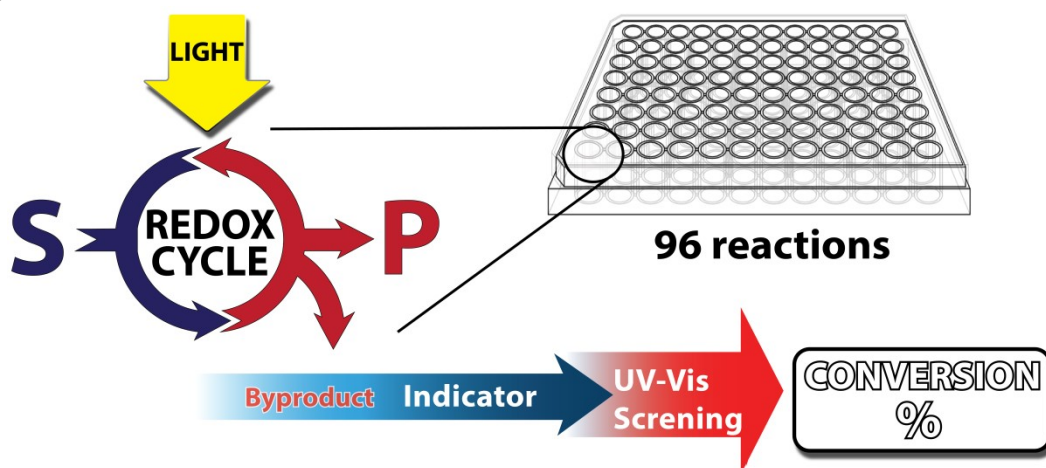
5	Light Upconverting soft particles: Triplet-triplet annihilation in the phospholipid bilayer of self-assembled vesicles	87
5.1	Introduction.....	88
5.2	Results and discussion.....	90
5.2.1	TTA inside the bilayer.....	90
5.2.2	TTA with the sensitizer on the surface of the membrane.....	91
5.2.3	TTA on the surface of the membrane.....	93
5.2.4	Different lipids.....	94
5.2.5	Effect of dilution.....	95
5.3	Conclusions.....	96
5.4	Experimental part.....	97
5.4.1	General methods and materials.....	97
5.4.2	Synthesis.....	98
5.4.3	Preparation and characterization of the vesicles.....	100
5.4.4	TTA measurements.....	103
5.4.5	NMR spectra.....	106
5.5	References.....	109
6	Fast colorimetric screening for visible light photocatalytic oxidation and reduction reactions	113
6.1	Introduction.....	114
6.2	Results and discussion.....	116
6.2.1	Screening of photocatalytic oxidations.....	116
6.2.2	Screening of photocatalytic reductions.....	119
6.2.3	Screening of photocatalyst stability.....	122
6.3	Conclusions.....	124
6.4	Experimental part.....	125
6.4.1	General methods and materials.....	125
6.4.2	Indicators.....	125
6.4.3	Reactor.....	129
6.4.4	Oxidation of benzyl alcohols and amines.....	131

6.4.5	Hydroxylation of boronic acids.....	132
6.4.6	Stability of the dyes	134
6.4.7	Aryl radical generation	137
6.4.8	List of used commercial drugs.....	143
6.4.9	Synthetic procedure for dehalogenation of selected drugs.....	144
6.5	References	148
7	Summary	154
8	Zusammenfassung	156
9	Abbreviations	158
10	Curriculum Vitae	161
11	Acknowledgement	165

1 Introduction - short overview



Vesicles are artificial liposomes whose surface can be modified by an addition of amphiphilic compounds. This approach provides a facile method for an introduction of various chemical species into close proximity with use of a simple self-assembly process. Such artificial soft particles have found a broad use in drug delivery, sensing, imaging and catalysis.



Visible light photocatalysis is an emerging field of synthetic chemistry. Therefore, a simple and facile method for rapid screening is required. We propose a photometric evaluation of the conversion using known indicators. Highly parallel investigation is possible by a directly irradiated microtiter plate as reaction vessel allowing 96 reactions at once.

1.1 Functionalised vesicles

Amphiphiles are molecules which combine hydrophobic and hydrophilic properties. When such compounds dissolve in water, they self-assemble into supramolecular systems.¹ Depending on the nature of the amphiphiles, they usually form micelles or vesicles (Figure 1.1).

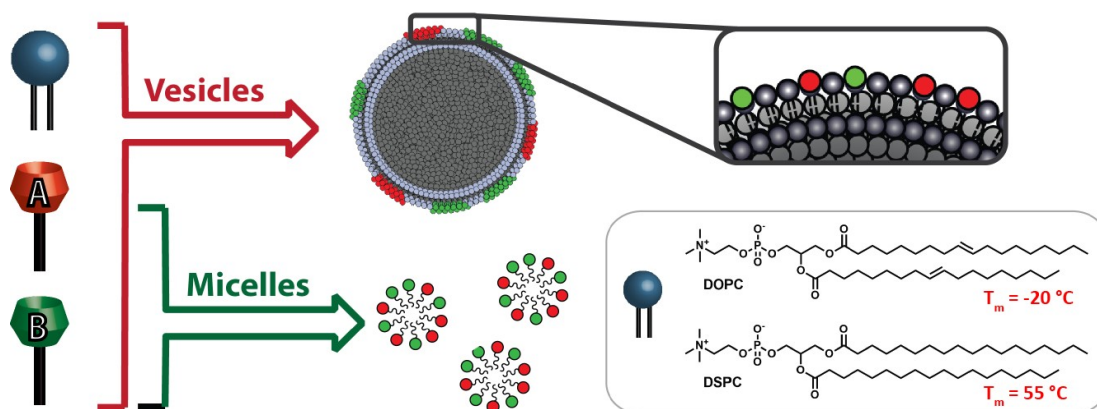


Figure 1.1 Construction of micelles and vesicles.

1,2-Dioleoyl-*sn*-glycero-3-phosphocholine (DOPC) and 1,2-distearoyl-*sn*-glycero-3-phosphocholine (DSPC) (Figure 1.1) are zwitterionic, phosphatidylcholine lipids equipped with two fatty-acid residues and are a common choice for an assembly of vesicles in aqueous solutions. Presence of the double bond in oleic acid of DOPC has a big impact on the fluidity of the membrane described by the transition temperature (T_m). At this temperature, the rigid gel-phase bilayer with a hindered lateral movement changes to fluid, so it is essentially a melting point of the membrane. DOPC provides vesicles with fluid membrane at room temperature, in contrast to a rigid bilayer of the DSPC. Fluidity of the vesicular membrane has a major influence on processes occurring on its surface.²

Vesicles can serve as a supramolecular platform into which we are able to co-embed various amphiphilic species. Using custom-made amphiphiles, we can functionalize its surface. Such molecules present in the membrane have much higher local concentration compared with a bulk solution and only 2-dimensional freedom of movement. Higher concentration increases the possible chemical and physical interaction between different amphiphiles. This offers a quick and facile method for exploring interactions between molecules without the need of labourous synthesis of their covalently-bound analogues. This feature was successfully used in our group for sensing. In these systems, receptor and reporter amphiphiles are co-

embedded on the vesicles (Figure 1.2, left). Metal complexes with a high binding affinity towards the analyte are used as receptor and a reporter is usually an amphiphilic dye, which reacts to a binding event of the receptor by changing its spectroscopic properties (absorbance, fluorescence). Such vesicular probes were developed for phosphates, imidazole species or by using aptamers for a detection of thrombin.^{3, 4, 5, 6} Imprinting on the membrane provided receptors for more complex molecules with two binding events, such as short peptides.^{7, 8, 9}

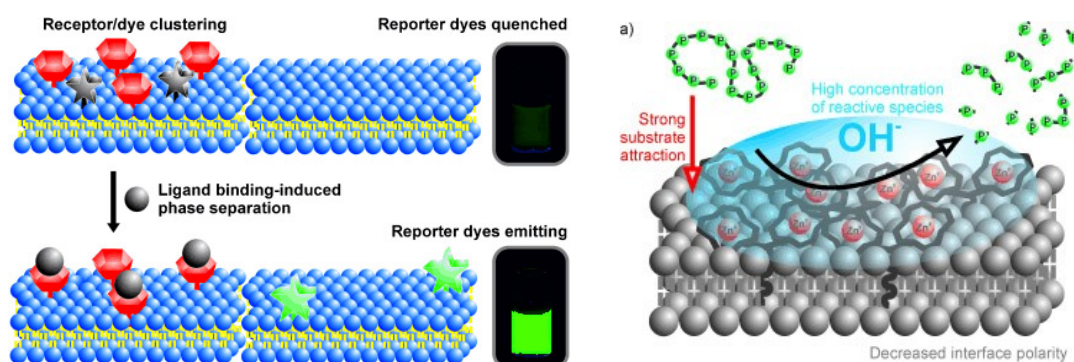


Figure 1.2 Vesicular sensing (left) and catalytic hydrolysis (right).

This phenomenon where two species interact and induce changes in spectroscopic properties raised the question if such interaction could be beneficial also in catalysis. Micellar catalysis is known for decades and numerous examples were published.^{10, 11} On the contrary to the highly dynamic micellar solutions, vesicles are a stable constructs, which might improve cooperative effects on the surface. Since they are ubiquitously prepared in aqueous solutions, it is apparent to examine catalytic reactions, which could benefit from the water–bilayer interface. In our group, the use of vesicles for photocatalytic water splitting was utilised.^{12, 13, 14} With the use of buffer, we can examine the catalytic hydrolysis at biological pH 7.4 and obtain artificial nucleases, which are able to effectively hydrolyse DNA.^{15, 16} It was found that a zinc complex co-embedded into the surface of the membrane increases the activity dramatically (Figure 1.2, right).¹⁶

In this work, I tried to extend our knowledge of the cooperative effects on the vesicular surface to identify better systems for catalytic hydrolysis. I focused on inducing activity by membrane additives, which resulted in higher hydrolytic activity in hydrolysis of aryl esters (Chapter 2). I showed that also selectivity can be affected by using chiral additives, which prompts the hydrolysis of one enantiomer of chiral-activated esters (Chapter 3). Later, I examined a simplified system where a complicated metal complex was replaced by

lanthanide anions, which by simple adhesion to the surface of the membrane increase their hydrolytic activity (Chapter 4).

We learned that the membrane induces cooperative effects simply by increasing the statistical probability for two molecules to come in close proximity. This is also very important in many physical processes like non-radiative energy transfers, such as FRET. Therefore, we decided to examine triplet–triplet annihilation (TTA) upconversion process in the vesicular systems (Chapter 5).¹⁷ This upconversion process consists of several intermolecular energy transfers, which should be favoured in vesicles. We were able to show that vesicles not only exhibit TTA, but also provide soft particles with molar upconversion efficiency that is independent of the concentration of the solution.

1.2 Rapid screening of photocatalytic reactions

Small unilamellar vesicles are systems, which are extremely hard to visualise on a molecular level without altering some of the main properties. This forces us to use indirect methods of analysis. Most of the surface interactions were demonstrated using principles of FRET or sensitising the phosphorescence. For kinetic measurements, we adopted microtiterplate technology for evaluation of a large amount of samples. These experiences lead us to reconsider the typical approach to screening methods for synthetic reactions. Especially in the emerging field of visible light photocatalysis,¹⁸ where numerous transformations are being developed every day and state of the art technique for analysis like GC or HPLC are slow and costly. We have chosen a different approach and developed a method where we screen reaction conversions through the analysis of formed by-products. These are identical throughout the substrate scope and by employing an indicator, we were able to photometrically screen conversions of such reactions. Combining it with microtiterplate technology, we established and tested a rapid screening technique for visible light photocatalysis (Figure 1.3, Chapter 6).

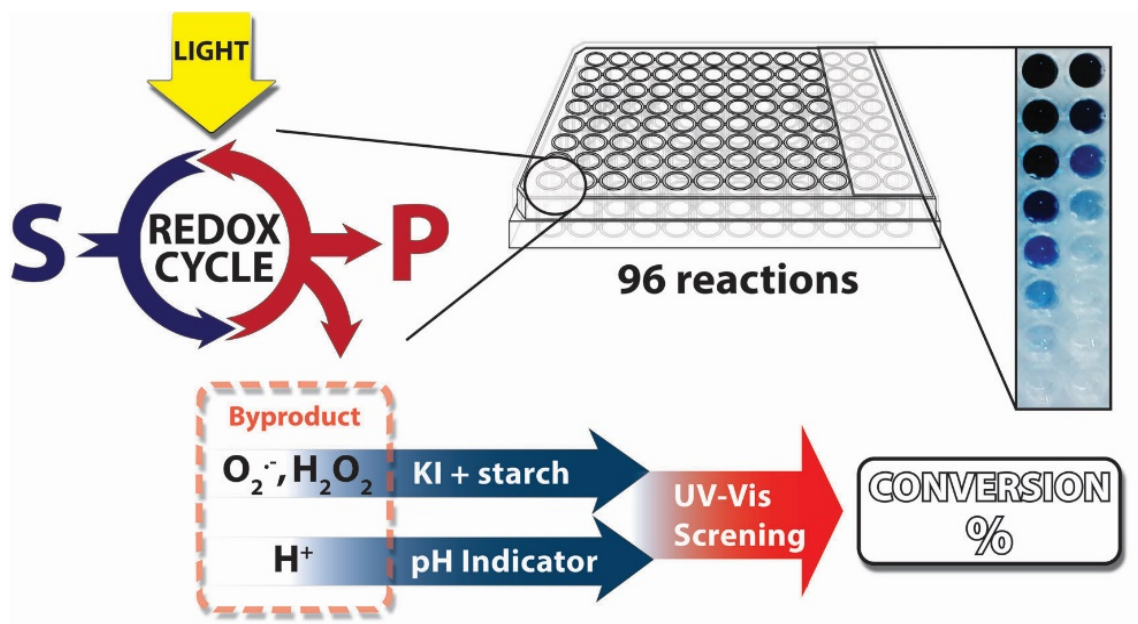


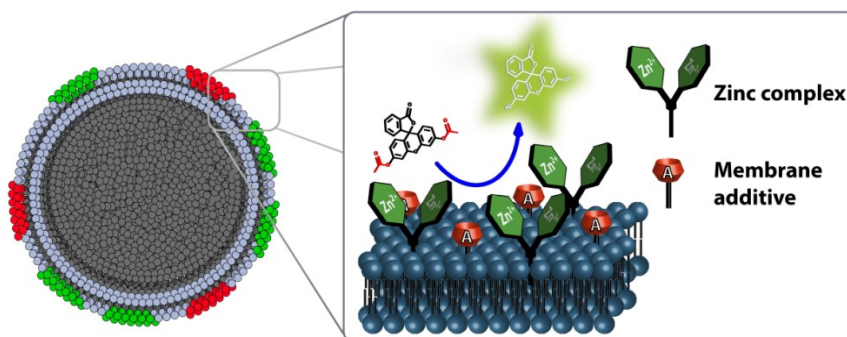
Figure 1.3 Principle of the screening method for a visible light photocatalysis.

1.3 References

1. Franks, F., *Water A Comprehensive Treatise: Volume 4: Aqueous Solutions of Amphiphiles and Macromolecules*. Springer US: 1975; Vol. 4, p 839.
2. Eze, M. O., Phase transitions in phospholipid bilayers: Lateral phase separations play vital roles in biomembranes. *Biochem. Educ.* **1991**, *19* (4), 204-208.
3. Muller, A.; König, B., Preparation of luminescent chemosensors by post-functionalization of vesicle surfaces. *Org. Biomol. Chem.* **2015**, *13* (6), 1690-1699.
4. Gruber, B.; König, B., Self-Assembled Vesicles with Functionalized Membranes. *Chem. Eur. J.* **2013**, *19* (2), 438-448.
5. Balk, S.; Maitra, U.; König, B., Terbium(iii)-cholate functionalized vesicles as luminescent indicators for the enzymatic conversion of dihydroxynaphthalene diesters. *Chem. Commun.* **2014**, *50* (58), 7852-7854.
6. Muller, A.; König, B., Vesicular aptasensor for the detection of thrombin. *Chem. Commun.* **2014**, *50* (84), 12665-12668.
7. Gruber, B.; Balk, S.; Stadlbauer, S.; König, B., Dynamic Interface Imprinting: High-Affinity Peptide Binding Sites Assembled by Analyte-Induced Recruiting of Membrane Receptors. *Angew. Chem. Int. Ed.* **2012**, *51* (40), 10060-10063.
8. Balk, S.; König, B., Thermally induced molecular imprinting of luminescent vesicles. *J. Inclusion Phenom. Macrocyclic Chem.* **2014**, *81* (1), 135-139.
9. Banerjee, S.; König, B., Molecular Imprinting of Luminescent Vesicles. *J. Am. Chem. Soc.* **2013**, *135* (8), 2967-2970.
10. Rathman, J. F., Micellar catalysis. *Curr. Opin. Colloid Interface Sci.* **1996**, *1* (4), 514-518.
11. La Sorella, G.; Strukul, G.; Scarso, A., Recent advances in catalysis in micellar media. *Green Chem.* **2015**, *17* (2), 644-683.
12. Hansen, M.; Li, F.; Sun, L.; König, B., Photocatalytic water oxidation at soft interfaces. *Chem. Sci.* **2014**, *5* (7), 2683-2687.
13. Troppmann, S.; Brandes, E.; Motschmann, H.; Li, F.; Wang, M.; Sun, L.; König, B., Enhanced Photocatalytic Hydrogen Production by Adsorption of an [FeFe]-Hydrogenase Subunit Mimic on Self-Assembled Membranes. *Eur. J. Inorg. Chem.* **2016**, *2016* (4), 554-560.
14. Troppmann, S.; König, B., Functionalized Membranes for Photocatalytic Hydrogen Production. *Chem. Eur. J.* **2014**, *20* (45), 14570-14574.

15. Mancin, F.; Scrimin, P.; Tecilla, P.; Tonellato, U., Artificial metallonucleases. *Chem. Commun.* **2005**, (20), 2540-2548.
16. Gruber, B.; Kataev, E.; Aschenbrenner, J.; Stadlbauer, S.; König, B., Vesicles and Micelles from Amphiphilic Zinc(II)–Cyclen Complexes as Highly Potent Promoters of Hydrolytic DNA Cleavage. *J. Am. Chem. Soc.* **2011**, 133 (51), 20704-20707.
17. Zhao, J.; Ji, S.; Guo, H., Triplet-triplet annihilation based upconversion: from triplet sensitizers and triplet acceptors to upconversion quantum yields. *RSC Adv.* **2011**, 1 (6), 937-950.
18. Schultz, D. M.; Yoon, T. P., Solar Synthesis: Prospects in Visible Light Photocatalysis. *Science* **2014**, 343 (6174).

2 Cooperative hydrolysis of aryl esters on functionalized membrane surfaces and in micellar solutions



Catalytic hydrolysis of peptides, proteins, phosphates or carboxylate esters in nature is catalysed by enzymes, which are efficient, fast and selective. Most of the hydrolytic chemical catalysts published so far mimic the active site of enzymes and contain metal complexes and amino acid residues. Their synthesis can be laborious, while the hydrolytic activity is still limited compared to enzymes. We present an approach that uses fluid membranes of vesicles and micelles as a support for amphiphilic additives, which cooperatively cleave aryl ester bonds. The membrane anchored bis-Zn(II)-complex **1** is hydrolytically active and hydrolyses fluorescein diacetate (**FDA**) with a second order rate constant (k_2) of $0.9 \text{ M}^{-1} \text{ s}^{-1}$. The hydrolytic activity is modulated by co-embedded membrane additives, bearing common amino acid side chain functional groups. With this approach, the hydrolytic activity of the system is enhanced up to 16 fold in comparison with cyclen **1** ($k_2 = 14.7 \text{ M}^{-1} \text{ s}^{-1}$). DOPC and DSPC lipids form at room temperature fluid or gel phase membranes, respectively. Omitting the lipid, micellar solutions were obtained with hydrolytic activity reaching $k_2 = 13.4 \text{ M}^{-1} \text{ s}^{-1}$. It is shown that cooperative hydrolysis is favoured in fluid membranes and micelles, allowing the active moieties to arrange freely. The embedding and dynamic self-assembly of membrane active components in fluid membranes and micelles provide facile access to hydrolytically active soft interfaces.

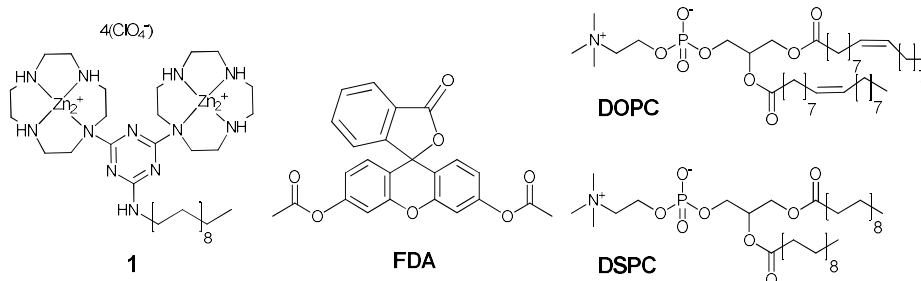
This chapter was published in:

M. Poznik and B. König, "Cooperative hydrolysis of aryl esters on functionalized membrane surfaces and in micellar solutions", *Org. Biomol. Chem.*, **2014**, 12, 3175–3180

M. Poznik performed the experimental work and wrote the manuscript. B. König supervised the project and is corresponding author.

2.1 Introduction

Carboxyesters are ubiquitously found in nature. They are involved in many biological processes and present in everyday life. Esters of drugs are better transported through membranes with respect to free drugs and cleaved inside cells by esterases. This is often used as pro-drug concept in pharmaceutical sciences.¹ Peptides, proteins, phosphate and carboxy esters, respectively are catalytically hydrolysed by natural enzymes and many attempts to design artificial hydrolysing enzymes have been reported over time, but their efficiency is still limited when compared to the natural models.^{2, 3} Most hydrolases contain metal ions such as zinc(II) (carboxypeptidase A, astacin) in their active centres.⁴ The stabilisation of the transition state during hydrolysis occurs by hydrogen bonding of the ester group to amino acid residues of the enzyme protein backbone. Histidine, tyrosine and glutamine often participate in the activation of the substrate. The crucial properties of the enzyme active centre are the appropriate distance and geometry of all participating groups, their dynamics during the reaction, the microenvironment created by the folded enzyme and the ability to bind the substrate. Combining all such features in one organic molecule is challenging or even impossible and covalent enzyme models may be incapable of adjusting the conformation for an efficient hydrolysis.^{2, 5, 6}



Scheme 2.1 Amphiphilic bis-Zn-cyclen **1** used as a hydrolytic metal center, fluorescein diacetate (**FDA**) used as a fluorescent probe and supporting lipids for providing fluid (**DOPC**) and gel phase (**DSPC**) membranes.

To investigate an alternative approach, we used functionalized membrane surfaces of vesicles and micelles for the cooperative hydrolysis of esters (Figure 2.1) with zinc complex **1** (Scheme 2.1) as a hydrolytically active metal center. This complex is known to coordinate water molecules and due to its Lewis acidity it produces hydroxide anions used for hydrolysis reactions at neutral pH.^{7, 8} The reaction rate was found to increase dramatically once complex **1** was embedded in a lipid membrane or in micelles.⁹ Embedded in

membranes, complex **1** may also serve as a ligand for the molecular recognition of phosphate anions.¹⁰

The effect of micellar catalysis of surfactant solutions has been studied and described in detail in the literature.^{11, 12} It was discovered that positively charged surfactants, such as tetraammonium salts, amines etc. embedded in micelles cleave p-nitrophenol esters in buffered solutions at pH 7 with a high efficiency.^{13, 14, 15} This effect is most likely caused by the high local concentration of the polar functional groups on the surface. Metallomicelles were also intensively studied for their increased hydrolytic activity with respect to homogeneous solution.^{16, 17}

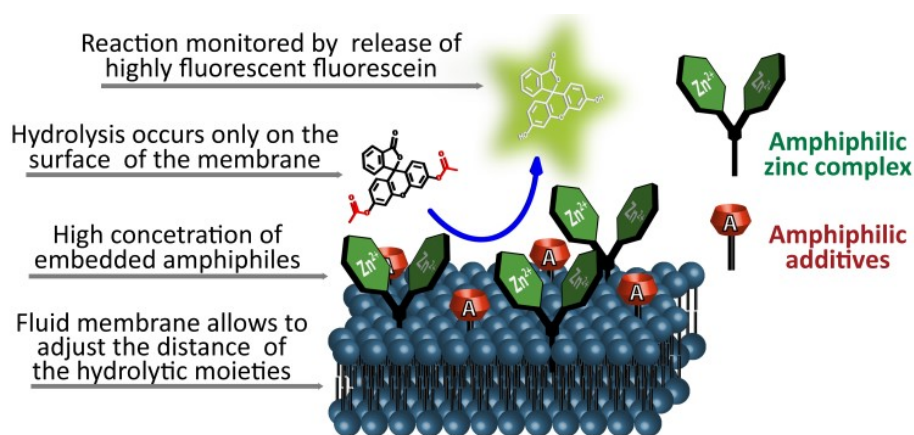


Figure 2.1 Concept of the proposed membrane hydrolysis.

The proposed cooperative catalytic effect by combining embedded metal complexes and membrane additives on the surface of a vesicular membrane is depicted in Figure 2.1. Soft interfaces are important for many biological processes and found use also in artificial systems.¹⁸ A potential advantage using a 2D functionalized membrane for hydrolysis is the non-covalent assembly of the components in a two dimensional fashion. In the fluid membrane of a vesicle, the hydrolytic active components may statistically arrange in distances optimal for hydrolysis. This concept offers the easy and facile testing of different combinations of components and their possible cooperative action. Micellar solutions of cyclen **1** and membrane additives were also examined for their hydrolytic activity. However, an advantage of the vesicular systems is that their structure is better defined and the effects of different membrane additives can be compared easier. The membrane active amphiphilic molecules are, most likely, not randomly distributed in the membrane, but form clusters and patches. Complete phase separation or limited mobility in the membrane might inhibit the cooperative action (Figure 2.2).¹⁹

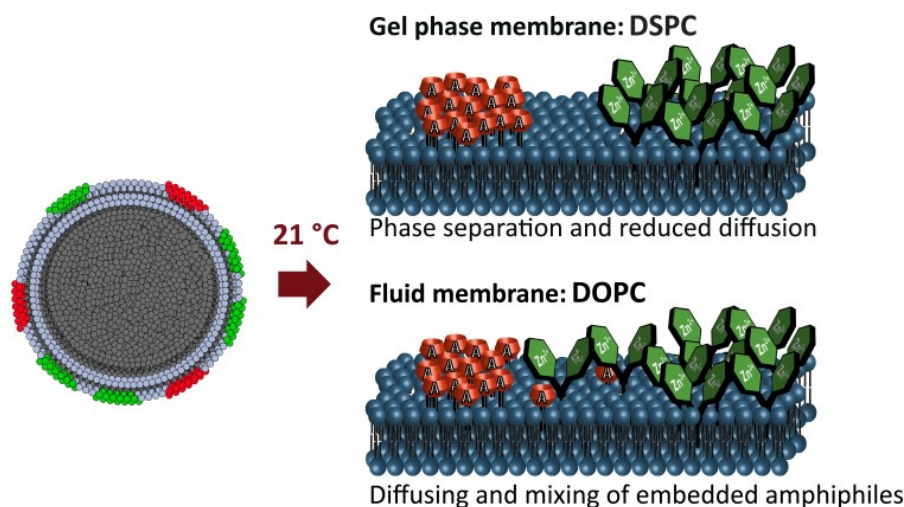


Figure 2.2 Expected patch formation in different phospholipid membranes.

To support this concept a well-described FRET pair of two amphiphilic fluorescent dyes was co-embedded into membranes (Figure 2.3).²⁰ The amphiphilic dye **TAMRA** exhibits in close proximity to amphiphilic carboxyfluorescein **CF** an emission at 580 nm after FRET, if irradiated at 495 nm. Both amphiphilic dyes were embedded in DOPC and DSPC membrane, respectively (Scheme 2.1).

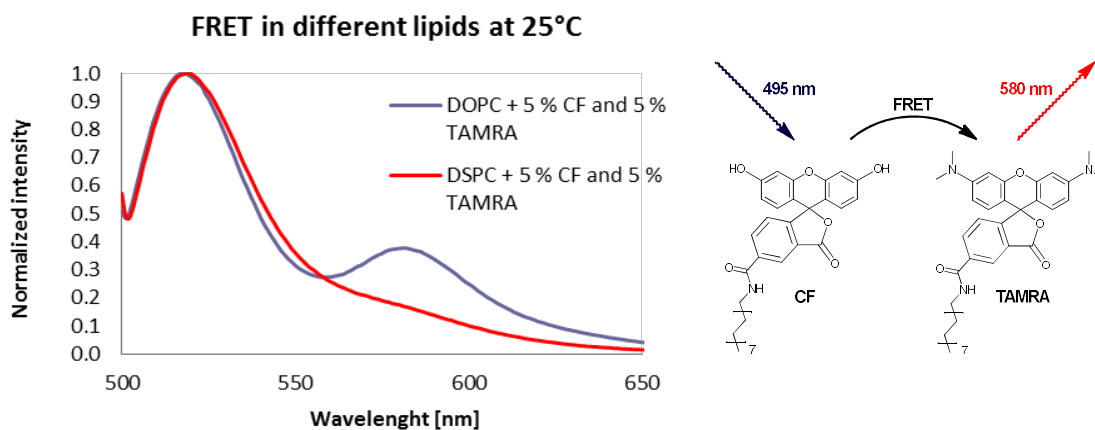
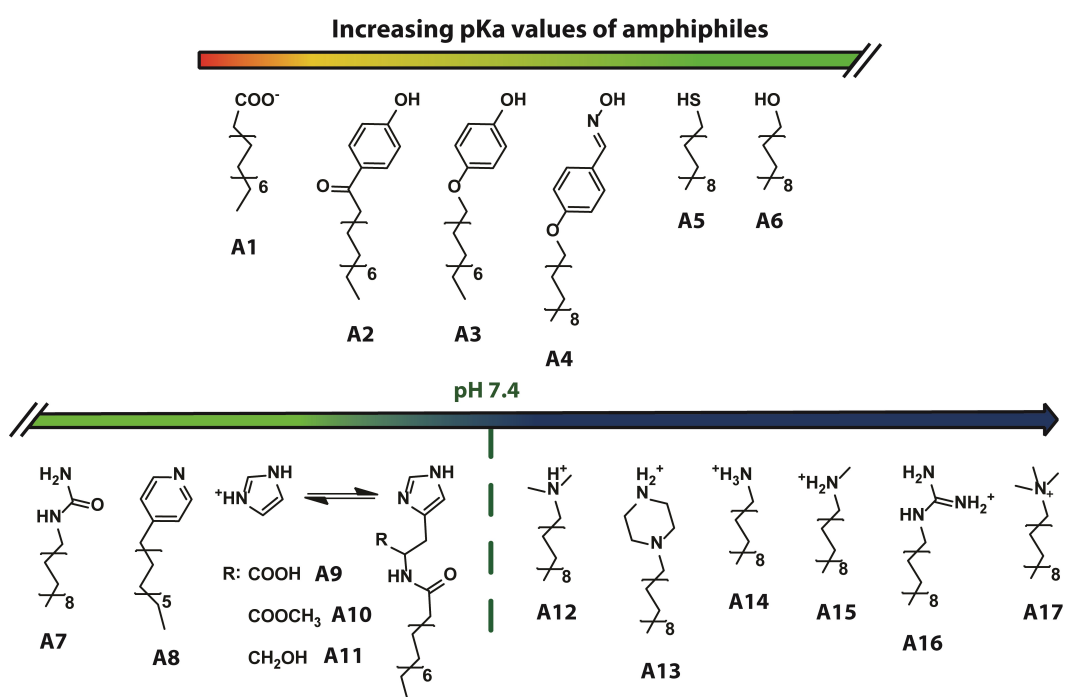


Figure 2.3 Emission spectra of **CF** (0.025 mM) and **TAMRA** (0.025 mM) mixture in various lipids ($\lambda_{\text{exc}} = 495 \text{ nm}$) and the mechanism of FRET.

The unsaturated lipid DOPC forms a fluid membrane at room temperature due to its transition temperature of $-20 \text{ }^\circ\text{C}$. DSPC yields a rigid gel phase membrane at room temperature (transition temp. $55 \text{ }^\circ\text{C}$). The FRET is observed only in the fluid membrane of

DOPC lipids, which indicates partially mixed patch formation under these conditions (Figure 2.3).

Membrane additives (Scheme 2.2) were designed to support the hydrolysis reaction resembling functional groups that are present in the active centers of hydrolytic enzymes, e.g. imidazole, phenol, acids or amides. Micellar hydrolytic activity has been reported previously for amines, oximes and histidine.^{21, 22} The series was extended to cover a larger range of acidic, neutral, basic and cationic functional groups. Amphiphiles are grouped in Scheme 2.2 according to the increasing pK_a values of corresponding non-amphiphilic molecules (see experimental part for the reported literature values).



Scheme 2.2 Membrane additives investigated for cooperative hydrolysis in their expected protonation state at pH 7.4, grouped by pK_a values of the functional group.

2.2 Results and discussion

2.2.1 Vesicular hydrolysis

The hydrolytic activity was monitored using fluorescein diacetate (**FDA**, Scheme 2.1), a substrate for membrane esterases, often used for evaluating the viability of cell samples.^{23, 24} **FDA** is a non-fluorescent diaryl ester whose fluorescence is triggered by the cleavage of its ester groups. The often used p-nitrophenol esters are more labile towards hydrolysis and their photometric determination is less sensitive than the measurement of fluorescence.

	DOPC		DSPC	
	k_{obs} 10^{-5}s^{-1}	k_{obs}^0 10^{-5}s^{-1}	k_{obs} 10^{-5}s^{-1}	k_{obs}^0 10^{-5}s^{-1}
Zn-cyclen 1 [5 mol%]	0.26	-	2.14	-
with membrane additive [10 mol%]				
A1	0.07	0.01	0.6	0.01
A2	0.9	0.03	2.1	0.02
A3	0.3	0.02	2.5	0.02
A4	2.4	0.03	2.2	0.01
A5	0.4	0.03	1.9	0.02
A6	0.4	0.02	2.6	0.02
A7	0.5	0.04	1.4	0.02
A8	0.4	0.05	1.9	0.02
A9	4.0	0.5	21.6	0.8
A10	4.4	0.9	6.0	0.3
A11	11.9	3.3	9.3	1.2
A12	0.9	0.05	4.2	0.03
A13	10.9	4.0	5.0	0.1
A14	17.2	9.8	5.3	0.08
A15	7.6	2.5	4.2	0.05
A16	1.6	0.05	3.3	0.04
A17	0.9	0.03	3.9	0.03

Table 2.1 Hydrolytic activity of vesicular systems : k_{obs} : 10 mol % of amphiphiles (0.05 mM) and 5 mol. % of cyclen **1** (0.025 mM) relative to the lipids in DOPC, DSPC membrane, k_{obs}^0 : hydrolytic rates for systems without **1**.

All measurements were performed under pseudo first-order-reaction conditions and the rate constant of hydrolysis (k_{obs}) was derived from the slope of the increased fluorescein concentration over 20 min (s^{-1}) and from the initial **FDA** concentration. The concentration of

the released fluorescein was determined using a recorded calibration curve in vesicular solutions not exceeding its linear region (see experimental part). All reported membrane additives were tested in vesicular membranes prepared by sonication above their transition temperature from both DOPC and DSPC in the presence of bis-Zn-cyclen **1**. To properly examine the hydrolysis, the best composition of the membrane was found to be 5 mol % of **1**, 10 mol. % of the respective membrane additive and 85 mol % of phospholipid. Hydrolytic activity was determined also for vesicles containing only the zinc cyclen complex **1** (5 mol %) or exclusively non-metal ion containing membrane additives (10 mol %). The measurements indicate, which species is mainly responsible for the hydrolysis. All data are summarized in Table 2.1 (values sorted according to Scheme 2.2).

Bis-Zn-cyclen **1** embedded in the membrane showed a higher activity towards hydrolysis than a non-amphiphilic solution of **1** (see experimental part), which confirms previous observations for bis(4-nitrophenyl) phosphate.⁹ Non-amphiphilic models of membrane additives were also tested for hydrolytic activity but none was observed (see experimental part). We found that **1** is much more active in rigid DSPC- than in fluid DOPC-membranes. Compounds **A9**, **A10**, **A11**, **A13**, **A14** and **A15**, respectively exhibit high rates of hydrolysis in the absence of **1** in the membrane, often exceeding the rate of sole cyclen **1**. These compounds have functional groups that have been previously reported to be hydrolytically active in micellar solutions.

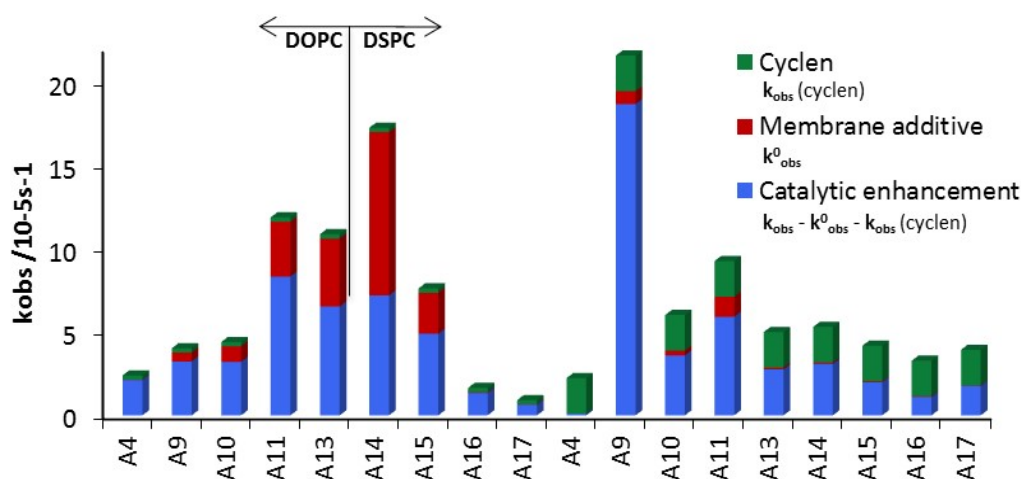


Figure 2.4 Comparison of the hydrolytic effects in selected vesicle compositions.

Only palmitic acid **A1** caused a notable drop in the hydrolytic activity. The coordination of its carboxylate group to bis-Zn-cyclen **1** may provide a rational explanation for the inhibition. Amphiphiles which are expected to be neutral at the investigated pH = 7.4, **A7**, **A8**, **A3**, **A5**

and **A6**, respectively (for DSPC also **A2**, **A4**) induced only small changes in the hydrolytic activity. High-polar and basic membrane additives exhibited the highest hydrolytic activity in combination with cyclen **1**. A comparison of hydrolytic rates of membranes containing only cyclen **1** or its combination with a membrane additive (Figure 2.4) clearly indicates cooperative effects.

Figure 2.4 shows that selected membrane additives (**A4**, **A9**, **A10**, **A11**, **A13**, **A14**, **A15**, **A16**, and **A17**) are hydrolytically more active in fluid membranes. With exception of **A9** a larger increase of the hydrolytic rate is observed in DOPC membranes than in DSPC. The effect is most pronounced for membrane additives that are only hydrolytically active in combination with complex **1**, such as oxime **A4** (ninefold higher activity), phenol **A2** (threefold) and guanidinium **A17** (threefold). A rationale may be the higher dynamics of embedded amphiphiles in the membrane. All membrane additives that increase the hydrolytic activity of complex **1** have some common structural features. All compounds bear a N-O or H-O bond and are at pH 7 either neutral with a pKa value close to 7 (imidazole: 6.95, phenol: 8.05) or are protonated (amines, guanidinium). Protonated membrane additives **A** with more hydrogen atoms tend to accelerate the hydrolysis more: The addition of the primary octadecylamine **A14** induced a more than 10 times faster hydrolysis compared to the tertiary amine **A12** in DOPC.

The hydrolytic effect of micellar solutions with polar head groups is often credited to the high local concentration of positive charge on the surface, therefore creating a local high concentration of hydroxide ions, but the example of trimethylammonium salt **A17** shows that this effect is only small in comparison with cations generated by protonation (amines, guanidinium). The observations indicate that the rate enhancing effect of some membrane additives may have its origin in creating hydrogen bonds, which stabilize the transition state of substrate hydrolysis reaction.

2.2.2 Micellar hydrolysis

Kinetic measurements of micellar solutions were done under the same conditions as described for the vesicular solutions. The concentration of every component was kept constant and only the lipids were omitted in the preparation step. Concentrations of amphiphiles were exceeding their cmc values (cmc for cyclen **1** is less than 0.01 mM, see experimental part). Fluorescence is strongly quenched in the co-micellar solutions and the hydrolysis was therefore monitored by absorption spectroscopy. Pseudo first-order-reaction rate constants of hydrolysis (k_{obs}) were calculated from the slope of the increased fluorescein

absorption band ($\lambda_{max} = 505$ nm) over 3 min ($M s^{-1}$) divided by the initial FDA concentration (see experimental part).

	k_{obs} $10^{-5} s^{-1}$	k_{obs}^0 $10^{-5} s^{-1}$
Zn-cyclen 1	8.6	-
with additive		
A9	34.6	n.d.
A11	30.7	0.5
A14	22.4	1.7

Table 2.2 Hydrolytic activity of micellar systems: k_{obs} : rate of system with cyclen 1 (0.025 mM) and membrane additives (0.05 mM), k_{obs}^0 : micellar solutions of membrane additives. Same concentration as for vesicular measurements is used.

For micellar hydrolysis only the membrane additives **A9**, **A11**, **A14** were tested, because they gave best results in vesicular systems. An enhancement of the hydrolytic activity was observed for micelles of cyclen 1 with respect to the vesicular solution. On the contrary, the membrane additives without the lipid were less active (**A11**, **A14**) or insoluble (**A9**). Co-micellar solutions gave high catalytic activity towards hydrolysis in all three tested system exceeding the activity of vesicles. An average 3-fold increase of activity in comparison to micellar cyclen 1 solution without membrane additive implies the existence of co-micelles and cooperative effects in the hydrolysis.

2.2.3 Mechanism and kinetics

For mechanistic studies, various concentrations of vesicular and micellar solutions were used and the observed pseudo-first-order kinetic rate constants were plotted against the overall cyclen 1 concentration in the solutions (Figure 2.5). The reaction mechanism with embedded cyclen 1 tends to be different for DSPC and micelles than for DOPC membranes. Two kinetic models were used: second-order kinetics were observed in the case of DSPC vesicles and micelles with k_{obs} linearly dependent on the concentration of cyclen 1 in solution. In contrast, DOPC vesicles show a Michaelis–Menten type behaviour of saturation kinetics. Apparently, a complex of substrate and catalyst is formed, which then undergoes the hydrolysis reaction. The kinetic data were non-linear fitted using equation (1.1) according to previously published studies.²⁵

$$k_{obs} = \frac{k_{cat}c_{cyclen}}{K_M + c_{cyclen}} \quad (1)$$

K_M describes the stability of the catalyst-substrate complex and k_{cat} the rate of its decomposition to product and catalyst. In a fluid DOPC membrane, Zn-cyclen 1 shows

saturation kinetics even without the presence of a membrane additive, but in a rigid DSPC membrane and in micelles the hydrolysis rate increases linearly with the Zn-cyclen **1** concentration.

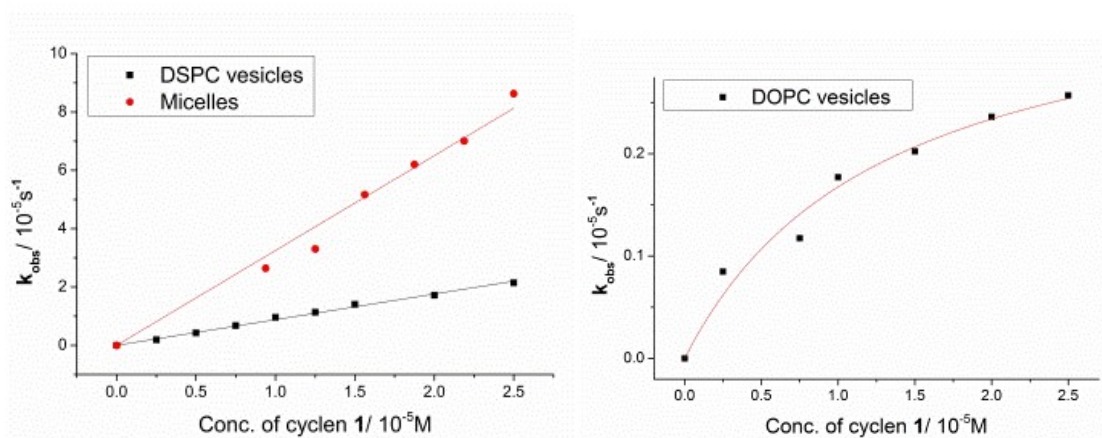


Figure 2.5 Second order kinetics for DSPC vesicle and micelles (left) and saturation kinetics for DOPC (right) containing cyclen **1**.

The kinetics of functionalized membranes with the highest hydrolytic activity consisting of cyclen **1** and membrane additives **A4**, **A14**, **A9** or **A11** were recorded and fitted to linear and non-linear (1) models. The derived constants are summarized in Table 2.3 (for data evaluation, see experimental part).

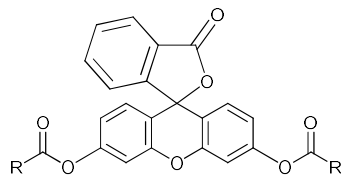
		k_{cat} 10^{-5} s^{-1}	K_M 10^{-5} M	$k_2' (k_{cat}/K_M)$ $\text{M}^{-1}\cdot\text{s}^{-1}$	k_2 $\text{M}^{-1}\cdot\text{s}^{-1}$
DOPC	Only cyclen 1 (5 %)	0.3	0.7	0.5	–
	5 % 1 + 10 % A4	10.4	8.4	1.2	–
	5 % 1 + 10 % A9	–	–	–	1.6
	5 % 1 + 10 % A11	40.9	9.3	4.4	–
	5 % 1 + 10 % A14	44.2	3.0	14.7	–
DSPC	Only cyclen 1 (5 %)	–	–	–	0.9
	5 % 1 + 10 % A4	–	–	–	0.9
	5 % 1 + 10 % A9	–	–	–	8.4
	5 % 1 + 10 % A11	–	–	–	3.7
	5 % 1 + 10 % A14	11.1	2.7	4.1	–
micelle.	Only cyclen 1	–	–	–	3.2
	1 + A9	–	–	–	13.4
	1 + A11	–	–	–	12.9
	1 + A14	–	–	–	7.8

Table 2.3 Second order rate constants: Only best performing systems selected.

For a better comparison of second order rate constants and reactions following a Michaelis–Menten kinetics, the initial slope was calculated dividing k_{cat} by K_M (k_2). For most of the functionalized DOPC membranes non-linear fitting gave better results as they followed not a single kinetic models, whereas rigid DSPC systems showed mostly linear correlations.

The membrane additive **A9** behaves different from the other functionalized lipids and shows a linear second-order kinetic also in the DOPC. Embedded amine **A14** leads to a saturation kinetic also in DSPC vesicles. Micelles of cyclen **1** and membrane additives showed the best hydrolytic activity.

To study the effect of lipophilicity and sterical hindrance of the ester group on the hydrolysis rate, a series of fluorescein esters was prepared (Table 2.4). All these compounds were tested under the same conditions as previously described and pseudo-first order hydrolytic rates were recorded for the three best performing membrane compositions with DSPC and DOPC lipids (Table 2.1, 2.2).



Name ^{pr.}	R	logP ^c
FDA ^a	CH ₃	3.20
F-C2 ^a	CH ₂ CH ₃	4.22
F-Ph ^b	Ph	4.41
F- <i>i</i> Pr ^b	<i>i</i> Pr	4.93
F-C3 ^b	(CH ₂) ₂ CH ₃	5.24
F- <i>t</i> Bu ^b	<i>t</i> Bu	5.75
F-C7 ^b	(CH ₂) ₆ CH ₃	9.31
F-C15 ^b	(CH ₂) ₁₄ CH ₃	17.47

Table 2.4 Fluorescein diesters: ^a Prepared from the acid chloride; ^b Prepared from the acid anhydride; ^c Values obtained from ACDlabs software.

Figure 2.6 shows that the trends in hydrolysis for the different esters remain the same in the different vesicular systems (for data, see experimental part); the molecular structure of the ester does not significantly affect the mechanism. The reactivity of the different esters is not affected by the membrane fluidity (DOPC *vs.* DSPC). The highest hydrolytic activity was reached for **FDA**, the least lipophilic ester (Figure 2.6). With increasing lipophilicity of the esters, the hydrolytic activity decreases. The lowest rates of hydrolysis were recorded for phenyl or *t*Bu esters (**F-Ph**, **F-*t*Bu**), which are more stable due to steric hindrance.

The trend in vesicular catalytic hydrolysis of the esters follows the reactivity for spontaneous hydrolysis. The stabilizing effect of increasing lipophilicity is less pronounced for reactions in vesicular solutions.

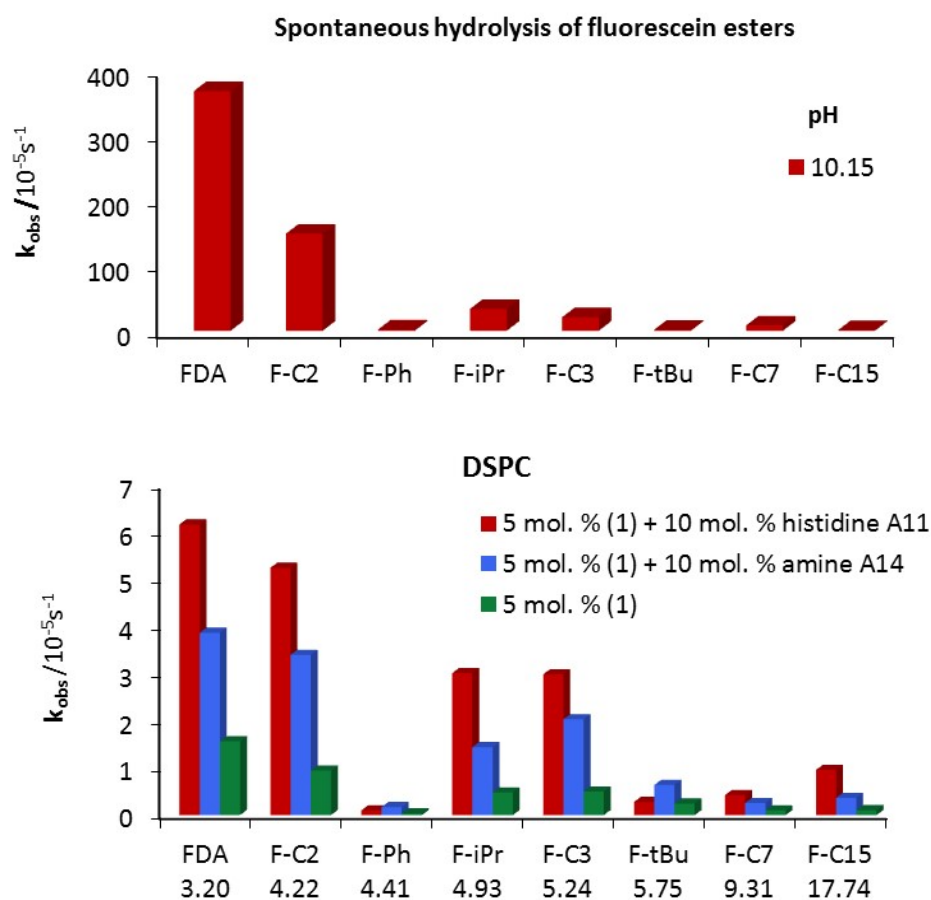


Figure 2.6 Hydrolysis of fluorescein esters (0.02 mM) spontaneously at pH 10.15 and by functionalized DSPC membranes at pH 7.4.

2.2.4 Comparison with hydrolytic enzymes

A direct comparison of kinetic data from the literature can be challenging due to different substrates and variations in the reaction conditions. Therefore commercially available hydrolytic enzymes were used under identical conditions to benchmark the hydrolytic rate of the functionalized vesicles. Porcine liver esterase and the lipase *Candida rugosa*, typical enzymes used in organic synthesis, were selected. Kinetic data were derived using the same non-linear fit as for vesicles to obtain k_{cat} and K_{M} . Since the enzymes are produced by extraction and no exact purity is given by the supplier, kinetic constants were calculated in weight concentration (mg ml^{-1}) for enzymes and vesicles. For vesicles the weight of cyclen complex 1, membrane additive A and the lipid was considered (see experimental part for data).

DOPC membranes functionalized with cyclen **1** and amine **A14** reach the activity of the two purchased enzymes (Table 2.5). However, the catalytic activity of the enzym active site still remains much higher compared to cyclen complex **1** and membrane additives, as the vesicles contain many hydrolytic active sites on their surface, while each enzyme has only one active centre.

	k_{cat} 10^{-5} s^{-1}	K_{M} 10^{-1} mg/ml	$k_2' (k_{\text{cat}}/K_{\text{M}})$ $10^{-4} (\text{mg/ml})^{-1} \cdot \text{s}^{-1}$
Porcine liver esterase	68.7	0.08	858
Lipase <i>Candida rugosa</i>	73.2	0.4	166
DOPC 5 % 1 + 10% A14	44.2	0.2	391

Table 2.5 Comparison of enzymatic and vesicular hydrolysis of **FDA**

2.3 Conclusions

Soft surfaces with ester hydrolysis activity were obtained by co-embedding of bis-Zn-cyclen complex **1** and amphiphilic membrane additives into a phospholipid membrane of a vesicle or producing a micellar solution. For many combinations of membrane additives and bis-Zn-cyclen complex **1** an increase of the hydrolytic activity up to 25 fold in comparison to complex **1** was observed. DOPC membranes that are fluid at the reaction temperature lead to more pronounced cooperative action of the membrane embedded amphiphiles and Michaelis-Menten saturation kinetic was observed for such membranes. Micellar solutions showed also higher activity when metal complex and additive are present. The functionalized vesicles with the highest hydrolytic activity were compared with two commercially available enzymes under identical reaction conditions. Considering the overall weight of the catalytic systems their hydrolysis activity towards fluorescein diesters is comparable.

In conclusion, we observed a significantly increased hydrolytic activity of functionalized vesicles and micelles at neutral pH towards carboxylesters, if Lewis acidic bis-Zn-cyclen complex **1** and functionalized amphiphiles are used concertedly. Their assembly has to be dynamic, as in DOPC membranes or micelles, to gain a cooperative hydrolytic effect.

2.4 Experimental Part

2.4.1 General Methods and Material

Dynamic Light Scattering

DLS measurements were performed on a Malvern Zetasizer Nano at 25 °C using 1 cm disposable polystyrene cuvettes (VWR).

NMR Spectra

Bruker Avance 300 (^1H : 300.1 MHz, ^{13}C : 75.5 MHz, T = 300 K). The chemical shifts are reported in δ [ppm] relative to external standards (solvent residual peak). The spectra were analysed by first order, the coupling constants are given in Hertz [Hz]. Characterization of the signals: s = singlet, d = doublet, t = triplet, q = quartet, m = multiplet, dd = double doublet, dt = double triplet. Integration is determined as the relative number of atoms. Error of reported values: chemical shift: 0.01 ppm for ^1H NMR, 0.1 ppm for ^{13}C NMR and 0.1 Hz for coupling constants. The solvent used is reported for each spectrum.

Mass Spectra

Finnigan MAT TSQ 7000 (ESI).

General

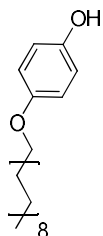
Thin layer chromatography (TLC) analyses were performed on silica gel 60 F-254 with a 0.2 mm layer thickness. Detection via UV light at 254 nm / 326 nm or through staining with KMnO_4 . Column chromatography was performed on silica gel (70–230 mesh) from Merck, flash chromatography on Biotage Isolera one using silica gel (230–400 mesh) from Merck. Commercially available solvents of standard quality were used. Starting materials were purchased from either Acros or Sigma-Aldrich and used without any further purification. Phospholipids were purchased from Avanti Polar Lipids Inc. Commercially available solvents of standard quality were used. If otherwise stated, purification and drying was done according to accepted general procedures. Enzymes were purchased from Sigma Aldrich.

2.4.2 Synthesis of membrane additives used as membrane additives

Zinc complex **1** was synthesized previously according to the published procedure.²⁶ Membrane additives **A1**, **A5**, **A6**, **A14**, **9-4**, **A17** were purchased and used as received, compound **A12** was recrystallized from ethanol prior to use. Amphiphiles **A2**²⁷, **A8**²⁸, **A7**²⁹,

A6³⁰, **A13**³¹, **A9**²¹, **A10**²¹, **A11**²¹, **CF**³², **TAMRA**³³ were synthesised according to published procedures. Amphiphiles **A3**, **A16**^{34, 35} (Scheme 2.3) were prepared by modified, published procedures.

4-Octadecyloxyphenol (**A3**)



Octadecylbromide (1.0 g, 3.0 mmol), hydroquinone (1.651 g, 15 mmol) and potassium carbonate (4.14 g, 30 mmol) were suspended in dry acetonitrile (60 ml), heated to 90 °C under nitrogen atmosphere and stirred for 12 h. After cooling, the solvent was evaporated and the residue suspended in water, which was adjusted with aq. HCl to be acidic in pH. The aqueous mixture was extracted with diethylether (3 × 60 ml) and the combined organic layers were dried over magnesium sulphate. Solids were filtered off and the solvent was removed *in vacuo*. The residue was purified by flash chromatography (PE with a gradient, up to 30% of EA) to obtain 500 mg (46%) of compound **A3** in form of white powder.

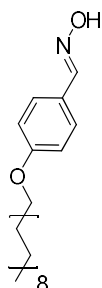
Yield: 46%.

T_m: 93 °C (lit 91-92 °C)

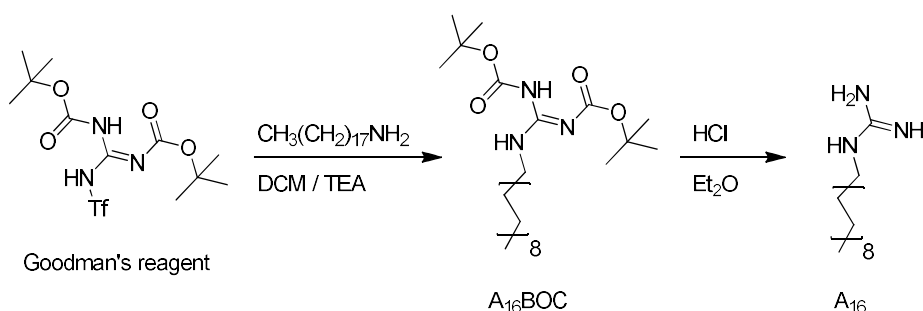
¹H NMR (300 MHz; CDCl₃): δ 6.89 – 6.57 (m, 4H), 3.89 (t, *J* = 6.6 Hz, 2H), 1.85 – 1.60 (m, 2H), 1.25 (s, 30H), 0.88 (t, *J* = 6.6 Hz, 3H).

¹³C NMR (75 MHz; CDCl₃): δ 153.35, 149.28, 115.99, 115.58, 68.71, 31.96, 29.73 (7C), 29.69, 29.64, 29.62, 26.45, 29.40 (2C), 26.08, 22.73, 14.17.

MS (ESI(+)): *m/z* [MH⁺].

4-Octadecyloxybenzaldehyde oxime³⁰ (A6)

Yield: 76%.

T_m: 84 °C¹H NMR (300 MHz; CDCl₃): δ 8.08 (s, 1H), 7.50 (d, *J* = 8.8 Hz, 2H), 6.89 (d, *J* = 8.8 Hz, 2H), 3.97 (t, *J* = 6.6 Hz, 2H), 1.86 – 1.71 (m, 2H), 1.51 – 1.16 (m, 30H), 0.88 (t, *J* = 6.8 Hz, 3H).¹³C NMR (75 MHz; CDCl₃): δ 160.70, 150.00, 128.48 (2C), 124.35, 114.76 (2C), 68.13, 31.95, 29.73 (7C), 29.69, 29.62, 29.59, 29.39, 29.19, 26.03, 22.72, 14.15.**MS** (ESI(+)): *m/z* 390.34 [MH⁺].**Scheme 2.3** Synthesis of 1-octadecylguanidine (**A16**)**1,3-Bis-(tert-butoxycarbonyl)-2-octadecyl-guanidine (A16-BOC)**

Octadecylamine (93 mg, 0.345 mmol) was dissolved in dry DCM (5 ml) and triethylamine (18 mg, 0.172 mmol) was added. The reaction mixture cooled in an ice bath under nitrogen atmosphere. A solution of Goodman's reagent (100 mg, 0.25 mmol) in dry DCM (5 ml) was added drop wise over a period of 5 minutes. The ice bath was removed and the reaction mixture stirred at RT overnight. The solvent was removed under reduced pressure and the residue was purified by column chromatography (EA:PE; 1:10) to obtain 100 mg (56%) of product **A16-BOC** in form of colourless oil.

$^1\text{H NMR}$ (300 MHz; CDCl_3): δ 3.46 – 3.30 (m, 2H), 1.60 – 1.50 (m, 2H), 1.49 (s, 9H), 1.50 (s, 9H), 1.19 – 1.39 (m, 30H), 0.93 – 0.79 (m, 3H).

$^{13}\text{C NMR}$ (75 MHz; CDCl_3): δ 156.10, 153.34, 83.01, 41.03, 31.95, 29.85 (9C), 29.60, 29.50, 29.39, 29.29, 28.97, 28.32 (3C), 28.09 (3C), 26.87, 22.72, 14.16.

MS (ESI(+)): m/z 512.44 [MH^+].

1-Octadecylguanidine (A16)

Boc protected guanidine **A16-BOC** (90 mg, 0.16 mmol) was dissolved in dry diethylether (5 ml), a saturated solution of HCl in diethylether (15 ml) was added and reaction mixture was stirred at room temp for 3 days. Solvents were removed *in vacuo* and the residue was purified by crystallisation from THF to obtain 45 mg (73%) of 1-octadecylguanidium (**A16**) in form of white crystals.

T_m: 153 °C decomp. (lit³⁶ 230.5 °C)

$^1\text{H NMR}$ (300 MHz; MeOD): δ 3.16 (t, $J = 7.1$ Hz, 2H), 1.63 – 1.50 (m, 2H), 1.25 – 1.43 (m, 30H), 0.90 (t, $J = 6.7$ Hz, 3H)

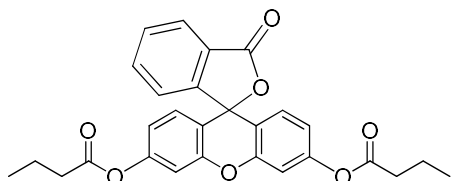
$^{13}\text{C NMR}$ (75 MHz; MeOD): δ 42.52, 33.13, 30.83 (9C), 30.75, 30.71, 30.53, 30.40, 29.95, 27.76, 23.79, 14.50.

MS (ESI(+)): m/z 312.34 [MH^+].

2.4.3 Synthesis of fluorescein esters

Esters **FDA** and **F-C2** were prepared by known procedures from the anhydrides of the parent acids.³⁷ Esters **F-C3**, **F-C7**, **F-C15**, **F-Ph**, **F-*i*Pr**, **F-*t*Bu** were prepared from chlorides of the acid. Fluorescein (200 mg, 0.602 mmol, 1 eqv) was suspended in dry toluene (15 ml) followed by addition of carboxychloride (1.204, 2 eqv), triethylamine (0.167 ml, 1.204 mmol, 2 eqv) and DMAP (5 mg). The reaction mixture was stirred under nitrogen atmosphere for 24 h. Solids were filtered off and washed with toluene. Solvent was removed under reduced pressure and the residue was purified two times by flash chromatography (petrolether with gradient, up to 30%, of ethyl acetate) or crystallization.

Fluorescein dibutyrate (F-C3)



Yield: 65%.

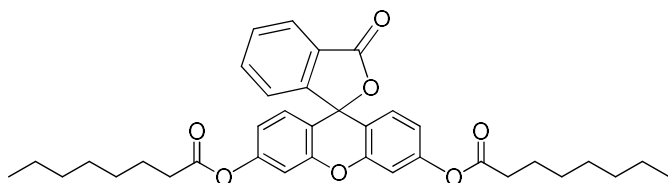
T_m: 139 °C (lit³⁷ 123 °C)

¹H NMR (300 MHz; CDCl₃): δ 8.02 (dd, *J* = 6.5, 1.3 Hz, 1H), 7.73 – 7.54 (m, 2H), 7.21 – 7.12 (m, 1H), 7.08 (dd, *J* = 1.8, 0.7 Hz, 2H), 6.89 – 6.72 (m, 4H), 2.54 (t, *J* = 7.4 Hz, 4H), 1.77 (h, *J* = 7.4 Hz, 4H), 1.02 (t, *J* = 7.4 Hz, 6H).

¹³C NMR (75 MHz; CDCl₃): δ 171.59, 169.18, 152.9, 152.15, 151.58, 135.33, 130.09, 128.96, 126.11, 125.21, 124.09, 117.80, 116.33, 110.40, 81.73, 36.15, 18.36, 13.62.

MS (ESI(+)): *m/z* 473.16 [MH⁺].

Fluorescein dioctanoate (F-C7)



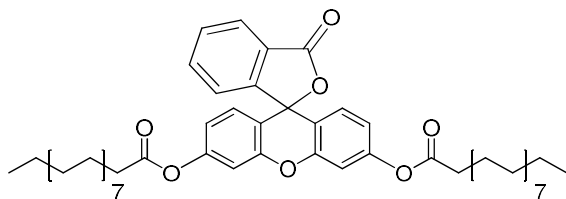
Yield: 77 %.

T_m: 49.3 °C (lit³⁷ 49 °C)

¹H NMR (300 MHz; CDCl₃): δ 8.03 (dd, *J* = 6.5, 1.3 Hz, 1H), 7.73 – 7.57 (m, 2H), 7.22 – 7.14 (m, 1H), 7.08 (dd, *J* = 1.9, 0.6 Hz, 2H), 6.88 – 6.74 (m, 4H), 2.56 (t, *J* = 7.5 Hz, 4H), 1.83 – 1.68 (m, 4H), 1.51 – 1.22 (m, 16H), 0.71 – 0.91 (m, 6H).

¹³C NMR (75 MHz; CDCl₃) δ 171.80, 169.22, 152.94, 152.16, 151.58, 135.30, 130.06, 128.96, 126.12, 125.23, 124.10, 117.78, 116.31, 110.39, 81.76, 34.36, 31.65, 29.03, 28.92, 24.85, 22.61, 14.10.

MS (ESI(+)): *m/z* 585.28 [MH⁺].

Fluorescein dipalmitoate (F-C15)

Purified by additional crystallisation from toluene.

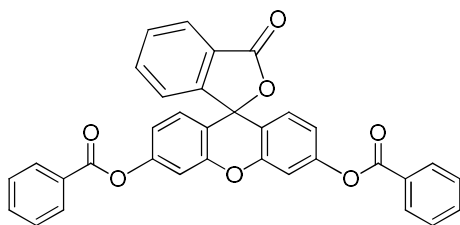
Yield: 43%.

T_m: 78 °C (lit³⁷ 69 °C)

¹H NMR (300 MHz; CDCl₃): δ 8.03 (dd, *J* = 6.5, 1.1 Hz, 1H), 7.74 – 7.55 (m, 2H), 7.18 (d, *J* = 7.0 Hz, 1H), 7.08 (d, *J* = 1.4 Hz, 2H), 6.86 – 6.71 (m, 4H), 2.56 (t, *J* = 7.5 Hz, 4H), 1.84 – 1.66 (m, 4H), 1.50 – 1.13 (m, 48H), 0.88 (t, *J* = 6.7 Hz, 6H).

¹³C NMR (75 MHz; CDCl₃): δ 171.78, 169.19, 152.96, 152.16, 151.58, 135.28, 130.04, 128.95, 126.13, 125.23, 124.10, 117.78, 116.32, 110.39, 81.74, 34.37, 31.95, 29.75 – 29.66 (bs, 5C), 29.62, 29.48, 29.39, 29.26, 29.09, 24.85, 22.72, 14.16.

MS (ESI(+)): *m/z* 585.28 [MH⁺].

Fluorescein dibenzoate (F-Ph)

Yield: 60%.

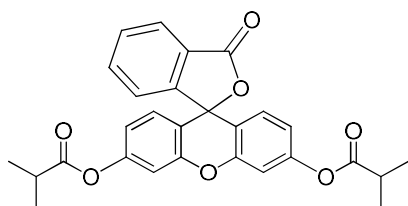
T_m: 217 °C (lit³⁸ 208-210 °C)

¹H NMR (300 MHz; CDCl₃): δ 8.27 – 8.14 (m, 4H), 8.07 (d, *J* = 7.1 Hz, 1H), 7.78 – 7.59 (m, 4H), 7.52 (t, *J* = 7.6 Hz, 4H), 7.31 – 7.16 (m, 3H), 6.95 (dt, *J* = 17.8, 5.4 Hz, 4H).

¹³C NMR (75 MHz; CDCl₃): δ 169.25, 164.66, 152.99, 152.39, 151.70, 135.40, 134.00, 130.31, 130.14, 129.10, 128.99, 128.72, 126.15, 125.29, 124.17, 117.98, 116.58, 110.66, 81.78.

MS (ESI(+)): *m/z* 541.13 [MH⁺].

Fluorescein diisobutyrate (F-iPr)



Yield: 70%.

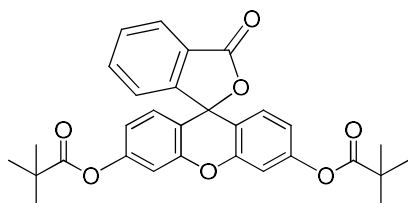
T_m: 155.6 °C

¹H NMR (300 MHz; CDCl₃): δ 8.02 (dt, *J* = 9.5, 5.1 Hz, 1H), 7.73 – 7.55 (m, 2H), 7.21 – 7.13 (m, 1H), 7.07 (dd, *J* = 2.0, 0.5 Hz, 2H), 6.87 – 6.74 (m, 4H), 2.80 (hept, *J* = 7.0 Hz, 2H), 1.31 (dd, *J* = 7.0, 0.6 Hz, 12H).

¹³C NMR (75 MHz; CDCl₃): δ 175.07, 169.23, 152.98, 152.32, 151.59, 135.31, 130.06, 128.94, 126.10, 125.23, 124.08, 117.72, 116.28, 110.33, 81.76, 34.19, 18.87.

MS (ESI(+)): *m/z* 473.16 [MH⁺].

Fluorescein dipivaloate (F-tBu)



Yield: 50%.

T_m: 99.6 °C

¹H NMR (300 MHz; CDCl₃): δ 8.02 (dt, *J* = 9.9, 5.1 Hz, 1H), 7.73 – 7.55 (m, 2H), 7.20 – 7.10 (m, 1H), 7.06 (t, *J* = 4.7 Hz, 2H), 6.79 (dt, *J* = 8.7, 5.4 Hz, 4H), 1.35 (s, 18H).

¹³C NMR (75 MHz; CDCl₃): δ 176.55, 169.26, 153.05, 152.57, 151.58, 135.32, 130.06, 128.91, 126.05, 125.22, 124.04, 117.72, 116.24, 110.32, 81.76, 39.20, 27.08.

MS (ESI(+)): *m/z* 501.19 [MH⁺].

2.4.4 Preparation and characterization of the membrane

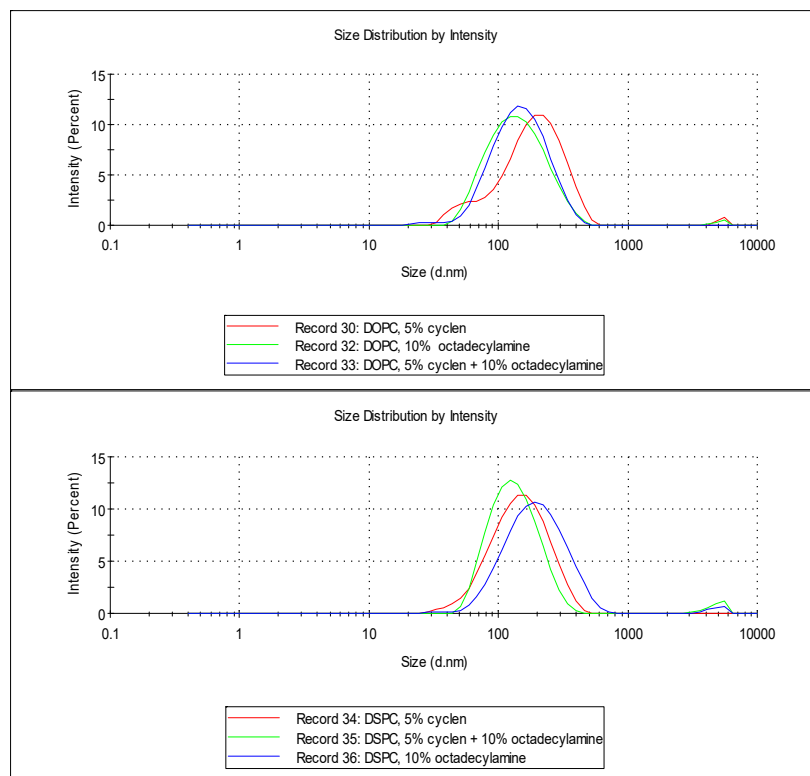


Figure 2.7 Examples of DLS measurement of mixtures made from lipids DSPC, DOPC (0.475 mM) with 5 % of cyclen **1** (0.025 mM), 5 % of cyclen **1** (0.025 mM) + 10 % octadecylamine **A14** (0.05 mM) and 10 % octadecylamine **A14** (0.05 mM)

Solutions of vesicles were prepared by a well-established procedure.³⁹ Membranes were prepared by sonication or treatment in a thermomixer of emulsions of amphiphiles in 25 mM HEPES (pH = 7.4) buffer for 10-20 min at 70 °C and used with or without an extrusion step. Micellar solutions were prepared by the same procedure with the exception of no addition of lipids. For each system the catalytic activity was determined and DLS analysis provided the size distribution of the vesicles. Measurements showed that there is only a small difference between the activities of membranes prepared by different procedures. DLS measurements (Figure 2.7) show that differently produced membranes are mostly in the shape of approximately 150 nm vesicles and do not change with composition. All measurements in this publication refer to vesicles prepared by sonication at a temperature higher than the transition temperature of the lipid used without extrusion step.

2.4.5 Determination of cmc value for cyclen 1

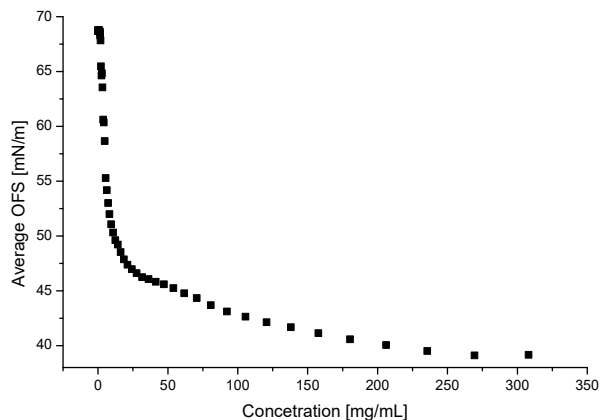


Figure 2.8 Isotherm of surface tension of the aqueous solution of Zn complex 1

2.4.6 Calibration curves for fluorescein concentration

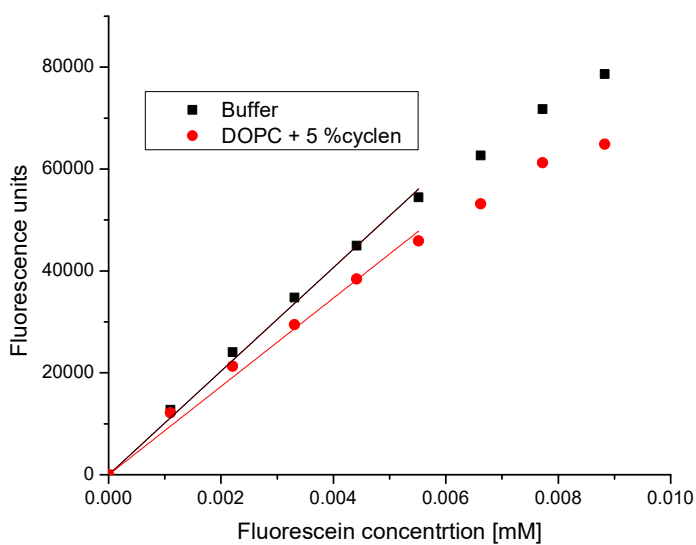


Figure 2.9 Fluorescein calibration curves.

The recorded fluorescence corresponds to the fluorescein produced by hydrolysis of FDA. To determine the fluorescein concentration a calibration curve was recorded. In vesicular solutions containing cyclen 1 the intensity of fluorescein is slightly quenched. Linear

regression was applied to determine the slope $k_{\text{buffer}} = 1.02 \times 10^{10}$ f.u./M and $k_{\text{vesicles}} = 8.67 \times 10^9$ f.u./M, which was used for calculations of pseudo first order kinetic constants. These rates were derived from the linear region of the calibration curve (up to 50 000 fluorescence unit). Membrane additives and lipids did not change the emission signal in the concentration range of the calibration curve so k_{vesicles} was used in all cases.

2.4.7 Estimated pKa values of membrane additives

Membrane additives	pKa	model compound (lit. ref.)
A1	4.76	acetic acid ⁴⁰
A2	8.05	4-acylphenol ⁴⁰
A3	10.20	4-methoxyphenol ⁴⁰
A4	11.16	4-methoxybenzaloxim ⁴¹
A5	12.00	methanthiol ⁴⁰
A6	15.54	methanol ⁴⁰
pKa of conj. Acid		
A7	0.18	urea ⁴⁰
A8	5.14	pyridine ⁴⁰
A9	6.95	imidazol ⁴⁰
A10	6.95	imidazol ⁴⁰
A11	6.95	imidazol ⁴⁰
A12	9.76	trimethylamine ⁴⁰
A13	9.82	piperazine ⁴⁰
A14	10.62	methylamine ⁴⁰
A15	10.64	dimethylamine ⁴⁰
A16	13.71	guanidin ⁴⁰

Table 2.6 Table of pKa values used as a estimated values for amphiphilic compound.

Compounds with short alkyl chains were chosen for the approximate determination of pKa values of membrane additive used for their sorting in Scheme 2.2.

2.4.8 Kinetic measurements

All the fluorescence measurements were performed in the FLUOstar Omega micro-titre plate reader using excitation filter at 485 nm and emission 520 nm. For every measurement 200 scans were performed over 16 hours. The fluorescein concentration was determined from calibration curves. The observed kinetic hydrolysis constant was calculated from the initial slope of the recorded increase of fluorescence. Each well of the micro-titre plate contained 200 μ l of the solution in 25 mM HEPES (pH = 7.4) buffer with a total concentration of the

amphiphiles of 0.5 mM (different lipids and amounts of membrane additives and cyclen) and 0.02 mM of the substrate (**FDA**). Stock solutions of the ester were made in DMSO: buffer (32: 1) resulting in the presence of 1.5 vol. % of DMSO in all measured solution. The same procedure was used for all fluorescein esters.

For micellar hydrolysis the same solutions and concentrations were used as for vesicles, but the increase of fluorescence concentration was measured with a Cary 50 UV-Vis spectrophotometer. Measurements were performed in 10 mm cuvette and the change of absorption was monitored at $\lambda_{\text{max}} = 505 \text{ nm}$ for 3 minutes. For evaluation of k_{obs} the published extinction coefficient for fluorescein of $76\,900 \text{ M}^{-1}\text{cm}^{-1}$ was used.⁴² All the measurements were repeated and did not exceed 10 % error.

Optimization of bis-Zn-cyclen 1 concentration in the membrane

The amount of embedded zinc-cyclen 1 in DSPC vesicles membranes was varied and the effect on hydrolytic activity determined (Figure 2.10).

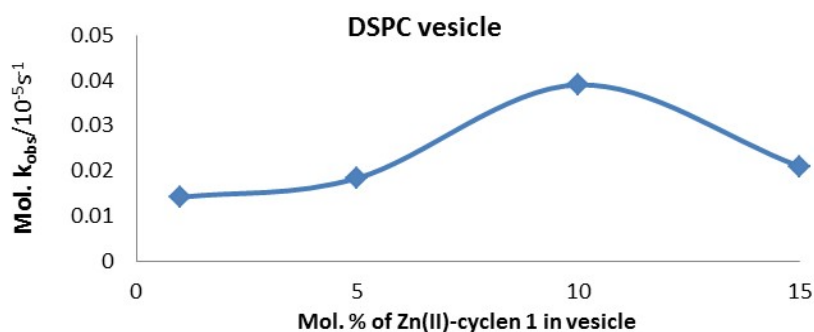


Figure 2.10 Hydrolytic activity on different cyclen 1 loading (0–) in DSPC vesicles.

The rate of the hydrolysis reaction increases with the amount of cyclen 1 embedded in the membrane, but decreases again above 10 % cyclen 1 with respect to the lipid. The hydrolysis rate as a function of the amount of complex 1, is highest with 5 mol. % of cyclen in the DSPC membrane. This amount of embedded complex 1 was used for all investigations.

Optimization of membrane additives concentration

The optimal ratio of membrane additive and cyclen for hydrolysis was determined for the DOPC membrane with embedded 5 mol% of bis-Zn-cyclen 1. Addition of more than 10 mol% of the supplement additive does not change the rate of hydrolysis any more (Figure 2.11). Therefore a ratio of 10 mol% of membrane additive and 5 mol% of cyclen with respect to the lipid was used for all kinetic measurements.

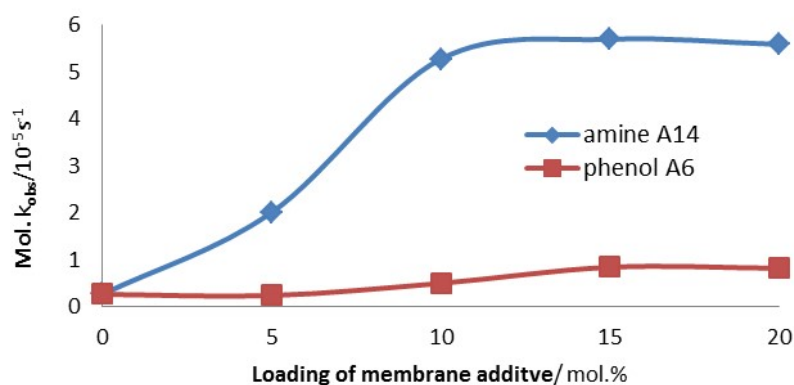


Figure 2.11 Dependence of the hydrolytic activity of 5 mol% bis-Zn-cyclen **1** (0.025 mM) in DOPC membranes with increasing amount of membrane additive **A14** and **A2** (0–0.1 mM).

Effect of different lipids

Lipid	T_m °C	5 % cyclen	5 % cyclen 1	10 % amine
		1	+ 10 % amine	A14
		k_{obs}	k_{obs}	k_{obs}^0
		$s^{-1} 10^{-5}$	$s^{-1} 10^{-5}$	$s^{-1} 10^{-5}$
DOPC	-20	0.23	14.09	4.65
DMPC	23	0.39	3.44	0.16
SMPC	30	0.87	4.89	0.28
DPPC	41	1.29	5.61	0.03
DSPC	55	1.57	4.36	0.77

Table 2.7 Hydrolytic rates of bis-Zn-cyclen **1** containing vesicles, T_m – transition temperature.

Different lipids with different transition temperature were examined for their hydrolytic properties with embedded bis-Zn-cyclen **1** (Figure 2.12, Table 2.7) and membrane additives. DOPC and DSPC lipids were used for the investigation of the membrane additives as they have a large difference in their transition temperature.

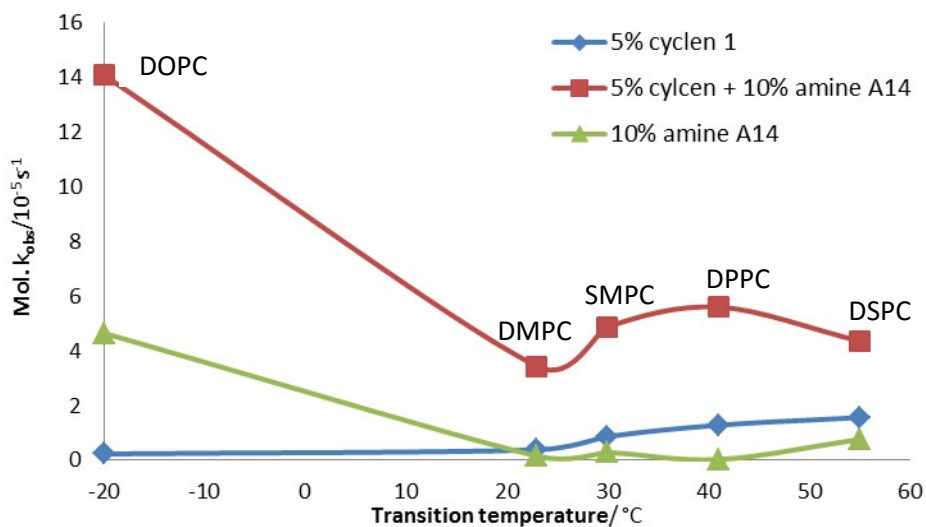


Figure 2.12 Hydrolytic rates of bis-Zn-cyclen **1** (0.025 mM) and/or amine **A14** (0.05 mM) containing vesicles made from various lipids compared with transition temperature of their membrane.

Various substrates

Selected functionalized vesicles were tested for their hydrolytic activity for different fluorescein esters.

		FDA	F-C2	F-Ph	F- <i>i</i> Pr	F-C3	F- <i>t</i> Bu	F-C7	F-C15
Lipophilicity ^a		3.20	4.22	4.41	4.93	5.24	5.75	9.31	17.47
DOPC	5 % Cyclen + 10 % A11	10.69	9.07	0.04	4.69	5.54	0.15	0.27	0.48
	5 % Cyclen + 10 % 10-2	17.44	12.55	0.11	2.86	4.29	0.07	0.36	0.55
	5 % Cyclen	0.27	0.17	0.00	0.07	0.07	0.02	0.01	0.05
DSPC	5 % Cyclen + 10 % A11	6.17	5.25	0.10	3.02	2.99	0.28	0.42	0.96
	5 % Cyclen + 10 % 10-2	3.87	3.40	0.17	1.44	2.03	0.64	0.26	0.37
	5 % Cyclen	1.57	0.94	0.04	0.48	0.50	0.24	0.10	0.10

Table 2.8 Hydrolytic rates (10^{-5} s^{-1}) of different fluorescein esters using selected membrane systems, ^a Lipophilicity was calculated using software ACDlabs.

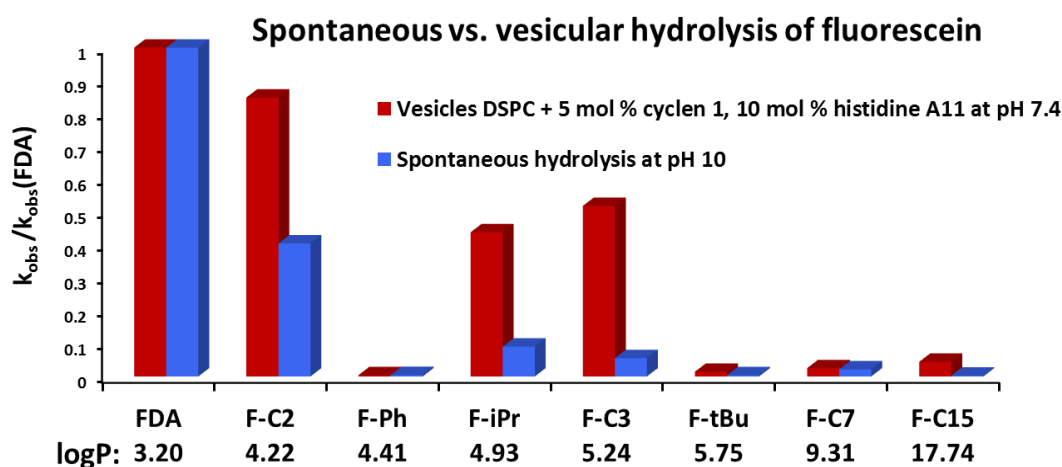


Figure 2.13 Comparison of the ratios of k_{obs} for different fluorescein esters (0.02 mM) hydrolysed spontaneously and by vesicles at

2.4.9 Processing of the kinetic data

Vesicular hydrolysis

For every measurement 200 scans were performed over 16 hours at 25°C. Using pseudo first order conditions the rate constant of hydrolysis (k_{obs}) was derived from the slope of the increasing fluorescein concentration over 20 min (s^{-1}) and the initial concentration of FDA (Figure 2.14).

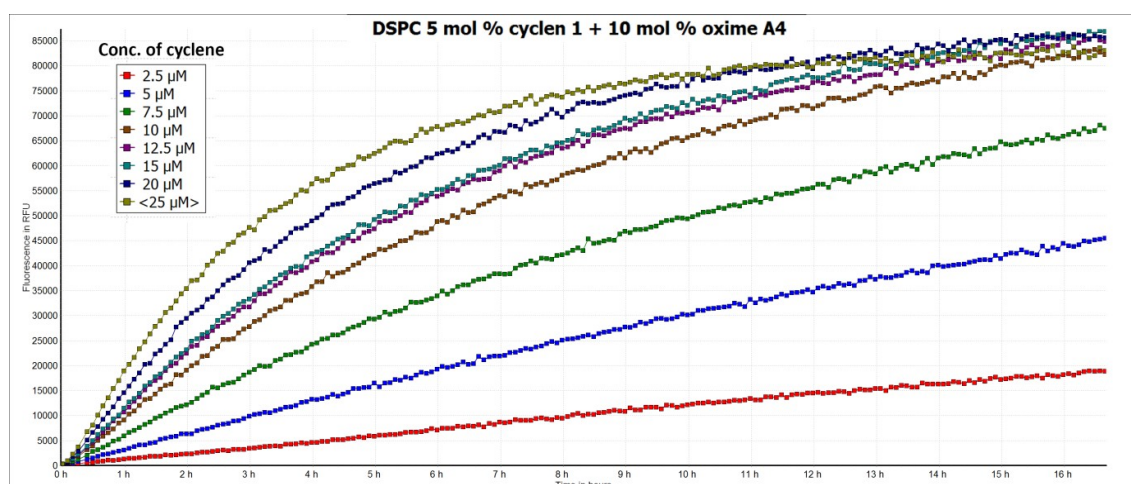
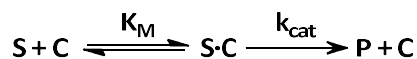


Figure 2.14 Example of kinetic data used for determination of k_{obs} for DOPC (0.425 mM), 5 mol % cyclen 1 (0.025 mM), 10 mol % oxime A4 (0.05 mM).


Scheme 2.4 Model for saturation kinetics.

The simple model for saturation kinetics can be described by equations (1) and (2):

$$\frac{d[P]}{dt} = k_{obs}\{[S]_0 + [C \cdot S]\} = k_{cat}[C \cdot S] \quad (1)$$

$$K_M = [C \cdot S]/[C]_0[S]_0 \quad (2)$$

Equation (3) is derived from equations (1) and (2), and was used for non-linear fitting. As concentration of catalyst, the overall cyclen complex 1 concentration in solution was used.

$$k_{obs} = \frac{k_{cat}c_{cyclen}}{K_M + c_{cyclen}} \quad (3)$$

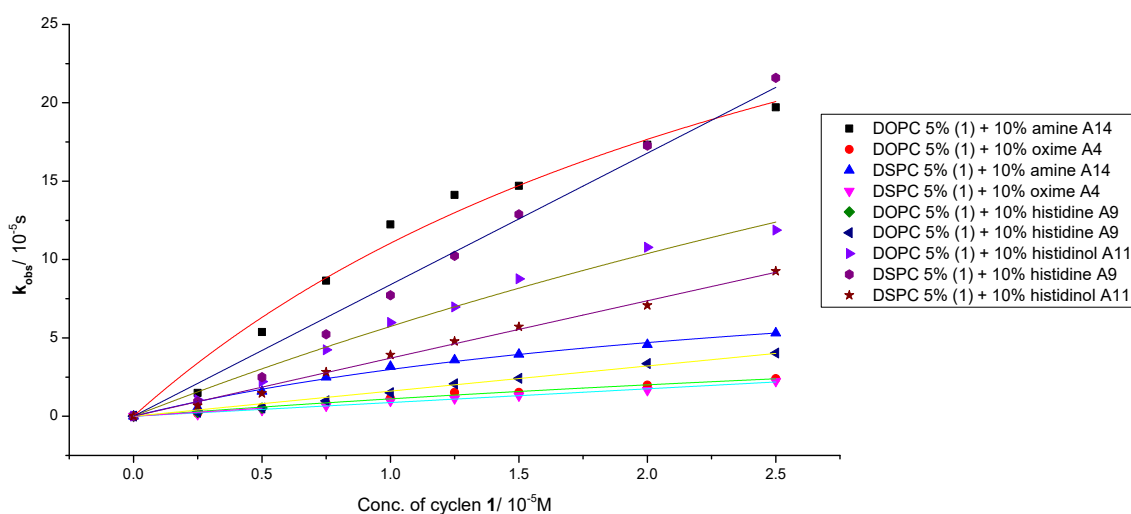


Figure 2.15 Plot of data and fitted curves of for determining the second rate constants for micellar solutions.

The exact molecular reaction mechanism is different from the kinetic model, because two ester groups of **FDA** need to be cleaved and the substrate- catalyst complex can consist of several cyclen complexes **1** and membrane additives **A**.

Micellar hydrolysis

Measurements were performed at 25°C under pseudo first order conditions. The hydrolysis rate constants (k_{obs}) were derived from the slope of increasing fluorescein concentration over 3 min (s^{-1}) and the initial concentration of FDA (Figure 2.16).

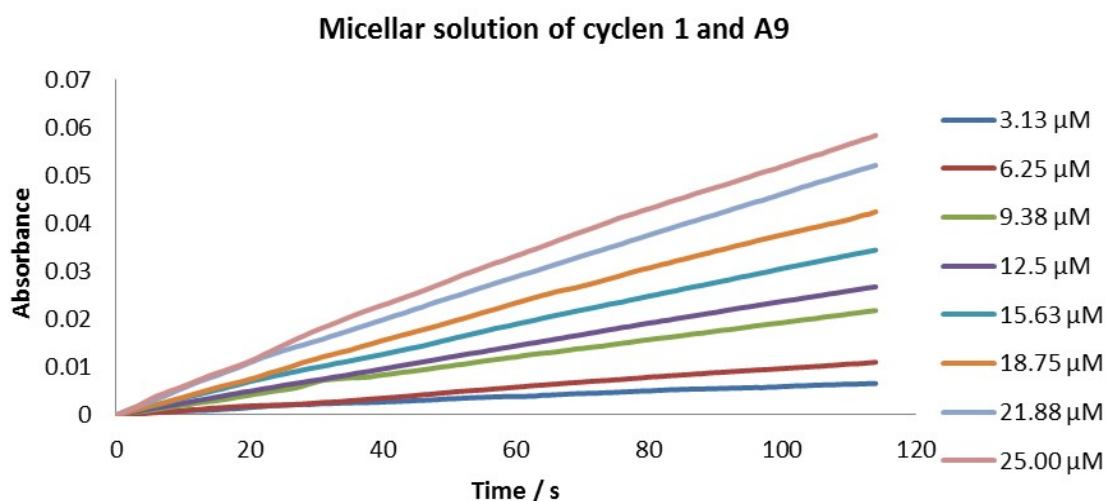


Figure 2.16 Kinetic data used for determination of k_{obs} in micellar solution of cyclen 1 and histidine A9.

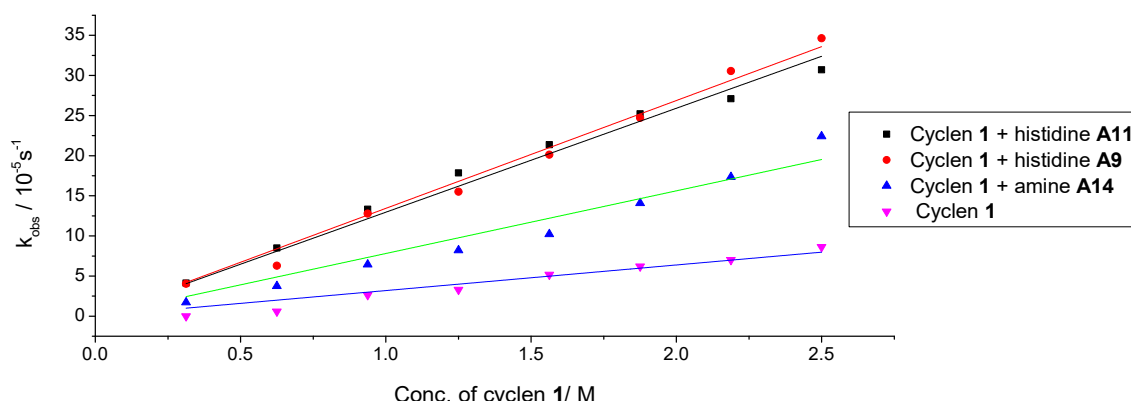


Figure 2.17 Fitted data of determining the second order rate constants for micellar solutions.

Comparison with enzymes

All the enzymes were purchased from Sigma Aldrich and were used fresh as delivered. Stock solutions of enzymes were made in 25 mM HEPES buffer in concentration 0.5 mg/ml and were used in the same manners as vesicular solutions. Kinetic measurements for obtaining k_{obs} were performed similarly as for vesicular solutions (Figure 2.18). Same conditions and

models were applied for processing the data; weight concentrations instead of molarities were used. For comparison with the enzymatic K_M values the data for vesicle solutions were recalculated from molar activity to mass activity considering the composition 85 mol % DOPC, 5 mol % cyclen **1**, 10 mol % **A14** by the equation (4).

$$K_M \left(\left(\frac{\text{mg}}{\text{ml}} \right)^{-1} \text{s}^{-1} \right) = K_M (M^{-1} \text{s}^{-1}) \cdot (0.85 \cdot M_{\text{DOPC}} + 0.05 \cdot M_{\text{cyclen 1}} + 0.10 \cdot M_{\text{A14}}) \quad (4)$$

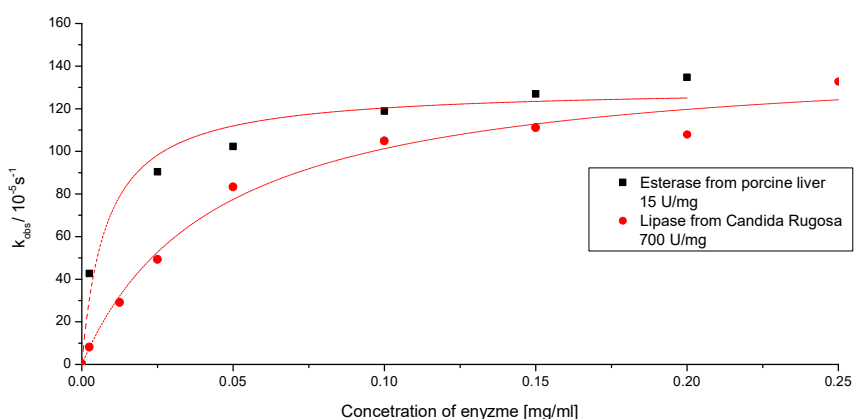
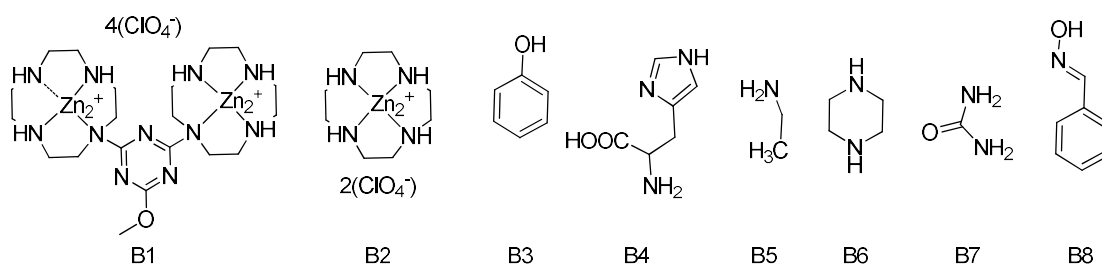


Figure 2.18 Kinetic data for enzymes.

Control experiments

All functional groups of the amphiphilic compounds were tested for their hydrolytic properties in homogeneous solution. For this purpose the corresponding molecules lacking the alkyl chain (Scheme 2.5) were tested under the same conditions as the amphiphilic samples (Table 2.9).



Scheme 2.5 Water soluble non-amphiphilic derivatives of Zn-cyclen complexes and membrane additives.

None of these compounds induced noticeable hydrolytic activity in comparison to the spontaneous hydrolysis of the **FDA** in buffer (Table 2.9).

Compound	k_{obs} $\text{s}^{-1} 10^{-5}$
B1	0.003
B2	0.006
B3	0.0035
B4	0.004
B5	0.003
B6	0.004
B7	0.003
B8	0.005
5 mol % cyclen*	0.24
DOPC only	0.005
Buffer only	0.003

Table 2.9 Initial rates of samples prepared using same method, but non amphiphilic molecules of membrane additives and cyclen **1**. For comparison the hydrolysis rates for bis- Zn-cyclen **1** in DOPC membrane (*) and spontaneous hydrolysis in buffer under identical conditions are given.

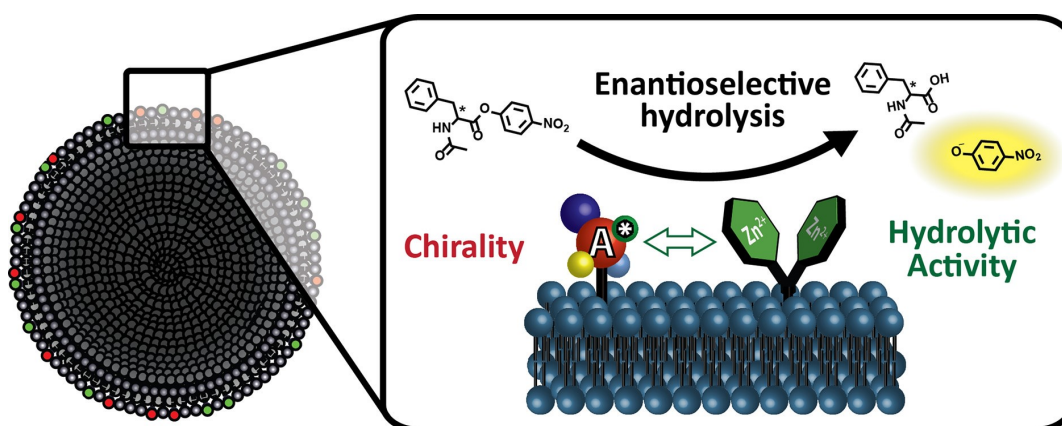
2.5 References

1. Testa, B.; Mayer, J. M., Introduction: Metabolic Hydrolysis and Prodrug Design. In *Hydrolysis in Drug and Prodrug Metabolism*, Verlag Helvetica Chimica Acta: 2006; pp 1-9.
2. Chin, J., Developing artificial hydrolytic metalloenzymes by a unified mechanistic approach. *Acc. Chem. Res.* **1991**, *24* (5), 145-152.
3. Murakami, Y.; Kikuchi, J.-i.; Hisaeda, Y.; Hayashida, O., Artificial Enzymes. *Chem. Rev.* **1996**, *96* (2), 721-758.
4. Christianson, D. W.; Cox, J. D., Catalysis by metal-activated hydroxide in zinc and manganese metalloenzymes. *Annu. Rev. Biochem* **1999**, *68* (1), 33-57.
5. Kimura, E., Dimetallic hydrolases and their models. *Curr. Opin. Chem. Biol.* **2000**, *4* (2), 207-213.
6. Mancin, F.; Scrimin, P.; Tecilla, P., Progress in artificial metallonucleases. *Chem. Commun.* **2012**, *48* (45), 5545-5559.
7. Subat, M.; Woinaroschy, K.; Anthofer, S.; Malterer, B.; König, B., 1,4,7,10-Tetraazacyclododecane Metal Complexes as Potent Promoters of Carboxyester Hydrolysis under Physiological Conditions. *Inorg. Chem.* **2007**, *46* (10), 4336-4356.
8. Subat, M.; Woinaroschy, K.; Gerstl, C.; Sarkar, B.; Kaim, W.; König, B., 1,4,7,10-Tetraazacyclododecane Metal Complexes as Potent Promoters of Phosphodiester Hydrolysis under Physiological Conditions. *Inorg. Chem.* **2008**, *47* (11), 4661-4668.
9. Gruber, B.; Kataev, E.; Aschenbrenner, J.; Stadlbauer, S.; König, B., Vesicles and Micelles from Amphiphilic Zinc(II)-Cyclen Complexes as Highly Potent Promoters of Hydrolytic DNA Cleavage. *J. Am. Chem. Soc.* **2011**, *133* (51), 20704-20707.
10. Gruber, B.; König, B., Self-Assembled Vesicles with Functionalized Membranes. *Chem. Eur. J.* **2013**, *19* (2), 438-448.
11. Moss, R. A.; Sunshine, W. L., Micellar catalysis of ester hydrolysis. Influence of chirality and head group structure in simple surfactants. *J. Org. Chem.* **1974**, *39* (8), 1083-1089.
12. Mancin, F.; Scrimin, P.; Tecilla, P.; Tonellato, U., Amphiphilic metalloaggregates: Catalysis, transport, and sensing. *Coord. Chem. Rev.* **2009**, *253* (17-18), 2150-2165.
13. Bunton, C. A.; Fendler, E. J.; Sepulveda, G. L.; Yang, K.-U., Micellar-catalyzed hydrolysis of nitrophenyl phosphates. *J. Am. Chem. Soc.* **1968**, *90* (20), 5512-5518.
14. Moss, R. A.; Sunshine, W. L., Micellar catalysis of ester hydrolysis. Influence of chirality and head group structure in simple surfactants. *J. Org. Chem.* **1974**, *39* (8), 1083-1089.
15. Kunitake, T.; Okahata, Y.; Sakamoto, T., Multifunctional hydrolytic catalyses. 8. Remarkable acceleration of the hydrolysis of p-nitrophenyl acetate by micellar bifunctional catalysts. *J. Am. Chem. Soc.* **1976**, *98* (24), 7799-7806.

16. Scrimin, P.; Tecilla, P.; Tonellato, U., Metallomicelles as catalysts of the hydrolysis of carboxylic and phosphoric acid esters. *J. Org. Chem.* **1991**, *56* (1), 161-166.
17. Zhang, J.; Meng, X.-G.; Zeng, X.-C.; Yu, X.-Q., Metallomicellar supramolecular systems and their applications in catalytic reactions. *Coord. Chem. Rev.* **2009**, *253* (17-18), 2166-2177.
18. Scrimin, P.; Tecilla, P., Model membranes: developments in functional micelles and vesicles. *Curr. Opin. Chem. Biol.* **1999**, *3* (6), 730-735.
19. Grochmal, A.; Ferrero, E.; Milanese, L.; Tomas, S., Modulation of In-Membrane Receptor Clustering upon Binding of Multivalent Ligands. *J. Am. Chem. Soc.* **2013**, *135* (27), 10172-10177.
20. Gruber, B.; Balk, S.; Stadlbauer, S.; König, B., Dynamic Interface Imprinting: High-Affinity Peptide Binding Sites Assembled by Analyte-Induced Recruiting of Membrane Receptors. *Angew. Chem. Int. Ed.* **2012**, *51* (40), 10060-10063.
21. You, J.-S.; Yu, X.-Q.; Su, X.-Y.; Wang, T.; Xiang, Q.-X.; Yang, M.; Xie, R.-G., Hydrolytic metalloenzyme models: Enantioselective hydrolysis of long chain α -amino acid esters by chiral metallomicelles composed of lipophilic l-histidinol. *J. Mol. Catal. A: Chem.* **2003**, *202* (1-2), 17-22.
22. Epstein, J.; Kaminski, J.; Bodor, N.; Enever, R.; Sowa, J.; Higuchi, T., Micellar acceleration of organophosphate hydrolysis by hydroximinomethylpyridinium type surfactants. *J. Org. Chem.* **1978**, *43* (14), 2816-2821.
23. Swisher, R.; Carroll, G., Fluorescein diacetate hydrolysis as an estimator of microbial biomass on coniferous needle surfaces. *Microb Ecol* **1980**, *6* (3), 217-226.
24. Steward, N.; Martin, R.; Engasser, J. M.; Goergen, J. L., A new methodology for plant cell viability assessment using intracellular esterase activity. *Plant Cell Reports* **1999**, *19* (2), 171-176.
25. Kim, D. H.; Lee, S. S., Origin of rate-acceleration in ester hydrolysis with metalloprotease mimics. *Biorg. Med. Chem.* **2000**, *8* (3), 647-652.
26. Turygin, D. S.; Subat, M.; Raitman, O. A.; Arslanov, V. V.; König, B.; Kalinina, M. A., Cooperative Self-Assembly of Adenosine and Uridine Nucleotides on a 2D Synthetic Template. *Angew. Chem. Int. Ed.* **2006**, *45* (32), 5340-5344.
27. Tian, H.-Y.; Li, H.-J.; Chen, Y.-J.; Wang, D.; Li, C.-J., Development of Highly Effective Encapsulating Surfactants for Mukaiyama Aldol Reactions in Water. *Ind. Eng. Chem. Res.* **2002**, *41* (18), 4523-4527.
28. Herbert, M.; Galindo, A. n.; Montilla, F., Methyltrioxorhenium Complexes of Polydimethylsiloxane-Functionalized Pyridine as Efficient Olefin Epoxidation Catalysts in Solventless and Low-Polar Solvent Conditions. *Organometallics* **2009**, *28* (9), 2855-2863.
29. li, Y.; Wang, Q.; Cai, W., Construction of Novel Terbium Green Emissive Gels and Their Unique Thermal Degradation Processes. *J. Cluster Sci.* **2012**, *23* (1), 147-154.

30. Pakulski, M. M.; Mahato, S. K.; Bosiak, M. J.; Krzeminski, M. P.; Zaidlewicz, M., Enantioselective reduction of ketoxime ethers with borane–oxazaborolidines and synthesis of the key intermediate leading to (S)-rivastigmine. *Tetrahedron: Asymmetry* **2012**, *23* (9), 716-721.
31. Boukli, L.; Touaibia, M.; Meddad-Belhabich, N.; Djimdé, A.; Park, C.-H.; Kim, J.-J.; Yoon, J.-H.; Lamouri, A.; Heymans, F., Design of new potent and selective secretory phospholipase A2 inhibitors. Part 5: Synthesis and biological activity of 1-alkyl-4-[4,5-dihydro-1,2,4-[4H]-oxadiazol-5-one-3-ylmethylbenz-4'-yl(oyl)] piperazines. *Biorg. Med. Chem.* **2008**, *16* (3), 1242-1253.
32. Gruber, B.; Stadlbauer, S.; Späth, A.; Weiss, S.; Kalinina, M.; König, B., Modular Chemosensors from Self-Assembled Vesicle Membranes with Amphiphilic Binding Sites and Reporter Dyes. *Angew. Chem. Int. Ed.* **2010**, *49* (39), 7125-7128.
33. Balk, S. Synthesis of functionalized vesicles for FRET based distance measurements. Master, University of Regensburg, 2010.
34. Späth, A.; König, B., Ditopic crown ether–guanidinium ion receptors for the molecular recognition of amino acids and small peptides. *Tetrahedron* **2010**, *66* (10), 1859-1873.
35. J, B. T.; M, T.; M, G., PREPARATION AND USE OF N,N'-DI-BOC-N"-TRIFLYLGUANIDINE. *Org. Synth.* **2004**, *Coll. Vol. 10*, 266.
36. Short, J. H.; Biermacher, U.; Dunnigan, D. A.; Leth, T. D., Sympathetic Nervous System Blocking Agents. Derivatives of Guanidine and Related Compounds1. *J. Med. Chem.* **1963**, *6* (3), 275-283.
37. Ge, F.-Y.; Chen, L.-G.; Zhou, X.-L.; Pan, H.-Y.; Yan, F.-Y.; Bai, G.-Y.; Yan, X.-L., Synthesis and study on hydrolytic properties of fluorescein esters. *Dyes Pigm.* **2007**, *72* (3), 322-326.
38. Eshghi, H.; Mirzaie, N.; Asoodeh, A., Synthesis of fluorescein aromatic esters in the presence of P2O5/SiO2 as catalyst and their hydrolysis studies in the presence of lipase. *Dyes Pigm.* **2011**, *89* (2), 120-126.
39. Gruber, B.; Stadlbauer, S.; Woinaroschy, K.; König, B., Luminescent vesicular receptors for the recognition of biologically important phosphate species. *Org. Biomol. Chem.* **2010**, *8* (16), 3704-3714.
40. Williams, R.; Jencks, W. P.; Westheimer, F. H. pKa Values.
41. Pícha, J.; Cibulka, R.; Hampl, F.; Liška, F.; Pytela, O.; Pařík, P., Reactivity of p-Substituted Benzaldoximes in the Cleavage of p-Nitrophenyl Acetate: Kinetics and Mechanism. *Collect. Czech. Chem. Commun.* **2004**, *69* (2), 397-413.
42. Sjöback, R.; Nygren, J.; Kubista, M., Absorption and fluorescence properties of fluorescein. *Spectrochim. Acta Mol. Biomol. Spectros.* **1995**, *51* (6), L7-L21.

3 Enantioselective ester hydrolysis by an achiral catalyst co-embedded with chiral amphiphiles into a vesicle membrane



Co-Co-embedding of an amphiphilic non-chiral hydrolysis catalyst with amphiphilic chiral additives into the membrane of a phospholipid vesicle induces different rates of ester hydrolysis for enantiomeric amino acid esters.

This chapter was published in:

M. Poznik and B. König, " Enantioselective ester hydrolysis by an achiral catalyst co-embedded with chiral amphiphiles into a vesicle membrane ",
RSC Adv., **2016**, 6, 44456-44458

M. Poznik performed the experimental work and wrote the manuscript. B. König supervised the project and is corresponding author.

3.1 Introduction

The origin of chirality in nature,¹ why natural molecules are homochiral, and how such a rapid amplification of single enantiomers occurred, are still unanswered questions.^{2, 3} Synthetic chemistry uses chiral catalyst or ligands to convert achiral substrates enantio-selective.⁴ The reactant and the source of chirality require typical close contact. The simple addition of chiral additives to the reaction mixture or using enantiopure chiral solvents^{5, 6} provide none or minute enantioselectivity. The intermolecular chirality transfer improves in 3D networks, such as chiral MOFs^{7, 8} or micellar solutions.^{9, 10, 11, 12}

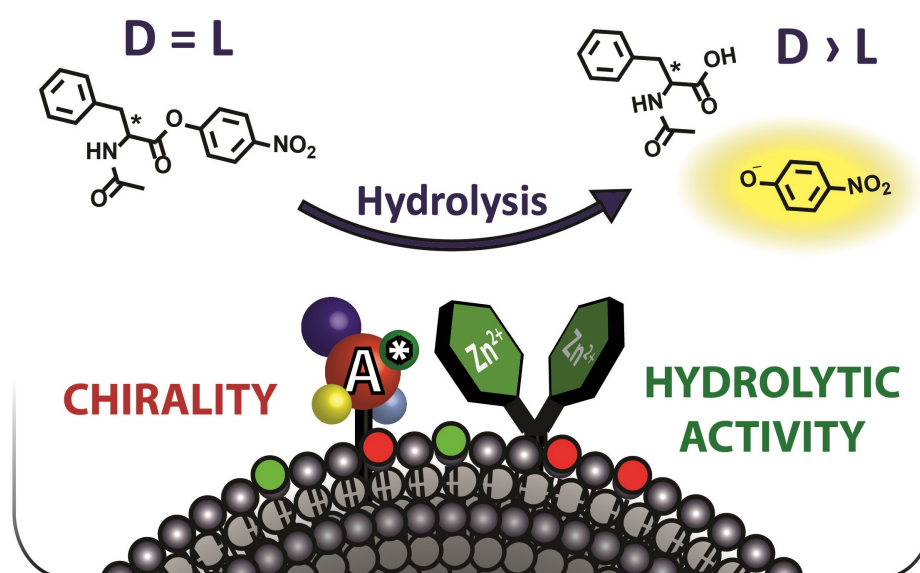


Figure 3.1 Proposed concept of additive-induced enantioselectivity in a hydrolytic reaction.

The Raymond group reported an approach where chiral selfassembled capsules induce stereoselective reactions of achiral substrates by weak interactions.^{13, 14, 15}

We report here the hydrolysis of enantiomeric amino acid esters on the modified surface of phospholipid vesicles (Figure 3.1). A chiral, catalytically inactive membrane additive is co-embedded with a catalytically active achiral metal complex Zn₂Cy into the phospholipid membrane.^{12, 16} The membrane serves as two-dimensional platform with higher concentration of the amphiphilic membrane additives compared to the bulk solution.¹⁷ This proximity of the chiral additive to the achiral metal complex affects its selectivity in ester hydrolysis and induces thereby different reaction rates for both enantiomers.

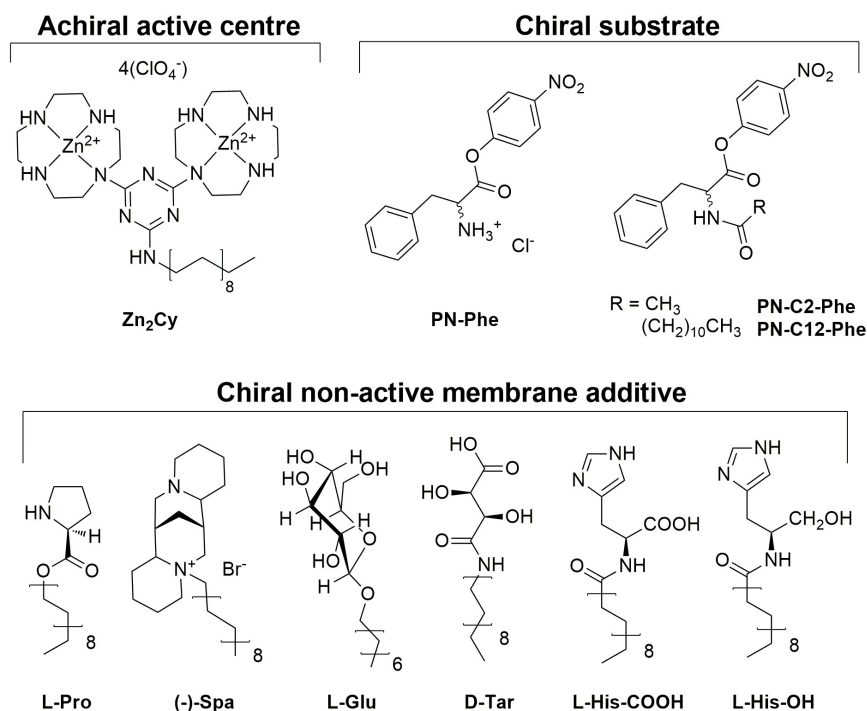


Figure 3.2 Molecular structures of the achiral catalyst for hydrolysis, racemic substrates and chiral membrane additives.

The bis-zinc-cyclen complex **Zn₂Cy** is anchored into the surface of the vesicle by its lipophilic alkyl chain and promotes the hydrolysis of activated carboxylic esters as previously reported (Figure 3.2).¹⁸ The Lewis acidic zinc ions coordinate one water molecule and the ester functionality. Enantiopure amphiphilic derivatives of L-proline **L-Pro**, (-)-sparteine **(-)-Spa**, L-glucose **L-Glu**, L-tartaric acid **L-Tar** and L-histidine **L-His-COOH** and the corresponding alcohol **L-His-OH** were used as chiral membrane additives. Enantiometrically pure 4-nitrophenol esters of phenylalanine, **PN-Phe**, serve as substrates for the catalysed hydrolysis. Upon cleavage of the ester bond, the coloured 4-nitrophenolate anion is released, which enables a facile determination of the reaction progress. However, derivatives **PN-Phe** with free amine group show fast spontaneous hydrolysis under the reaction conditions. Therefore compounds **PN-C12-Phe** and **PN-C2-Phe** with a protected amino-group were prepared, which are stable in the absence of the hydrolysis catalyst.

3.2 Results and discussion

All measurements were done in buffered solutions (HEPES buffer, 25 mM, 7.4 pH), at room temperature. Samples were prepared by sonication according to a previously reported procedure to form micellar solutions or 100 nm unilamellar functionalised vesicles.¹⁸ The rate of substrate hydrolysis was determined colorimetrically as an increase in absorbance intensity at 400 nm (absorption maximum of 4-nitrophenol at pH 7.4; no other species absorb at this wavelength). Relative error of the measurement was estimated to be below 10 % (Figure 3.3).

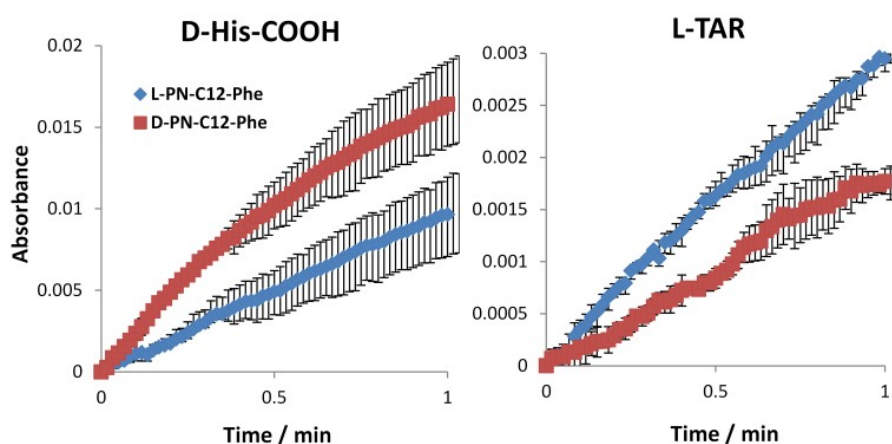


Figure 3.3 Examples of the kinetic data for hydrolysis of the **PN-C12-Phe** substrate by vesicular solution (85 % DOPC), **Zn₂Cy** (5%) and amphiphilic additive (10%).

Pseudo first order rate constants were calculated using the initial slope method. Every membrane additive was examined as a sole micellar solution (without lipid or **Zn₂Cy**), co-micellar solution (without lipid in the presence of **Zn₂Cy**), and in vesicular membranes with 1,2-dioleoyl-*sn*-glycero-3-phosphocholine (DOPC) and 1,2-distearoyl-*sn*-glycero-3-phosphocholine (DSPC) lipids (5 mol. % **Zn₂Cy**, 10 mol. % membrane additive, 85 mol. % lipid). Lipids differ in their transition temperatures providing fluid (DOPC) and rigid (DSPC) membranes at room temperature. We measured the hydrolytic rate constants separately for the two enantiomers of the substrate **PN-C12-Phe**. This substrate is equipped with a long alkyl chain, which increases its lipophilicity and the adsorption to the surface of the membrane. The initial hydrolysis rates for different functionalized vesicles and co-micelles are summarised in Table 3.1.

	DOPC		DSPC		Co-micelles		No cyclen No lipid	
	k_L	k_D	k_L	k_D	k_L	k_D	k_L	k_D
ZnCy₂	31	30	65	50	201	198		
L-Pro	15	15	63	61	166	159	– ^a	– ^a
(-)-Spa	28	26	50	41	277	236	– ^a	– ^a
L-Glu	13	15	28	28	229	242	– ^a	– ^a
L-Tar	24	14	26	24	46	46	– ^a	– ^a
L-His-COOH	212	113	153	129	214	286	11	2
D-His-COOH	127	233	<i>n.d.</i>	<i>n.d.</i>	<i>n.d.</i>	<i>n.d.</i>	<i>n.d.</i>	<i>n.d.</i>
L-His-OH	339	327	357	287	513	384	6	4

Table 3.1 Pseudo first order kinetic rate constants for the hydrolysis of the L and D enantiomer of **P-C12-Phe** using different systems. All kinetic values are given in 10^{-3}s^{-1} . ^a no effect on hydrolysis observed.

3.2.1 Kinetic effects

Hydrolysis of the ester **PN-C12-Phe** is favoured in micellar solutions (Table 3.1). Confirming previous results,¹⁸ membrane additives can affect the hydrolysis activity in vesicular and co-micellar solutions significant.

In DOPC membranes the hydrolytic rates are affected by two types of membrane additives: tartrate **L-Tar** decreases and histidine derivatives **L-His-COOH** and **L-His-OH** increase the initial rate of ester hydrolysis (Table 3.1). These observations are in accordance to effects on the previously studied hydrolysis of fluorescein diacetate by **Zn₂Cy**.¹⁸

3.2.2 Enantiodiscrimination in ester hydrolysis

The rates of ester hydrolysis were determined for both enantiomers as previously reported for micellar solutions.¹⁰ The largest relative difference in hydrolysis rates for the enantiomeric esters is observed in DOPC vesicles with addition of amphiphilic tartrate **L-Tar** or histidine acid **L-His-COOH** as membrane additives (Figure 3.4).

Both compounds contain free carboxy group. When the carboxyl group of histidine is reduced the effect in vesicles is lost. This indicates that the free acid might have a crucial role in this cooperative action. In buffered solution the acid is deprotonated and might interact with the Lewis acidic zinc complex. This interaction is weak in bulk solution, but may significantly increase due to the close proximity of the binding partners at the vesicular surface. In fluid DOPC membranes, embedded components diffuse and may thereby arrange optimal for the catalysis. In gel phase DSPC added amphiphiles form patches with restricted

lateral movement decreasing the possibility for cooperative effects.^{19, 20, 21} This was also previously observed by us.¹⁸

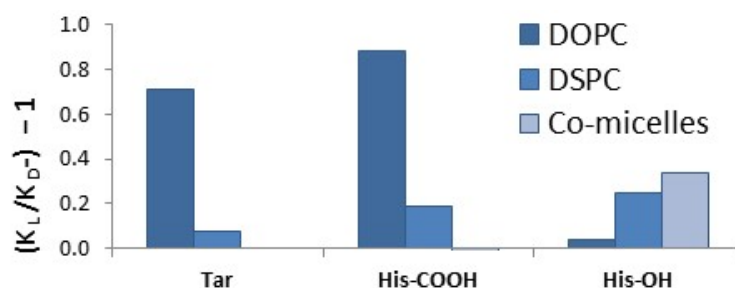


Figure 3.4 Effect of membrane additives on the relative ratio of ester hydrolysis rates of enantiomeric amino acid esters represented by the fraction of pseudo first order kinetic constants.

Other membrane additives than tartrate or histidine do not show considerable effects on the relative hydrolysis rate of the enantiomeric esters. Substrates **PN-C2-Phe** and **Pn-Phe** exhibit similar enantioselective enhancement (Table 3.2).

	k_L [$10^{-3} s^{-1}$]	k_D [$10^{-3} s^{-1}$]
PN-C2-Phe	35	17
PN-Phe	2059	1204

Table 3.2 Pseudo first order rate constants of hydrolysis for both enantiomers by a vesicular solution of **Zn₂Cy** (5 mol. %), **L-Tar** (10 mol. %) and **DOPC** (85 mol. %).

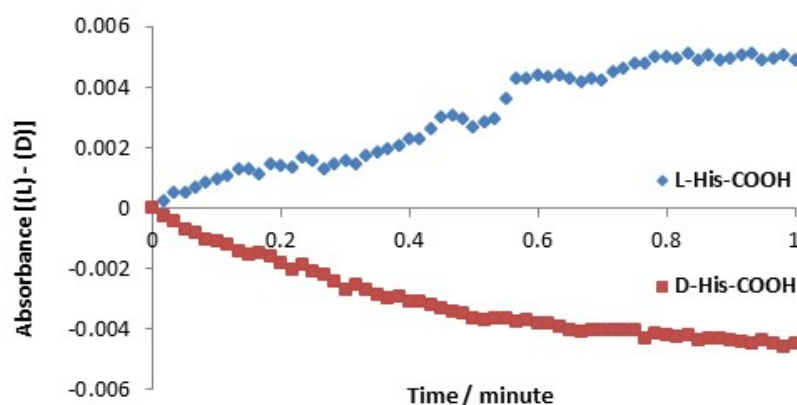


Figure 3.5 Recorded difference in kinetics of L and D **PN-C12-Phe** substrate hydrolysis by vesicular solution (85 % **DOPC**) with L or D **His-COOH** (10 %) and **ZnCy₂** (5%)

In order to confirm our observation we prepared the enantiomeric amphiphilic histidine **D-His-COOH**. This compound was investigated under identical conditions as **L-His-COOH**

and induced a similar hydrolysis rate enhancement of **D-PN-C12-Phe** (Figure 3.5), but with opposite enantioselectivity.

In addition, the effect of the membrane additive loading on the enantioselectivity of the hydrolysis was investigated for **D-His-COOH** (Figure 3.6). Addition of 10 mol. % provided the highest relative difference between the hydrolysis rate constants.

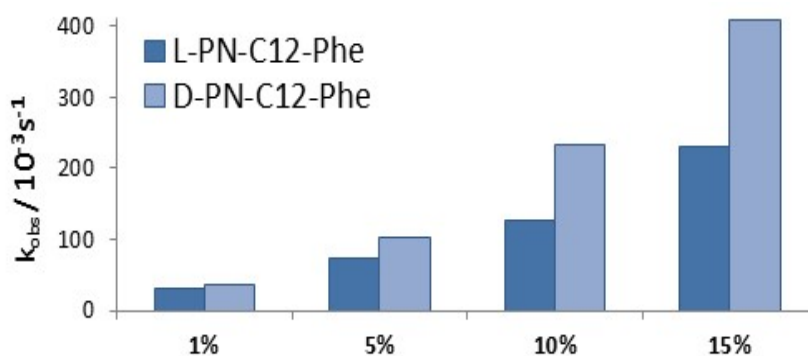


Figure 3.6 Pseudo first order rate constants of hydrolysis for both enantiomers by a vesicular solution of **Zn₂Cy** (5 mol. %) and DOPC with varied loadings of **D-His-COOH**.

3.3 Conclusions

The relative catalytic hydrolysis rates of enantiomeric amino acid esters with a non-chiral catalyst become significantly different, if the catalyst is co-embedded into the surface of DOPC vesicles with chiral amphiphiles. The rates for enantiomeric phenylalanine nitrophenyl esters differ by a factor of two with co-embedded amphiphiles based on tartaric acid or histidine. This resembles an ee of approx. up to 40%, which may be expected for reactions performed from racemate. The fluidity of the membrane is essential to achieve catalytic enantiodiscrimination and therefore only observed in DOPC vesicles. Although the measured rate differences may not be useful for practical applications, the results prove that the intermolecular interaction between a Lewis acidic metal complex, chiral amphiphiles and activated amino acid esters co-embedded into a fluid membrane without covalent connection can affect reaction rates enantioselective.

3.4 Experimental part

3.4.1 General methods and materials

Solvents were used as p.a. grade or dried and distilled according to common procedures.

NMR-Spectroscopy: NMR-spectra were recorded on a Bruker Avance 400 (^1H : 400 MHz, ^{13}C : 101 MHz, T = 300 K) or a Bruker Avance 300 (^1H : 300 MHz, ^{13}C : 75 MHz, T = 295 K) using the solvent residual peak as internal reference (CDCl_3 : δ H 7.26). The chemical shifts are reported in δ [ppm] relative to internal standards (solvent residual peak). The spectra were analyzed by first order, the coupling constants J are given in Hertz [Hz]. Characterization of the signals: s = singlet, d = doublet, t = triplet, m = multiplet. Integration is determined as the relative number of atoms. Error of reported values: chemical shift: 0.01 ppm for ^1H -NMR, 0.1 ppm for ^{13}C -NMR and 0.1 Hz for coupling constants. The solvent used is reported for each spectrum.

Thin Layer Chromatography: Aluminum plates coated with silica gel (ALUGRAM Xtra SIL G/UV₂₅₄ from Macherey-Nagel) were used. Detection was done by UV light (254 nm, 366 nm) or oxidation, using a KMnO_4 -solution.

Polarimetry: Polarimetry measured in 1 dm cuvette on a PERKIN-ELMER 241 polarimeter.

UV/Vis-Spectroscopy: UV/Vis Spectra were recorded on a Cary 50 UV/Vis spectrophotometer.

Dynamic Light Scattering: DLS measurements were performed on a Malvern Zetasizer Nano at 25 °C using 1 cm disposable polystyrene cuvettes (VWR).

3.4.2 Synthesis

The synthesis of the metal complex **Zn₂Cy** was previously reported and the compound was prepared in the same manner.²² Substrates **L(D)-PN-C12-Phe** were prepared via DCC coupling of BOC protected L(D)-phenylalanine followed by deprotection with saturated HCL in diethylether and consecutive acylation with octadecanoyl chloride. Acetylated compounds **L(D)-PN-C2-Phe** were prepared either by acylation of amine in 4-nitrophenyl-alanine **PN-Phe** (D enantiomere) or via DCC coupling of 4-nitrophenol and N-acetyl-phenylalanine (L enantiomere) (Figure 3.7).

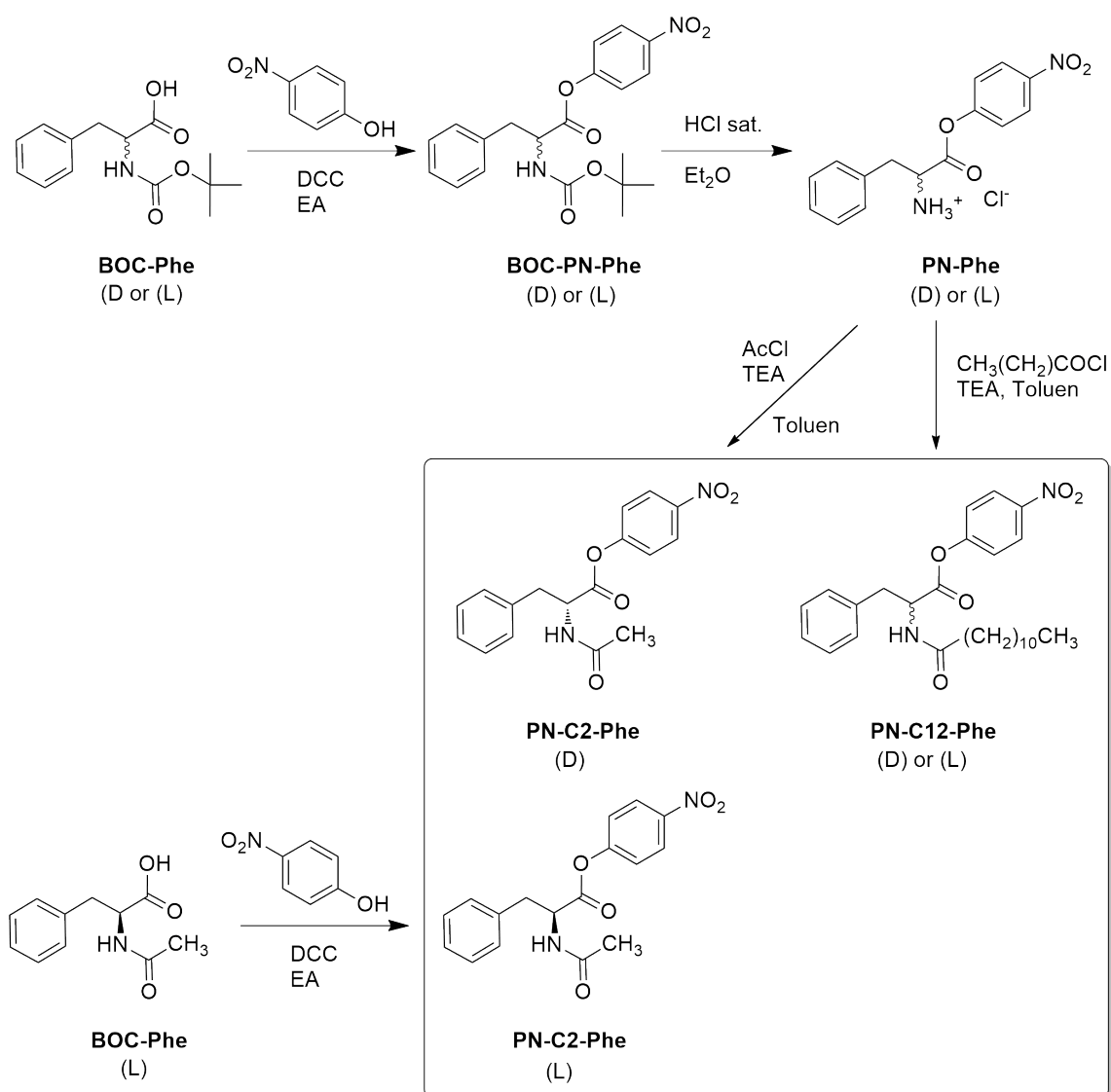
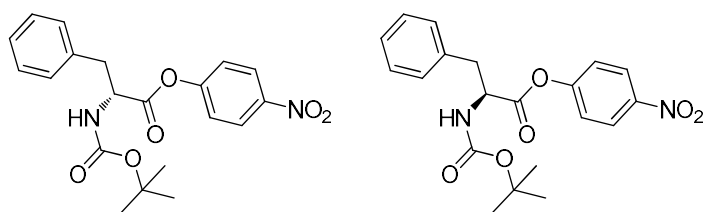


Figure 3.7 Synthesis of the substrates.

(L) and (D) 4-Nitrophenyl-Boc-phenylalaninate (Boc-Phe)²³



(L)-Phenylalanine (2.38 g, 9 mmol), 4-nitrophenol (1.25 g, 9 mmol) and DCC (1.95 g, 9.45 mmol) were dissolved in dry ethylacetate (35 mL) equipped with drying tube and stirred overnight. Solids were filtered off and washed with water (30 ml) and saturated aq. NaHCO₃

(30 ml). The aqueous phase was extracted with ethyl acetate (2 x 30 ml). Combined organic layers were washed with brine and dried over MgSO_4 . Solids were filtered off and solvent removed in *vacuo*. Crude product was recrystallized from ethanol to obtain 1.8 g (52 %) of **L-Boc-Phe** enantiomer in form of white crystals.

D-Boc-Phe was obtained by the same procedure in 43 % yield.

$^1\text{H NMR}$ (300 MHz; CDCl_3): δ 8.24 (d, $J = 9.0$ Hz, 2H), 7.41 – 7.27 (m, 3H), 7.25 – 7.20 (m, 2H), 7.14 (d, $J = 9.0$ Hz, 2H), 5.10 – 5.00 (m, 1H), 4.71 – 4.85 (m, 1H), 3.32 – 2.92 (m, 2H), 1.44 (s, 9H).

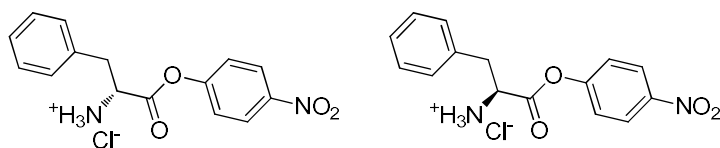
$^{13}\text{C NMR}$ (75 MHz; CDCl_3): δ 170.1, 155.2, 145.5, 135.4, 129.4, 128.9, 127.5, 125.3, 122.3, 80.6, 77.2, 54.7, 38.2, 28.3.

MS (ESI(+)): m/z 409.15 [MNa^+].

(L) $[\alpha]_D^{21} = -9.2^\circ$ (CHCl_3)

(D) $[\alpha]_D^{21} = 9.1^\circ$ (CHCl_3)

(L) and (D) 4-Nitrophenyl phenylalaninate (PN-Phe)²⁴



Protected L-phenylalaninate **L-Boc-Phe** (387 mg, 1.00 mmol) was suspended in sat. HCl diethylether solution (20 mL) and stirred under the drying tube at room temperature for 3 h. Solvent was removed in *vacuo* and the residue was recrystallized from methanol to obtain 223 mg (69 %) of product **L-PN-Phe** in form of white needles.

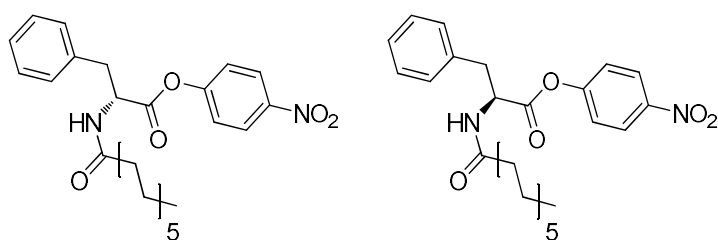
The D-enantiomere was obtained by the same procedure in 53 % yield.

$^1\text{H NMR}$ (300 MHz; MeOD): δ 8.38 – 8.17 (m, 2H), 7.50 – 7.20 (m, 7H), 4.70 (dd, $J = 8.6, 5.7$ Hz, 1H), 3.48 – 3.36 (m, 2H).

$^{13}\text{C NMR}$ (75 MHz; MeOD): δ 168.5, 155.7, 147.5, 135.2, 130.7, 130.4, 129.3, 126.4, 123.6, 55.4, 37.7.

(L) $[\alpha]_D^{21} = -53.8^\circ$ (DMSO)

(D) $[\alpha]_D^{21} = 54.6^\circ$ (DMSO)

(L) and (D) 4-Nitrophenyl *N*-dodecanoylphenylalaninate (PN-C12-Phe)¹⁰

The ammonium salt of **D-PN-Phe** (200 mg, 0.62 mmol) was suspended in toluene (20 mL) and triethylamine (157 mg, 1.55 mmol) was added under nitrogen atmosphere. Subsequently dodecanoyl chloride (271 mg, 1.24 mmol) was added and mixture was stirred at room temperature for 1h. Solids were filtered off and washed with toluene. Solvent was removed from filtrate in *vacuo* and the residue was purified by flash chromatography (PE → PE:EA, 1:1). 190 mg (65 %) of the product **D-PN-C12-Phe** obtained in form of oil which crystallized at RT. To obtain highest purity, substrates were recrystallized from ethanol.

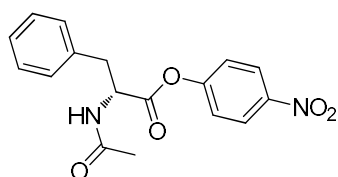
The L-enantiomer was obtained by the same procedure in 40 % yield.

¹H NMR (300 MHz; CDCl₃): δ 8.38 – 8.19 (m, 2H), 7.44 – 7.29 (m, 3H), 7.29 – 7.05 (m, 4H), 5.94 (t, *J* = 9.9 Hz, 1H), 5.15 – 4.98 (m, 1H), 3.32 – 3.17 (m, 2H), 2.30 – 2.07 (m, 2H), 1.57 (dd, *J* = 27.4, 20.4 Hz, 2H), 1.43 – 1.13 (m, 16H), 0.87 (t, *J* = 6.7 Hz, 3H).

¹³C NMR (75 MHz; CDCl₃): NMR resonance data are identical with the literature.¹⁰

(L) $[\alpha]_D^{21} = -15.7^\circ$ (DMSO)

(D) $[\alpha]_D^{21} = 17.0^\circ$ (DMSO)

(D) 4-Nitrophenyl *N*-acetylphenylalaninate (D-PN-C2-Phe)²³

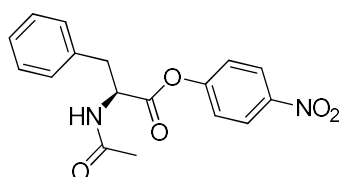
The ammonium salt of 4-nitrophenyl D-phenylalaninate (77 mg, 0.24 mmol) was suspended in toluene (10 mL) and triethylamine (60 mg, 0.60 mmol) was added under nitrogen atmosphere. Subsequently acyl chloride (38 mg, 0.48 mmol) was added and mixture was stirred at room temperature for 1h. Solids were filtered off and washed with toluene. Solvent was removed from filtrate in *vacuo* and the residue was purified by flash chromatography (PE:EA, 0:1 → 1:1). The residue was recrystallized from ethanol to obtain 46 mg (58 %) of product **L-PN-C2-Phe** in form of white crystals.

^1H NMR (300 MHz; CDCl_3): δ 8.30 – 8.19 (m, 2H), 7.42 – 7.28 (m, 3H), 7.25 – 7.19 (m, 2H), 7.19 – 7.08 (m, 2H), 5.95 (d, $J = 7.2$ Hz, 1H), 5.07 (dd, $J = 13.8, 6.5$ Hz, 1H), 3.35 – 3.15 (m, 2H), 2.05 (s, 3H).

^{13}C NMR (75 MHz; CDCl_3): NMR resonance data are identical with the literature.

(D) $[\alpha]_D^{21} = 1.6^\circ$ (DMSO)

(L) 4-Nitrophenyl *N*-acetylphenylalaninate (L-PN-C2-Phe)



N-Acetyl *L*-phenylalanine (324 mg, 1.56 mmol), 4-nitrophenol (218 mg, 1.56 mmol) and DCC (354 mg, 1.72 mmol) were dissolved in dry ethyl acetate (20 mL), the reaction flask was equipped with drying tube and the reaction mixture was stirred overnight. Solids were filtered off and washed with water (20 ml) and saturated aq. NaHCO_3 (15 ml). The aqueous phase was extracted with ethyl acetate (2 x 20 ml). Combined organic layers were washed with brine and dried over MgSO_4 . Solids were filtered off and solvent removed in *vacuo*. The crude product was recrystallized from ethanol to obtain 300 mg (58 %) of **L-PN-Ac-Phe** in form of white crystals.

^1H NMR (300 MHz; CDCl_3): δ same as for D derivative.

^{13}C - NMR (75 MHz; CDCl_3): δ same as for D derivative.

(L) $[\alpha]_D^{21} = -1.5^\circ$ (DMSO)

3.4.3 Synthesis of the membrane additives

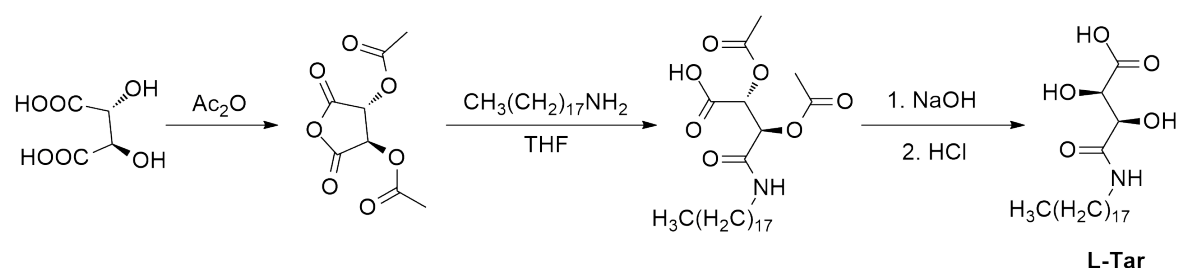
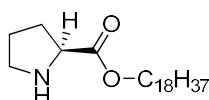


Figure 3.8 Synthesis of the tartrate derivative **L-Tar**.

Glucose **L-Glu** was purchased by Sigma Aldrich. L-Histidine derivatives **L-His-COOH** and **L-His-OH** were prepared according to known procedure.¹⁰ Spartein (**-)-Spa** and proline **L-Pro** derivatives were prepared by alkylation (for (**-)-Spa**) or esterification (for **L-Pro**) with octadecylbromide or alcohol.^{25, 26} Amphiphilic tartrate derivative **L-Tar** was prepared from L-tartrate by a series of protection and amide bond formation steps with octadecylamine and anhydride to obtain amphiphilic free acids according to Figure 3.8.

L-Proline octadecyl ester (**L-Pro**)



L-Proline (772 mg, 6.710 mmol) and octadecanole (8 g, 29.57 mmol) were heated up to 60 °C producing viscous suspension. Thionyl chloride (880 mg, 7.40 mmol) was added followed by DMAP (4 mg, 0.03 mmol). The reaction mixture was stirred at 60 °C for 5 h. Afterwards DCM (20 ml) was added and the suspension was cooled down to 0 °C. After a dropwise addition of triethylamine (1154 mg, 11.41 mmol), the reaction mixture was stirred for additional 3 h. Et₂O (10 ml) was added and the precipitated crude product was filtered off. The residue was purified by column chromatography (PE:EA; 1:1). The product **L-Pro** 270 mg (11 %) was obtained as a white crystalline solid.

¹H NMR (300 MHz, CDCl₃): δ 4.10 (t, *J* = 6.7 Hz, 2H), 3.75 (dd, *J* = 8.7, 5.5 Hz, 1H), 3.08 (dt, *J* = 10.2, 6.5 Hz, 1H), 2.90 (dt, *J* = 10.2, 6.7 Hz, 1H), 2.29 (bs, 1H), 2.12 (m, 1H), 1.92 – 1.59 (m, 5H), 1.39 – 1.20 (m, 30H), 0.87 (t, *J* = 6.7 Hz, 3H).

¹³C NMR (101 MHz, CDCl₃): δ 175.6, 65.1, 59.8, 47.1, 31.9, 30.3, 29.7, 29.7, 29.6, 29.6, 29.5, 29.4, 29.2, 28.6, 25.9, 25.5, 22.7, 14.1.

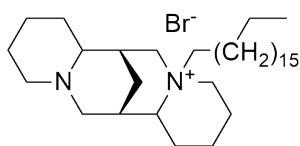
MS (ESI(+)): *m/z* = 368.35 [MH⁺]

T_m: 145–150 °C

The NMR-data identical to the literature reference.²⁵

[α]_D²¹ = - 24.8° (CHCl₃)

(-)-*N*-Octadecylsparteinium ((-)-Spa)²⁶



A mixture of (-)-spartein (611 mg, 2.6 mmol), octadecylbromide (869 mg, 2.6 mmol), potassium carbonate (3g, 21.7 mmol) and sodium iodide (3 g, 20.0 mmol) in MeCN:DMF (40 ml, 1:1) was refluxed under nitrogen atmosphere for 15 hours. After cooling to room temperature the reaction mixture was poured on crushed ice and the formed precipitate was filtered off. After recrystallization from diethyl ether the pure product was obtain in form of a white solid.

Yield: 0.6 g; 41 %

¹H NMR (300 MHz, CDCl₃): δ 3.39 (t, J = 6.9 Hz, 2H), 2.84 – 2.63 (m, 5H), 2.52 (d, J = 10.9 Hz, 2H), 2.34 (dd, J = 11.2, 3.4 Hz, 2H), 2.13 – 1.77 (m, 12H), 1.78 – 1.63 (m, 4H), 1.63 – 0.96 (m, 33H), 0.86 (t, J = 6.6 Hz, 3H).

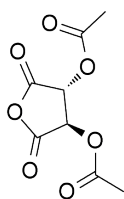
¹³C NMR (75 MHz, CDCl₃): δ 64.2, 63.1, 51.5, 32.2, 31.9, 29.7, 29.6, 29.5, 29.40, 29.2, 26.2, 22.8, 22.7, 14.1.

MS (ESI(+)): m/z = 487.49 [M⁺]

T_m: 71–75 °C

[α]_D²¹ = - 5.0° (DMSO)

2,5-Dioxotetrahydrofuran-3,4-diyl diacetate²⁷



Sulfuric acid (0.12 ml, 2.25 mmol) was added dropwise to a suspension of L-tartratic acid (4.0 g, 27 mmol) in acetic anhydrid (13.6 g, 133 mmol) and the reaction mixture was stirred at 140 °C for 1 h. The reaction mixture was cooled in an ice bath and the formed crystals were washed with toluene (2 × 3 ml) and Et₂O (10 ml). The white crystalline product was dried under vacuum.

Yield: 4.28 g; 73%

$^1\text{H NMR}$ (300 MHz, CDCl_3): δ 5.68 (s, 2H), 2.23 (s, 6H).

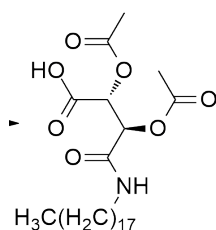
$^{13}\text{C NMR}$ (75 MHz, CDCl_3): δ 169.8, 163.4, 72.1, 20.1.

MS (APCI EIC(+)): $m/z = 217.03$ [MH^+]

T_m : 130–132 °C

$[\alpha]_D^{21} = 37.9^\circ$ (DMSO)

L-2,3-Bis(acetyloxy)-3-(octadecylcarbamoyl)propanoic acid²⁸



1-Aminooctadecane (624 mg; 2.31 mmol) was added to a solution of 2,5-dioxotetrahydrofuran-3,4-diyl diacetate (500 mg; 2.31 mmol) in THF (20 ml) and the reaction mixture was stirred at room temperature for 16 h; the reaction was monitored by TLC (PE:EA; 1:1). The solvent was removed in *vacuo* to obtain the pure product in form of a white crystalline solid.

Yield: 1.12 g; 99%

$^1\text{H NMR}$ (400 MHz, CDCl_3): δ 6.27 (t, $J = 5.7$ Hz, 1H), 5.76 (d, $J = 2.5$ Hz, 1H), 5.60 (d, $J = 2.5$ Hz, 1H), 3.33 (m, 1H), 3.19 (m, 1H), 2.17 (s, 3H), 2.11 (s, 3H), 1.48 (tt, $J = 6.6, 6.0$ Hz, 2H), 1.37 – 1.12 (m, 30H), 0.86 (t, $J = 6.8$ Hz, 3H).

$^{13}\text{C NMR}$ (101 MHz, CDCl_3): δ 169.9, 169.5, 169.0, 166.0, 72.8, 72.0, 71.2, 67.9, 39.7, 31.9, 29.7, 29.7, 29.6, 29.5, 29.4, 29.4, 29.3, 26.8, 26.6, 25.5, 22.7, 20.6, 20.3, 14.1.

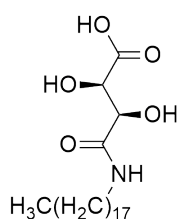
MS (ESI(+)): $m/z = 486.34$ [MH^+]

T_m : 80–83 °C

The NMR-data match the literature reference.²⁸

$[\alpha]_D^{21} = -8.2^\circ$ (DMSO)

L-2,3-Bis(hydroxy)-3-(octadecylcarbamoyl)propanoic acid (L-Tar)



Diacetate-N-octadecyl-4-amino-L-tartrate (204 mg; 0.420 mmol) and NaOH (52 mg; 1.30 mmol) were dissolved in a mixture of H₂O (10 ml) in MeOH (20 ml) and stirred at room temperature for 4 h. The precipitated crude product was filtered off and washed with HCl_{aq} (1 M; 8 ml). The product, a white crystalline solid, was crystallized from MeOH (10 ml).

Yield: 72 mg; 43%

¹H NMR (400 MHz, DMSO): δ 7.63 (t, *J* = 5.9 Hz, 1H), 4.32 (d, *J* = 1.8 Hz, 1H), 4.17 (s, 1H), 3.07 (dd, *J* = 13.9, 6.2 Hz, 2H), 1.40 (m, 2H), 1.24 (m, 30H), 0.86 (t, *J* = 6.8 Hz, 3H).

¹³C NMR (101 MHz, DMSO): δ 173.8, 170.9, 72.9, 71.5, 38.3, 31.2, 29.1, 28.9, 28.9, 28.7, 28.6, 26.2, 22.0, 13.8.

MS (ESI(+)): *m/z* = 402.33 [MH⁺]

T_m: 139–146 °C

[α]_D²¹ = 30.1° (DMSO)

3.4.4 Preparation and characterization of the vesicles

Micellar Solutions

Appropriate aliquots of a stock solution of Zn₂Cy (CHCl₃, 1 mM, 150 μl) were added to a solution of the membrane additive (0.5 mM; 600 μl), the mixture of amphiphiles was dried in a thermomixer at 75 °C, residual solvent was removed in *vacuo* for 15 min. HEPES-buffer (25 mM; pH = 7.4; 3 ml) was added and micelles were formed in the ultrasonic bath (70 °C, 20 min). For the blank measurements cyclen Zn₂Cy was omitted.

Vesicular Solutions

Out of the stock solutions of membrane additives (0.5 mM, CHCl₃) 600 μl was combined with either DOPC (CHCl₃, 4.3 mM, 593 μl) or DSPC (CHCl₃, 6.36 mM, 401 μl) and a solution of bis-Zn(II)-cyclen Zn₂Cy (CHCl₃, 1mM, 150 μl) was added, the mixture of amphiphiles was dried in a thermomixer at 75 °C, the residual solvent was removed in *vacuo* for 15 min. HEPES-buffer (25 mM; pH = 7.4; 3 ml) was added and vesicles were formed in the ultrasonic

bath (70 °C, 20 min). Vesicles formed via sonication were approximately 100 nm in size and stable for days (Figure 3.9).

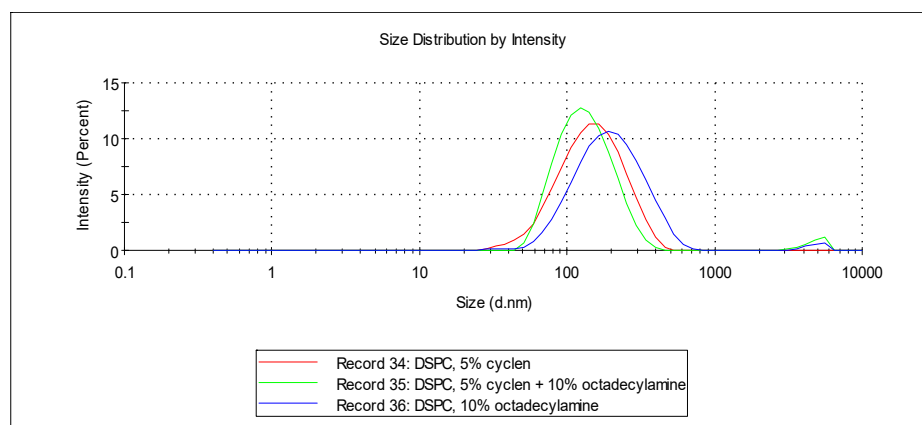


Figure 3.9 DLS measurement of vesicles with selected amphiphiles.

Kinetic measurements

The kinetics of the hydrolysis was monitored using the two enantiopure substrates (L) and (D). From a freshly prepared stock solution of substrate (1 mM in MeCN) was added 7 μ l to a 700 μ l of buffered vesicular solution (0.05 mM **Zn₂Cy**, 0.1 mM membrane additive, 0.85 mM phospholipid). The same procedure was used for micellar solutions. The kinetic measurement was started after shaking 5 times (20 sec). The reaction kinetics of the hydrolysis was recorded as the increase of absorbance at the absorption maximum of 4-nitrophenol at pH 7.4 ($\lambda_{\text{max}} = 400$ nm) in buffered solution (25 mM, HEPES). The extinction coefficient used for 4-nitrophenol at pH 7.4 ($\epsilon = 9.8 \text{ mM}^{-1}\text{cm}^{-1}$) was reported previously.²⁹ The hydrolysis was carried out under pseudo first order conditions and rate constants were derived from the initial slope plotting changes in absorbance vs reaction time. Measurements were done in triplicates in case of **L-Tar**, **D** and **L-His-COOH**, **L-His-OH** and standard deviations for the slope was calculated to be below 10%. The hydrolysis of the substrates **PN-Phe** and **PN-C2-Phe** was performed at pH 7.4 using tartrate **L-Tar** as membrane additive in DOPC bilayer with cyclen **ZnCy₂**.

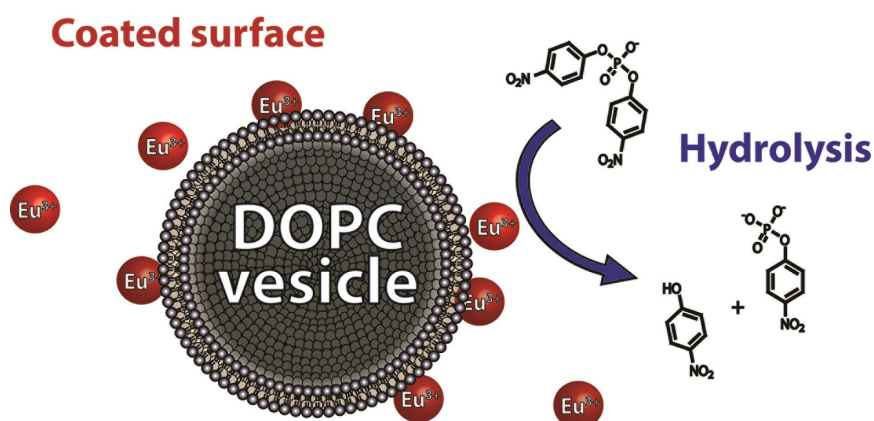
3.5 References

1. Mason, S., The origin of chirality in nature. *Trends Pharmacol. Sci.* **1986**, *7*, 20-23.
2. Blackmond, D. G., The Origin of Biological Homochirality. *Cold Spring Harbor Perspectives in Biology* **2010**, *2* (5), a002147.
3. Bonner, W., The origin and amplification of biomolecular chirality. *Origins Life Evol. Biosphere* **1991**, *21* (2), 59-111.
4. Walsh, P. J.; Kozlowski, M. C., *Fundamentals of Asymmetric Catalysis*. Macmillan Education: 2008; p 750.
5. Tulashie, S. K.; Lorenz, H.; Hilfert, L.; Edelman, F. T.; Seidel-Morgenstern, A., Potential of Chiral Solvents for Enantioselective Crystallization. 1. Evaluation of Thermodynamic Effects. *Cryst. Growth Des.* **2008**, *8* (9), 3408-3414.
6. Tulashie, S. K.; Lorenz, H.; Seidel-Morgenstern, A., Potential of Chiral Solvents for Enantioselective Crystallization. 2. Evaluation of Kinetic Effects. *Cryst. Growth Des.* **2009**, *9* (5), 2387-2392.
7. Ma, L.; Abney, C.; Lin, W., Enantioselective catalysis with homochiral metal-organic frameworks. *Chem. Soc. Rev.* **2009**, *38* (5), 1248-1256.
8. García-Simón, C.; Gramage-Doria, R.; Raouf-moghaddam, S.; Parella, T.; Costas, M.; Ribas, X.; Reek, J. N. H., Enantioselective Hydroformylation by a Rh-Catalyst Entrapped in a Supramolecular Metallo Cage. *J. Am. Chem. Soc.* **2015**, *137* (7), 2680-2687.
9. You, J.; Yu, X.; Li, X.; Yan, Q.; Xie, R., Enantioselective hydrolysis of long chain α -amino acid esters by chiral sulfur-containing macrocyclic metallomicelles. *Tetrahedron: Asymmetry* **1998**, *9* (7), 1197-1203.
10. You, J.-S.; Yu, X.-Q.; Su, X.-Y.; Wang, T.; Xiang, Q.-X.; Yang, M.; Xie, R.-G., Hydrolytic metalloenzyme models: Enantioselective hydrolysis of long chain α -amino acid esters by chiral metallomicelles composed of lipophilic l-histidinol. *J. Mol. Catal. A: Chem.* **2003**, *202* (1-2), 17-22.
11. Moss, R. A.; Sunshine, W. L., Micellar catalysis of ester hydrolysis. Influence of chirality and head group structure in simple surfactants. *J. Org. Chem.* **1974**, *39* (8), 1083-1089.
12. Mancin, F.; Scrimin, P.; Tecilla, P.; Tonellato, U., Amphiphilic metalloaggregates: Catalysis, transport, and sensing. *Coord. Chem. Rev.* **2009**, *253* (17-18), 2150-2165.
13. Brown, C. J.; Bergman, R. G.; Raymond, K. N., Enantioselective Catalysis of the Aza-Cope Rearrangement by a Chiral Supramolecular Assembly. *J. Am. Chem. Soc.* **2009**, *131* (48), 17530-17531.

14. Brown, C. J.; Toste, F. D.; Bergman, R. G.; Raymond, K. N., Supramolecular Catalysis in Metal–Ligand Cluster Hosts. *Chem. Rev.* **2015**, *115* (9), 3012-3035.
15. Zhao, C.; Toste, F. D.; Raymond, K. N.; Bergman, R. G., Nucleophilic Substitution Catalyzed by a Supramolecular Cavity Proceeds with Retention of Absolute Stereochemistry. *J. Am. Chem. Soc.* **2014**, *136* (41), 14409-14412.
16. Mancin, F.; Scrimin, P.; Tecilla, P., Progress in artificial metallonucleases. *Chem. Commun.* **2012**, *48* (45), 5545-5559.
17. Gruber, B.; König, B., Self-Assembled Vesicles with Functionalized Membranes. *Chem. Eur. J.* **2013**, *19* (2), 438-448.
18. Poznik, M.; König, B., Cooperative hydrolysis of aryl esters on functionalized membrane surfaces and in micellar solutions. *Org. Biomol. Chem.* **2014**, *12* (20), 3175-3180.
19. Shimshick, E. J.; McConnell, H. M., Lateral phase separation in phospholipid membranes. *Biochemistry* **1973**, *12* (12), 2351-2360.
20. Müller, H.-J.; Galla, H.-J., Chain length and pressure dependence of lipid translational diffusion. *European Biophysics Journal* **1987**, *14* (8), 485-491.
21. Heberle, F. A.; Feigenson, G. W., Phase Separation in Lipid Membranes. *Cold Spring Harbor Perspectives in Biology* **2011**, *3* (4), a004630.
22. Turygin, D. S.; Subat, M.; Raitman, O. A.; Arslanov, V. V.; König, B.; Kalinina, M. A., Cooperative Self-Assembly of Adenosine and Uridine Nucleotides on a 2D Synthetic Template. *Angew. Chem. Int. Ed.* **2006**, *45* (32), 5340-5344.
23. Volkmann, A.; Brüggemann, O., Catalysis of an ester hydrolysis applying molecularly imprinted polymer shells based on an immobilised chiral template. *React. Funct. Polym.* **2006**, *66* (12), 1725-1733.
24. Riechers, A.; Grauer, A.; Ritter, S.; Sperl, B.; Berg, T.; König, B., Binding of phosphorylated peptides and inhibition of their interaction with disease-relevant human proteins by synthetic metal-chelate receptors. *J. Mol. Recognit.* **2010**, *23* (3), 329-334.
25. Kadyrov, R., Low Catalyst Loading in Ring-Closing Metathesis Reactions. *Chem. Eur. J.* **2013**, *19* (3), 1002-1012.
26. Ogino, I.; Davis, M. E., Molecular sieve synthesis using alkylated sparteine derivatives as structure-directing agents. *Microporous Mesoporous Mater.* **2004**, *67* (1), 67-78.
27. Shriner, R. L.; Furrow, C. L., DIACETYL-d-TARTARIC ANHYDRIDE. *Org. Synth.* **1955**, *35* (49).

28. Sobczak, M.; Nurzyńska, K.; Kolodziejcki, W., Seeking Polymeric Prodrugs of Norfloxacin. Part 2. Synthesis and Structural Analysis of Polyurethane Conjugates. *Molecules* **2010**, *15* (2), 842.
29. Poznik, M.; Maitra, U.; Konig, B., The interface makes a difference: lanthanide ion coated vesicles hydrolyze phosphodiesterases. *Org. Biomol. Chem.* **2015**, *13* (38), 9789-9792.

4 The interface makes a difference: Lanthanide ion coated vesicles hydrolyse phosphodiester



Lanthanide ions are strong Lewis acids. The complexation to a variety of ligands can further enhance the Lewis acidity allowing the hydrolysis of phosphoesters and even DNA. We show that the interaction of lanthanide ions with vesicles from zwitterionic phosphatidylcholine lipids give supramolecular structures in which the metal ion is loosely coordinated to the surface. This assembly provides a high density of Lewis-acidic metal centres, which hydrolyse phosphodiester with enhanced rates.

This chapter was published in:

M. Poznik, U. Maitra and B. König, "The interface makes a difference: lanthanide ion coated vesicles hydrolyze phosphodiester", *Org. Biomol. Chem.*, **2015**, *13*, 9789-9792

M. Poznik performed the experimental work and wrote the manuscript. U. Maitra and B. König supervised the project and are corresponding authors.

4.1 Introduction

Phosphodiester are among the most important functional groups in nature. They form the hydrolytically stable backbone of the DNA, which has an estimated half-life of over 30 million years.¹ Even though highest resistance towards degradation and alteration is required for the genetic material, DNA is processed by nucleases in cells. Great effort were therefore made developing artificial systems, which match the specificity and hydrolytic activity of native phosphodiester processing enzymes.^{2,3} Enzymes often contain metal cations in their active centres, which serve as Lewis acids promoting the ester cleavage. The same approach is frequently followed in enzyme mimics^{4,5} and lanthanides are used due their higher Lewis acidity replacing transition metal ions.⁶ Usually the lanthanide ion is coordinated by a ligand, but their synthesis and the preparation of complexes can be laborious. Simpler self-assembled structures with hydrolytic activity could be advantageous.

We report here the preparation of phospholipid vesicles with lanthanide ions bound to their surface promoting the hydrolysis of phosphodiester (Figure 4.1).

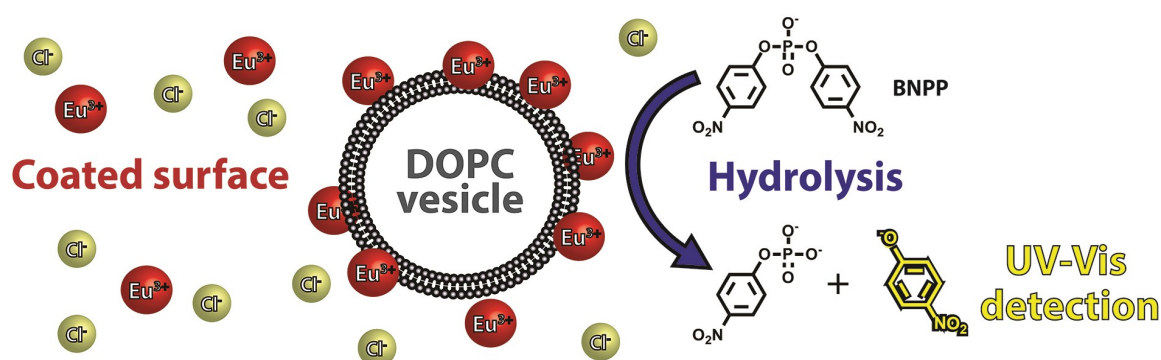


Figure 4.1 Phosphodiester hydrolysis with lanthanide ion coated vesicles.

The coordination of metal cations to the surface of bilayers was previously reported.^{7,8} The interaction of europium ions with phospholipids can be followed by changes in emission⁹ and mixtures of cerium cations with surfactants or anionic phospholipids have been reported as promoters of phosphodiester hydrolysis.^{10,11,12}

4.2 Results and discussion

4.2.1 Interaction of metal cations with DOPC vesicles

We have investigated the interaction of lanthanide cations and 100 nm vesicles prepared from the zwitterionic lipid 1,2-dioleoyl-*sn*-glycero-3-phosphocholine (DOPC). In order to achieve high hydrolytic activity of metal complexes it is important to retain their charge in the complex and keep open coordination sites for the interaction with substrates. Negatively charged ligands, such as carboxylates, decrease the overall charge in lanthanide complexes and therefore the hydrolytic activity. In the case of phospholipids the metal ion should interact with several phosphate moieties of the lipid membrane. However, since the vesicles are neutral the overall surface charge will increase by the lanthanide ion binding. †

Binding events on the surface of phospholipid vesicles can be monitored by the change of emission intensity of a co-embedded fluorescent dye (Figure 4.2).¹³

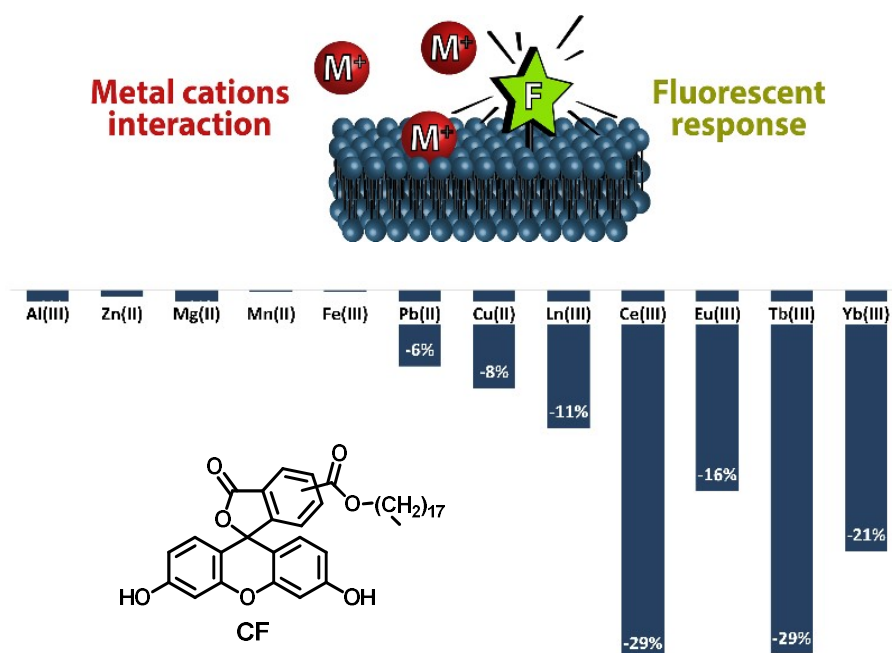


Figure 4.2 Effect of different metal ions (0.6 equiv. with resp. to carboxyfluorescein) on the emission intensity of membrane-embedded carboxyfluorescein 10 mol% in DOPC vesicles ($5 \cdot 10^{-5}$ mol/L) in aqueous HEPES buffer at pH 7.4.

Amphiphilic carboxyfluorescein (CF) exhibits a strong green fluorescence when embedded in DOPC. The addition of one equiv. of different metal salts with respect to the dye lead to a decrease in the emission intensity depending on the nature of the metal cation (Figure 4.2).

Cations with high charge density induced a larger decrease of the CF emission intensity. The emission intensity change can be explained by the alteration of the local environment on the surface of the vesicles, most likely due to metal ion binding. The relative change in emission intensity cannot be used to quantify the amount of metal ion binding to the membrane surface, as emission quenching effects of different metal ions will be very different, but these data provide a qualitative indication of which metal ions interact with the lipid membrane. Using identical conditions, but with *non-amphiphilic* carboxyfluorescein, the metal ion addition had no effect on the emission intensity (see experimental part).

Europium chloride has a very characteristic emission spectrum ($\lambda_{\text{exc}} = 394 \text{ nm}$) whose intensity is strongly influenced by the environment. Intensities of peaks and their ratios provide important information about the coordination around the europium ion. The peak at 615 nm is known as *hypersensitive transition* ($^5\text{D}_0\text{-}^7\text{F}_2$) and its intensity reflect changes in the ligand binding.¹⁴ Tracking the intensity changes at 615 nm compared to other emission maxima allows one to determine differences in ligand coordination.¹⁵ We observed an increase of the emission peak at 615 nm when DOPC was added to a buffered solution of europium chloride (see experimental part). This effect is likely due to the binding of europium ion to the phosphate moiety of the lipid.

To confirm the presence of europium ions close to the surface of the membrane, its emission was sensitized using pyrene (Figure 4.3). Pyrene has been reported to sensitise effectively the europium phosphorescence in sodium cholate gels.¹⁶ Pyrene locates due to its lipophilicity inside the phospholipid bilayer and when irradiated at 365 nm an increased emission of the europium ions was observed (Figure 4.3).

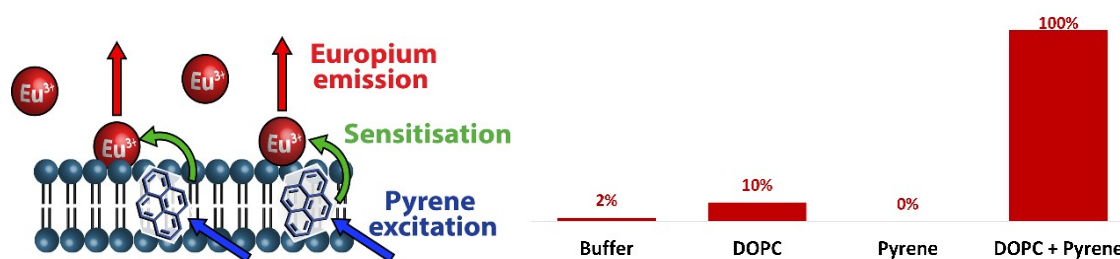


Figure 4.3 Sensitization of the emission of membrane-bound europium ions by membrane-incorporated pyrene (top). Relative emission intensity at 615 nm of 1 mM EuCl_3 solution in the presence and absence of lipid and pyrene.

The europium ions must be therefore close to the phospholipid membrane. No sensitisation by pyrene was observed in the absence of vesicles.

4.2.2 Hydrolysis of BNPP with different metal ions

Bis-4-nitrophenyl phosphate (BNPP) was used for investigating the phosphodiester hydrolysis activity of the membranes. The hydrolysis was monitored by the increase in the absorbance at 400 nm and pseudo first order rate constants were determined by the initial slope method (see experimental part). We examined different transition metal ions, which typically occur in hydrolases, and lanthanide ions (Figure 4.4). Equimolar amounts of the metal ions as their chloride salts and the lipid in form of DOPC vesicles were combined, incubated for 2 minutes, then BNPP was added and its hydrolysis monitored. Identical reactions were performed in the absence of the lipid (Figure 4.4). The hydrolytic activity for Fe(III), Cu(II), Zn(II) and Al(III) is low under these conditions with slight increases in the presence of the lipid. Significantly larger hydrolytic activity was observed for lanthanide salts, particular Yb(III) and Tb(III). Here the hydrolytic activity increased up to 7 fold in the presence of the lipid.

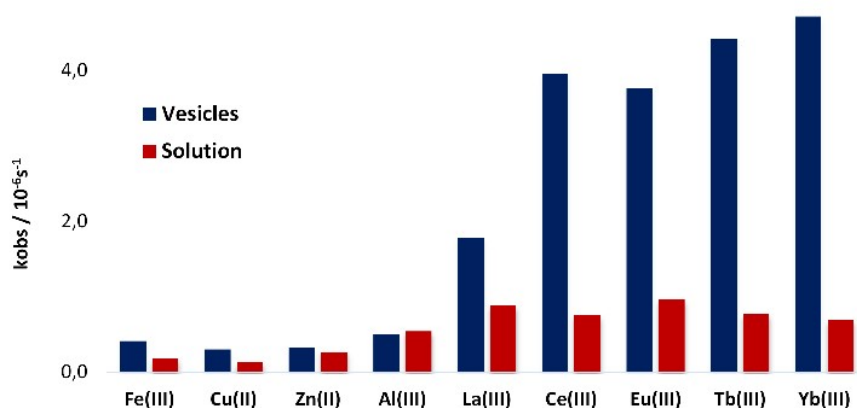


Figure 4.4 Pseudo first order rate constants for BNPP hydrolysis in aqueous solution (HEPES, pH 7.4) in the presence of different metal ions ($c = 10^{-4}$ mol/L) (red) and DOPC ($c = 10^{-4}$ mol/L) (blue) as 100 nm vesicles. Estimated error of the hydrolysis rate $\pm 5\%$ from three experiments.

4.2.3 Different lipids

All phospholipids used in this work were zwitterionic phosphatidyl choline lipids varying in length and saturation of the chain, which changes the physical behaviour of the membrane in particular the transition temperature from solid (gel) phase to liquid phase. This transition can greatly affect properties and behaviour of embedded amphiphiles, as phase separation

and lateral movements change. We examined five different phospholipids (DOPC, DMPC, SMPC, DPPC, DSPC) in the presence of europium ions to investigate the effect of the membrane properties on the hydrolytic activity towards BNPP (for data see experimental part). All measurements were conducted at room temperature and all examined lipids showed similar performance within the error limits of the experiment. Membranes that are in the liquid phase at this temperature gave a slight improvement of about 20 % in hydrolytic rate and overall conversion of BNPP after 24 h (see experimental part). A rationale for this observation may be the better adaptation of lipids and lanthanide ions to the optimal geometry required for a cooperative BNPP hydrolysis.¹⁷

4.2.4 Comparison of the hydrolytic properties

DOPC and europium salts were selected for further investigations. Second order rate constants were determined from the linear regression of pseudo first order rates of varying europium ion concentration for three ratios of Eu to DOPC: 2:1, 1:1 and 1:2 (see experimental part, Figure 4.18). The largest rate enhancement of the BNPP hydrolysis was observed for a ratio of Eu; DOPC of 1:1. In Table 4.1 we compare the hydrolytic rate of BNPP at comparable conditions for several lanthanide ion based hydrolysis catalysts. The europium – DOPC vesicles enhance the hydrolytic activity of europium compared to the salt by a factor of 17 and match rates of simple europium complexes. However, micellar and vesicular systems based on mono and binuclear amphiphilic complexes of cerium (IV) and zinc show significantly higher rates of BNPP hydrolysis.

System	k_2 ($M^{-1}s^{-1}$)	rel. k_2	T ($^{\circ}C$)	pH	Ref.
Eu: DOPC (1:1)	0.07	17	25	7.4	^a
EuCl ₃	0.004	1	25	7.4	^a
EuDO ₂ A ⁺	0.017		25	9.35	¹⁸
Eu(THED)	0.11		37	7,5	¹⁹
Eu:peptide	0.1–0.3		37	7.7	²⁰
Ce(IV)-micelles	0.6		37	7	²¹
Bis-Zn-cyclen micelles	7.9		25	7.4	²²
Bis-Zn-cyclen:DOPC	9.4		25	7.4	²²

Table 4.1 Comparison of the **BNPP** hydrolytic activity of Eu:DOPC (1:1) with other metal salts and complexes. ^a This work.

4.3 Conclusions

Lanthanide cations bind to the lipid-water interface of DOPC vesicles. The interaction of metal ions with the membrane was confirmed by induced changes of the spectroscopic properties of membrane embedded carboxyfluorescein. The sensitisation of the europium emission by membrane embedded pyrene verifies their close proximity to the interface. The higher local concentration of the lanthanide ions at the lipid interface is a likely rationale for the increased hydrolytic activity towards the activated phosphodiester BNPP by a factor of 17 compared to aqueous europium salts. Such hydrolytically active membranes may be used to coat objects providing hydrolytically active surfaces.

4.4 Experimental part

4.5 General methods and materials

General

Salts of metals were purchased from Acros or Sigma-Aldrich and used without any further purification. Phospholipids were purchased from Avanti Polar Lipids Inc. All solutions were prepared in miliQ deionised water or HEPES buffer (25 mM, 7.4 pH).

Dynamic Light Scattering

DLS measurements were performed on a Malvern Zetasizer Nano at 25 °C using 1 cm disposable polystyrene cuvettes (VWR).

Spectroscopy

Fluorescence of co-embedded carboxyfluorecein upon addition of metals was measured using FLUOstar Omega microtiter plate reader using excitation filter at 485 nm and emission filter 520 nm. Phosphorescence of Europium was recorded on Cary eclipse machine. Shimadzu UV-3600 Plus was used for all kinetic measurements.

4.5.1 Preparation and characterization of the vesicles

Vesicles were prepared by established procedure.¹³ Required amount of DOPC solution in chloroform (10 mM) was pipetted in a vial, evaporated in a stream of nitrogen and the residual solvent was removed in vacuo (30 min). Buffer was added to obtain the required concentration (1 mM) of DOPC and the mixture was sonicated for 15 min. The turbid emulsion was extruded through 100 nm polycarbonate membranes at room temperature to obtain uniform vesicles.

In case of different lipids, temperature of sonication and extrusion was always 10 °C above their transition temperature. In case of europium sensitisation, pyrene was added as chloroform solution in the first step of vesicle preparation.

Size and distribution of DOPC vesicles was determined by DLS before and after addition of europium chloride (Figure 4.5).

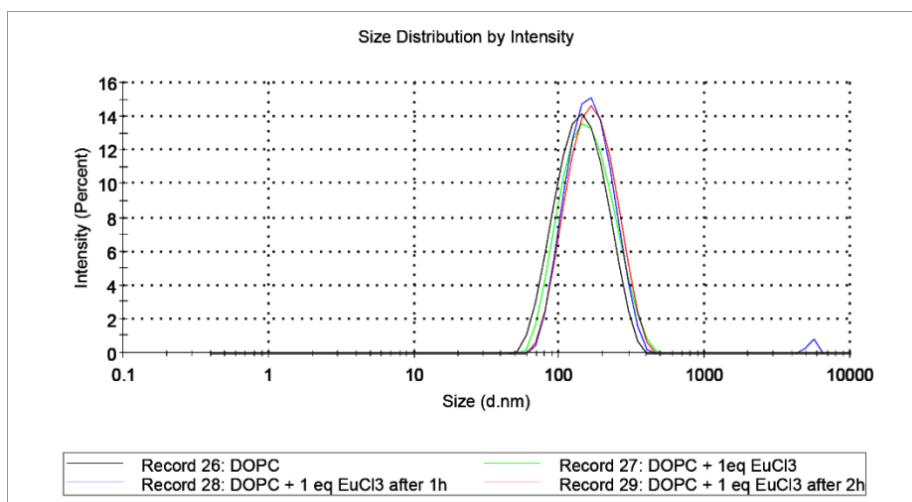


Figure 4.5 DLS measurement of vesicles before and after addition of equimolar amounts of europium chloride.

4.5.2 Detection of metal binding by carboxyfluorescein

A 96-well microtiter plate was used. In each well 90 μL of HEPES buffer, 10 μL of aqueous metal salt solution (100 μM) or miliQ water for the blank experiments and 25 μL of vesicular solution (0.25 mM) containing DOPC vesicles with 10 mol. % of amphiphilic carboxyfluorescein were pipetted.²³ The result of the measurements is the average of four experiments compared with the fluorescence intensity when no metal salt was added. Two salts of copper(II) were examined showing no difference in the fluorescent response due to different anions (Table 4.2).

AlCl_3	$\text{Zn}(\text{ClO}_4)_2$	MgCl_2	MnCl_2	FeCl_3	PbCl_2	$\text{Cr}(\text{ClO}_4)_3$	CuSO_4 CuCl_2	LnCl_3	CeCl_3	EuCl_3	TbCl_3	YbTf_3
-----------------	-----------------------------	-----------------	-----------------	-----------------	-----------------	-----------------------------	------------------------------------	-----------------	-----------------	-----------------	-----------------	-----------------

Table 4.2 Table of salts used for metal sensing.

Experiment with fluorescein or non derivatized carboxyfluorescein under the same conditions show no significant difference when the different metal ions were added (Figure 4.6).

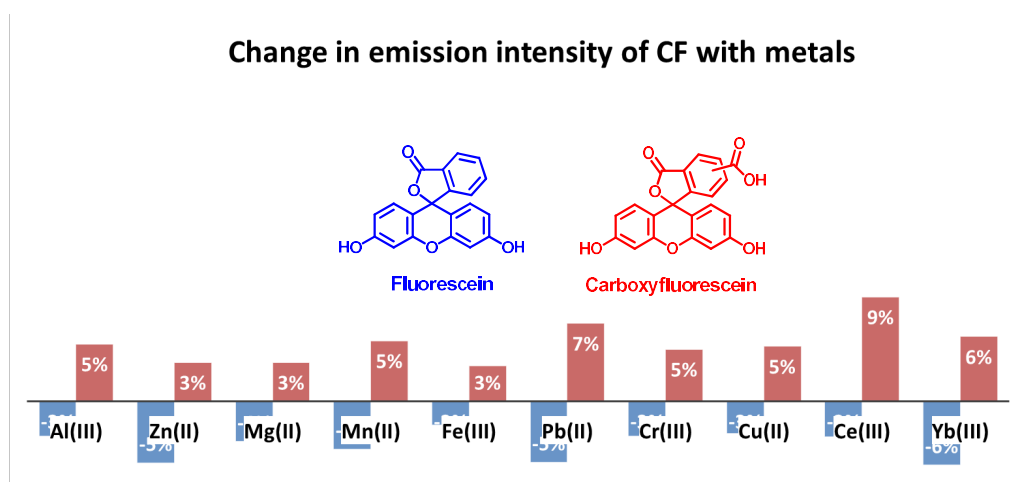


Figure 4.6 Fluorescence emission intensity changes of non-amphiphilic fluorescein derivatives upon addition of metal salts to a vesicular solution.

4.5.3 Europium phosphorescence in the presence of the DOPC membrane

The europium chloride concentration was always kept at 1 mM (either in MiliQ water or HEPES buffer) and the DOPC lipid concentration was varied from 0–5 mM. The emulsion was sonicated for 30 min to obtain a clear vesicular solution. Samples were excited at $\lambda_{ex}=394$ nm and phosphorescence was measured after 100 μ s.

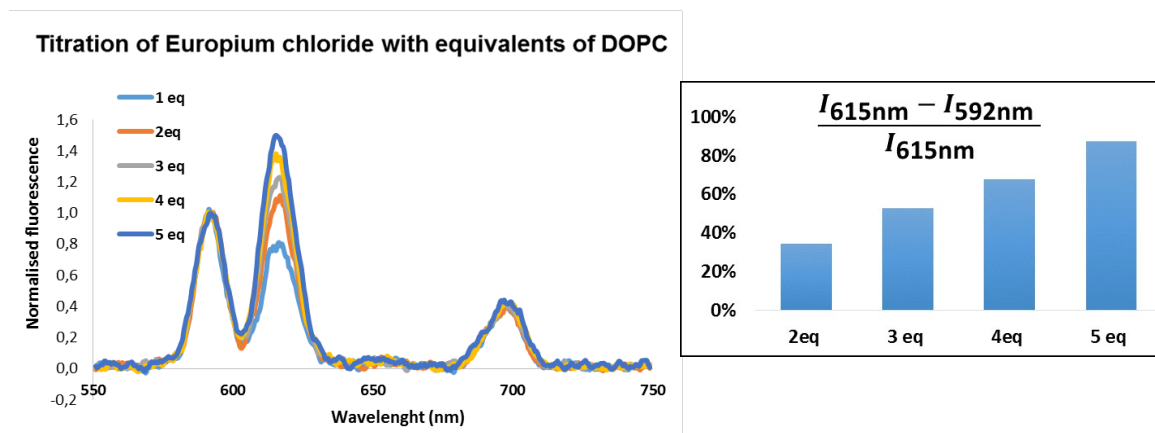


Figure 4.7 Europium ion emission depending on the amount of DOPC present.

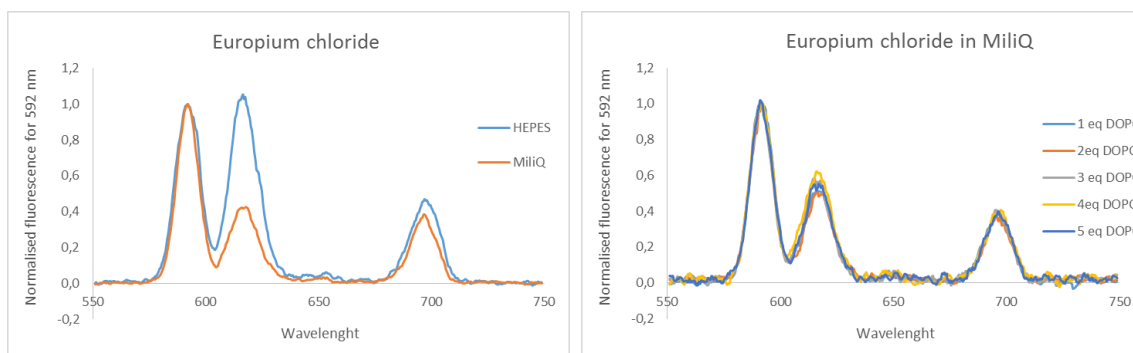


Figure 4.8 Europium ion emission in MiliQ water (left) or HEPES (25 mM) buffered aqueous solution.

4.5.4 Sensitisation of europium emission by pyrene

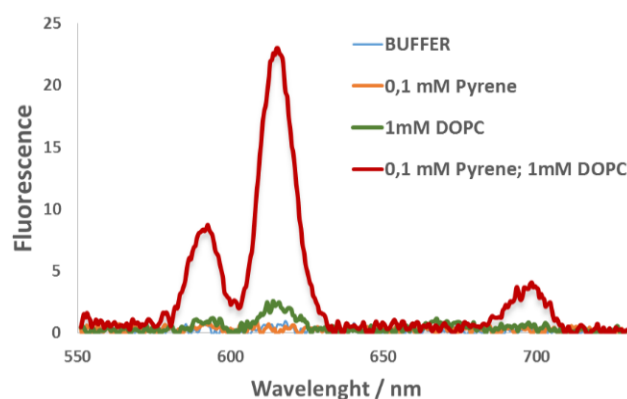


Figure 4.9 Full spectra of pyrene sensitisation.

In sensitisation experiments solutions of europium chloride (1mM) with vesicles containing 10 mol. % of pyrene in the DOPC membrane (1mM) were used. Pyrene was added as a stock solution in chloroform (with or without DOPC) and then evaporated and re-dissolved in buffer. Pyrene was excited at $\lambda_{ex}= 336$ nm and the phosphorescence of europium (after 100 μ s) was recorded.

The effect of the substrate and products for hydrolysis on the emission intensity was examined by addition of 1 eq of the respective compound in buffer to obtain the same final concentration of the europium salt and vesicles as for the previous sensitisation measurements. Phenyl phosphate and diethylphosphate were chosen for their slow or no hydrolysis during the course of the measurements (Figure 4.10).

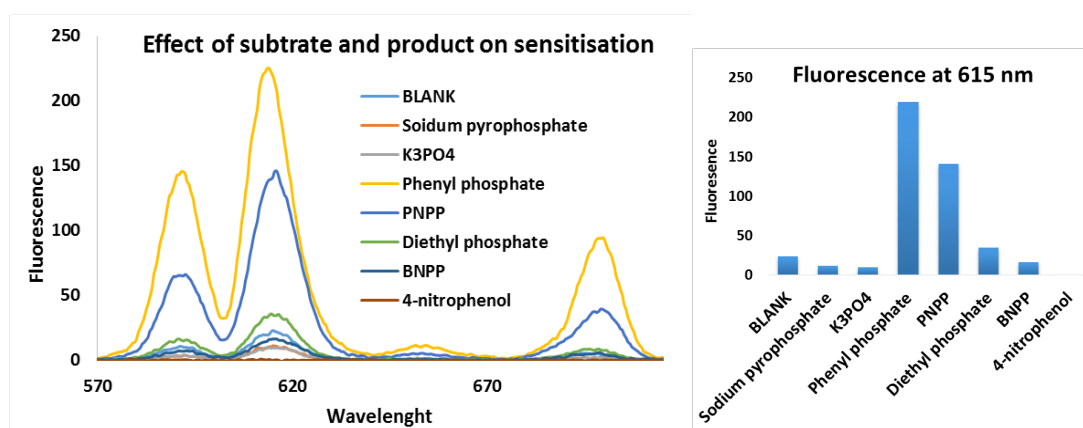


Figure 4.10 Effect of different phosphates on the europium ion emission intensity using pyrene sensitisation.

4.5.5 Kinetic measurements

All the measurements were done at 25 °C with extruded vesicles (1mM of DOPC) in HEPES buffer (25 mM, 7.4 pH).

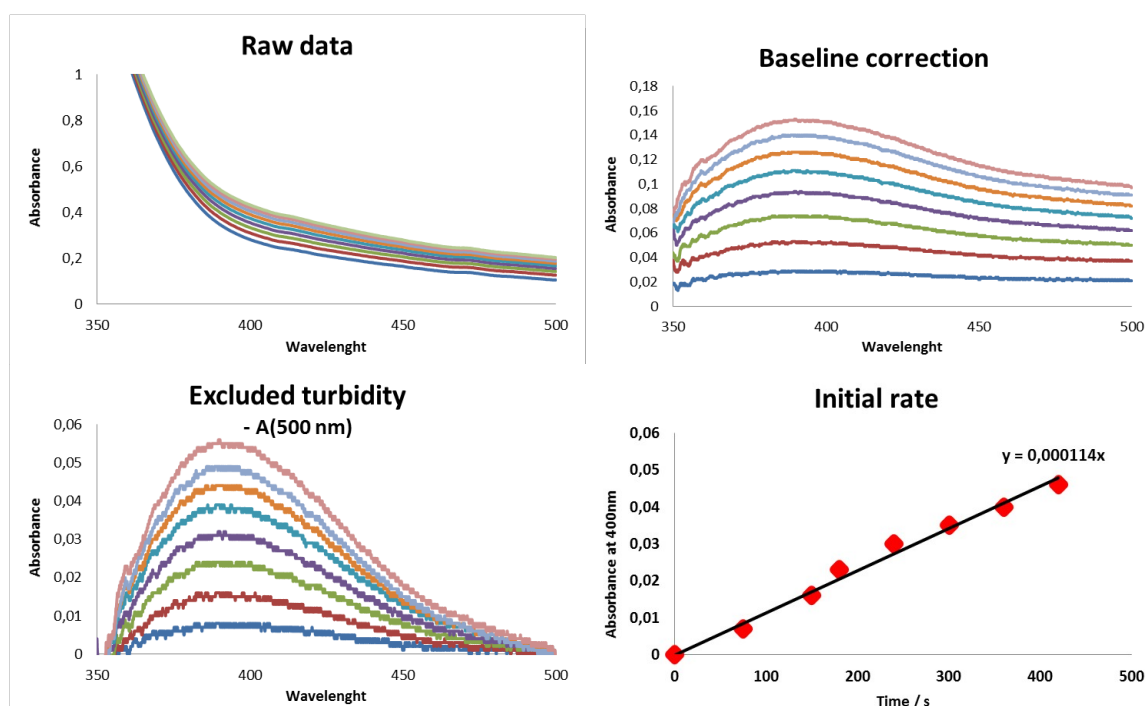


Figure 4.11 Example of the kinetic data evaluation.

All the stock solutions were prepared prior to use, BNPP in HEPES buffer (2 mM), europium salt solutions were prepared by diluting a 10 mM stock solution in miliQ water with buffer to obtain 1 mM solutions. Initially, the vesicular solution was added to the buffer to obtain the required concentration for measurements followed by the addition of europium salts. After 2 min of incubation the substrate (BNPP) was added and the increase of absorbance was monitored spectroscopically over 10 min at two wavelengths (500 nm and 400 nm). Increasing turbidity was excluded by subtracting absorbance at 500 nm (no absorption of product) from the value of the para-nitro-phenolate maximum absorption at 400 nm (Figure 4.11). The initial rate was calculated as a slope of the increasing absorbance. Pseudo first order rate constants were determined using the absorption coefficient obtained from the 4-nitrophenol calibration curve. The estimated error of the kinetic measurement is smaller than 5 %.

Calibration curve for 4-nitrophenol in HEPES buffer

Initial rates of reaction were determined from the increase of the absorbance of 4-nitrophenol. 4-Nitrophenol can be present in solution in protonated and deprotonated form, therefore we determined its absorption coefficient under our reaction conditions of 7.4 pH in 25 mM HEPES buffer via calibration curve ($\epsilon = 9.8 \text{ mM}^{-1}\text{cm}^{-1}$, Figure 4.12).

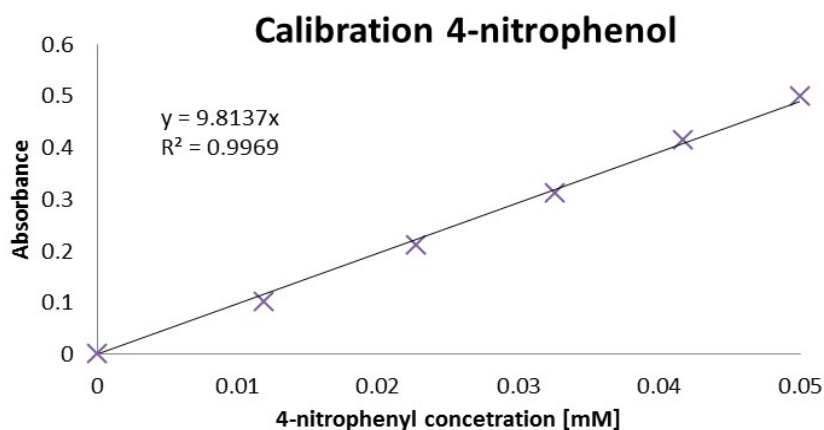


Figure 4.12 4-Nitrophenol absorption calibration curve in HEPES buffer.

Screening of metals

In a 1 cm quartz cuvette was added 300 μL of buffer followed with 50 μL of DOPC vesicles. 50 μL of metal salt solution or buffer was added (1mM) and incubated for 2 minutes. Measurement started after the addition 100 μL of BNPP stock solution.

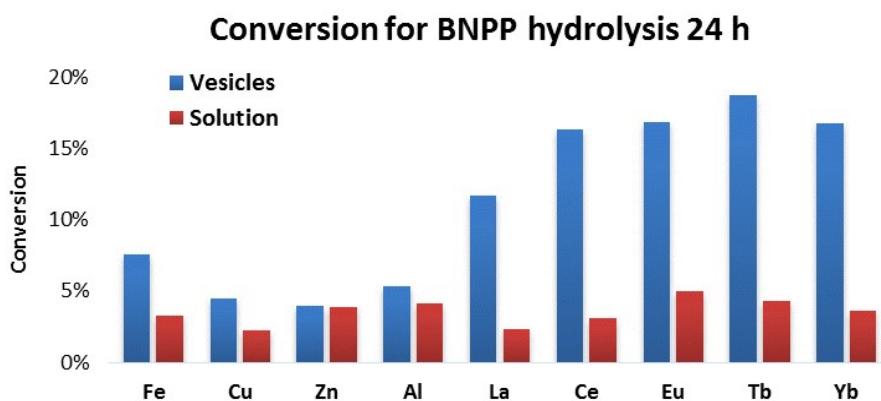


Figure 4.13 Conversion of substrate after 24 h for different metals.

FeCl ₃	CuSO ₄	ZnCl ₂	Al(NO ₃) ₃	La(NO ₃) ₃	CeCl ₃	EuCl ₃	TbCl ₃	YbAc ₃
-------------------	-------------------	-------------------	-----------------------------------	-----------------------------------	-------------------	-------------------	-------------------	-------------------

Table 4.3 Table of metal salts used for screening.

Screening of lipids

Same measurement conditions were used for the screening of lipids using only europium chloride and varying lipids.

Lipid	DOPC	DMPC	SMPC	DPPC	DSPC
Transition temperature (°C)	-20	23	30	41	55

Table 4.4 Transition temperatures of lipids.

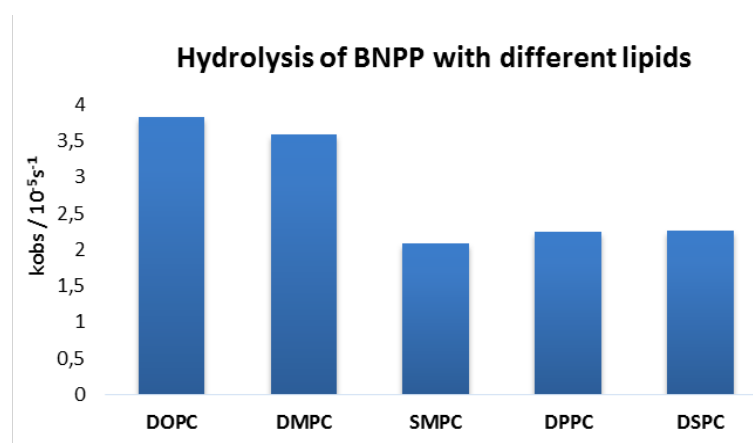


Figure 4.14 Pseudo first order rate constants for different lipids.

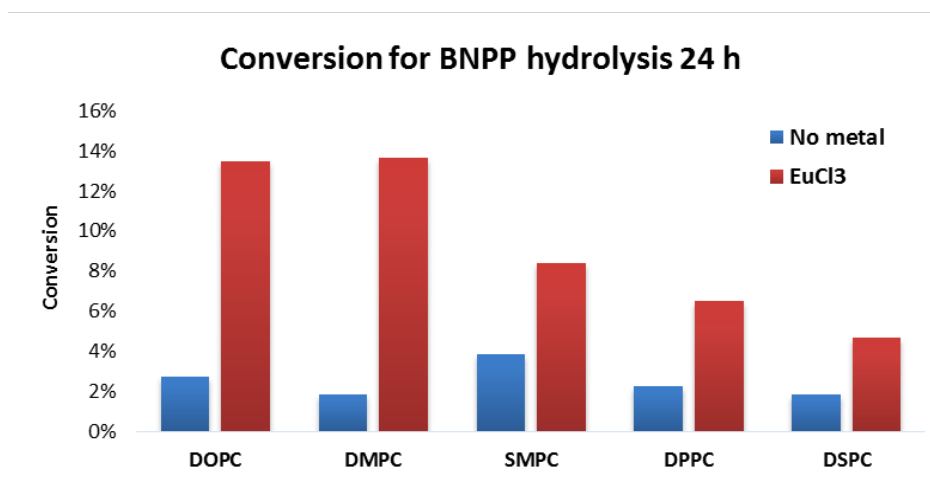


Figure 4.15 Conversion of BNPP ($c = 0.4 \text{ m M}$) using different lipids ($c = 0.1 \text{ mM}$) with and without the addition of europium chloride ($c = 0.1 \text{ mM}$) in HEPES buffer ($c = 25 \text{ mM}$, 7.4 pH). Conversion of BNPP ($c = 0.4 \text{ mM}$) using different lipids ($c = 0.1 \text{ mM}$) with and without the addition of europium chloride ($c = 0.1 \text{ mM}$) in HEPES buffer ($c = 25 \text{ mM}$, 7.4 pH).

Optimisation of the Eu:DOPC ratio

Same conditions were used for the measurements as in the previous investigations.

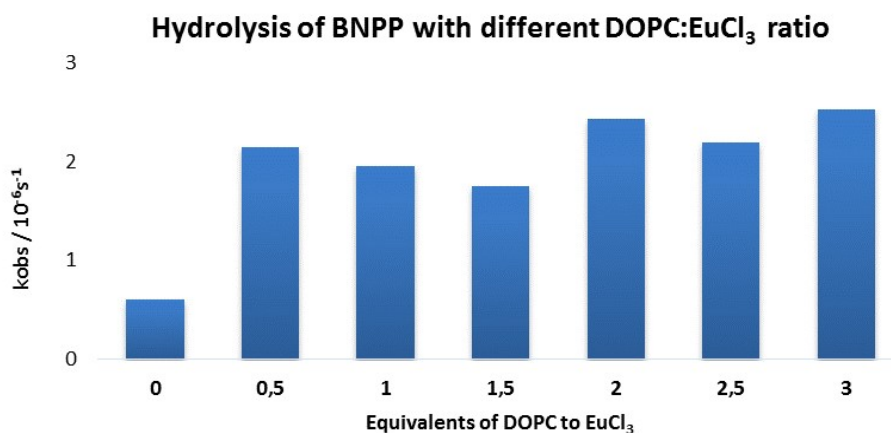


Figure 4.16 Pseudo first order rate constants for BNPP hydrolysis with increasing amounts of DOPC. The concentration of europium salts is kept constant (0.1 mM).

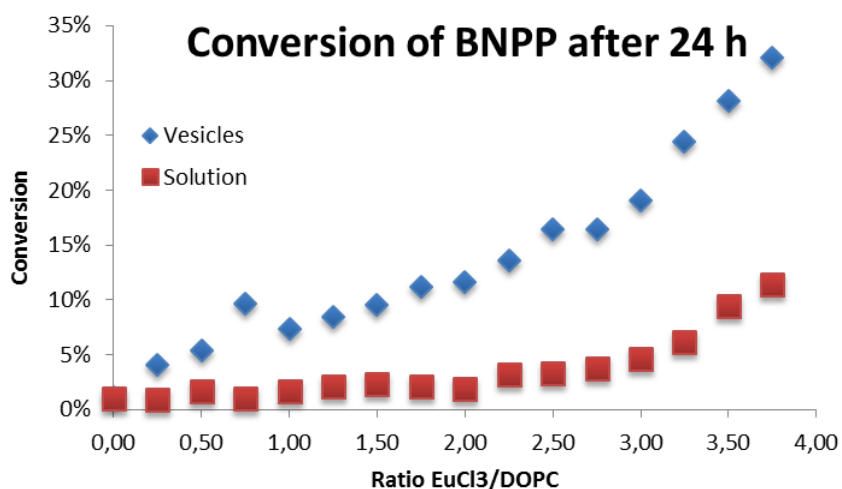


Figure 4.17 Conversion of BNPP after 24 h for increasing amount of europium. The DOPC concentration is constant (0.1 mM), only the europium ion concentration is increased (0.1–0.4 mM).

Second order rate constants

Second order rate constants were derived from pseudo first order rate constants recorded at different europium salt concentrations.

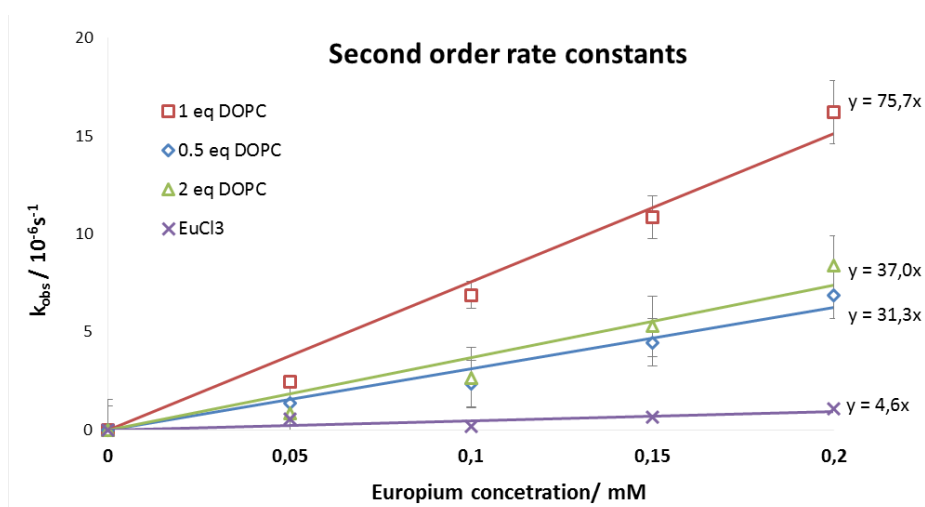


Figure 4.18 Determination of second order rate constant for EuCl₃:DOPC in ratio 1:1 (red), 1:2 (green), 2:1 (blue).

Monophosphate hydrolysis

Attempts to use monophosphate esters as substrates for hydrolysis resulted in rapid precipitation in the presence of DOPC vesicles. Therefore in most cases no hydrolytic rates

could be measured. The hydrolysis of 4-nitrophenylphosphate (PNPP) by europium chloride measured after 24 hours is comparable in the presence or absence of lipids (Figure 4.19).

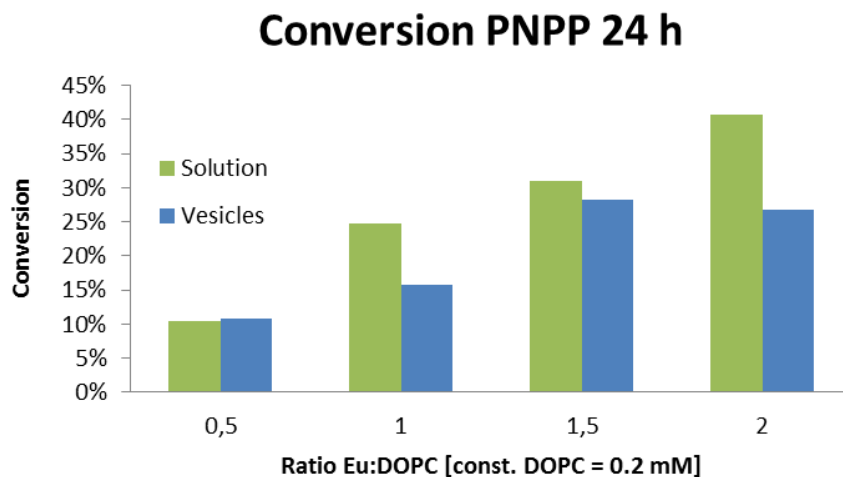


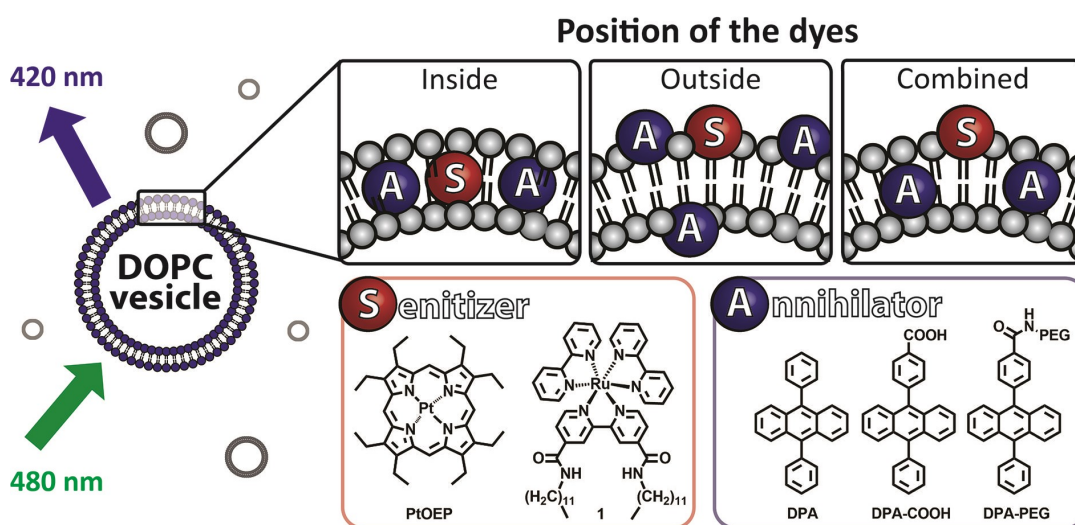
Figure 4.19 Conversion of PNPP (0.4 mM) after 24h using europium chloride in the presence and absence of DOPC membranes.

4.6 References

- ‡ The chloride counter anions will neither tightly coordinate the lanthanide cation in aqueous solution nor bind to the zwitterionic headgroup of the lipid.
1. Schroeder, G. K.; Lad, C.; Wyman, P.; Williams, N. H.; Wolfenden, R., The time required for water attack at the phosphorus atom of simple phosphodiester and of DNA. *Proc. Natl. Acad. Sci. U.S.A.* **2006**, *103* (11), 4052-4055.
 2. Zenkova, M. A., *Artificial Nucleases*. Springer-Verlag Berlin Heidelberg: 2004; p 292.
 3. Cowan, J. A., Chemical nucleases. *Curr. Opin. Chem. Biol.* **2001**, *5* (6), 634-642.
 4. Mancin, F.; Scrimin, P.; Tecilla, P.; Tonellato, U., Amphiphilic metalloaggregates: Catalysis, transport, and sensing. *Coord. Chem. Rev.* **2009**, *253* (17-18), 2150-2165.
 5. Mancin, F.; Scrimin, P.; Tecilla, P., Progress in artificial metallonucleases. *Chem. Commun.* **2012**, *48* (45), 5545-5559.
 6. Franklin, S. J., Lanthanide-mediated DNA hydrolysis. *Curr. Opin. Chem. Biol.* **2001**, *5* (2), 201-208.
 7. Jones, M. N.; Hammond, K.; Reboiras, M. D.; Acerete, C.; Jackson, S. M.; Nogueira, M.; Nicholas, A. R., The interaction of lanthanum ions with dipalmitoylphosphatidylcholine—phosphatidylinositol vesicles. *Colloids and Surfaces A* **1986**, *18* (1), 75-91.
 8. Altenbach, C.; Seelig, J., Calcium binding to phosphatidylcholine bilayers as studied by deuterium magnetic resonance. Evidence for the formation of a calcium complex with two phospholipid molecules. *Biochemistry* **1984**, *23* (17), 3913-3920.
 9. Saris, N.-E. L., Europium phosphorescence as a probe of binding to phospholipids. *Chem. Phys. Lipids* **1983**, *34* (1), 1-5.
 10. Bracken, K.; Moss, R. A.; Ragunathan, K. G., Remarkably Rapid Cleavage of a Model Phosphodiester by Complexed Ceric Ions in Aqueous Micellar Solutions. *J. Am. Chem. Soc.* **1997**, *119* (39), 9323-9324.
 11. Kimizuka, N.; Watanabe, E.; Kunitake, T., Lanthanide Ion-Mediated Hydrolysis of DNA on Phosphate Bilayer Membrane. *Chem. Lett.* **1999**, *28* (1), 29-30.
 12. Sumaoka, J.; Igawa, T.; Furuki, K.; Komiyama, M., Homogeneous Ce(IV) Complexes for Efficient Hydrolysis of Plasmid DNA. *Chem. Lett.* **2000**, *29* (1), 56-57.
 13. Gruber, B.; Stadlbauer, S.; Woinaroschy, K.; König, B., Luminescent vesicular receptors for the recognition of biologically important phosphate species. *Org. Biomol. Chem.* **2010**, *8* (16), 3704-3714.
 14. Eliseeva, S. V.; Bunzli, J.-C. G., Lanthanide luminescence for functional materials and biosciences. *Chem. Soc. Rev.* **2010**, *39* (1), 189-227.

15. Gallagher, P. K., Absorption and Fluorescence of Europium(III) in Aqueous Solutions. *J. Chem. Phys.* **1964**, *41* (10), 3061-3069.
16. Bhowmik, S.; Banerjee, S.; Maitra, U., A self-assembled, luminescent europium cholate hydrogel: a novel approach towards lanthanide sensitization. *Chem. Commun.* **2010**, *46* (45), 8642-8644.
17. Poznik, M.; Konig, B., Cooperative hydrolysis of aryl esters on functionalized membrane surfaces and in micellar solutions. *Org. Biomol. Chem.* **2014**, *12* (20), 3175-3180.
18. Chang, C. A.; Wu, B. H.; Kuan, B. Y., Macrocyclic Lanthanide Complexes as Artificial Nucleases and Ribonucleases: Effects of pH, Metal Ionic Radii, Number of Coordinated Water Molecules, Charge, and Concentrations of the Metal Complexes. *Inorg. Chem.* **2005**, *44* (19), 6646-6654.
19. Morrow, J. R.; Aures, K.; Epstein, D., Metal ion promoted attack of an alcohol on a phosphate diester: modelling the role of metal ions in RNA self-splicing reactions. *J. Chem. Soc., Chem. Commun.* **1995**, (23), 2431-2432.
20. Welch, J. T.; Sirish, M.; Lindstrom, K. M.; Franklin, S. J., De Novo Nucleases Based on HTH and EF-Hand Chimeras. *Inorg. Chem.* **2001**, *40* (9), 1982-1984.
21. Bonomi, R.; Scrimin, P.; Mancin, F., Phosphate diesters cleavage mediated by Ce(IV) complexes self-assembled on gold nanoparticles. *Org. Biomol. Chem.* **2010**, *8* (11), 2622-2626.
22. Gruber, B.; Kataev, E.; Aschenbrenner, J.; Stadlbauer, S.; König, B., Vesicles and Micelles from Amphiphilic Zinc(II)-Cyclen Complexes as Highly Potent Promoters of Hydrolytic DNA Cleavage. *J. Am. Chem. Soc.* **2011**, *133* (51), 20704-20707.
23. Gruber, B.; Stadlbauer, S.; Späth, A.; Weiss, S.; Kalinina, M.; König, B., Modular Chemosensors from Self-Assembled Vesicle Membranes with Amphiphilic Binding Sites and Reporter Dyes. *Angewandte Chemie International Edition* **2010**, *49* (39), 7125-7128.

5 Light Upconverting soft particles: Triplet-triplet annihilation in the phospholipid bilayer of self-assembled vesicles



Large unilamellar vesicles (100 nm) were functionalised to obtain supramolecular particles capable of light upconversion in pure aqueous media. Triplet-triplet annihilation of diphenylanthracene (DPA) leading to delayed fluorescence at 420 nm was used to upconvert the light absorbed by embedded metal complex sensitizers. The lipid type and the chromophore position in the membrane affect the TTA intensity, which remains constant over a large concentration range.

This chapter was published in:

M. Poznik, U. Faltermeier, B. Dick and B. König, "Light upconverting soft particles: triplet-triplet annihilation in the phospholipid bilayer of self-assembled vesicles", *RSC Adv.* **2016**, 6, 41947–41950

M. Poznik performed the experimental work and wrote the manuscript, U. Faltermaier operated the laser and evaluated delayed fluorescence, B. Dick supervised and performed data fitting, B. König supervised the project and is corresponding author.

5.1 Introduction

Increasing the efficiency of light harvesting is an important task in natural photosynthesis as well in industrial solar systems. For some applications, high energies or short irradiation wavelength are required.¹ Therefore, up-converting (UC) processes producing photons of higher energy by combination of low energy photons have been developed.² Different systems showing upconversion are known, but most of them provide only low quantum yields or require specific conditions.³ In recent years, significant effort was put into the development of triplet-triplet annihilation (TTA) upconversion processes and their applications.

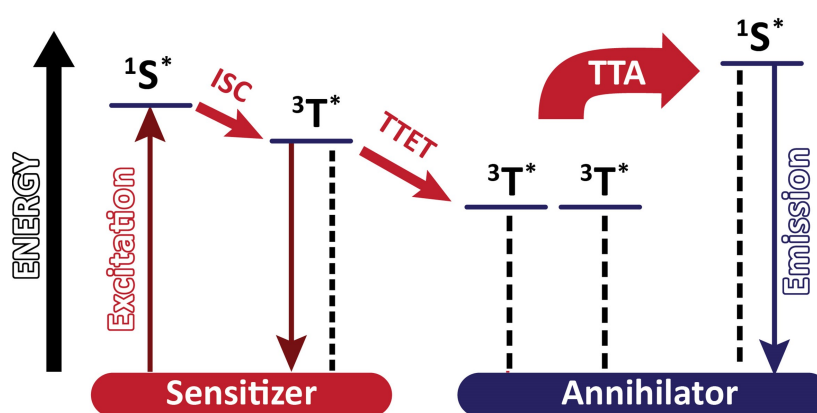


Figure 5.1 Schematic representation of the triplet-triplet annihilation process.

In this process low energy photons are absorbed by sensitizers, which after intersystem crossing (ISC) perform triplet-triplet energy transfer (TTET) with an annihilator dye. Two annihilator molecules then undergo TTA and singlet emission is observed (Figure 5.1).^{4, 5} TTA upconversion was used in sensing,⁶ in flexible LCDs⁷ and in bioimaging.⁸ The process has some advantages in comparison with other UC processes as it works with low excitation intensities and provides a relatively high quantum yield.⁹ Many pairs of sensitizers and annihilators were found to exhibit TTA in organic solvents,¹⁰ polymers,^{11, 12} dendrimers¹³ and other supramolecular systems.^{14, 15} However, most dyes used for TTA are lipophilic and only soluble in organic solvents. TTA systems operating in aqueous media use upconverting nanocapsules, micellar solutions or giant unilamellar vesicles.^{16, 17, 18, 19} As the preparation of such water soluble TTA systems can be laborious we present here a supramolecular self-assembly approach based on large vesicles (100 nm) with embedded dyes exhibiting TTA (Figure 5.2). In this system, platinum porphyrin **PtOEP** and an amphiphilic derivative of tris-(bipyridine)ruthenium(II) **1** are used as sensitizers. They are co-embedded in the membrane

and appear inside (PtOEP) or on the outer part of the bilayer (1). Lipophilic diphenyl-anthracene DPA used as an annihilator is present inside the bilayer. Two other amphiphilic derivatives of DPA (DPA-COOH, DPA-PEG, Figure 5.2) were examined in order to test the effect of the position of the annihilator in the membrane.

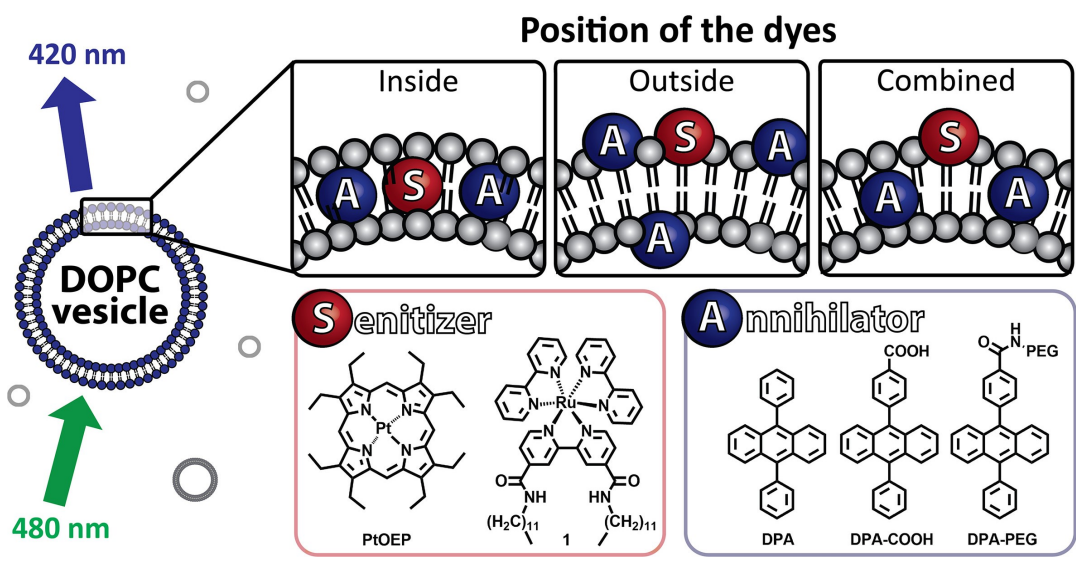


Figure 5.2 Used dyes and their assembly in the upconverting DOPC vesicles.

5.2 Results and discussion

The porphyrin complex **PtOEP** is a known TTA sensitizer.²⁰ The amphiphilic sensitizer **1** was previously prepared in our group and used in vesicular systems.²¹ It co-embeds well in the membrane and creates stable vesicles with a variety of lipids. **DPA** was chosen as annihilator for its ability to perform triplet-triplet energy transfer with both sensitizers.¹¹ Due to its molecular structure it neither forms photodimers, nor excimers upon excitation.^{11, 22} Combinations of sensitizers and annihilators were introduced to DOPC vesicles to study the behaviour of the TTA. Vesicles were prepared according to known procedures and loading of the compounds co-embedded in the membrane did not exceed 11 mol%. All prepared vesicles were used fresh and were stable more than 24 h (see experimental part, Figure 5.12). We used a OPO pumped by a Nd:YAG laser to excite the sensitizers (**PtOEP**: 532 nm, **1**: 480 nm) and recorded the observed delayed fluorescence of annihilator with a Streak Camera.²³

5.2.1 TTA inside the bilayer

A recent report by Askes *et al.* shows that the confinement inside the DOPC bilayer does not affect TTA between palladium complex and perylene.¹⁶

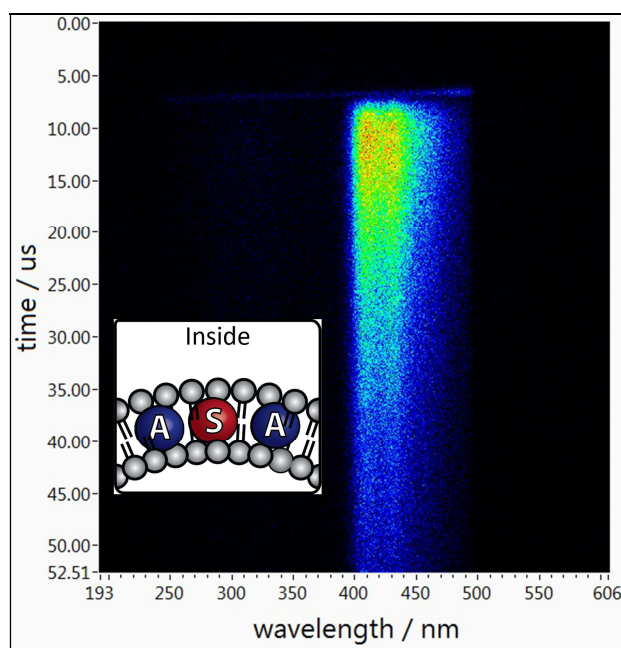


Figure 5.3 Delayed emission of DPA when both dyes are co-embedded inside the bilayer. The system contains **DPA** (0.06 mM), **PtOEP** (0.02 mM) in aq. DOPC vesicles (0.92 mM).

Our selected pair of dyes operates at shorter wavelengths. Both **PtOEP** and **DPA** are lipophilic compounds and locate inside the phospholipid bilayer. A strong delayed fluorescence of **DPA** is observed when the sensitizer is excited (Figure 5.3).

5.2.2 TTA with the sensitizer on the surface of the membrane

Sensitizer **1** is amphiphilic and expected to assemble with its polar head group at the surface of the bilayer. We examined TTA using **DPA** and **1** in water, in methanol and in aqueous solution containing DOPC vesicles (Figure 5.4). When the same amounts of dyes were used in the vesicular solution, the absorbance of **DPA** was drastically reduced by 50 % in comparison to the same concentrations in methanol (Figure 5.4, left). This indicates that high local **DPA** concentration inside the bilayer result in the formation of larger aggregates, which are still present in vesicular solution, but do not absorb light. We studied the absorption and emission spectra of **DPA** in the vesicular systems (see experimental part, Figure 5.11) and observed the highest absorption intensity for 4 mol% loading of **DPA**, which corresponded also to the highest fluorescence emission intensity (Figure 5.4, left).[‡] With membrane loadings exceeding 4 mol%, the shape and intensity of the emission spectra change, which might be explained by the formation of aggregates in the membrane. This was confirmed by experiments where 3 volume equivalents of methanol were added to the vesicular solutions to burst and dissolve the vesicles, which restored the original fluorescence intensity of the chromophores (see experimental part, Figure 5.13).

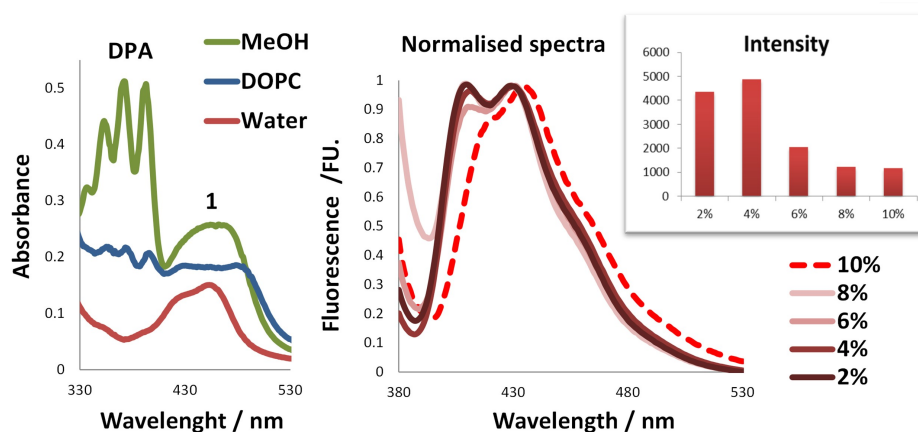


Figure 5.4 *Left*; UV-Vis spectra of different systems containing **DPA** (0.06 mM) and **1** (0.02 mM) in aq. DOPC vesicles (0.92 mM) (blue), plain MiliQ water (red) or methanol (green). *Right*; Fluorescence ($\lambda_{\text{ex}} = 374 \text{ nm}$) of DOPC (0.89–0.97 mM) vesicles with different molar loading of **DPA** in presence of 1 mol% of **1** (0.01 mM). Intensity integrated from 390nm to 580 nm.

For sensitizer **1**, the differences of the photophysical properties between homogeneous solution and embedded in the membrane were much less pronounced (Figure 5.4). We used these optimised concentrations of sensitizer and annihilator and recorded TTA in vesicles and solutions (Figure 5.5).

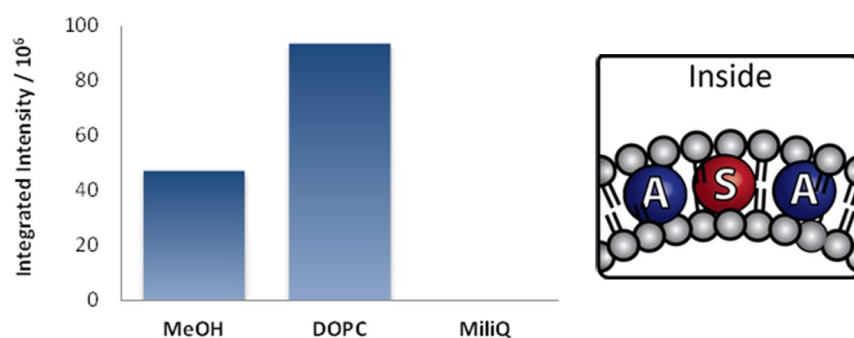


Figure 5.5 TTA intensity^s in vesicles containing **DPA** (0.06 mM) and **1** (0.02 mM) in aq. DOPC vesicles (0.92 mM), MiliQ water or methanol.

DPA is negligibly soluble in water (see experimental part, Figure 5.10). Due to this fact, no delayed fluorescence is observed in aqueous solution (Figure 5.5). The mixture was prepared in the same manner as vesicular solutions except the absence of the lipid. If lipids are present, a delayed fluorescence due to TTA is observed with twofold intensity compared with the methanol solution of the same concentration (Figure 5.5). This can be attributed to higher local concentration of the dyes involved in TTA.

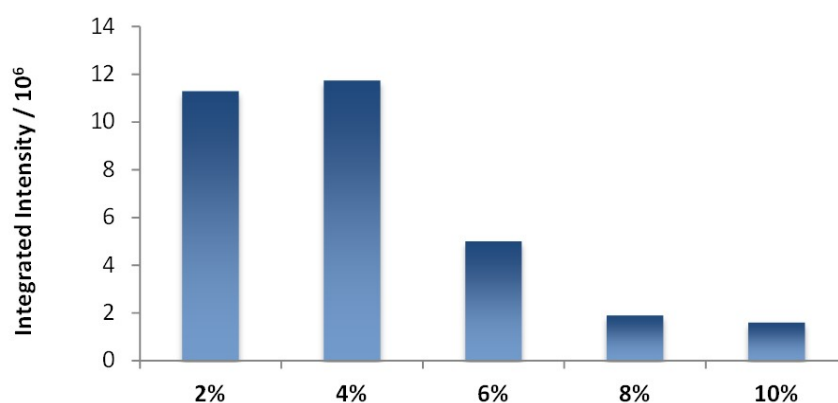
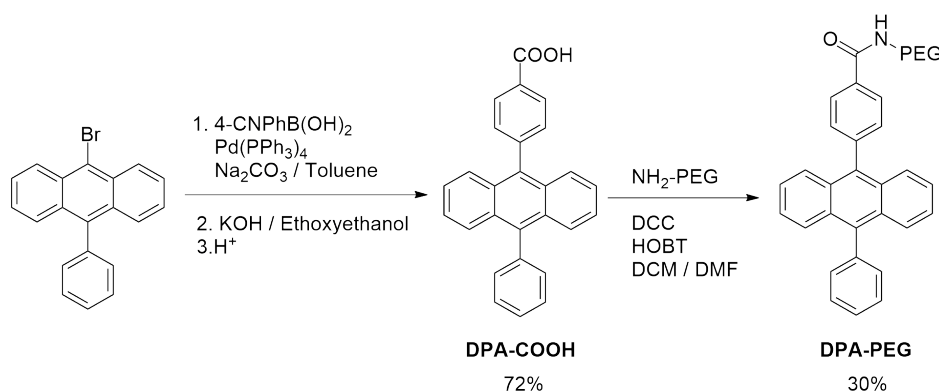


Figure 5.6 Intensity^s of TTA in DOPC (0.89–0.97 mM) vesicles with different molar loading of **DPA** in presence of 1 mol% of **1** (0.01 mM).

In order to increase the intensity of TTA, often a large excess of the annihilator is used to improve the efficiency of the triplet-triplet energy transfer to annihilator molecules. Therefore, we prepared vesicular solutions varying the ratio of **DPA** from 2 to 10 equivalents, respective to the sensitizer **1**, which concentration was kept constant. Only a small increase in intensity is achieved by changing from 2 to 4 eq. of **DPA** (2 to 4 %). Larger excess of **DPA** leads to significantly reduced emission intensities (Figure 5.6). This corresponds well with effect of aggregation observed on fluorescence intensity.

5.2.3 TTA on the surface of the membrane

During TTA upconversion two intermolecular processes (TTET, TTA) take place. The close proximity of the dyes plays a key role in its efficiency. In order to assemble all dyes at the water lipid interface, we prepared two derivatives of **DPA** bearing a polar head group (Scheme 5.1).



Scheme 5.1 Synthesis of **DPA** amphiphiles.

The carboxylic acid in **DPA-COOH** serves as a small polar head group, which was further functionalized with a polyethylene glycol chain ($M_r = 5000$) giving **DPA-PEG**. Both compounds showed similar absorption and emission properties (see experimental part, Figure 5.14).

When used as previously, **DPA** derivatives with sensitizer **1** yielded stable 100 nm vesicles (see experimental part, Figure 5.15). The TTA intensity is clearly enhanced when amphiphilic **DPA** derivatives are used in DOPC vesicles (Figure 5.7).

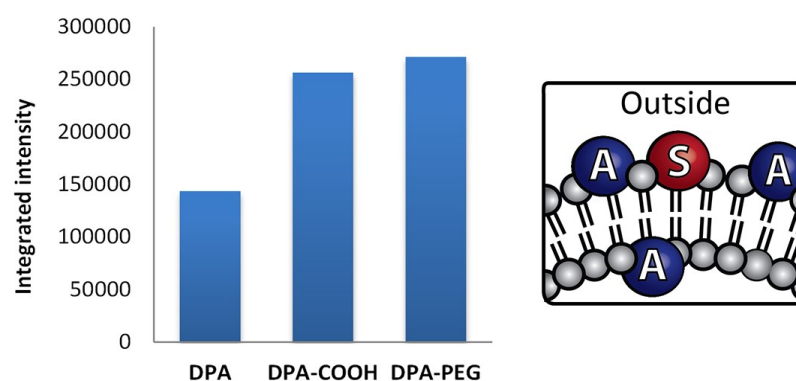


Figure 5.7 Intensity^s of delayed fluorescence in vesicles containing **DPA** or derivatives (0.06 mM) and **1** (0.02 mM) in DOPC vesicles (0.92 mM) in MiliQ water.

5.2.4 Different lipids

The membrane mobility within vesicles depends on the chemical nature of the lipids and is characterized by the transition temperature between gel and liquid phase. Below the transition temperature the lateral movement of membrane embedded compounds is inhibited. Under the same conditions as for DOPC ($T_m = -17\text{ }^\circ\text{C}$) we tested DSPC ($T_m = 55\text{ }^\circ\text{C}$) and DMPC ($T_m = 24\text{ }^\circ\text{C}$). Only low (DMPC) or no (DSPC) TTA was observed in comparison with DOPC (Figure 5.8). DSPC-based membranes are rigid as a result of the high transition temperature of the lipid. This is known to induce phase separation and clustering of molecules on the membrane surface and similar effects might be expected inside the bilayer.

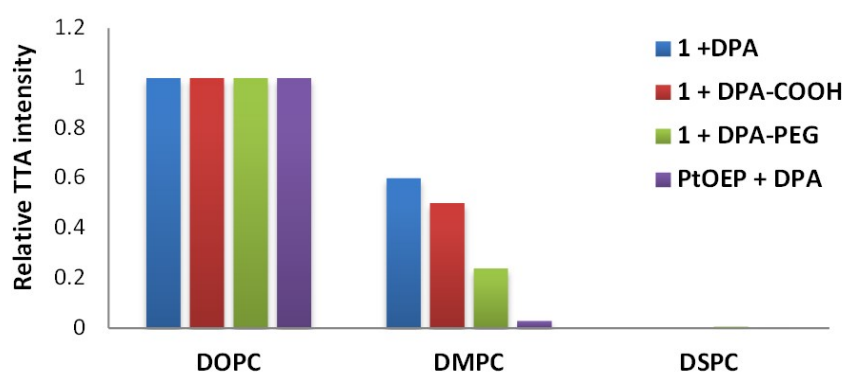


Figure 5.8 Relative intensity of TTA depending on the nature of the vesicle lipid (0.95 mM). The vesicles are functionalised with **DPA** derivatives (0.04 mM) and sensitizers (0.01 mM). For each TTA system the intensity^s in DOPC vesicles is used as 100 % value.

DMPC on the other hand is a lipid, which should give at room temperature a similarly fluid membrane as DOPC, but the intensity of TTA is proportionally lower at the same **DPA** loadings. The shape of fluorescence spectra indicate that **DPA** behaves in DMPC membrane similar as in DOPC at higher loadings (see experimental part, Figure 5.16) and forms aggregates. It can be concluded that a fluid membrane is essential for effective TTA in vesicle membranes.

5.2.5 Effect of dilution

In homogenous TTA systems, dilution leads to a nonlinear decrease of the intensity of delayed fluorescence of **DPA** due to the lower rate of TTET and TTA. Contrary, in the vesicular membrane the local concentration of the dyes does not change significantly upon dilution of the solution; only the overall concentration of the vesicles decreases. Therefore, the upconverting system is functionally independent on the concentration and emission intensity decreases linearly upon dilution (Figure 5.9). Fitting of the time resolved emission measurements with a simple model described in the experimental part shows no significant change in the dynamics of the system. The rate constant for the decay of the sensitizer k_1 was in the range of 4.99 to $5.20 \times 10^4 \text{ s}^{-1}$ and the rate constant for the decay of the annihilator showed values from 1.44 to $1.62 \times 10^4 \text{ s}^{-1}$.

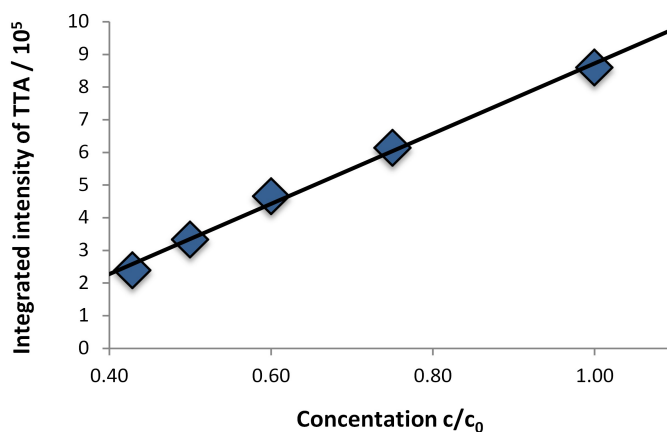


Figure 5.9 Integrated intensity⁵ of TTA for different dilutions of the solution shows linear dependency. Starting concentration c_0 (concentration of all amphiphiles) of the solution: DOPC (0.93 mM) vesicles functionalised with **1** (0.01 mM) and **DPA** (0.06 mM) in MiliQ water.

5.3 Conclusions

Functionalized DOPC vesicles exhibiting TTA were prepared by co-embedding dyes in different positions in the phospholipid bilayer of the vesicles. Three derivatives of the annihilator were used with two sensitizers. The vesicles are stable and exhibit twice as intense TTA compared to a methanolic solution of the dyes at identical concentrations. The ratios between sensitizer and annihilator dye and their respective concentrations in the membrane were optimized to yield the best TTA efficiency. Fluidity of the membrane is essential for effective TTA of the embedded dyes. Solutions of the functionalized vesicles can be diluted retaining their molar intensity of TTA, allowing their use at low concentrations for imaging applications. Additional functionalization of the outer membrane surface for specific applications can be readily envisaged.

The simple preparation by self-assembly and easy variations of type and ratio of dyes makes visible light upconverting functionalized vesicles a valuable alternative to TTA in homogeneous solution.

5.4 Experimental part

5.4.1 General methods and materials

Diphenylantracen **DPA** was purchased from TCI chemicals and **PtOEP** from Sigma Aldrich, both compounds were used as delivered. 9-Bromo-10-phenylanthracene²⁴ and amphiphilic sensitizer Tris(bipyridine)ruthenium(II)²¹ **1** were prepared according to published procedure. All used lipids were purchased from Avanti Polar Lipids Inc. All aqueous solutions were prepared in MiliQ deionised water.

NMR-Spectroscopy: NMR-spectra were recorded on a Bruker Avance 300 (¹H: 300 MHz, ¹³C: 75 MHz, T = 295 K) using the solvent residual peak as internal reference (CDCl₃: δ H 7.26). The chemical shifts are reported in δ [ppm] relative to internal standards (solvent residual peak). The spectra were analyzed by first order, the coupling constants *J* are given in Hertz [Hz]. Integration is determined as the relative number of atoms. Error of reported values: chemical shift: 0.01 ppm for ¹H-NMR, 0.1 ppm for ¹³C-NMR and 0.1 Hz for coupling constants. The solvent used is reported for each spectrum.

Thin Layer Chromatography: Aluminium plates coated with silica gel (ALUGRAM Xtra SIL G/UV₂₅₄ from Macherey-Nagel) were used. Detection was done by UV light (254 nm, 366 nm) or oxidation, using a KMnO₄-solution.

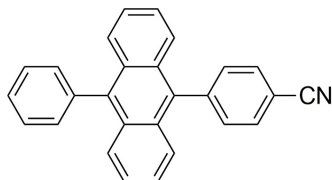
Spectroscopy: UV/Vis Spectra were recorded on a Cary 50 UV/Vis spectrophotometer, fluorescence of dyes on Horiba Fluoromax.

Dynamic Light Scattering: DLS measurements were performed on a Malvern Zetasizer Nano at 25 °C using 1 cm disposable polystyrene cuvettes (VWR).

Time resolved measurements: The time resolved fluorescence spectra were recorded using an optical parametric oscillator pumped by a Nd:YAG Laser (Surelite II and Surelite OPO Plus, Continuum) as excitation source. The fluorescence light was recorded by the combination of a spectrograph (Burker 200is, grating 100 lines / 100mm), a streak camera (C7700, Hamamatsu Photonics) and a CCD camera (ORCA-CR, Hamamatsu Photonics). The software provided by Hamamatsu (HPD-TA, Hamamatsu Photonics) was used to record the fluorescence in photon counting mode.

5.4.2 Synthesis

4-(10-Phenylanthracen-9-yl)benzonitrile (DPA-CN)²⁵



9-Bromo-10-phenylanthracene (473 mg, 1.42 mmol), 4-cyanophenylboronic acid (314 mg, 2.14 mmol) and K_2CO_3 (1969 mg, 14.25 mmol) were suspended in ethanol (5 mL) and toluene (20 mL). The reaction mixture was flushed with nitrogen for 20 min. Afterwards $Pd(PPh_3)_4$ (83 mg, 0.07 mmol) was added and the reaction was refluxed under nitrogen for 24 h. After cooling to room temperature, brine (10 mL) was added and the mixture was extracted with toluene (3×15 mL). The combined organic layers were dried over $MgSO_4$, solids were filter off and the solvent removed under reduced pressure. The residue was purified by flash chromatography (gradient: 100 % petroleum ether to 50 % petroleum ether and 50 % dichloromethane) to obtain 471 mg (93 %) of product **DPA-CN** in form of white crystals.

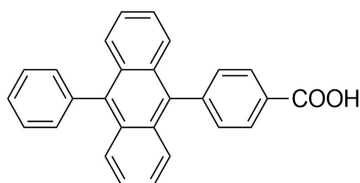
1H NMR (300 MHz, $CDCl_3$): δ 7.98 – 7.89 (m, 2H), 7.79 – 7.68 (m, 2H), 7.68 – 7.51 (m, 7H), 7.51 – 7.43 (m, 2H), 7.43 – 7.31 (m, 4H).

^{13}C NMR (75 MHz, $CDCl_3$): δ 144.6, 138.7, 138.3, 134.5, 132.4, 132.3, 131.2, 129.8, 129.4, 128.5, 127.7, 127.3, 126.0, 125.8, 125.2, 119.0, 111.6.

MS (EI(+)): $m/z = 355.13 [M^+]$

T_m : 278–279 °C

4-(10-Phenylanthracen-9-yl)benzoic acid (DPA-COOH)²⁶



A pellet of KOH (662 mg, 11.82 mmol) was added to a suspension of derivative **DPA-CN** (300 mg, 0.84 mmol) in water (15 mL) and 2-ethoxyethanol (30 mL). The reaction mixture was refluxed for 4 h. After cooling aq. HCl was added dropwise to reach acidic pH followed by additional water (50 mL). The suspension was extracted with diethylether (3×50 mL),

combined organic layers were washed with water (10 mL), brine (10 mL) and dried over MgSO_4 . Solids were filter off and the residue was purified via column chromatography (gradient: petroleum ether with 50 % ethyl acetate to 100 % ethyl acetate) to obtain 242 mg (77 %) product **DPA-COOH** in form of white solid.

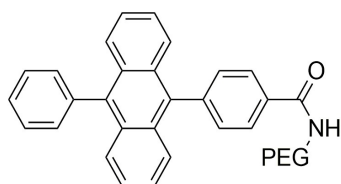
$^1\text{H NMR}$ (300 MHz, DMSO): δ 8.27 – 8.13 (m, 3H), 7.72 – 7.50 (m, 10H), 7.49 – 7.40 (m, 5H).

$^{13}\text{C NMR}$ (75 MHz, DMSO): δ 167.7, 141.2, 138.0, 136.8, 135.7, 133.6, 130.7, 130.8, 129.1, 128.9, 128.6, 127.7, 126.4, 126.1, 125.6, 125.5.

MS (ESI(+)): $m/z = 374.15$ [MH^+]

T_m : 304–308 °C

Polyethyleneglycol 4-(10-phenylanthracen-9-yl)benzamid (DPA-PEG)²⁷



In nitrogen atmosphere the acid **DPA-COOH** (100 mg, 0.26 mmol) was suspended in dry DCM (15 mL) and additional dry DMF was added under stirring until the acid dissolved. DCC (28 mg, 0.13 mmol) was added and stirring continued for 15 min. Consecutively methoxypolyethylene glycol amine 5000 (668 mg, 0.134 mmol) was added as a solution in dry DCM (5 mL) followed by HOBT (20 mg, 0.134 mmol) in dry DMF (5 mL). The reaction mixture was stirred at RT for 24 h. DCM was removed in *vacuo*. The residue was treated with diethylether, a precipitate was filtered off and washed with cold diethylether. The obtained solid was recrystallized three times from ethanol and dried in *vacuo* to obtain 300 mg (41 %) of polymer **DPA-PEG** in form of a white solid. Loading of the dye in the polymer was calculated to be: 74 % (via $^1\text{H NMR}$).

$^1\text{H NMR}$ (300 MHz, CDCl_3): δ 8.04 (d, $J = 7.7$ Hz, 2H), 7.74 – 7.28 (m, 15H), 3.85 – 3.31 (m, 614H).

T_m : 50–57 °C

5.4.3 Preparation and characterization of the vesicles

Vesicle preparation

Vesicles were prepared according to known procedures.²⁸ From stock solutions of lipids and dyes the required ratio of compounds was mixed, solvent was evaporated in a stream of nitrogen and in *vacuo*. The residue was dissolved in MiliQ water to obtain the solution of all amphiphiles with a concentration of 1mM. The emulsion was sonicated and extruded through polycarbonate membrane with 100 nm pores to obtain vesicles with the desired size. Samples were bubbled with nitrogen for 15 min during sonication step and 10 min prior and during the measurements.

Different systems

Absorption spectra for sensitizer **1** and annihilator **DPA** were measured individually and compared with the mixture of the components under three different conditions (Figure 5.10).

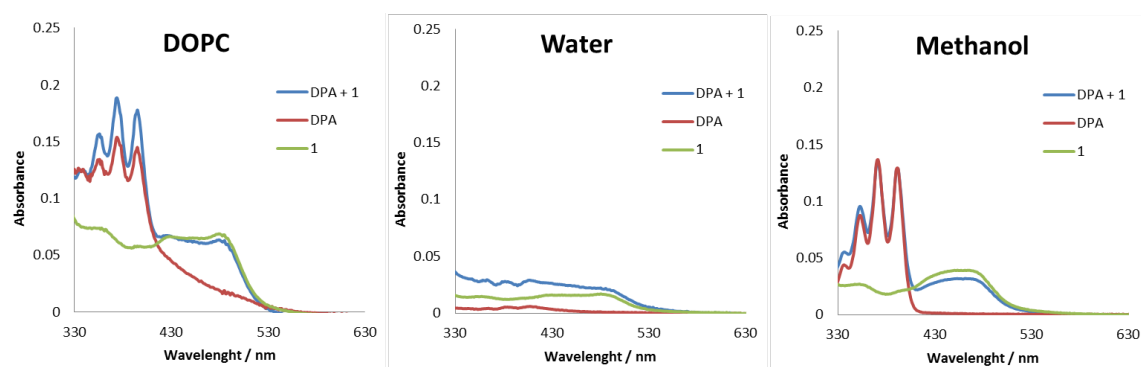


Figure 5.10 UV-Vis spectra of different systems containing **DPA** (0.04 mM) or **1** (0.01 mM) or their mixture in aq. DOPC vesicles (0.95 mM), MiliQ water or Methanol.

All concentrations are identical. **DPA** is nearly insoluble in water.

Loading of DPA in Vesicles

Different loadings of **DPA** in DOPC vesicles were examined. Highest fluorescence intensity and absorption for **DPA** is observed for system with 4 mol % of **DPA** in DOPC membrane (with 1 mol % of **1**) (Figure 5.11).

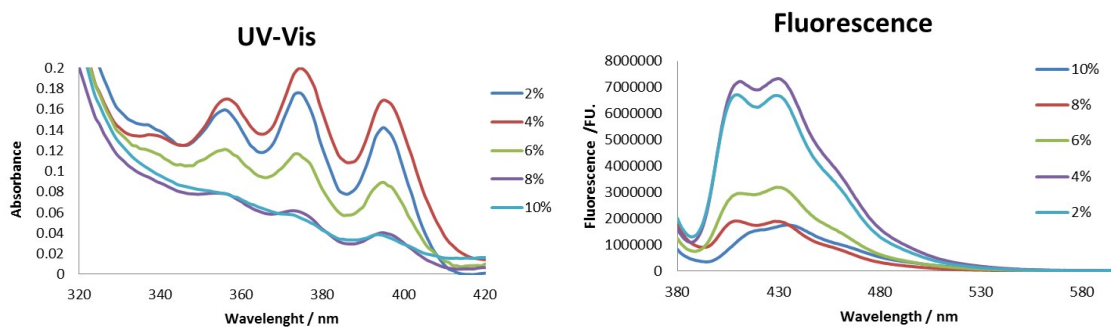


Figure 5.11 Absorption and emission spectra of DOPC vesicles with different molar loading of DPA in presence of 1 mol % of **1** (0.01 mM). Concentration of DOPC is always calculated to give 1 mM of all amphiphiles (0.89–0.97 mM).

Vesicles are stable after extrusion for 24 h at room temperature (Figure 5.12) and only vesicles with 10 mol. % of DPA exhibited a higher polydispersity index showing inferior stability with increased loading.

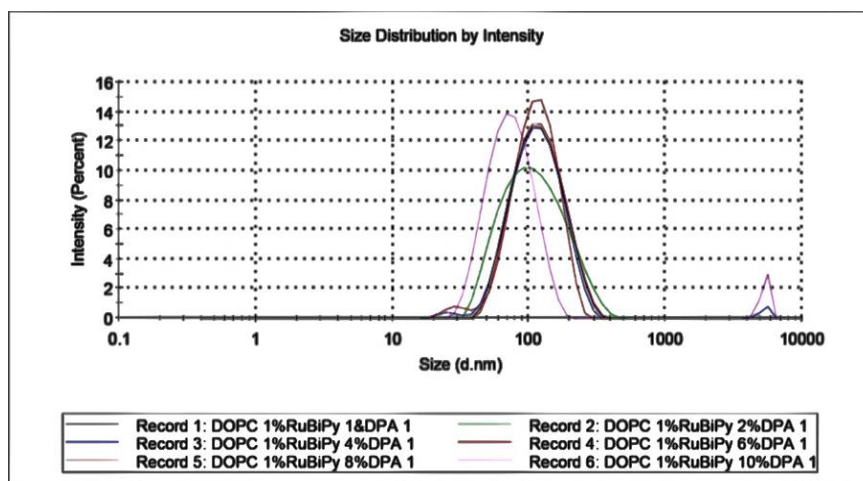


Figure 5.12 DLS measurement for DOPC (0.89–0.97 mM) vesicles with 1 mol. % **1** (0.01 mM) and different loadings of DPA (1–10 mol. %) after 24 h.

Disassembling of vesicles by methanol addition

Extruded vesicles can be dissolved by addition of 3 vol. eq. of methanol. The recovered fluorescence and absorbance indicates an aggregation and self-quenching of DPA in the bilayer (Figure 5.13). With 2 vol. eq. of methanol vesicles do not disintegrate immediately.

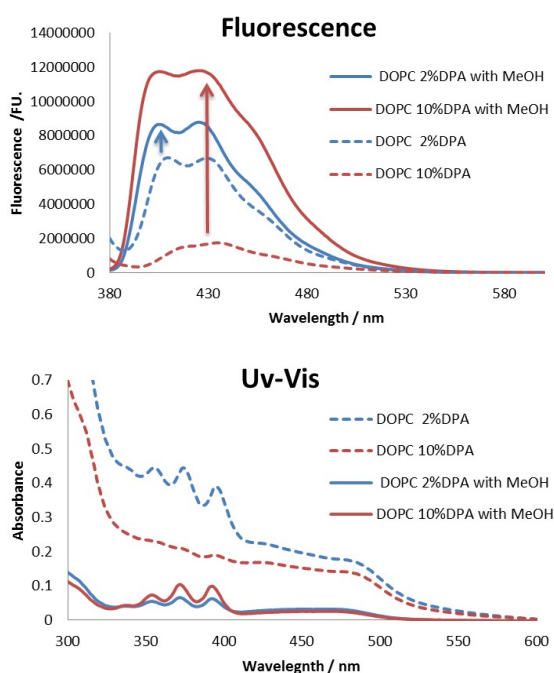


Figure 5.13 Absorption and emission spectra of aq. vesicular solution of DOPC (0.89, 0.97 mM) vesicles functionalised with 1 mol % of **1** (0.01 mM) and 2 or 10 mol % of **DPA** (0.02, 0.1 mM) before and after addition of 3 vol. eq of MeOH.

Amphiphilic DPA derivatives

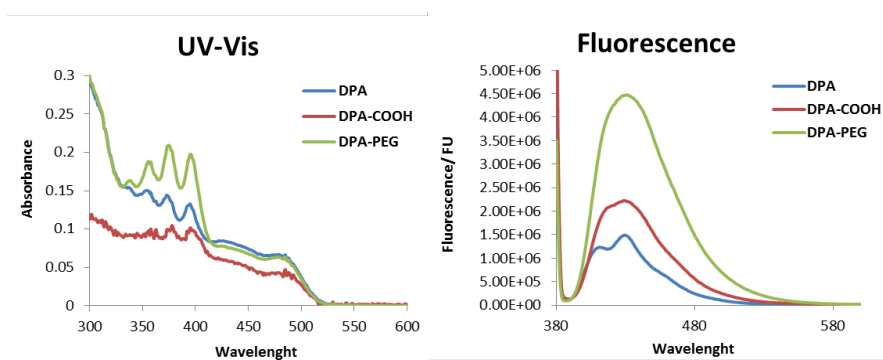


Figure 5.14 Absorption and emission spectra of aq. vesicular solution of DOPC (0.95 mM) vesicles functionalised with 1 mol % of **1** (0.01 mM) and 4 mol % of **DPA**, **DPA-COOH** or **DPA-PEG** (0.04 mM).

Vesicles with amphiphilic derivatives of **DPA** (**DPA-COOH**, **DPA-PEG**) were prepared in the same manner as for **DPA** and yielded stable 100 nm vesicles just by simple sonication (Figure 5.15)

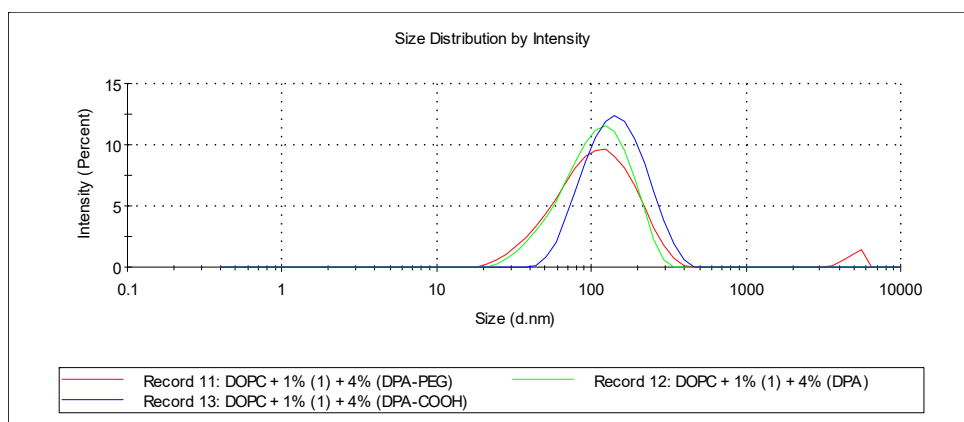


Figure 5.15 Size distribution of DOPC vesicles: 1 mol % of **1** (0.01 mM) and 4 mol % of **DPA** derivatives (0.04 mM) and 95 mol % DOPC (0.95 mM).

Lipids

Vesicular systems with different lipids were prepared in the same manner as for DOPC with exception for DSPC where the solution during sonication and extrusion was heated to 70 °C to be above the transition temperature of the lipid (for DSPC 55 °C). Optical spectra of the obtained systems were measured (Figure 5.16).

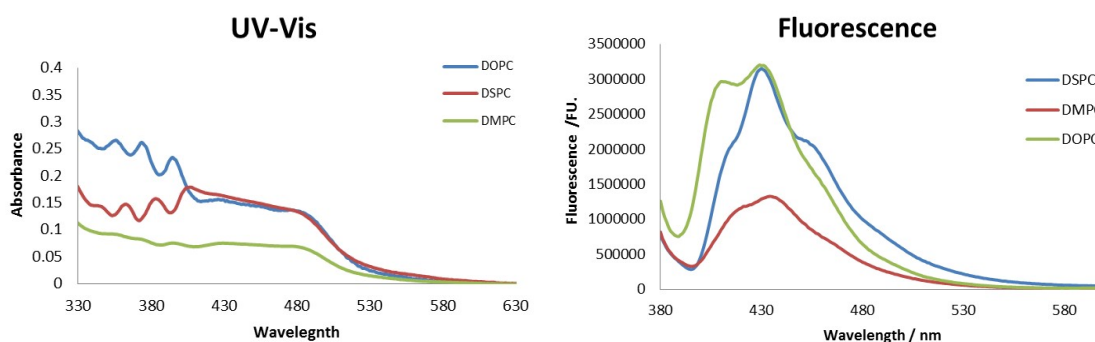


Figure 5.16 Absorption and emission spectra of vesicular systems with different lipids (0.97 mM) functionalised with 1 mol % **1** (0.01 mM) and 6 mol % of **DPA** (0.06 mM) in MilliQ water.

5.4.4 TTA measurements

TTA delayed fluorescence was recorded by photon counting. Measurement data is saved as a 2D Matrix for 512 lines and 512 columns, so that every line is a spectrum at a given time and every column is a time trace at a given wavelength. The intensity values for the delayed

fluorescence were calculated by summation over all cells in the 2D Matrix that fall in a specified time and wavelength range. This range was from 370 nm to 470 nm and from 2 μ s (to avoid the scattered excitation light) after the excitation event to the end of the measurement. Fluorescence spectra and time traces were always displayed as a sum over a range several μ s or nm.

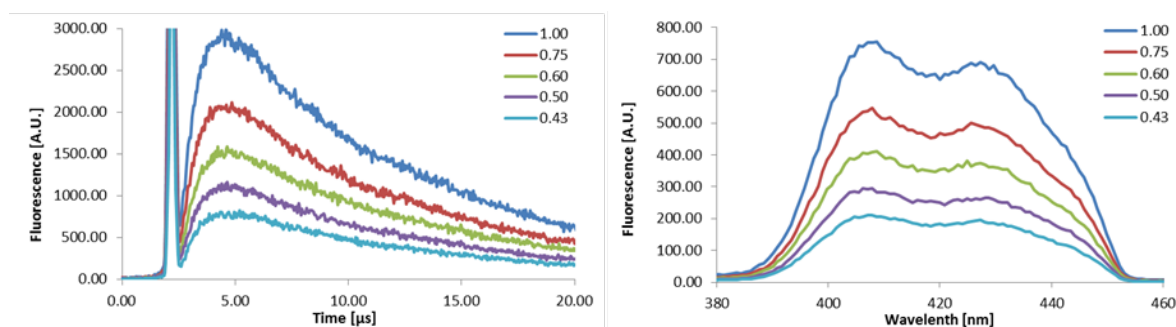


Figure 5.17 Example of measured delayed fluorescence in dilution experiments for DOPC vesicles (0.93 mM) with **1** (0.01 mM) and **DPA** (0.06 mM). Spectra correspond with relative dilution c/c_0 . The time traces are averaged over 405 nm to 430 nm and the spectra are the average from 2 μ s after the excitation to the end of the measurement.

The time dependence of the delayed fluorescence could be modeled very well by a simple model. The sensitizer triplet can decay spontaneously (k_s), through energy transfer to the annihilator ($k_{ET}[A]$), through quenching by other compounds in the sample, and by triplet-triplet annihilation. If we neglect the last process, the time dependence will be monoexponential.

$$c_s(t) = c_s(0) \exp(-k_1 t); k_1 = k_s + k_{ET}[A]_0$$

Where we have subsumed all pseudo first order quenching processes into k_s . The annihilator triplet is produced from the sensitizer and decays both spontaneously and by triplet triplet annihilation (TTA)

$$\frac{dc_A}{dt} = k_{ET}[A]_0 c_s - k_A c_A - k_{TTA} c_A^2$$

If we assume that TTA makes a negligible contribution to the decay, the time dependence of c_A is given by

$$c_A(t) = \frac{k_{ET}[A]_0}{k_1 - k_A} (\exp(-k_A t) - \exp(-k_1 t))$$

And the time dependence of the delayed fluorescence is given by

$$F(t) = \Phi_F k_{TTA} c_A^2$$

Where Φ_F is the fluorescence quantum yield of the excited singlet state of the acceptor. A fit of this model to the data yields the two rate constants and the amplitude. We observe values from 5.0 to $5.2 \times 10^4 \text{ s}^{-1}$ for k_A and values from 1.44 to $1.61 \times 10^6 \text{ s}^{-1}$ for k_1 . The amplitude increase linearly with the acceptor concentration (Figure 5.18).

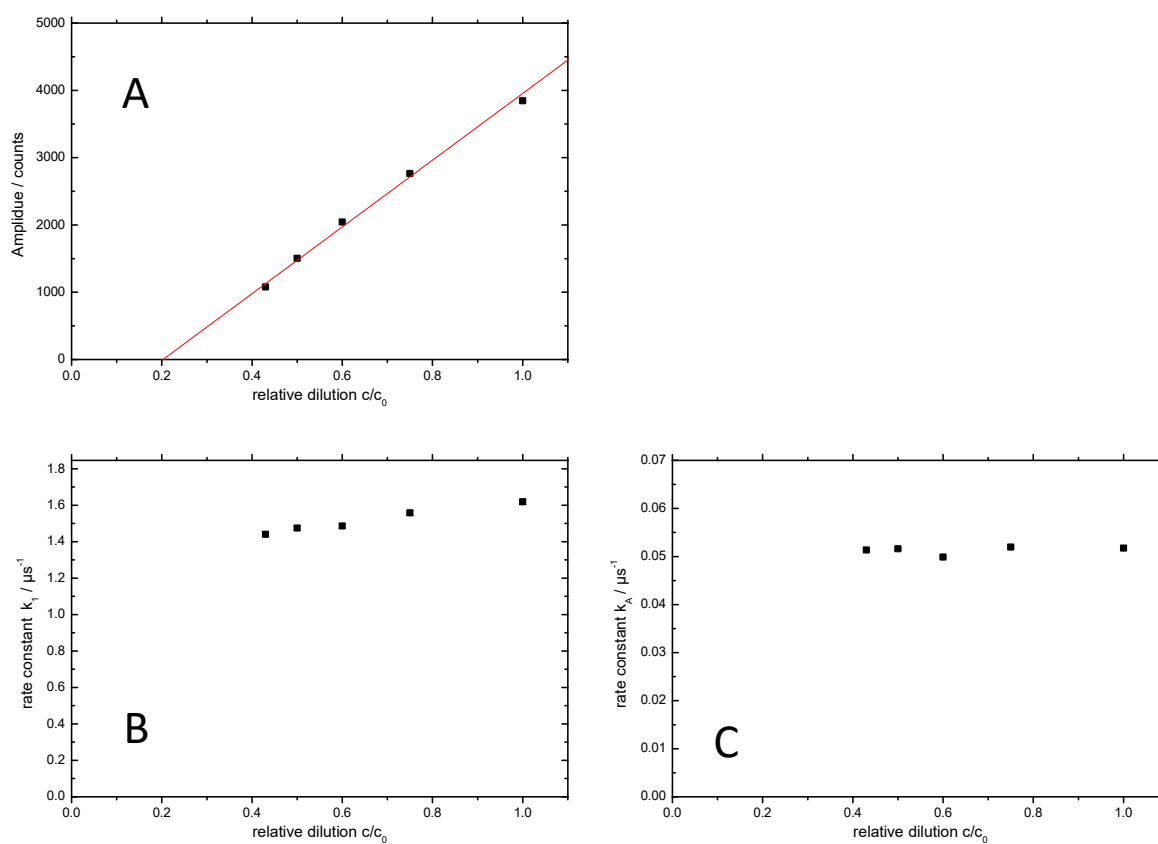
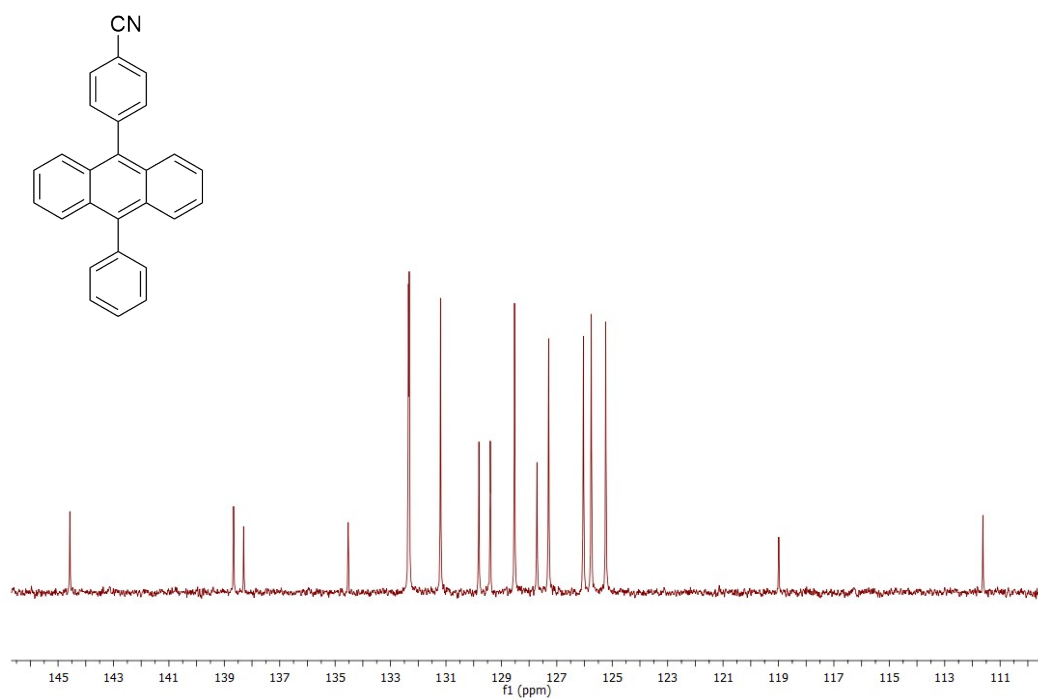
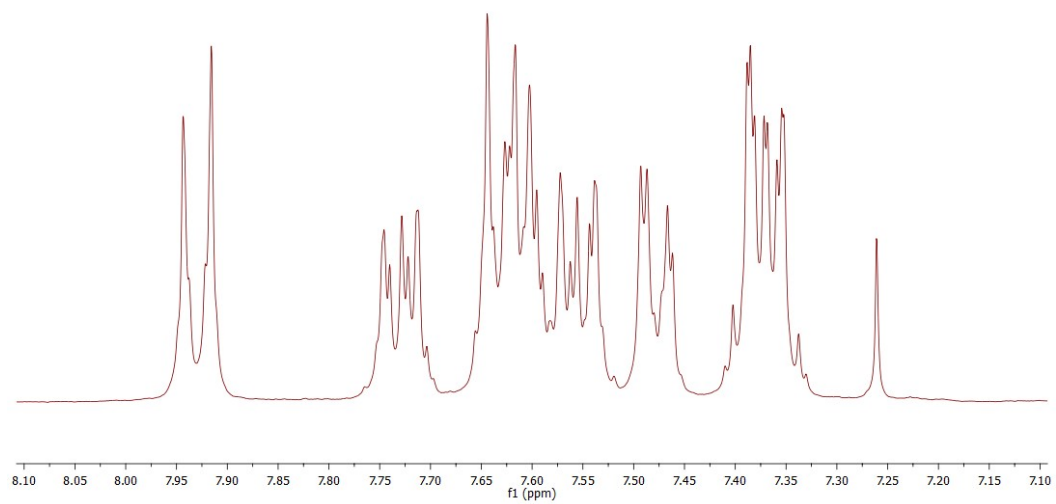
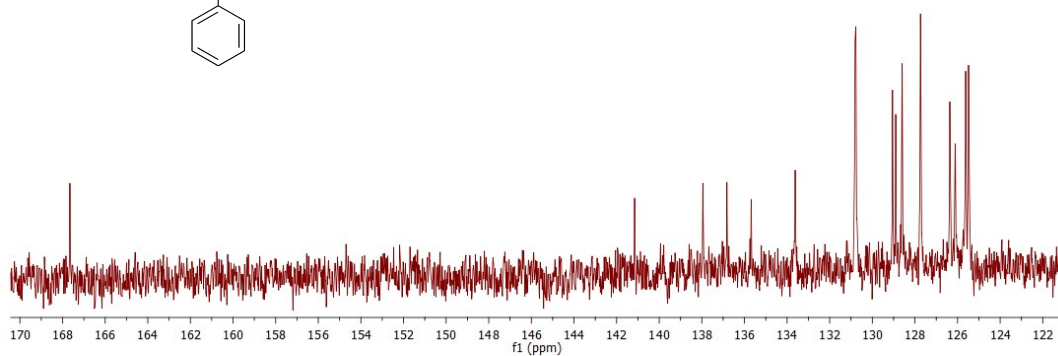
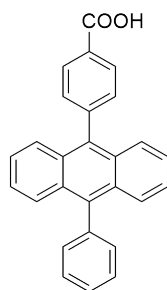
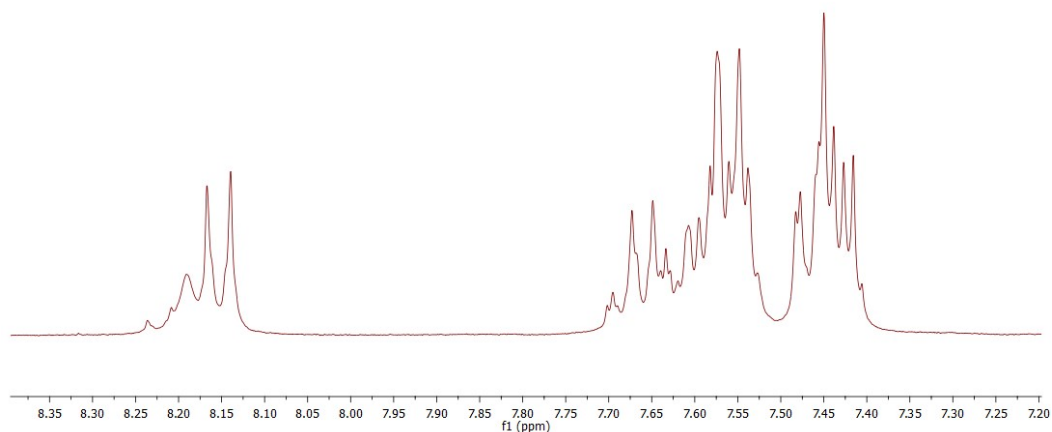
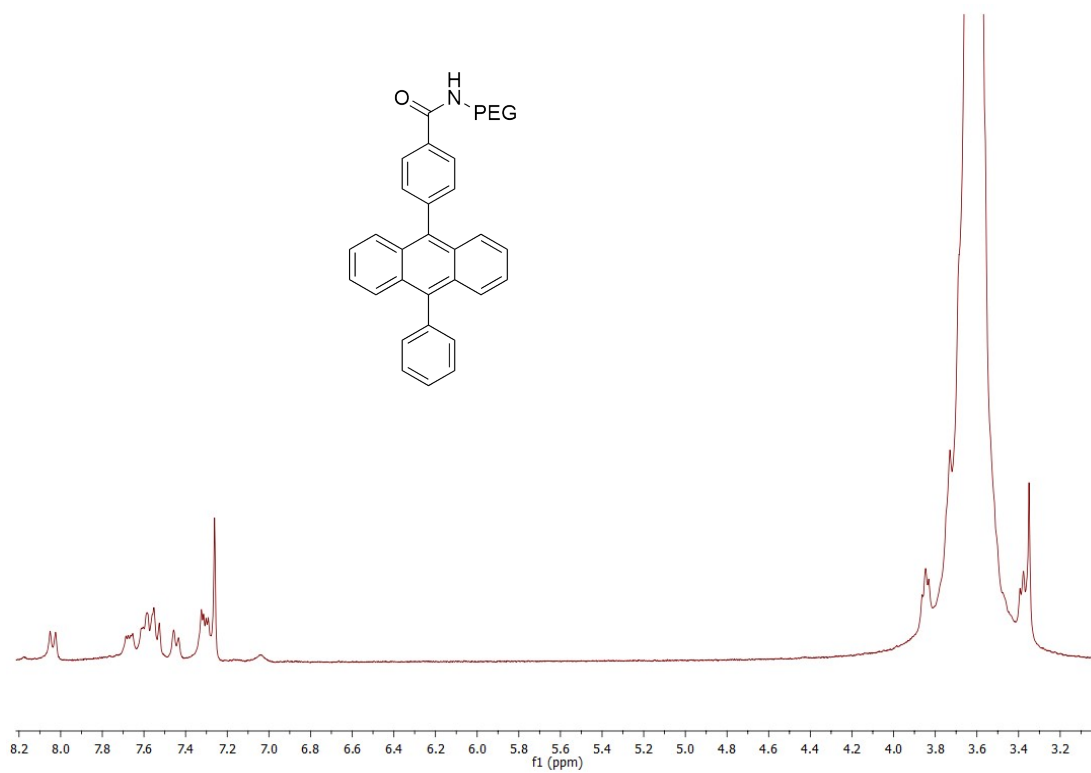


Figure 5.18 Plots of the Amplitude (A) rate constants k_A (B) and k_1 (C) vs the relative concentration of vesicles corresponding to the measurements displayed in Figure 5.17.

5.4.5 NMR spectra







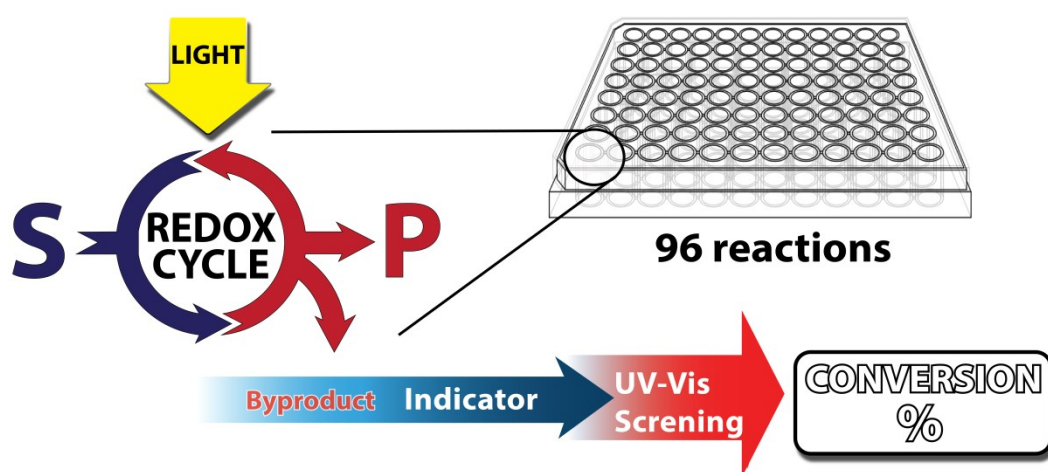
5.5 References

- ‡ The compared fluorescence emission intensities belong to systems with different absorption spectra.
- § The Intensity is the sum of all counting events from 2 μ s after excitation to the end of the measurement from 365 to 480 nm.
1. Huang, X.; Han, S.; Huang, W.; Liu, X., Enhancing solar cell efficiency: the search for luminescent materials as spectral converters. *Chem. Soc. Rev.* **2013**, *42* (1), 173-201.
 2. He, G. S.; Tan, L.-S.; Zheng, Q.; Prasad, P. N., Multiphoton Absorbing Materials: Molecular Designs, Characterizations, and Applications. *Chem. Rev.* **2008**, *108* (4), 1245-1330.
 3. Scheps, R., Upconversion laser processes. *PROG QUANT ELECTRON* **1996**, *20* (4), 271-358.
 4. Singh-Rachford, T. N.; Castellano, F. N., Photon upconversion based on sensitized triplet-triplet annihilation. *Coord. Chem. Rev.* **2010**, *254* (21-22), 2560-2573.
 5. Briggs, J. A.; Atre, A. C.; Dionne, J. A., Narrow-bandwidth solar upconversion: Case studies of existing systems and generalized fundamental limits. *J. Appl. Phys.* **2013**, *113* (12), 124509.
 6. Borisov, S. M.; Larndorfer, C.; Klimant, I., Triplet-Triplet Annihilation-Based Anti-Stokes Oxygen Sensing Materials with a Very Broad Dynamic Range. *Adv. Funct. Mater.* **2012**, *22* (20), 4360-4368.
 7. Tzenka, M.; Vladimir, Y.; Gabriele, N.; Stanislav, B., Annihilation assisted upconversion: all-organic, flexible and transparent multicolour display. *New J. Phys.* **2008**, *10* (10), 103002.
 8. Liu, Q.; Yang, T.; Feng, W.; Li, F., Blue-Emissive Upconversion Nanoparticles for Low-Power-Excited Bioimaging in Vivo. *J. Am. Chem. Soc.* **2012**, *134* (11), 5390-5397.
 9. Balushev, S.; Yakutkin, V.; Miteva, T.; Wegner, G.; Roberts, T.; Nelles, G.; Yasuda, A.; Chernov, S.; Aleshchenkov, S.; Cheprakov, A., A general approach for non-coherently excited annihilation up-conversion: transforming the solar-spectrum. *New J. Phys.* **2008**, *10* (1), 013007.
 10. Zhao, J.; Ji, S.; Guo, H., Triplet-triplet annihilation based upconversion: from triplet sensitizers and triplet acceptors to upconversion quantum yields. *RSC Adv.* **2011**, *1* (6), 937-950.
 11. Boutin, P. C.; Ghiggino, K. P.; Kelly, T. L.; Steer, R. P., Photon Upconversion by Triplet-Triplet Annihilation in Ru(bpy)₃- and DPA-Functionalized Polymers. *J. Phys. Chem. Lett.* **2013**, *4* (23), 4113-4118.

12. Simon, Y. C.; Weder, C., Low-power photon upconversion through triplet-triplet annihilation in polymers. *J. Mater. Chem.* **2012**, *22* (39), 20817-20830.
13. Tanaka, K.; Inafuku, K.; Chujo, Y., Environment-responsive upconversion based on dendrimer-supported efficient triplet-triplet annihilation in aqueous media. *Chem. Commun.* **2010**, *46* (24), 4378-4380.
14. Katta, K.; Busko, D.; Avlasevich, Y.; Muñoz-Espí, R.; Balushev, S.; Landfester, K., Synthesis of Triplet-Triplet Annihilation Upconversion Nanocapsules Under Protective Conditions. *Macromol. Rapid Commun.* **2015**, *36* (11), 1084-1088.
15. Ceroni, P., Energy Up-Conversion by Low-Power Excitation: New Applications of an Old Concept. *Chem. Eur. J.* **2011**, *17* (35), 9560-9564.
16. Askes, S. H. C.; Mora, N. L.; Harkes, R.; Koning, R. I.; Koster, B.; Schmidt, T.; Kros, A.; Bonnet, S., Imaging the lipid bilayer of giant unilamellar vesicles using red-to-blue light upconversion. *Chem. Commun.* **2015**, *51* (44), 9137-9140.
17. Andrey, T.; Dmitry, B.; Stanislav, B.; Tzenka, M.; Katharina, L., Micellar carrier for triplet-triplet annihilation-assisted photon energy upconversion in a water environment. *New J. Phys.* **2011**, *13* (8), 083035.
18. Kim, J.-H.; Kim, J.-H., Encapsulated Triplet-Triplet Annihilation-Based Upconversion in the Aqueous Phase for Sub-Band-Gap Semiconductor Photocatalysis. *J. Am. Chem. Soc.* **2012**, *134* (42), 17478-17481.
19. Askes, S. H. C.; Kloz, M.; Bruylants, G.; Kennis, J. T. M.; Bonnet, S., Triplet-triplet annihilation upconversion followed by FRET for the red light activation of a photodissociative ruthenium complex in liposomes. *PCCP* **2015**, *17* (41), 27380-27390.
20. Merkel, P. B.; Dinnocenzo, J. P., Low-power green-to-blue and blue-to-UV upconversion in rigid polymer films. *J. Lumin.* **2009**, *129* (3), 303-306.
21. Hansen, M.; Li, F.; Sun, L.; Konig, B., Photocatalytic water oxidation at soft interfaces. *Chem. Sci.* **2014**, *5* (7), 2683-2687.
22. Rohatgi-Mukherjee, K. K., *Fundamentals of Photochemistry*. Wiley: 1978.
23. Kutta, R.-J.; Langenbacher, T.; Kensy, U.; Dick, B., Setup and performance of a streak camera apparatus for transient absorption measurements in the ns to ms range. *Appl. Phys. B* **2013**, *111* (2), 203-216.
24. Hu, J.-Y.; Pu, Y.-J.; Yamashita, Y.; Satoh, F.; Kawata, S.; Katagiri, H.; Sasabe, H.; Kido, J., Excimer-emitting single molecules with stacked [small pi]-conjugated groups covalently linked at the 1,8-positions of naphthalene for highly efficient blue and green OLEDs. *J. Mater. Chem. C* **2013**, *1* (24), 3871-3878.

25. Hu, J.-Y.; Pu, Y.-J.; Satoh, F.; Kawata, S.; Katagiri, H.; Sasabe, H.; Kido, J., Bisanthracene-Based Donor–Acceptor-type Light-Emitting Dopants: Highly Efficient Deep-Blue Emission in Organic Light-Emitting Devices. *Adv. Funct. Mater.* **2014**, *24* (14), 2064-2071.
26. Baek, N. S.; Kim, Y. H.; Roh, S. G.; Kwak, B. K.; Kim, H. K., The First Inert and Photostable Encapsulated Lanthanide(III) Complexes Based on Dendritic 9,10-Diphenylanthracene Ligands: Synthesis, Strong Near-Infrared Emission Enhancement, and Photophysical Studies. *Adv. Funct. Mater.* **2006**, *16* (14), 1873-1882.
27. Fischer, P. M.; Zheleva, D. I., Liquid-phase peptide synthesis on polyethylene glycol (PEG) supports using strategies based on the 9-fluorenylmethoxycarbonyl amino protecting group: application of PEGylated peptides in biochemical assays. *J. Pept. Sci.* **2002**, *8* (9), 529-542.
28. Poznik, M.; Maitra, U.; Konig, B., The interface makes a difference: lanthanide ion coated vesicles hydrolyze phosphodiester. *Org. Biomol. Chem.* **2015**, *13* (38), 9789-9792.

6 Fast colorimetric screening for visible light photocatalytic oxidation and reduction reactions



Fast screening accelerates the discovery and optimization of chemical reactions. Here, we present the parallel irradiation and evaluation of 96 visible light photocatalytic reactions in a microtiter plate. After completion, a chemical indicator is added, allowing the spectroscopic determination of the formed stoichiometric by-products. Their quantity correlates in many cases with the conversion of starting materials and yield of photochemical reaction products. We demonstrate the concept with known photooxidations of organic compounds by riboflavin tetraacetate (**RFTA**) and reproduce published results and gas chromatographic analyses by a colorimetric assay. Two new photocatalysts for the hydroxylation of boronic acids and new substrates for the photocatalytic generation of arylradicals from arylhalides were identified. By screening of a series of drug molecules containing arylhalides new photochemical dehalogenation reactions were found. The presented methods enable laboratories lacking sophisticated high-throughput instrumental analysis to perform parallel optimization and scope determination of photocatalytic oxidation and reduction reactions.

This chapter is a manuscript prepared for submission to a journal.

M. Poznik performed the experimental work and wrote the manuscript. B. König supervised the project and is corresponding author.

6.1 Introduction

The discovery of new reactions is of key importance in organic chemistry. For applications in synthesis new transformations must be optimized and their scope and limitations defined. This typically requires the exhaustive systematic variation of many reaction parameters. Individual yield determination by product isolation or calibrated chromatographic methods, such as GC or HPLC, is laborious, slow and expensive. In recent years organic chemists increasingly used advanced instrumentation and automation to accelerate discovery and optimization steps^{1, 2} leading to the development of various high throughput screening methods.^{3, 4} The scope of techniques ranges from multidimensional directed or undirected screens for reactivity discovery,^{5, 6, 7} over robustness⁸ and functional group tolerance^{9, 10} assays to parallel reaction optimization protocols.^{11, 12} These are usually performed in microvials or microfluidic system.^{13, 14} The bottleneck of such screening methods is typically the analysis of the reaction outcome, which often utilizes GC,¹⁵ HPLC¹⁶ and MS^{5, 6, 17} techniques. Even though analysis based on chromatographic separation of all compounds present in the reaction mixture, their identification and database correlation allows the most accurate and detailed evaluation of an experiment, such an approach is not available to all laboratories due to lack of equipment. We therefore present here a low cost colorimetric screening as an alternative for the initial assessment of photoredox catalytic reactions (Figure 6.1). Naturally, less accurate analysis will provide less reliable evaluation results, but this limitation may be compensated by the faster and broader application in laboratories lacking high end instrumentation.

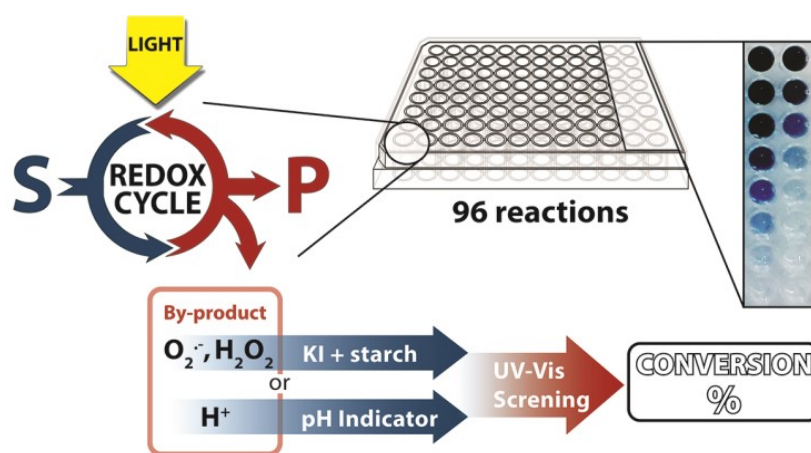


Figure 6.1 Parallel screening of visible light photocatalytic reactions generating oxidative by-products or protons. S = starting material; P = product.

Visible light photocatalytic transformations have received a lot of attention in organic synthesis over the last decade.^{18, 19, 20, 21, 22, 23, 24} MacMillan showed with his approach of accelerated serendipity that by random high-throughput screening, new reactions can be discovered, and a mechanism-based screening method to accelerate discovery was recently reported by Glorius.²⁵ A focused screening of radical photo-catalysed methylations by DiRocco demonstrated reactions in microtiter plates linked with UPLC-MS for the optimization of solvent and catalyst combination.²⁶

An alternative screening procedure that does not require high end instrumentation may be based on a colorimetric assay.²⁷ They are easy to perform and evaluate. Numerous indicators were developed for the specific detection of functional groups,^{28, 29, 30, 31, 32} but this limits a general applicability. However, many photoredox reactions need a sacrificial electron donor or acceptor to complete the catalytic cycle. During this process, a few typical by-products are formed. While the substrates and products of different reactions may vary in their properties and structure, the by-products often remain identical, *e.g.* reduced dioxygen species such as H_2O_2 , $\text{O}_2^{\bullet-}$ or simply protons. Examples of reactivity screening using by-product analysis were reported before, but not applied recently or to photocatalytic reactions.^{33, 34, 35, 36} We describe a simple colorimetric indicator method to detect and quantify by-products of 96 photocatalytic reactions simultaneously. The by-product formation in these oxidation or dehalogenation reactions correlates in many cases with the reaction conversion and even with the product yield.

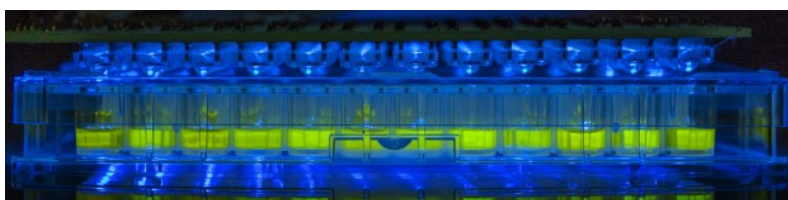


Figure 6.2 96 Well plate with LED irradiation.

Reactions were carried out in disposable polystyrene or clear polypropylene (for non-aqueous solutions) microtiter plates. Irradiation was performed with a custom-made 96 LED array. Each LED is positioned above one well and cooling is provided from the bottom (Figure 6.2). Reactions using oxygen as terminal oxidant were carried out at room temperature in air. Exclusion of oxygen was possible performing the reactions in a custom-made PMMA box flushed with nitrogen (see experimental part, Figure 6.14).

6.2 Results and discussion

6.2.1 Screening of photocatalytic oxidations

Air oxygen is a typical terminal oxidant in many photooxidation reactions generating hydrogen peroxide, superoxide anion or other reactive oxygen species. Mixtures of potassium iodide with starch give a strong blue colour when iodide is oxidized to iodine, which then forms a complex with amylose.^{37, 38} Starch indicator was previously employed in screening methods, but usually as an indicator of produced iodine and not hydrogen peroxide.^{31, 39} The reaction is very sensitive and can detect amounts of hydrogen peroxide as small as 50 μM when optimized for the microtiter plate reader (see experimental part, Figure 6.8). Fresh indicator was used for every measurement. In order for the indicator to work properly, the pH needs to be acidic and water is added in the detection step if the photoreactions were performed in organic solvents (see experimental part, Figure 6.10).

The well described photooxidation of benzyl alcohols and benzyl amines to benzaldehydes by riboflavin tetraacetate (**RFTA**) (Figure 6.3) was used to evaluate the screening method.^{40, 41} The photooxidation produces equimolar amounts of hydrogen peroxide when converting substrates to products.⁴² For a fast screening the reaction mixtures were only irradiated for 15 min; initial conversions produce sufficient hydrogen peroxide for a reliable detection and reaction conditions are more defined at low conversions facilitating a relative comparison.⁴³ Three benzyl alcohols were oxidized to the corresponding benzaldehydes and the reaction mixtures from the microtiter plate were analysed by GC and simultaneously evaluated spectroscopically after indicator addition (Figure 6.3). The product yield was estimated from the amount of released hydrogen peroxide determined by the KI-starch indicator using a calibration. Both methods provided very similar results, showing that the amount of hydrogen peroxide reflects the product formation in this photooxidation. For the screening of different substrates, relative reactivities are more useful than absolute yields. Therefore we normalized the obtained colorimetric response to the best converted substrate and correlated others by their relative reactivity. We expanded the scope of the screened benzyl alcohols. As expected from literature,⁴¹ electron-rich derivatives react best. Using published reaction conditions for the oxidation of benzylamines in the microtiter plate assay gave relative reactivities, which reflect the reported yields of completed reactions very well.⁴⁴ This shows that indicator response based on initial rates of reactions qualitatively correlates with isolated reaction yields for these photooxidations. Substrates that only serve as electron donor for the flavin, but are not converted into aldehydes, such as butylamine, can give stronger or weaker

false positive results.[†] The critical evaluation of the produced data is essential for most indirect screening methods.

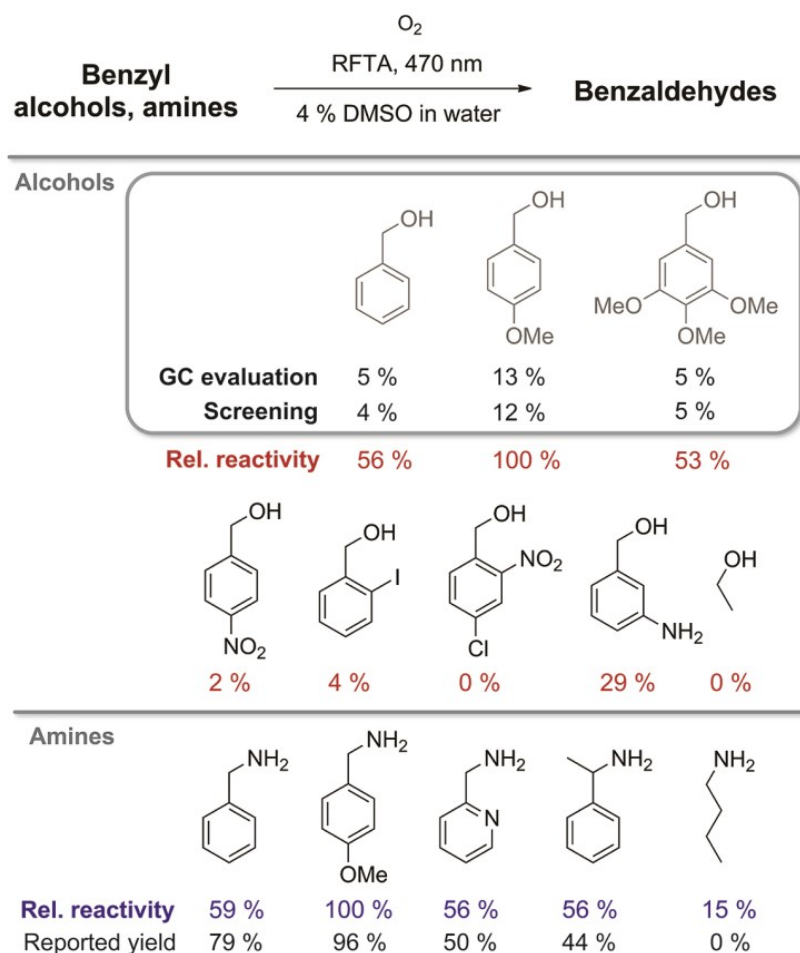


Figure 6.3 Solutions containing RFTA (1 mol. %) and the respective substrate were irradiated for 15 min in a microtiter plate (in MilliQ water with 4 % DMSO). Conversion was evaluated by a KI-starch indicator or with GC analysis. The relative reactivity of benzylamines was compared with reported product yields.⁴⁴

In the photocatalytic transformation of arylboronic acids to aryl alcohols introduced by *Zou et al.*, a photocatalytically produced superoxide radical is being consumed in the reaction (Figure 6.4).⁴⁵ Ruthenium-tris(bipyridiene) (**Ru(bpy)₃**) was initially used as photocatalyst and later replaced by methylene blue, rose bengal, MOFs and flavin derivatives.^{46, 47, 48, 49, 50, 51, 52} The presence of the reactive oxygen species in the mechanism inspired us to study this reaction in a screening approach with the goal to identify other organic photocatalysts and further optimize the reaction conditions (Figure 6.4).

We selected two catalysts with high oxidation potential: flavin **RFTA** and 9-mesityl-10-methylacridinium perchlorate (**ACR**). First we investigated different aliphatic amines as sacrificial electron donor. Triethyl amine was identified as donor with the highest photocatalytic production of superoxide radical anions. In the presence of boronic acid, the generated oxidant is consumed. The quantified amount of the photogenerated oxidant in the presence and in the absence of the boronic acid therefore indicates the reaction conversion.

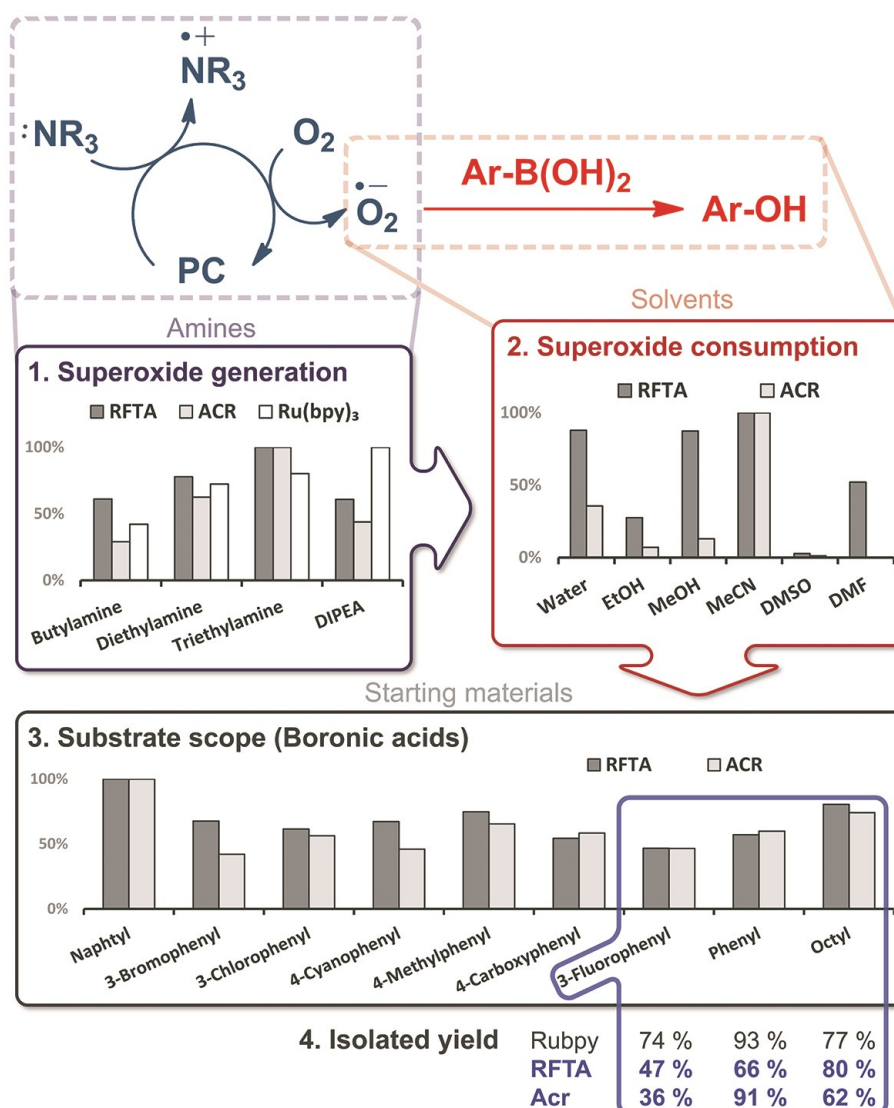


Figure 6.4 Optimization of **RFTA** and **ACR** as photocatalysts in the hydroxylation of boronic acids. The conditions are compared for three compounds with reported reaction conditions for **Ru(bpy)₃** catalyst after 16 h of irradiation (455 nm). Y axes represent relative reactivity.

This difference was recorded for 6 commonly used solvents; acetonitrile provided the best results. For comparison of a reaction in different solvents the indicator response was normalized (see experimental part, Table 6.3).[‡] The identified best conditions were then used for larger-scale, batch reactions of three substrates giving comparable yields after 16 h of irradiation as the previously used ruthenium catalyst under reported conditions (Figure 6.4).⁴⁵

6.2.2 Screening of photocatalytic reductions

Aryl halides have been photocatalytically transformed into aryl radicals, which can abstract a hydrogen atom yielding the corresponding dehalogenated product. Other reaction pathways are C-H arylation or addition to double bonds (Figure 6.5).^{53, 54} All reactions produce as stoichiometric by-product the corresponding acid H-X.⁵⁵ Although in many cases a base is used in excess to ensure high yields, pH changes may indicate the relative reactivity of different substrates or best conditions. We recently reported the visible light photoreduction of arylhalides,⁵⁵ using different perylene-3,4,9,10-bis(dicarboximide) (**PDI**) dyes as photocatalysts. The photocatalytic reaction of 4-bromoacetophenone with 1 eq. of DIPEA resulted in a slightly acidic reaction medium of approximately pH = 5. We therefore selected bromocresol green (**BCG**) as an appropriate indicator for this pH range. Reaction mixtures, in which the photocatalytic dehalogenation proceeds, give after addition of **BCG** a yellow colour, while a blue colour is observed for non-successful reaction trials (see experimental part, Figure 6.19). We correlated the relative change in absorbance at the indicator λ_{\max} absorption (617 nm) to a relative reactivity of the aryl halides investigated. All reactions were performed in DMF with 1 eq. DIPEA using **PDI**, **Ir(bpy)₃** and **Ru(ppy)₃** as photocatalysts under 470 nm irradiation (Figure 6.5).⁵⁶

In DMF solution the aryl radical abstracts a proton from the solvent or the sacrificial electron donor DIPEA and the dehalogenation product is formed.⁵⁷ Representative aryl halides were selected covering a wide range of reduction potentials to explore the substrate limits of the three photocatalysts.⁵⁸ Compounds octadecylbromide, 3-bromopyridine, 2-bromonaphthalene and 4-bromoanisole, which are very difficult to reduce, show only negligible colorimetric response (<10%). They are outside the available reduction potential of the investigated catalysts under the reaction conditions and no conversion can be expected. However, compounds from 9-bromoanthracene to 4-chlorobenzonitrile (Figure 6.5) requiring reduction potentials matching the reducing power of the catalysts, produce a detectable colour change (>10%). No colour change was detected in the case of 2-bromonitrobenzene, even though it has a redox potential lower than -1 V vs. SCE, and should therefore be reduced. Previous findings showed that 2-bromonitrobenzene is unable to produce the aryl

radical, as the radical anion is very stable and back electron transfer is favoured.⁵⁸ Conversion of 9-bromoanthracene to anthracene was monitored by UV-Vis spectra changes (see experimental part, Figure 6.20). Selected reactions of the screening were repeated on larger scale (10 eq. DIPEA, 455 nm) and the reaction outcome monitored by GC. The yields of the dehalogenated products correlate well with the relative reactivity derived from the colorimetric screening. The quick assay reproduces the accessible substrate scope and limitation of the three catalysts for the photocatalytic reaction well.

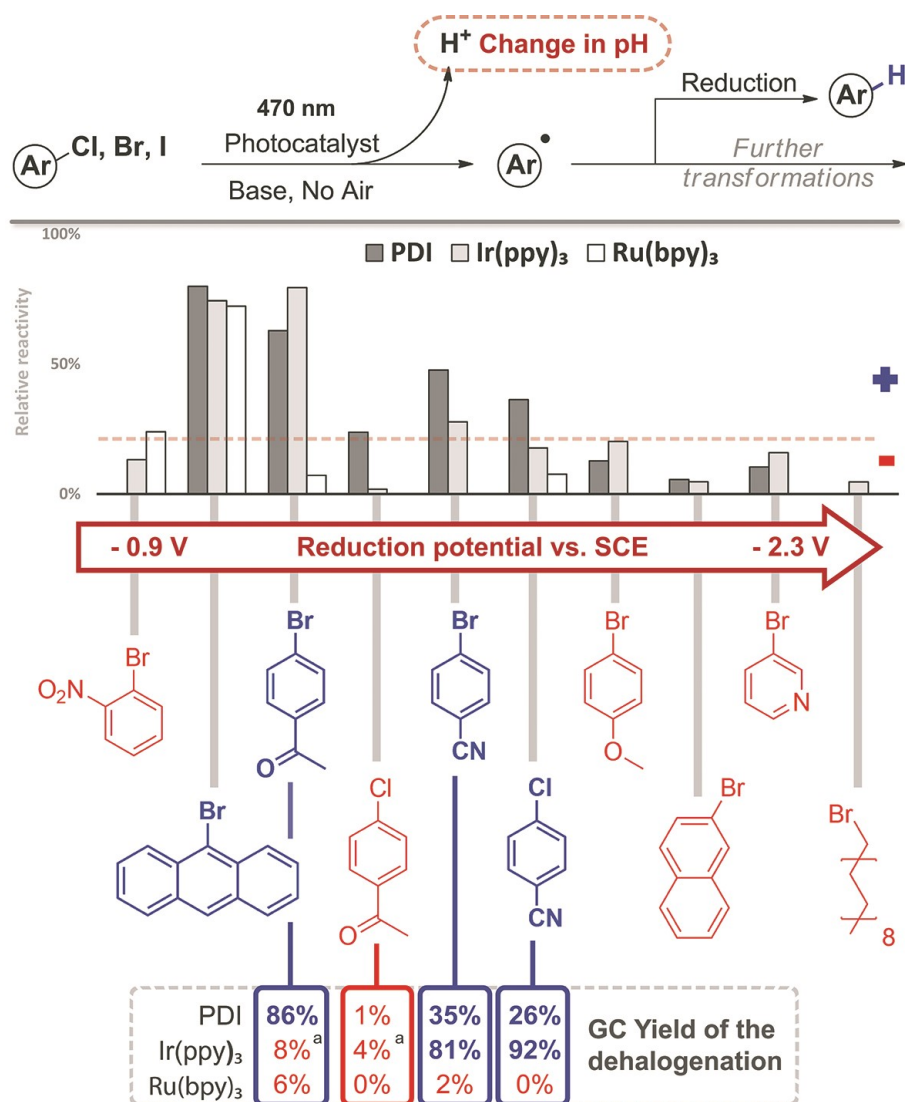


Figure 6.5 Screening results of the reduction of arylhalides. The compounds are given in the order of increasing reduction potential (V vs. SCE) potential.⁵⁸ Reaction conditions: (1 h, 470 nm, DMF, 1 mM substrate, 1 eq. DIPEA, 1 mol. % catalyst). GC comparison for selected compounds (12 h, 455 nm, DMF, 20 mM substrate, 10 eq. DIPEA, 1 mol. % catalyst (10 % for PDI)). ^a Full conversion but no yield of reduction product.

Next, a series of heteroaromatic halides were investigated for photocatalytic dehalogenation using the same procedure (Figure 6.6). 2-Chloropyrazine, 2-bromobenzophenone and 5-bromonicotinamide in combination with PDI or Ir(ppy)₃ showed moderate conversion in the assay (>10%), which was confirmed by GC, producing the corresponding dehalogenated compounds, although only in low to moderate yield.

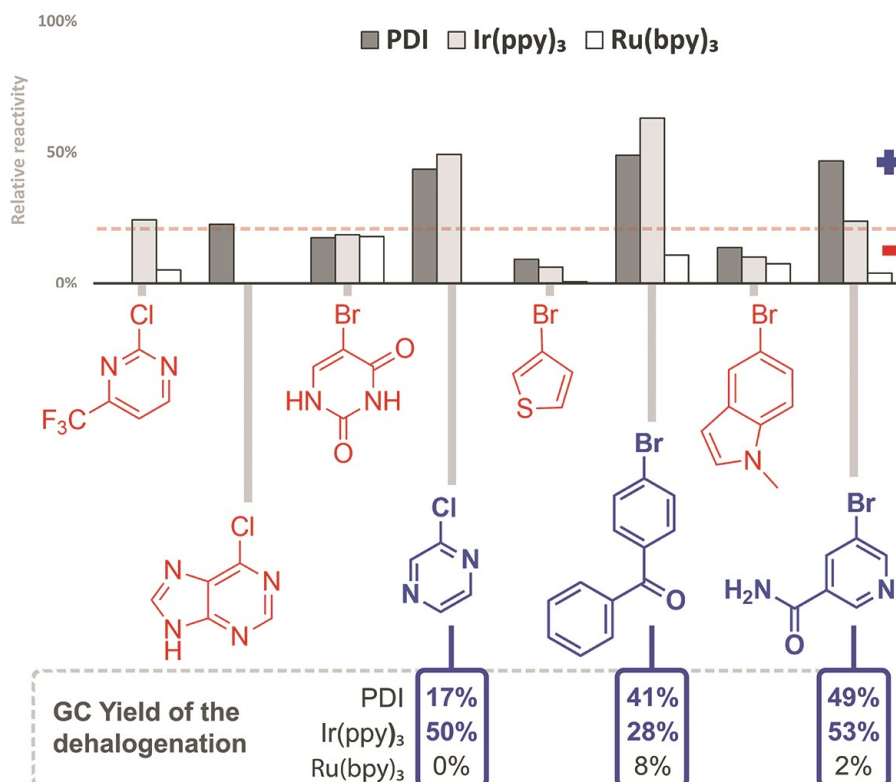


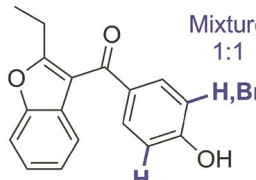
Figure 6.6 Screening results of the reduction of heteroaryl halides. Reaction conditions (1 h, 470 nm, DMF, 1 mM substrate, 1 eq. DIPEA, 1 mol. % catalyst) and its comparison with GC measurement (12h, 455 nm, DMF, 20 mM substrate, 10 eq. DIPEA, 1 mol. % catalyst (10 % for PDI)).

To test our method for the reactivity screening of more complex substrates, we selected fifteen commercially available drugs (structures available in experimental part) with arylhalide moiety (Table 6.1). The compounds were screened for a photocatalytic dehalogenation using the described assay. For three compounds, the acidification of the reaction mixture indicated a possible reactivity, and these were investigated individually on larger scale. The indication for bromazepam was found to be a false positive; the compound does not convert into the expected product. In the case of hydrochlorothiazide and benzbromarone we were able to isolate the dehalogenation products in moderate to good

yield (Table 6.1, bottom) applying any of the three tested catalysts. This shows that our method is useful for an initial reactivity screening of more complex molecules with different functional groups.

	PDI	Ir(ppy) ₃	Ru(bpy) ₃
Ambroxol-HCl	-	-	-
Amlodipinbesilat	-	-	-
Atorvastatin-Ca	-	-	-
Benzbromarone	-	• ^c	• ^a
Bromazepam	• ^d	-	-
Chlordiazepoxid	-	-	-
Diazepam	-	-	-
Glibenclamide	-	-	-
Griseofulvin	-	-	-
Hydrochlorothiazide	• ^b	• ^b	-
Meclofenoxate-HCl	-	-	-
Metoclopramide	-	-	-
Miconazole	-	-	-
Norfloxacin	-	-	-
Oxazepam	-	-	-

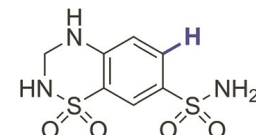
a,



Mixture 1:1

48 h, 455 nm, DMF, 10 eq. DIPEA
1 mol % Ru(bpy)₃ (**80 %**)

b,



48 h, 455 nm, DMF, 10 eq. DIPEA
10 mol % PDI (**10 %**)
1 mol % Ir(ppy)₃ (**20 %**)

Table 6.1 Screening of aryl-halide-moiety-containing commercial drugs for their possible photocatalytic dehalogenation: no response (-), moderate response (•). ^a Mixture of mono and di dehalogenated benzbromarone, ^b Dechlorinated hydrochlorothiazide. ^c Deeper fragmentation of the substrate. ^d No or very weak reaction.

6.2.3 Screening of photocatalyst stability

Crucial for all catalytic reactions is the stability of the catalyst. The photostability of the photocatalysts under the reaction conditions is essential to achieve a good overall performance of the reaction. We investigated therefore the potential bleaching of several typical photocatalysts under different reaction conditions. The dyes were tested in different solvents with addition of base (NaOH) or acid (CF₃COOH) in air and in nitrogen atmosphere (Table 6.2, for exact values see experimental part, Table 6.5). The summarized stability results

6.3 Conclusions

We have described and validated a simple high-throughput reactivity screening for photocatalytic reactions based on colorimetric detection of by-products. Reactive oxygen species and changes in pH were semi-quantitatively detected to monitor the reaction conversion of photooxidations and photodehalogenations. Using flavin photooxidations of benzyl alcohols and benzyl amines as example, the relative reactivities derived from the indicator responds reflect very well the reported product yields for the respective substrate. For the photooxidative conversion of boronic acids into phenols we identified two new photocatalysts by screening. As example for photoreduction reactions, the colorimetric screening for arylhalide dehalogenation was developed, and the indicator results were confirmed by GC for several substrates including more complex drug molecules. The reported method may find use for a facile initial screening of photocatalytic reactions and be a helpful tool in exploring reactivity or optimization without the need for sophisticated instrumentation. Using the described by-product detection by indicator approach enables laboratories with limited analytical capacities paralyzed screening, which may accelerate the discovery and application of new photocatalytic transformation in synthesis.

6.4 Experimental part

6.4.1 General methods and materials

General

All compounds and solvents were purchased from Sigma-Aldrich or Acros and used as delivered. UV-Vis clear flat bottom polystyrene and polypropylene 96 well microtiter plates were purchased from Grenier bio-one. In reactions with solvents, polypropylene microtiter plates were used. In all experiment was used deionised MiliQ water. Buffered solutions were prepared according to known literature.⁵⁹

NMR-Spectroscopy

NMR-spectra were recorded on a Bruker Avance 300 (¹H: 300 MHz, ¹³C: 75 MHz, T = 295 K) using the solvent residual peak as internal reference (CDCl₃: δ H 7.26). The chemical shifts are reported in δ [ppm] relative to internal standards (solvent residual peak). The spectra were analysed by first order, the coupling constants *J* are given in Hertz [Hz]. Integration is determined as the relative number of atoms. Error of reported values: chemical shift: 0.01 ppm for ¹H-NMR, 0.1 ppm for ¹³C-NMR and 0.1 Hz for coupling constants. The solvent used is reported for each spectrum.

GC chromatography

Performed using capillary column (length: 30 m; diam. 0.25 mm; film: 0.25 μ) with helium gas as carrier. Quantitative analysis was performed with an FID detector.

Spectroscopy

Absorption spectroscopy using microtiter plates was carried out by a plate reader OMEGA Fluorostar.

6.4.2 Indicators

KI-starch

The redox indicator consists of a solution of KI (0.1 mM) and starch (1 mg/mL) in MiliQ water with acetic acid (5 μL/mL). KI and starch were prepared as stock solutions in tenfold concentration and used for preparing the indicator prior to the measurement. The starch stock solution was boiled for 10 min to allow starch dissolving and used after cooling. If not stated differently, addition of 100 μL of indicator solution was used in each well to determine

the amount of produced hydrogen peroxide. Indicator response was measured as the difference of the optical densities at the absorption maxima (570 nm) of the formed complex between measured sample and blank (Figure 6.7). As a blank experiment, we used a sample with the same volume of solvent, while omitting the catalyst or the substrate. The read out for each well was obtained as the average of three measurements (every 20 s) five minutes after the addition of the indicator. The given values for each reaction are the average of at least three separate measurements (wells).

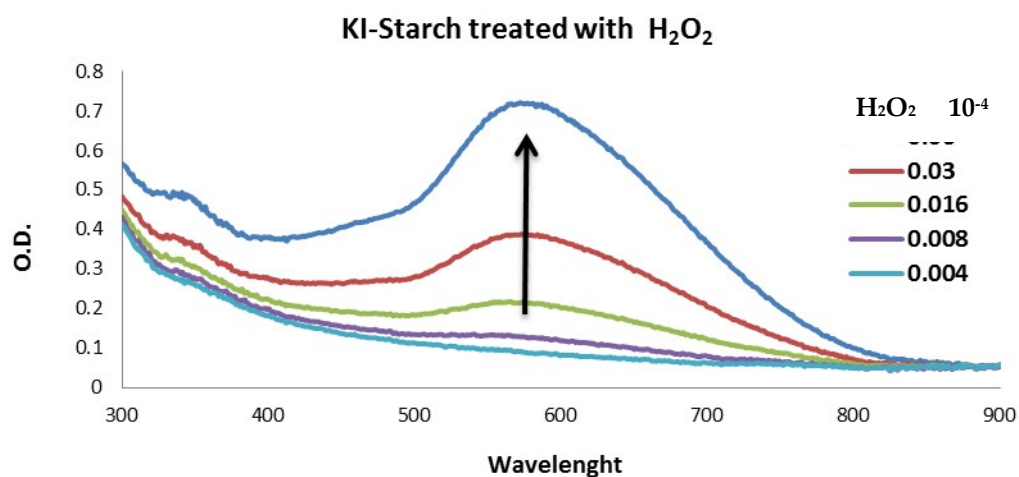


Figure 6.7 Recorded spectra of the KI-starch indicator after addition of hydrogen peroxide.

Indicator response to changing pH was measured using a series of citrate and phosphate buffers and a constant concentration of hydrogen peroxide (0.001 %) (Figure 6.8, left).

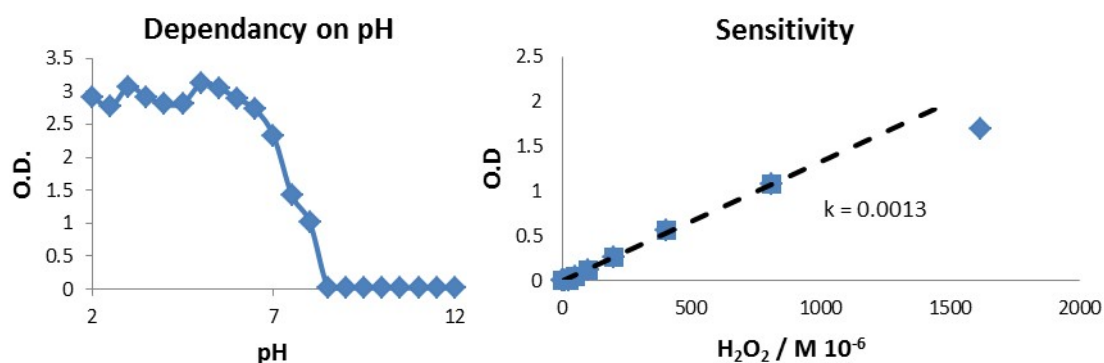
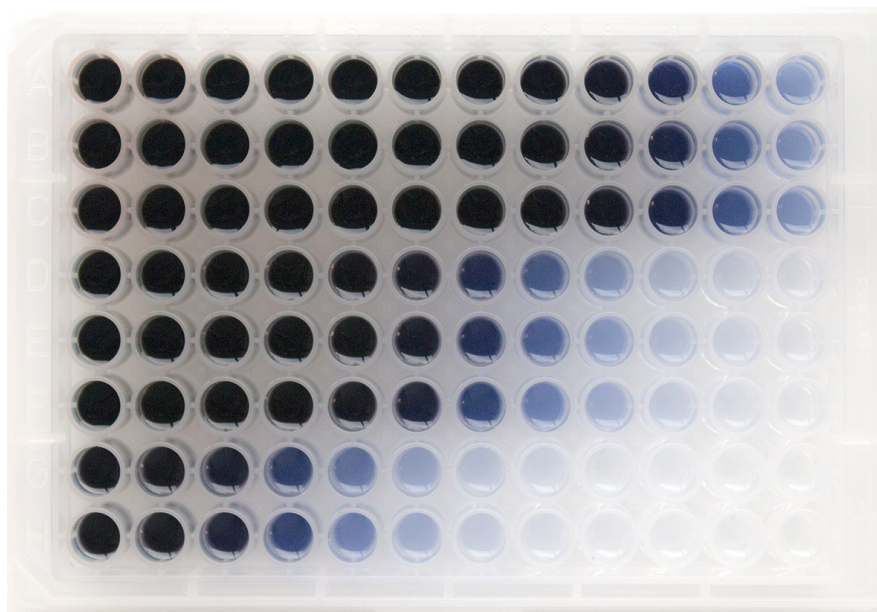


Figure 6.8 KI-starch indicator tested in microtiter plate reader for different pH (left) and different concentrations of H_2O_2 (right).

The sensitivity was measured in pure MiliQ water with changing concentration of hydrogen peroxide (Figure 6.8, right). All presented data were measured under conditions where the optical density of the indicator response did not exceed 1, hence Lambert-Beer law can be applied and calibration can be used (Figure 6.8, right).[§]



	1	2	3	4	5	6	7	8	9	10	11	12
A	1%	0.5%	0.3%	0.1%	0.06%	0.03%	0.02%	0.008%	0.004%	0.002%	0.001%	0.0005%
B	1%	0.5%	0.3%	0.1%	0.06%	0.03%	0.02%	0.008%	0.004%	0.002%	0.001%	0.0005%
C	1%	0.5%	0.3%	0.1%	0.06%	0.03%	0.02%	0.008%	0.004%	0.002%	0.001%	0.0005%
D	0.1%	0.05%	0.03%	0.01%	0.006%	0.003%	0.002%	0.0008%	0.0004%	0.0002%	0.0001%	0.00005%
E	0.1%	0.05%	0.03%	0.01%	0.006%	0.003%	0.002%	0.0008%	0.0004%	0.0002%	0.0001%	0.00005%
F	0.1%	0.05%	0.03%	0.01%	0.006%	0.003%	0.002%	0.0008%	0.0004%	0.0002%	0.0001%	0.00005%
G	0.01%	0.005%	0.003%	0.001%	0.0006%	0.0003%	0.0002%	0.0001%	0.00004%	0.00002%	0.00001%	0.000005%
H	0.01%	0.005%	0.003%	0.001%	0.0006%	0.0003%	0.0002%	0.0001%	0.00004%	0.00002%	0.00001%	0.000005%

Figure 6.9 Example of microtiter plate with gradient of hydrogen peroxide after 1 hour.

Indication in water:solvent mixtures

Response of the KI-Starch indicator to the presence of 0.01 % hydrogen peroxide in different aq. solutions of commonly used solvents was examined (Figure 6.10, left). As the ideal ratio, 80% of water in solvent was selected. Therefore all reactions, which were performed in organic solvents, were in 50 μ L scale and for evaluation 200 μ L of indicator solution was used to obtain the desired water content. For these solvent mixtures we measured linear dependencies on the hydrogen peroxide content (Figure 6.10, right).

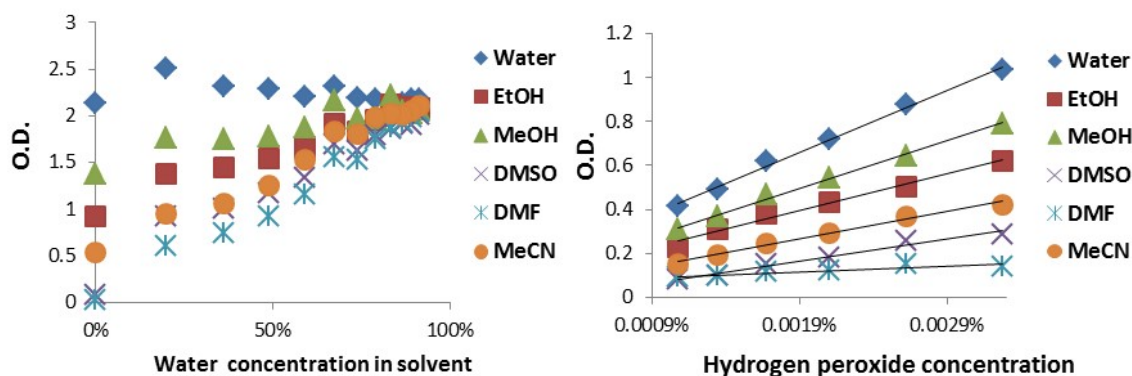


Figure 6.10 Response of the KI-Starch indicator on hydrogen peroxide in different solvent:water mixtures (left) and in water:solvent (80:20) mixtures for changing hydrogen peroxide concentration (right).

From the slope of the linear regression, an empirical solvent constant $a_{(\text{solvent})}$, which was used for calculation of the correct amount of produced hydrogen peroxide in different solvents, was derived. This constant resembles the calibration of the indicator response in different solvent normalized for water.

	Water	EtOH	MeOH	DMSO	DMF	MeCN
Slope	1181	454	875	281	433	773
$a_{(\text{solvet})}$	1.00	2.60	1.35	4.20	2.73	1.53

Table 6.3 Derived established solvent constants for the KI-Starch indicator.

pH Indicators

All pH indicators were used as a solutions (0.1 mM) in a mixture of ethanol:water (1:10). 50 μL of the indicator solution was always used per well. Response was measured as a change in optical density at the maxima of the respective indicator (phenolphthalein (555 nm), bromocresol green (615 nm), bromthymol blue (615 nm), methyl orange (507 nm)). All indicators were examined on the microtiter plate using buffered solutions (Figure 6.11).

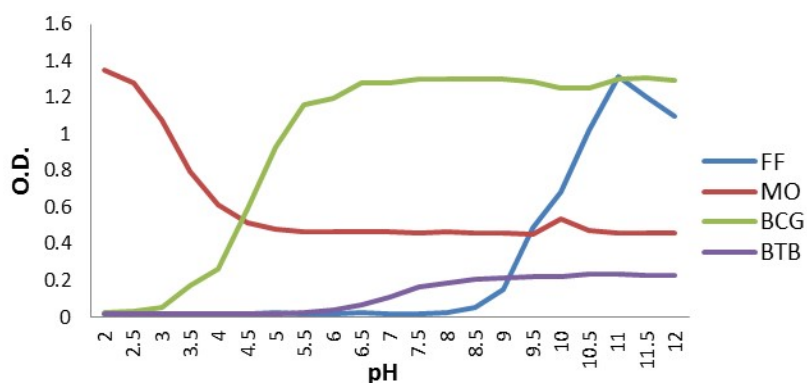


Figure 6.11 Different pH indicators (200 μ L volume in well, 0.05 mM): Phenolphthalein (FF), Bromocresol green (BCG), Bromthymol blue (BTB), Methyl orange (MO).

6.4.3 Reactor

Construction

The reactor consists of two parts (Figure 6.12). A hollow aluminum block at the bottom provides water cooling. It is manufactured to precisely hold the microtiter plate in the way that the metal is in contact with the flat bottom of the wells providing maximum cooling efficiency. Irradiation was carried out by a custom made 96 LED array positioned above the microtiter plate. Every well was irradiated by blue LED Superflux (LT-1229) at 20 mA. For experiments where oxygen has to be excluded, a PMMA box with appropriate connection and insulation was built, and the whole reactor was placed inside it (Figure 6.12, right).

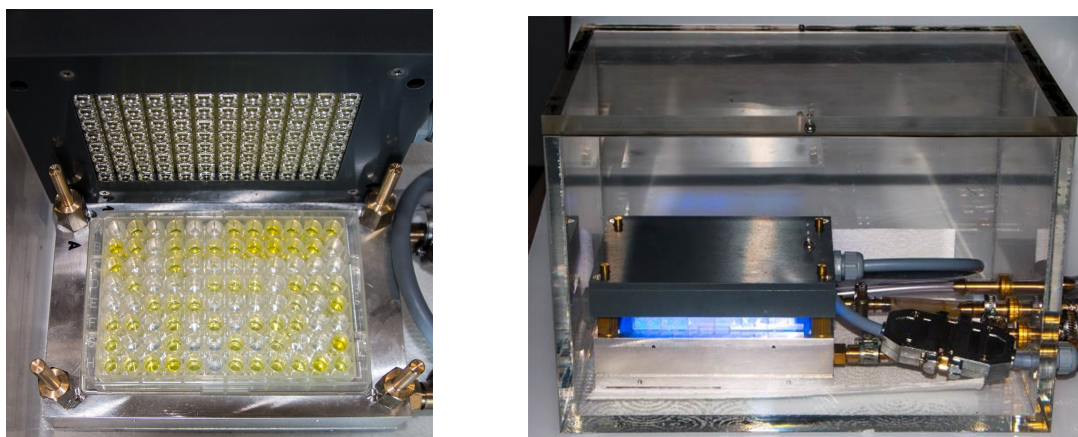
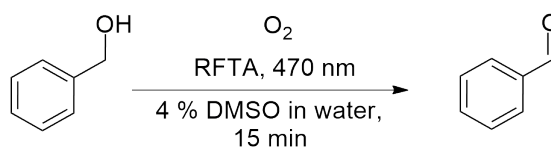


Figure 6.12 Experimental setup for microtiter plate irradiation.

Homogeneity of irradiation and error of the measurement

To test if the conditions are homogenous in the reactor an established reaction was performed in each well of the microtiter plate and evaluated by addition of KI-starch indicator (Scheme 6.1). Solution of benzyl alcohol (10 mM) and RFTA (0.1 mM) was prepared in aq. solution of DMSO (4 %) and 100 μ L pipetted in each of 96 wells. The microtiter plate was irradiated for 15 min and the conversion evaluated with KI-starch indicator.



Scheme 6.1 Oxidation of benzyl alcohol to aldehyde using RFTA.

Standard deviation was calculated for each well (Figure 6.13). Error of the measurement in microtiter plate using KI-starch indicator was determined to be 10 %. Slight difference in irradiation intensity is observed with increase intensity towards the centre of the plate. This was taken into account in designing the experiments and duplicate reactions were placed in edge and inner wells.

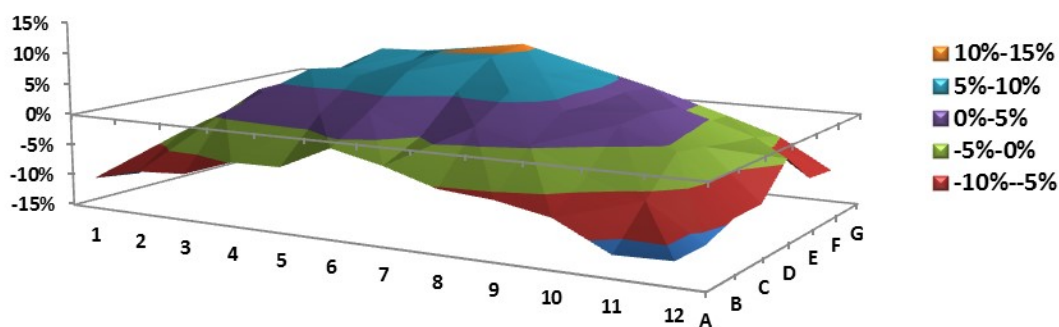


Figure 6.13 Relative deviation for each well from the average.

Exclusion of oxygen

A PMMA-box was equipped with an outlet, which was connected to a vacuum line and nitrogen source through a three-way valve. Exclusion of oxygen was performed by decreasing the pressure inside the box to 750 mBar followed by flushing it with pure nitrogen. The effectiveness of the process was evaluated by performing a photocatalytic

transformation of 4-methoxybenzyl alcohol to 4-methoxybenzaldehyde with **RFTA** (Figure 6.14).

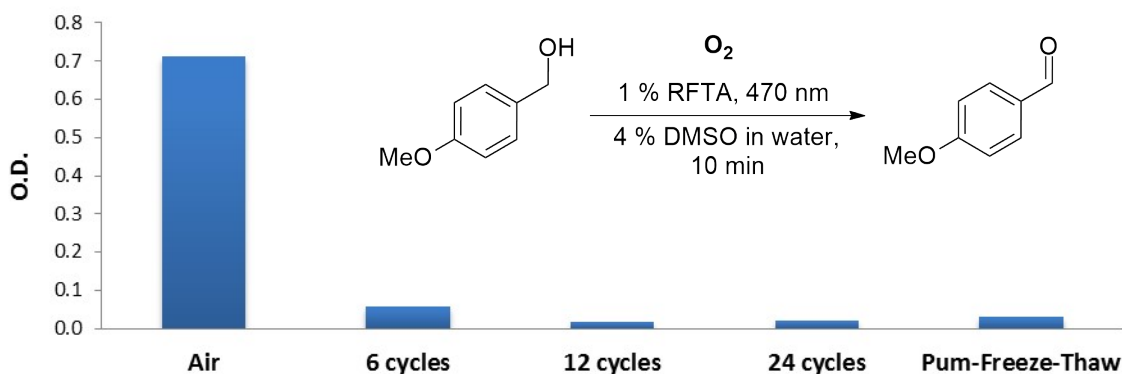


Figure 6.14 Response of the KI-starch indicator towards the oxidation of 4-methoxybenzyl alcohol performed under different oxygen exclusion technique.

Oxygen is required for completion of the catalytic cycle and the effect of the vacuum-nitrogen cycles on the conversion was examined (Figure 6.14). Results were compared to one reaction carried out in a vial where exclusion of the oxygen was achieved by pump-freeze-thaw technique, but the evaluation was done similarly in a microtiter plate using 100 μL of its solution. 12 cycles provide sufficient exclusion of the oxygen for the reaction not to occur and this procedure was used in all later reaction performed in absence of air.

6.4.4 Oxidation of benzyl alcohols and amines

Substrates (benzyl alcohols and amines) were prepared as stock solutions (4.16 mM) in MiliQ water and **RFTA** in DMSO (0.1 mM). Prior to the measurement 960 μL of the substrate and 40 μL of **RFTA** were mixed and 100 μL aliquots were pipetted into each well to obtain the required concentration of the substrate (4 mM) and photocatalyst (4 μM , 0.1 mol. %). After irradiation for 10 min 100 μL of KI-starch indicator was added in each well. The response was evaluated according to the procedure described above. Every microtiter plate experiment is the average of 8 measurements done in separate wells. As a blank reaction, a solution without substrate was used. The relative reactivity was calculated from the optical readout, which was normalized for the substrate with highest response.

GC Analysis

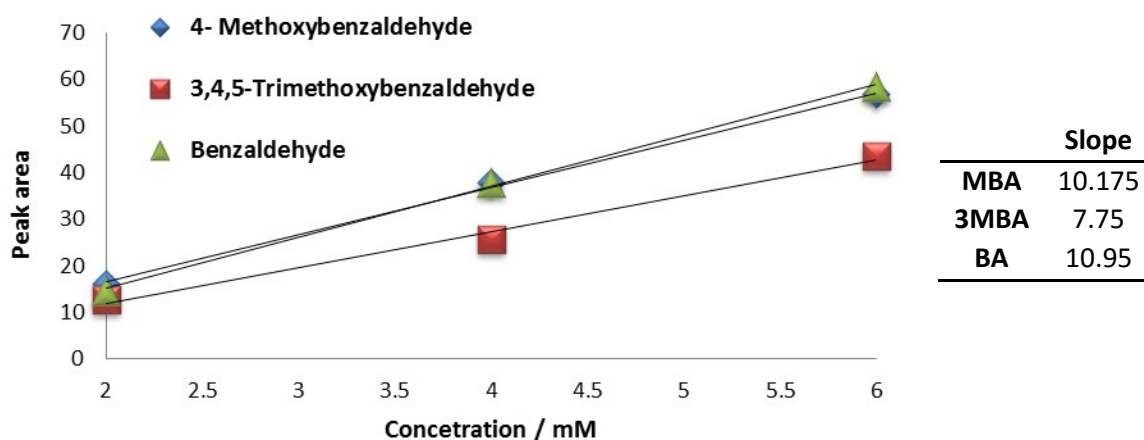


Figure 6.15 GC calibration for products of the transformation.

Three selected substrates were compared: benzyl alcohol (**BA**), 4-methoxybenzyl alcohol (**MBA**) and 3,4,5-trimethoxybenzyl alcohol (**3MBA**). GC calibration was performed in the range of the reaction concentration for the expected products of the oxidation (Figure 6.15). Measurements were performed in a similar manner as for the screening with a difference that solutions from 4 wells were combined, filtered and used for GC evaluation. Reaction conditions were altered to higher concentrations: substrate (10 mM), **RFTA** (0.01 mM), solvent (water with 4 % DMSO), loading (100 μ L in well), irradiation time (20 min).

6.4.5 Hydroxylation of boronic acids

Amine screening

All stock solutions were prepared and measurements were performed in MeCN. Each measurement comprised one well filled with a solution (50 μ L) of one dye (0.01 mM, 0.2 mol. %) and amine (5 mM). The array was irradiated for 5 min at 470 nm at room temperature. Then 200 μ L KI-starch indicator solution was added and the response evaluated as previously. As blank, a measurement without added amine was used. The blank experiment was performed for every catalyst independently. The given value is the average of three measurements. The relative reactivity of amines was evaluated as the optical response of the indicator normalized to the value of the best performing amine.

Solvent screening

Each measurement comprised two wells filled with a solution (65 μL) of one dye (**ACR**: 0.008 mM, 0.2 mol. % or **RFTA** 0.08mM, 2 mol. %) and triethylamine (5 mM) with and without phenylboronic acid (4 mM) in 6 different solvents. The microtiter plate was irradiated for 5 min at 470 nm at room temperature. Next, 200 μL of indicator solution was added and the indicator response evaluated as described before. A measurement without boronic acid was used as blank experiment. Difference in colorimetric response of blank (only amine) and sample (amine and boronic acid) was calculated for each case. These values for different solvents were then corrected by the above described solvent constant $a_{(\text{solvent})}$ (Table 6.3) in order to be able to compare them between each other. These values were then transformed into relative reactivity as described before by normalization to the best performing solvent for each dye separately.

Substrate screening

Each measurement comprised two wells filled with a solution (50 μL) of one dye (**ACR**: 0.008 mM, 0.2 mol. % or **RFTA** 0.08mM, 2 mol. %) and triethylamine (5 mM) with and without boronic acid (4 mM, 9 boronic acids) in acetonitrile. The microtiter plate was irradiated for 5 min at 470 nm at room temperature. Next, 200 μL of indicator solution was added. The evaluation of the relative reactivity was done in the same way as for the solvents.

Isolated compounds

General procedure

Tris(2,2'-bipyridyl)dichlororuthenium(II) hexahydrate (**Ru(bpy)₃**) (0.01 mmol, 0.02 eq.), octylboronic acid (0.5 mmol, 1.0 eq.) and DIPEA (1.0 mmol, 2.0 eq.) were dissolved in DMF (5 mL), placed in a crimp cap vial, flushed with nitrogen for 5 times and irradiated with 455 nm (high power LED) under stirring at room temperature for 16 h. Subsequently the reaction mixture was quenched with cold hydrochloric acid (5 ml, 10 %), and extracted with diethyl ether (3 \times 10 mL). The organic layers were combined, washed with brine (5 ml) and dried over MgSO_4 . Solids were filtered off, and the solvent was removed under reduced pressure. The residue was purified by flash chromatography (PE:EA, 9:1 \rightarrow 7:3) to obtain 50 mg (77 %) of octanol as colourless liquid.

	Amine	Solvent	Product / mg (%)		
			Octanol	Phenol	3-Fluorophenol
Ru	DIPEA	DMF	50 (70 %)	35 (74 %)	53 (93 %)
RFTA	TEA	MeCN	55 (80 %)	22 (47 %)	27 (66 %)
Acr	TEA	MeCN	40 (62 %)	17 (36 %)	52 (91 %)

Table 6.4 Conditions and yields of reactions for each catalyst and substrate.

NMR

1-Octanol:

^1H NMR (300 MHz, CDCl_3) δ 3.61 (t, $J = 6.7$ Hz, 2H), 2.21 (bs, 1H), 1.62 – 1.44 (m, 2H), 1.40 – 1.18 (m, 10H), 0.95 – 0.78 (m, 3H).

Phenol:

^1H NMR (300 MHz, CDCl_3) δ 7.33 – 7.15 (m, 2H), 7.00 – 6.90 (m, 1H), 6.90 – 6.79 (m, 2H), 5.20 (bs, 1H).

3-Fluorophenol:

^1H NMR (300 MHz, CDCl_3) δ 7.24 – 7.10 (m, 2H), 6.70 – 6.52 (m, 3H), 5.22 (bs, 1H).

6.4.6 Stability of the dyes

Each well of the microtiter plate (polypropylene) contained 220 μL of the dye solution (0.1 mM) in a different solvent. The full absorption spectra (200–800 nm) were recorded for each well prior to irradiation (470 nm) and then every 15 min over one hour. The dye content was derived from the optical density at the absorption maxima and its relative decrease through time was as assigned to bleaching (Figure 6.16). The slope of the linear bleaching of the dye over time was ascribed as relative stability of the dye in %/h (Table 6.5).

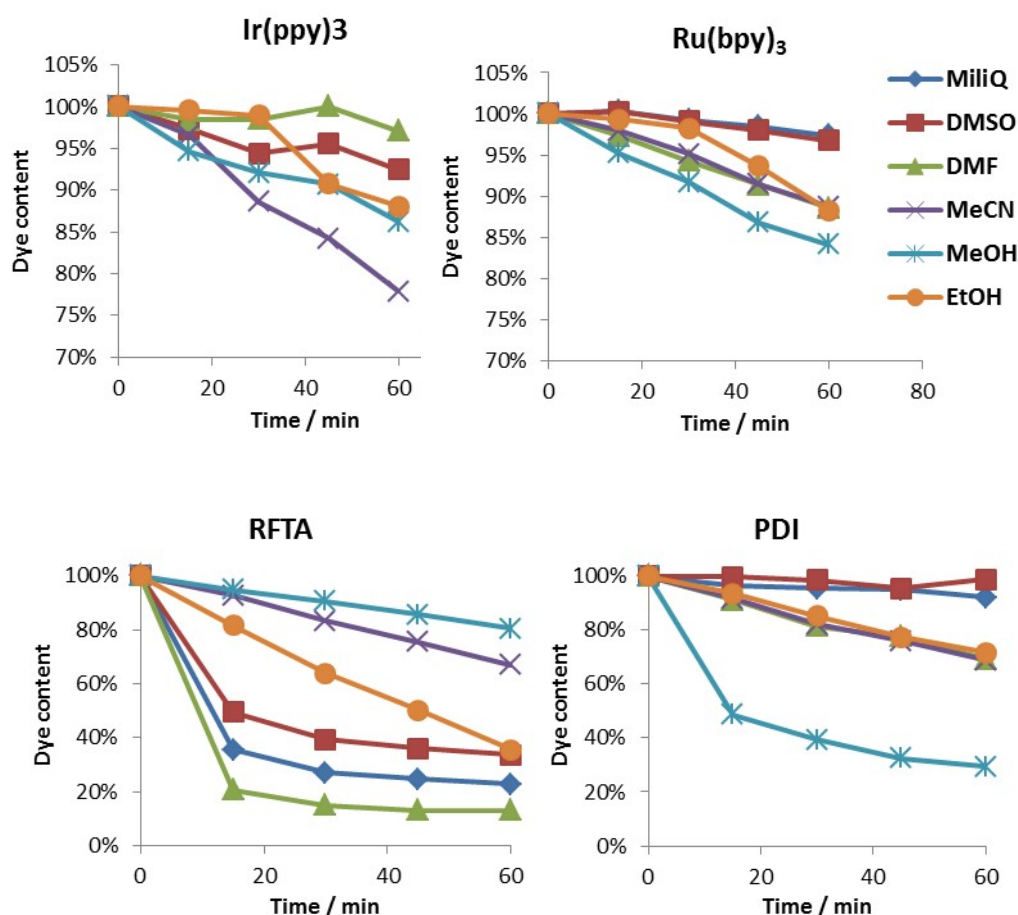


Figure 6.16 Examples of recorded data for photo-stability experiments. Irradiation with 470 nm LED setup was done in microtiter plate in presence of air at 20 °C. Concentration of each dye is 0.1 mM.

If the dye was too unstable, the fitting was performed on the linear part of the bleaching curve, which often exhibited complete bleaching in 1 h. For every solvent and dye the average of two measurements from two separate wells was used.

In the case of measurements done in nitrogen atmosphere only the measurement before and after 30 min irradiation was performed and the bleaching after 1 hour was calculated accordingly.

Measurements performed in the presence of acid or base were performed in the same condition with the difference that each solvent was a 10 mM solution of either trifluoroacetic acid or sodium hydroxide (in DMSO, DMF and MeCN concentration might be lower due to solubility). If potassium *tert*-butoxide was used as base, most of the dyes are unstable in aprotic solvents and show a strong colour change.

Abs. maxima	450 nm			375 nm			300 nm			420 nm			445 nm			490 nm		
	Water	96	97	61				94	100		92	95	34	0	0	0		
DMSO	9	95	98	97	94	100	99	100	100	76	80		0	0		100	97	
MeCN	86	88	82	89	98	100	94	94	98	0	0	92	0	0	66	75	70	0
DMF	78	88	64	75	77	83	96	99	86	81	90	46	0	67	12	88	69	68
MeOH	61	84	70	68	87	83	83	86	92	76	82	0	0	80	14	38	37	27
EtOH	73	88	55	71	87	93	90	92	108	75	79	0	0	36	38	78	71	66
Nitrogen																		
Water	98	97	49				90	88		93	87	48	0	0	2			
DMSO	100	100	100	100	100	100	100	63	99	59	39		0	0		0	82	
MeCN	93	81	59	92	94	100	88	78	98	0	0	100	0	0	76	11	66	10
DMF	59	53	30	84	92	77	87	89	100	50	10	85	0	0	0	81	79	0
MeOH	86	70	21	52	80	88	98	73	91	15	0	0	0	43	19	0	0	0
EtOH	83	81	19	83	92	92	84	95	100	36	36	0	0	0	59	81	53	82

Table 6.5 Relative photo stability of the dyes (under 470 nm irradiation in microtiter plate) provided as the rate (1-(% bleached)/h) which resembles amount of remained dye after 1 h irradiation at concentration 0.1 mM (220 μ L in well). Photo stability was measured in the presence of air (up) and its absence in nitrogen atmosphere (down) as well as under acidic (red) and basic (blue) conditions.

It is important to notice that absorption coefficients vary drastically at 470 nm and expected stability at different wavelength might differ (Figure 6.17).

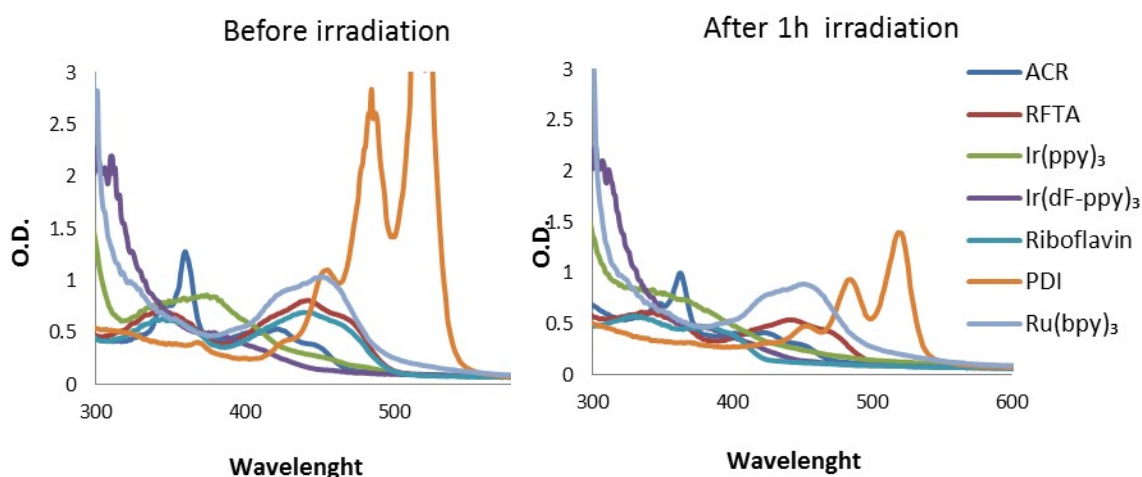


Figure 6.17 Recorded spectra during the experiment in acetonitrile before and after irradiation.

6.4.7 Aryl radical generation

Stock solutions of DIPEA (4 mM), dye (0.2 mM) and substrate (4 mM) were prepared fresh in DMF prior to each measurement. In a well, DIPEA (12.5 μL) and substrate (12.5 μL) were pipetted, followed by the respective dye (25 μL). Two sets of blank measurements were performed: omitting either the dye or the catalyst.

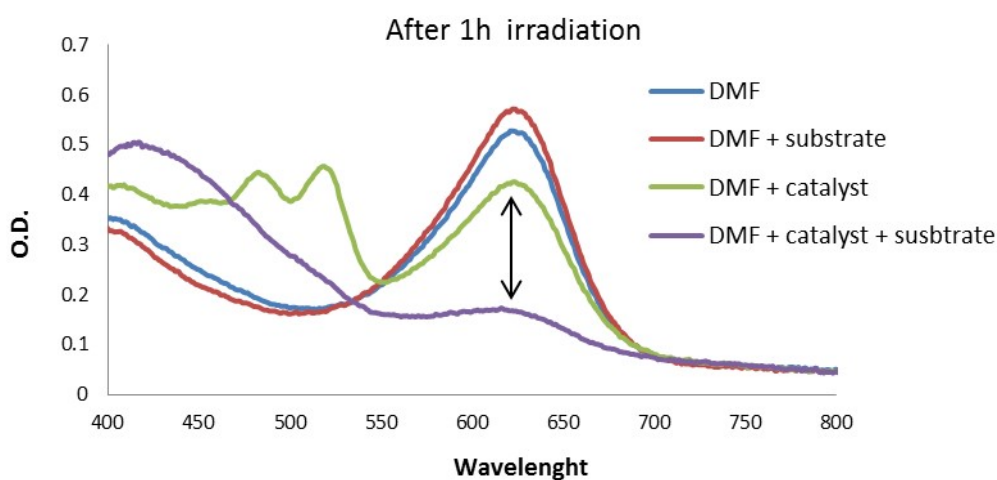


Figure 6.18 Example of spectra recorded for experiment performed with **PDI** and 4-bromoacetophenone after irradiation for 1 h and addition of **BCG** indicator.

The microtiter plate was placed in the reactor inside the gas-tight box, which was flushed with nitrogen (as described above) and irradiated for 1 h at 470 nm. Next, a solution of bromocresol green (**BCG**) (50 μL , 0.1 mM, 1:10 EtOH:H₂O) was added to each well and the full absorption spectra were recorded (250–850 nm) (Figure 6.18). For each sample the optical density at the maxima of the absorption of BCG (617 nm) was corrected to baseline by subtracting the O.D. value measured at 800 nm to obtain the absolute response of the indicator. Samples were investigated in pairs and the resulting average was used for calculations. The ratio between the substrate containing the sample and the blank with only the catalyst was subtracted from one, which resembles the relative reactivity of the substrate (Table 6.6).

	$-E_{ArX/ArX^{+-}}^0$ (V vs SCE) ^a	PDI	Ir(ppy) ₃	Ru(bpy) ₃
2-Chloronitrobenzene	0.99	0%	13%	24%
9-Bromoanthracene	1.7	80%	74%	72%
4'-Bromoacetophenone	1.84	63%	79%	7%
4-Chloroacetophenone	1.9	24%	2%	0%
4'-Bromobenzonitrile	1.94	48%	28%	0%
4-Chlorobenzonitrile	2.08	36%	18%	8%
4-Bromoanisole	–	13%	20%	0%
2-Bromonaphthalen	2.21	6%	5%	0%
3-Bromopyridin	2.23	10%	16%	0%
Bromooctadecane	–	0%	5%	0%

Table 6.6 Relative reactivity values obtained for different aryl halides with their redox potentials.
^a Reported values.⁵⁸

The relative reactivity was compared with the published redox potential of the aryl halides. An important aspect of the measurement to observe a high contrast between reacting and non-reacting substrates is to optimize the amine concentration and the irradiation time.[‡] In our case it was 1eq of DIPEA and 1h of irradiation.

	PDI	Ir(ppy) ₃	Ru(bpy) ₃
4'-Bromoacetophenone	53%	67%	0%
9-Bromoanthracene	68%	55%	54%
2-Chloro-4-(trifluoromethyl)pyrimidine	0%	24%	5%
6-Chloropurine	23%	0%	0%
5-Bromouracil	17%	19%	18%
2-Chloropyrazine	44%	49%	0%
3-Bromothiophene	9%	6%	1%
2-Bromobenzophenon	49%	63%	11%
5-Bromo-1-methylindol	14%	10%	7%
5-Bromonicotinamide	47%	24%	4%

Table 6.7 Relative reactivity values obtained for extended substrate scope.

Screening of heterocycles and benzophenone was performed in a similar fashion (Table 6.7).

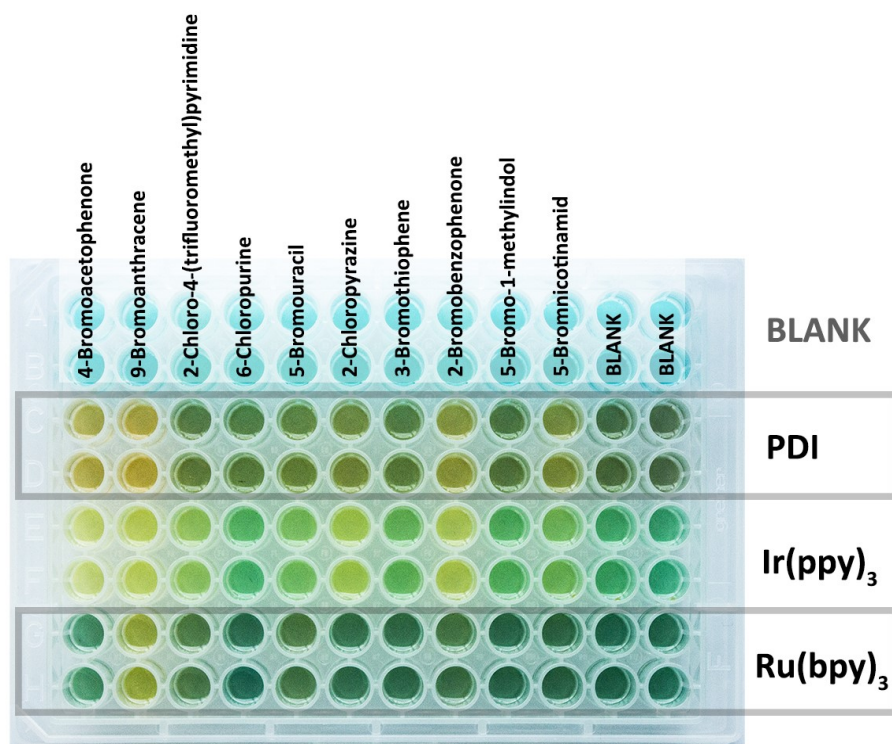


Figure 6.19 Picture of microtiter plate experiment after irradiation and addition of **BCG** indicator. Yellow color indicates increased acidity hence successful reaction.

UV analysis of the conversion

9-Bromoanthracene and anthracene have a distinct UV/Vis absorptions that were used to monitor the reaction with all three catalyst (Figure 6.20) confirming the expected transformation.

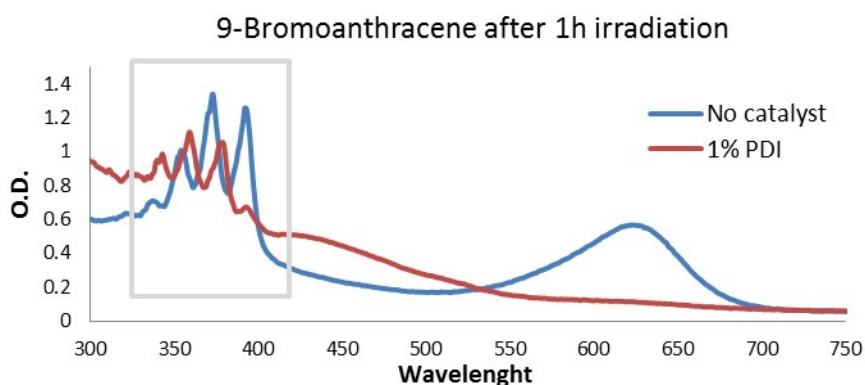


Figure 6.20 Recorded spectra of 9-bromoanthracene after 1 h irradiation in the presence and absence of the catalyst.

GC analysis

Three point calibrations were performed for all measured substrates and products (Figure 6.21).

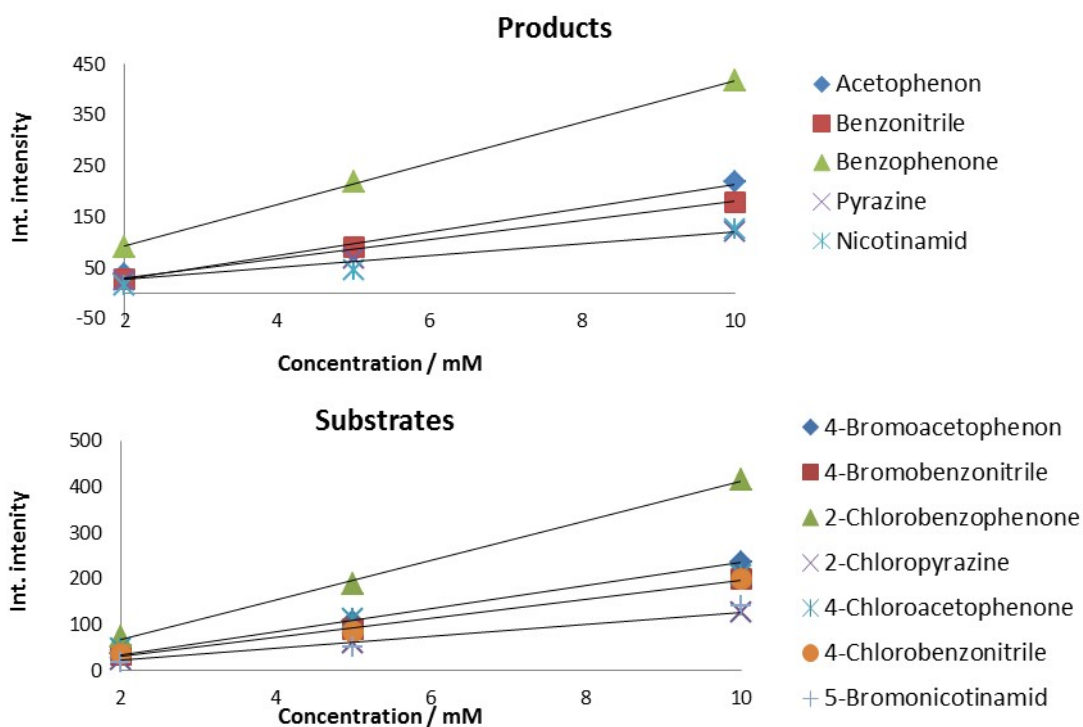


Figure 6.21 GC calibration for substrates and products.

All the GC measurements were performed in crimp-cap vials flushed with nitrogen and irradiated for 16 or 24 h. As shown above, the **PDI** dye is more prone to bleach. Therefore 10 mol% was used in contrary to 1 mol% in case of **Ru(bpy)₃** an **Ir(ppy)₃**. Reactions were performed in DMF with one substrate (20 mM) and DIPEA (10 eq., 200 mM) and irradiation was provided by high power LED (455 nm) for each crimp-cap vial. Samples were analysed by GC, and yields and conversion were calculated using the calibration (Table 6.8).

	Conversion			Yield		
	PDI	Ir(ppy) ₃	Ru(bpy) ₃	PDI	Ir(ppy) ₃	Ru(bpy) ₃
4-Bromoacetophenon	59%	84%	0%	86%	8%	6%
4-Chloroacetophenone	0%	89%	2%	1%	4%	0%
4-Bromobenzonitrile	28%	100%	0%	35%	81%	2%
4-Chlorobenzonitrile	14%	100%	0%	26%	92%	0%
2-Chloropyrazine	0%	65%	0%	17%	50%	0%
2-Bromobenzophenone	78%	100%	4%	41%	28%	8%
5-Bromnicotinamid	93%	100%	1%	49%	53%	2%

Table 6.8 Obtained conversions and yields via GC analysis.

Screening of commercially available drugs

Screening of the drugs was performed in the similar manner as for the aryl halides. The major difference is that they often bear an amine or acidic residue, which has to be taken into account for a correct readout of the assay. This was addressed by calculating the relative difference between the absorption at BCG maxima (617 nm) in plain DMF with only DIPEA and with the substrate. This represents the response due to the varying pKa of the compound. The relative colorimetric change in DMF was then subtracted from the one with catalyst after irradiation (Figure 6.22). If the obtained relative change in colour of the indicator was positive, acidification occurs upon irradiation in the presence of the catalyst. Values greater than 10 % were considered as hit (•) (Table 6.9). All drugs were compared with the reactivity of 9-bromoanthracene.

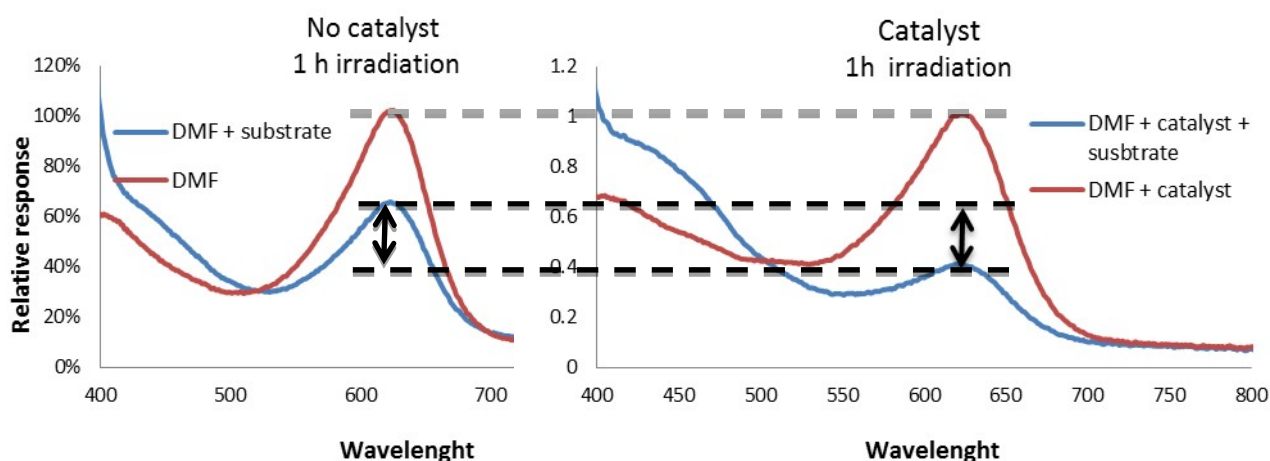


Figure 6.22 Illustration of colorimetric response evaluation for hydrochlorothiazide using Ru(bpy)₃ as catalyst.

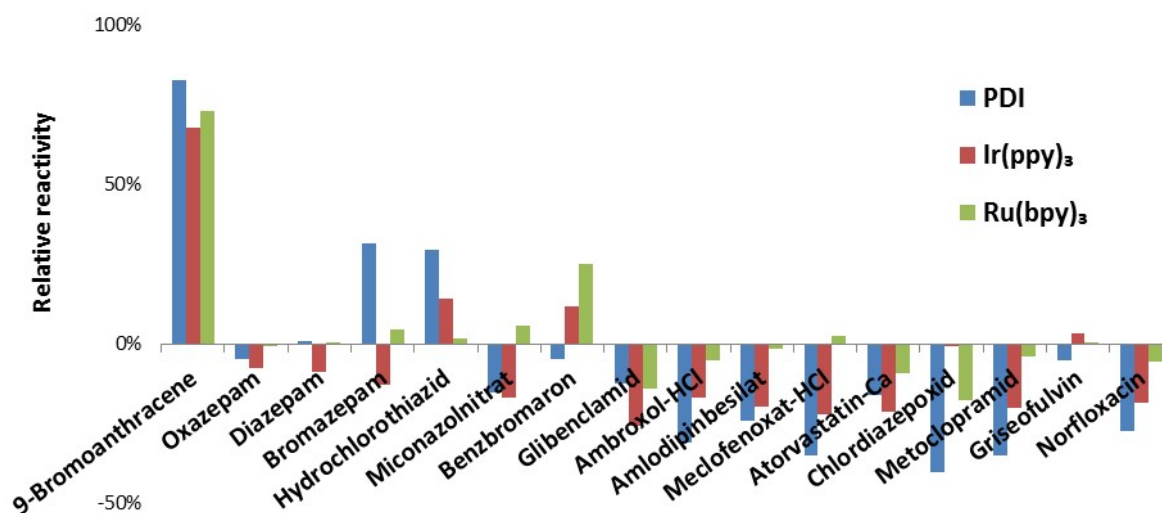
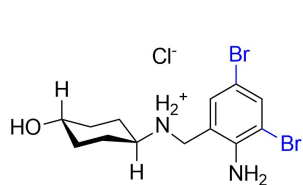


Figure 6.23 Relative reactivity of the selected drugs compared with reactivity of 9-bromoanthracene.

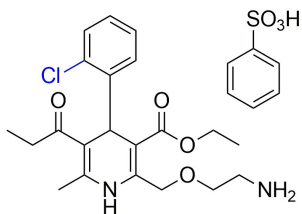
	PDI	Ir(ppy) ₃	Ru(bpy) ₃
9-Bromoanthracene	83%	68%	73%
Oxazepam	-5%	-7%	-1%
Diazepam	1%	-9%	0%
Bromazepam	31%	-13%	5%
Hydrochlorothiazide	29%	14%	2%
Miconazole	-15%	-17%	6%
Benzbromarone	-5%	12%	25%
Glibenclamid	-12%	-26%	-14%
Ambroxol-HCl	-31%	-17%	-5%
Amlodipinbesilat	-24%	-20%	-2%
Meclofenoxat-HCl	-35%	-22%	3%
Atorvastatin-Ca	-16%	-21%	-9%
Chlordiazepoxid	-40%	-1%	-18%
Metoclopramid	-35%	-20%	-4%
Griseofulvin	-5%	3%	1%
Norfloxacin	-27%	-19%	-6%

Table 6.9 Relative reactivity of the selected drugs compared with reactivity of 9-bromoanthracene.

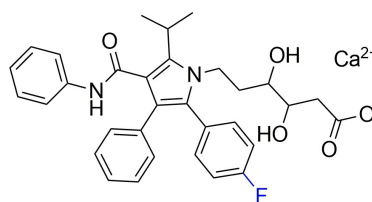
6.4.8 List of used commercial drugs



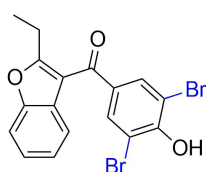
Ambroxol-HCl



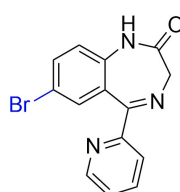
Amlopudinbesilat



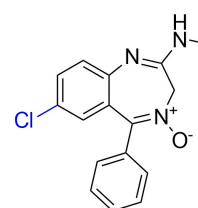
Atorvastatin-Ca



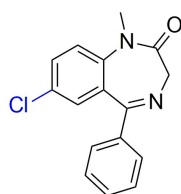
Benzbromarone



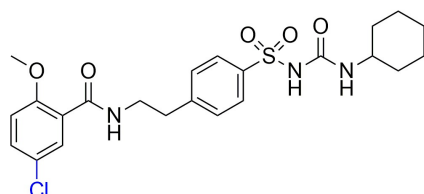
Bromazepam



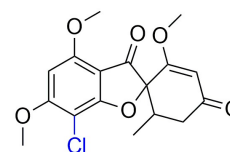
Chlorodiazepoxid



Diazepam



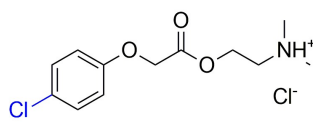
Glibenclamide



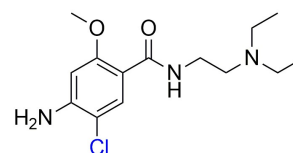
Griseofulvin



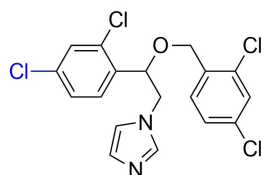
Hydrochlorothiazide



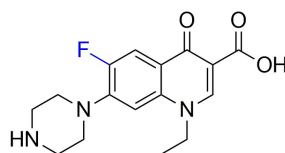
Meclofenoxate-HCl



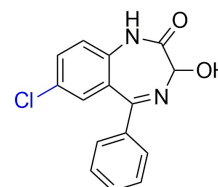
Metoclopramide



Miconazole



Norfloxacin



Oxazepam

6.4.9 Synthetic procedure for dehalogenation of selected drugs

Benzbromarone

Tris(2,2'-bipyridyl)ruthenium(II) chloride (**Ru(bpy)₃**) (0.5 mg, 0.006 mmol), benzbromarone (24 mg, 0.6 mmol) and DIPEA (93 μ L, 73 mg, 6 mmol) were dissolved in DMF (5 mL), placed into a crimp cap vial, flushed with nitrogen 5 times and irradiated with 455 nm (high power LED) under stirring at room temperature for 48 h. Subsequently, the reaction mixture was quenched with water (12 mL) and extracted with ethyl acetate (3 \times 3 mL). The organic layers were combined, washed with brine (1 mL) and dried over MgSO₄. Solids were filtered off and the solvent was removed under reduced pressure. The residue was purified by flash chromatography (PE:EA, 9:1 to 7:3) to obtain 14 mg (80 %) of the mixture of mono and non-brominated product in 1:1 ratio (according to NMR).

Obtained mixed NMR spectra correspond to the reported values.^{60, 61}

Monobrominated: MS (ESI(+)): $m/z = 345.0126$ [MH⁺]

Debrominated: MS (ESI(+)): $m/z = 267.1022$ [MH⁺]

Hydrochlorothiazide

Tris[2-phenylpyridinato-C2,N]iridium(III) (**Ir(ppy)₃**) (0.8 mg, 0.012 mmol), hydrochlorothiazide (36 mg, 1 mmol) and DIPEA (200 μ L, 157 mg, 12 mmol) were dissolved in DMF (5 mL), closed in crimp cap vial, flushed with nitrogen 5 times and irradiated with 455 nm (high power LED) under stirring at room temperature for 4 days. Subsequently, the reaction mixture was quenched with water (12 mL) and extracted with ethyl acetate (3 \times 3 mL). The organic layers were combined, washed with brine (1 mL) and dried over MgSO₄. Solids were filtered off and the solvent was removed under reduced pressure. The residue was purified by flash chromatography (PE:EA, 2:1 to 0:1) to obtain 12 mg (38 %) of the dechlorinated hydrochlorothiazide.

In the case of **PDI** (10 mol. %) 15 mg (50 %) of product were obtained.

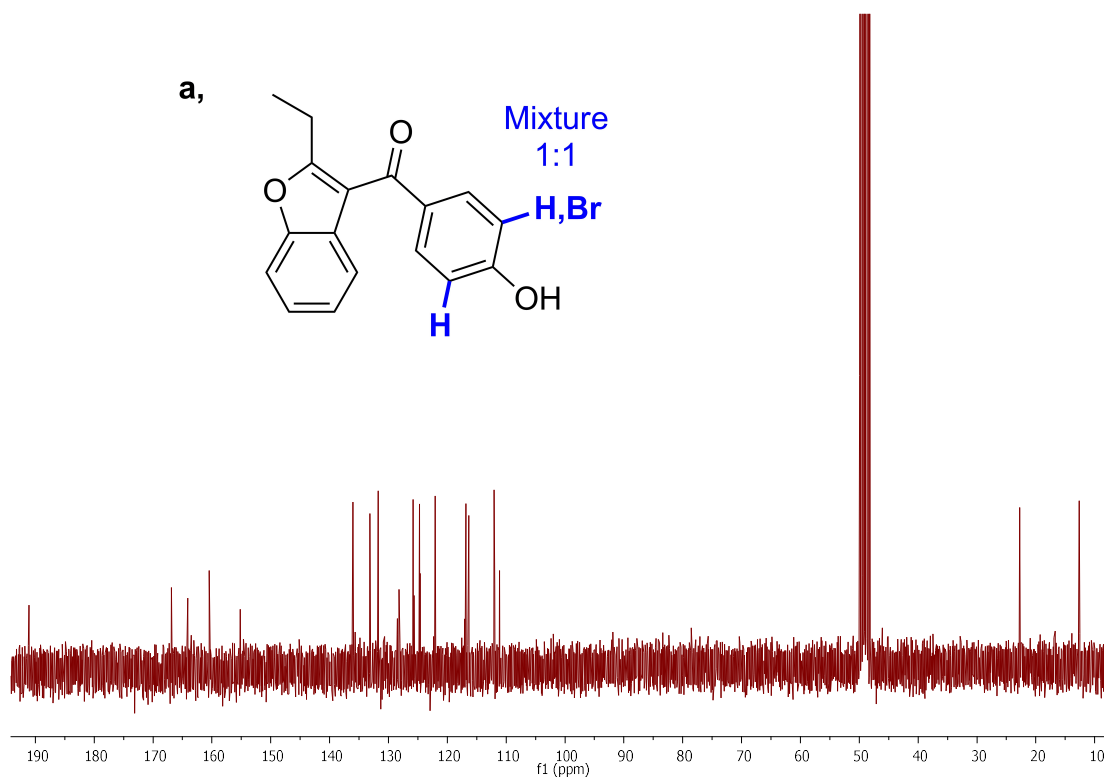
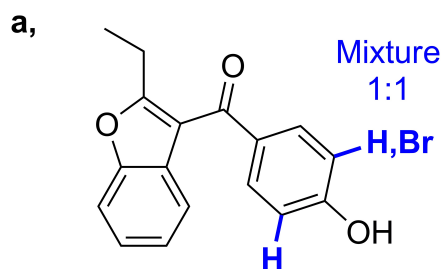
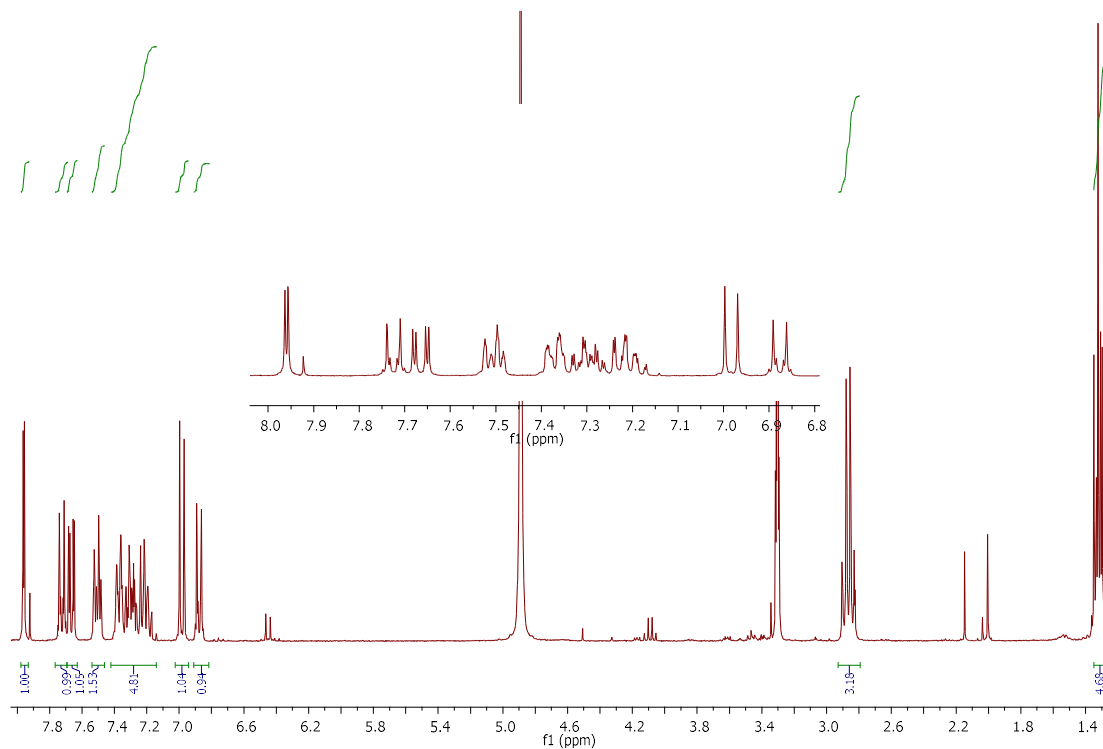
¹H NMR (400 MHz, MeOD) δ 8.04 (d, $J = 2.1$ Hz, 1H), 7.72 (dd, $J = 8.9, 2.2$ Hz, 1H), 6.85 (d, $J = 8.9$ Hz, 1H), 4.77 (s, 2H).

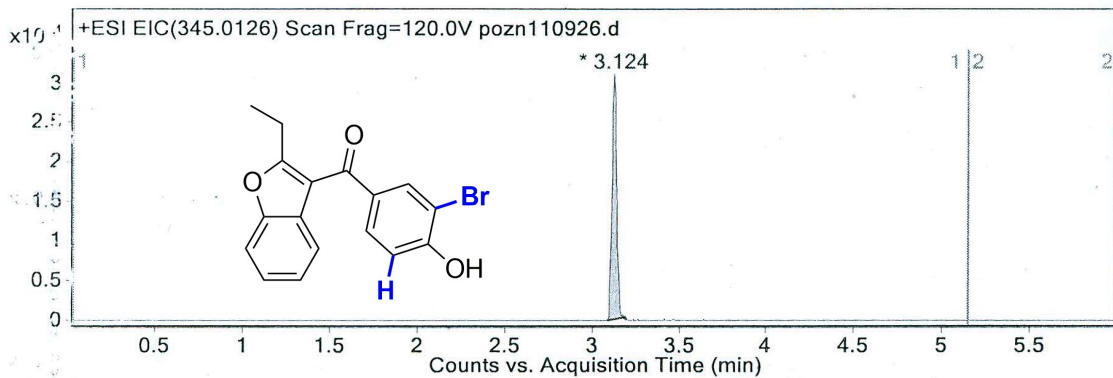
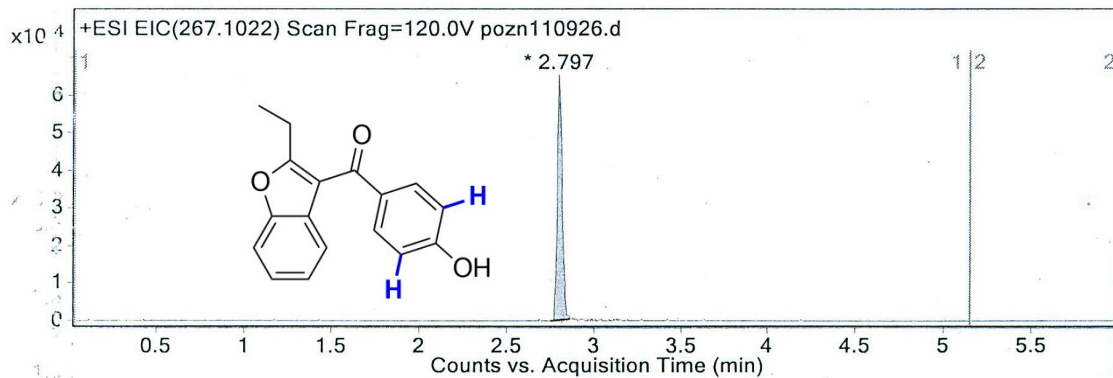
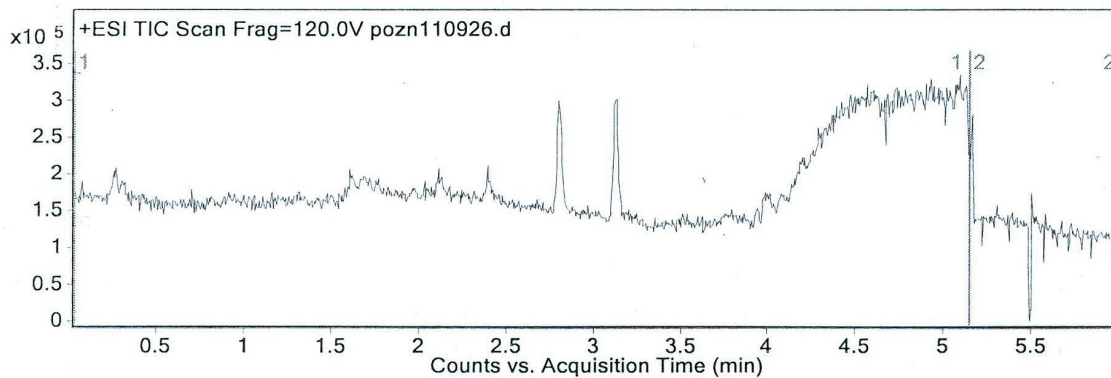
¹³C NMR (101 MHz, MeOD) δ 147.87, 130.85, 130.10, 123.10, 120.68, 115.74, 54.42.

MS (ESI(+)): $m/z = 264.011$ [MH⁺]

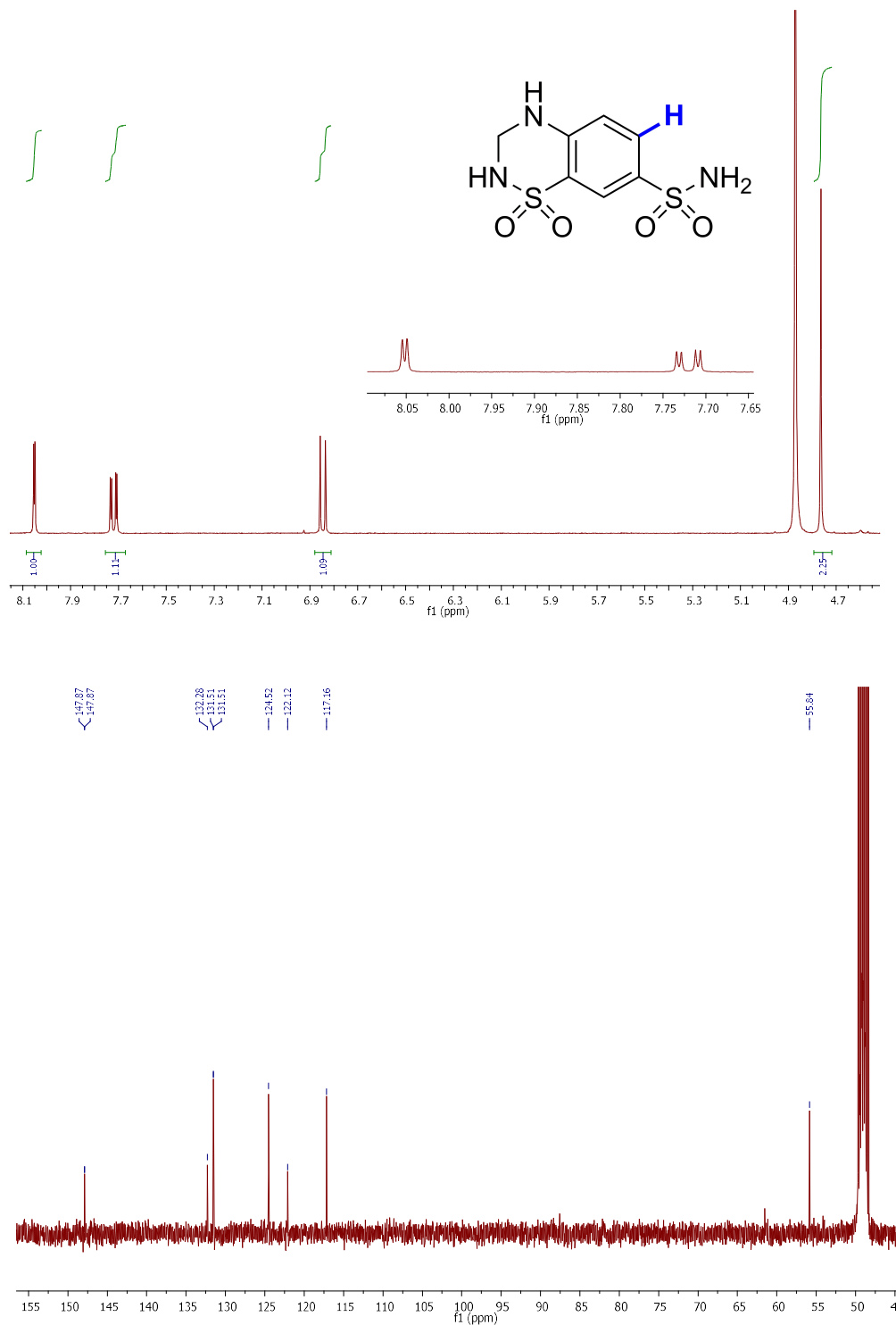
The measured NMR resonance signals correspond to the reported values.⁶²

Characterization of reduced benzbromarone





Characterization of reduced hydrochlorothiazide



6.5 References

- † All amines as electron rich nucleophiles are oxidized by flavin releasing reactive oxygen species.
- ¥ Big differences between slopes of calibration curves can cause changes in standard deviation for each solvent.
- § The calibration can strongly depend on the type and quality of the starch and the indicator preparation. Therefore is advised to prepare fresh indicator solution for every series of experiments to obtain comparable results.
- ‡ DMF might contain amines. Therefore amine-free DMF or pre-optimization of the correct concentration of added amine and irradiation time is required to achieve highest resolution.
1. Ley, S. V.; Fitzpatrick, D. E.; Ingham, R. J.; Myers, R. M., Organic Synthesis: March of the Machines. *Angew. Chem. Int. Ed.* **2015**, *54* (11), 3449-3464.
 2. Houston, J. G.; Banks, M., The chemical-biological interface: developments in automated and miniaturised screening technology. *Curr. Opin. Biotechnol.* **1997**, *8* (6), 734-740.
 3. Collins, K. D.; Gensch, T.; Glorius, F., Contemporary screening approaches to reaction discovery and development. *Nat Chem* **2014**, *6* (10), 859-871.
 4. Houben, C.; Lapkin, A. A., Automatic discovery and optimization of chemical processes. *Current Opinion in Chemical Engineering* **2015**, *9*, 1-7.
 5. Robbins, D. W.; Hartwig, J. F., A Simple, Multidimensional Approach to High-Throughput Discovery of Catalytic Reactions. *Science* **2011**, *333* (6048), 1423-1427.
 6. Buitrago Santanilla, A.; Regalado, E. L.; Pereira, T.; Shevlin, M.; Bateman, K.; Campeau, L.-C.; Schneeweis, J.; Berritt, S.; Shi, Z.-C.; Nantermet, P.; Liu, Y.; Helmy, R.; Welch, C. J.; Vachal, P.; Davies, I. W.; Cernak, T.; Dreher, S. D., Nanomole-scale high-throughput chemistry for the synthesis of complex molecules. *Science* **2015**, *347* (6217), 49-53.
 7. Ding, K.; Du, H.; Yuan, Y.; Long, J., Combinatorial Chemistry Approach to Chiral Catalyst Engineering and Screening: Rational Design and Serendipity. *Chem. Eur. J.* **2004**, *10* (12), 2872-2884.
 8. Collins, K. D.; Glorius, F., A robustness screen for the rapid assessment of chemical reactions. *Nat Chem* **2013**, *5* (7), 597-601.
 9. Kutchukian, P. S.; Dropinski, J. F.; Dykstra, K. D.; Li, B.; DiRocco, D. A.; Streckfuss, E. C.; Campeau, L.-C.; Cernak, T.; Vachal, P.; Davies, I. W.; Krska, S. W.; Dreher, S. D., Chemistry

- informer libraries: a chemoinformatics enabled approach to evaluate and advance synthetic methods. *Chem. Sci.* **2016**, *7* (4), 2604-2613.
- Collins, K. D.; Glorius, F., Intermolecular Reaction Screening as a Tool for Reaction Evaluation. *Acc. Chem. Res.* **2015**, *48* (3), 619-627.
 - Preshlock, S. M.; Ghaffari, B.; Maligres, P. E.; Krska, S. W.; Maleczka, R. E.; Smith, M. R., High-Throughput Optimization of Ir-Catalyzed C–H Borylation: A Tutorial for Practical Applications. *J. Am. Chem. Soc.* **2013**, *135* (20), 7572-7582.
 - Bellomo, A.; Celebi-Olcum, N.; Bu, X.; Rivera, N.; Ruck, R. T.; Welch, C. J.; Houk, K. N.; Dreher, S. D., Rapid Catalyst Identification for the Synthesis of the Pyrimidinone Core of HIV Integrase Inhibitors. *Angew. Chem. Int. Ed.* **2012**, *51* (28), 6912-6915.
 - Rodrigues, T.; Schneider, P.; Schneider, G., Accessing New Chemical Entities through Microfluidic Systems. *Angew. Chem. Int. Ed.* **2014**, *53* (23), 5750-5758.
 - Tucker, J. W.; Zhang, Y.; Jamison, T. F.; Stephenson, C. R. J., Visible-Light Photoredox Catalysis in Flow. *Angew. Chem. Int. Ed.* **2012**, *51* (17), 4144-4147.
 - Trapp, O., Gas chromatographic high-throughput screening techniques in catalysis. *J. Chromatogr. A* **2008**, *1184* (1–2), 160-190.
 - Cai, C.; Chung, J. Y. L.; McWilliams, J. C.; Sun, Y.; Shultz, C. S.; Palucki, M., From High-Throughput Catalyst Screening to Reaction Optimization: Detailed Investigation of Regioselective Suzuki Coupling of 1,6-Naphthyridone Dichloride. *Org. Process Res. Dev.* **2007**, *11* (3), 328-335.
 - Martin, V. I.; Goodell, J. R.; Ingham, O. J.; Porco, J. A.; Beeler, A. B., Multidimensional Reaction Screening for Photochemical Transformations as a Tool for Discovering New Chemotypes. *J. Org. Chem.* **2014**, *79* (9), 3838-3846.
 - König, B., *Chemical Photocatalysis*. 2013.
 - Yoon, T. P.; Ischay, M. A.; Du, J., Visible light photocatalysis as a greener approach to photochemical synthesis. *Nat Chem* **2010**, *2* (7), 527-532.
 - Schultz, D. M.; Yoon, T. P., Solar Synthesis: Prospects in Visible Light Photocatalysis. *Science* **2014**, *343* (6174).
 - Ibhadon, A.; Fitzpatrick, P., Heterogeneous Photocatalysis: Recent Advances and Applications. *Catalysts* **2013**, *3* (1), 189.
 - Adesina, A. A., Industrial exploitation of photocatalysis: progress, perspectives and prospects. *Catal. Surv. Asia* **8** (4), 265-273.

23. Langford, C. H., Photocatalysis—A Special Issue on a Unique Hybrid Area of Catalysis. *Catalysts* **2012**, 2 (3), 327.
24. Narayanam, J. M. R.; Stephenson, C. R. J., Visible light photoredox catalysis: applications in organic synthesis. *Chem. Soc. Rev.* **2011**, 40 (1), 102-113.
25. Hopkinson, M. N.; Gómez-Suárez, A.; Teders, M.; Sahoo, B.; Glorius, F., Accelerated Discovery in Photocatalysis using a Mechanism-Based Screening Method. *Angew. Chem. Int. Ed.* **2016**, 55 (13), 4361-4366.
26. DiRocco, D. A.; Dykstra, K.; Krska, S.; Vachal, P.; Conway, D. V.; Tudge, M., Late-Stage Functionalization of Biologically Active Heterocycles Through Photoredox Catalysis. *Angew. Chem. Int. Ed.* **2014**, 53 (19), 4802-4806.
27. Bicker, K. L.; Wiskur, S. L.; Lavigne, J. J., Colorimetric Sensor Design. In *Chemosensors*, John Wiley & Sons, Inc.: 2011; pp 275-295.
28. Lavastre, O.; Morken, J. P., Discovery of Novel Catalysts for Allylic Alkylation with a Visual Colorimetric Assay. *Angew. Chem. Int. Ed.* **1999**, 38 (21), 3163-3165.
29. Löber, O.; Kawatsura, M.; Hartwig, J. F., Palladium-Catalyzed Hydroamination of 1,3-Dienes: A Colorimetric Assay and Enantioselective Additions. *J. Am. Chem. Soc.* **2001**, 123 (18), 4366-4367.
30. Kawatsura, M.; Hartwig, J. F., Transition Metal-Catalyzed Addition of Amines to Acrylic Acid Derivatives. A High-Throughput Method for Evaluating Hydroamination of Primary and Secondary Alkylamines. *Organometallics* **2001**, 20 (10), 1960-1964.
31. Kim, S.; Jung, E.; Kim, M. J.; Pyo, A.; Palani, T.; Eom, M. S.; Han, M. S.; Lee, S., A simple, fast, and easy assay for transition metal-catalyzed coupling reactions using a paper-based colorimetric iodide sensor. *Chem. Commun.* **2012**, 48 (70), 8751-8753.
32. Eom, M. S.; Noh, J.; Kim, H.-S.; Yoo, S.; Han, M. S.; Lee, S., High-Throughput Screening Protocol for the Coupling Reactions of Aryl Halides Using a Colorimetric Chemosensor for Halide Ions. *Org. Lett.* **2016**, 18 (8), 1720-1723.
33. Copeland, G. T.; Miller, S. J., A Chemosensor-Based Approach to Catalyst Discovery in Solution and on Solid Support. *J. Am. Chem. Soc.* **1999**, 121 (17), 4306-4307.
34. Jarvo, E. R.; Evans, C. A.; Copeland, G. T.; Miller, S. J., Fluorescence-Based Screening of Asymmetric Acylation Catalysts through Parallel Enantiomer Analysis. Identification of a Catalyst for Tertiary Alcohol Resolution. *J. Org. Chem.* **2001**, 66 (16), 5522-5527.
35. Evans, C. A.; Miller, S. J., Proton-activated fluorescence as a tool for simultaneous screening of combinatorial chemical reactions. *Curr. Opin. Chem. Biol.* **2002**, 6 (3), 333-338.

36. Onaran, M. B.; Seto, C. T., Using a Lipase as a High-Throughput Screening Method for Measuring the Enantiomeric Excess of Allylic Acetates. *J. Org. Chem.* **2003**, *68* (21), 8136-8141.
37. Schmitz, G., The oxidation of iodine to iodate by hydrogen peroxide. *PCCP* **2001**, *3* (21), 4741-4746.
38. Rundle, R. E.; Foster, J. F.; Baldwin, R. R., On the Nature of the Starch—Iodine Complex1. *J. Am. Chem. Soc.* **1944**, *66* (12), 2116-2120.
39. Kurtovic, S.; Jansson, R.; Mannervik, B., Colorimetric endpoint assay for enzyme-catalyzed iodide ion release for high-throughput screening in microtiter plates. *Arch. Biochem. Biophys.* **2007**, *464* (2), 284-287.
40. Lechner, R.; Koenig, B., ChemInform Abstract: Oxidation and Deprotection of Primary Benzylamines by Visible Light Flavin Photocatalysis. *ChemInform* **2010**, *41* (40), no-no.
41. Schmaderer, H.; Hilgers, P.; Lechner, R.; König, B., Photooxidation of Benzyl Alcohols with Immobilized Flavins. *Adv. Synth. Catal.* **2009**, *351* (1-2), 163-174.
42. Megerle, U.; Wenninger, M.; Kutta, R.-J.; Lechner, R.; König, B.; Dick, B.; Riedle, E., Unraveling the flavin-catalyzed photooxidation of benzylic alcohol with transient absorption spectroscopy from sub-pico- to microseconds. *PCCP* **2011**, *13* (19), 8869-8880.
43. The initial rate of conversion of a reaction is often used to derive data for relative comparison.

Jones, R. A. Y., *Physical and Mechanistic Organic Chemistry (Cambridge Texts in Chemistry and Biochemistry)*. Cambridge University Press: 1979; p 368.
44. Lechner, R.; König, B., Oxidation and Deprotection of Primary Benzylamines by Visible Light Flavin Photocatalysis. *Synthesis* **2010**, *2010* (10), 1712-1718.
45. Zou, Y.-Q.; Chen, J.-R.; Liu, X.-P.; Lu, L.-Q.; Davis, R. L.; Jørgensen, K. A.; Xiao, W.-J., Highly Efficient Aerobic Oxidative Hydroxylation of Arylboronic Acids: Photoredox Catalysis Using Visible Light. *Angew. Chem.* **2012**, *124* (3), 808-812.
46. Pitre, S. P.; McTiernan, C. D.; Ismaili, H.; Scaiano, J. C., Mechanistic Insights and Kinetic Analysis for the Oxidative Hydroxylation of Arylboronic Acids by Visible Light Photoredox Catalysis: A Metal-Free Alternative. *J. Am. Chem. Soc.* **2013**, *135* (36), 13286-13289.
47. Kotoucova, H.; Strnadova, I.; Kovandova, M.; Chudoba, J.; Dvorakova, H.; Cibulka, R., Biomimetic aerobic oxidative hydroxylation of arylboronic acids to phenols catalysed by a flavin derivative. *Org. Biomol. Chem.* **2014**, *12* (13), 2137-2142.

48. Luo, J.; Zhang, X.; Zhang, J., Carbazolic Porous Organic Framework as an Efficient, Metal-Free Visible-Light Photocatalyst for Organic Synthesis. *ACS Catalysis* **2015**, *5* (4), 2250-2254.
49. Paul, A.; Chatterjee, D.; Rajkamal; Halder, T.; Banerjee, S.; Yadav, S., Metal free visible light photoredox activation of PhI(OAc)₂ for the conversion of arylboronic acids to phenols. *Tetrahedron Lett.* **2015**, *56* (19), 2496-2499.
50. Penders, I. G. T. M.; Amara, Z.; Horvath, R.; Rossen, K.; Poliakoff, M.; George, M. W., Photocatalytic hydroxylation of arylboronic acids using continuous flow reactors. *RSC Adv.* **2015**, *5* (9), 6501-6504.
51. Yu, X.; Cohen, S. M., Photocatalytic metal-organic frameworks for the aerobic oxidation of arylboronic acids. *Chem. Commun.* **2015**, *51* (48), 9880-9883.
52. Toyao, T.; Ueno, N.; Miyahara, K.; Matsui, Y.; Kim, T.-H.; Horiuchi, Y.; Ikeda, H.; Matsuoka, M., Visible-light, photoredox catalyzed, oxidative hydroxylation of arylboronic acids using a metal-organic framework containing tetrakis(carboxyphenyl)porphyrin groups. *Chem. Commun.* **2015**, *51* (89), 16103-16106.
53. Cheng, Y.; Gu, X.; Li, P., Visible-Light Photoredox in Homolytic Aromatic Substitution: Direct Arylation of Arenes with Aryl Halides. *Org. Lett.* **2013**, *15* (11), 2664-2667.
54. Kim, H.; Lee, C., Visible-Light-Induced Photocatalytic Reductive Transformations of Organohalides. *Angew. Chem.* **2012**, *124* (49), 12469-12472.
55. Ghosh, I.; Ghosh, T.; Bardagi, J. I.; König, B., Reduction of aryl halides by consecutive visible light-induced electron transfer processes. *Science* **2014**, *346* (6210), 725-728.
56. Prier, C. K.; Rankic, D. A.; MacMillan, D. W. C., Visible Light Photoredox Catalysis with Transition Metal Complexes: Applications in Organic Synthesis. *Chem. Rev.* **2013**, *113* (7), 5322-5363.
57. Majek, M.; Filace, F.; Jacobi von Wangelin, A., Visible Light Driven Hydro-/Deuterodefunctionalization of Anilines. *Chemistry - A European Journal* **2015**, *21* (12), 4518-4522.
58. Costentin, C.; Robert, M.; Savéant, J.-M., Fragmentation of Aryl Halide π Anion Radicals. Bending of the Cleaving Bond and Activation vs Driving Force Relationships. *J. Am. Chem. Soc.* **2004**, *126* (49), 16051-16057.
59. Carmody, W. R., An easily prepared wide range buffer series. *J. Chem. Educ.* **1963**, *40* (5), A386.
60. Wempe, M. F.; Quade, B.; Jutabha, P.; Iwen, T.; Frick, M.; Rice, P. J.; Wakui, S.; Endou, H., Human Uric Acid Transporter 1 (hURAT1): An Inhibitor Structure-Activity Relationship (SAR) Study. *Nucleosides, Nucleotides Nucleic Acids* **2011**, *30* (12), 1312-1323.

61. Wempe, M. F.; Jutabha, P.; Quade, B.; Iwen, T. J.; Frick, M. M.; Ross, I. R.; Rice, P. J.; Anzai, N.; Endou, H., Developing Potent Human Uric Acid Transporter 1 (hURAT1) Inhibitors. *J. Med. Chem.* **2011**, *54* (8), 2701-2713.
62. Monguchi, Y.; Kume, A.; Hattori, K.; Maegawa, T.; Sajiki, H., Pd/C–Et₃N-mediated catalytic hydrodechlorination of aromatic chlorides under mild conditions. *Tetrahedron* **2006**, *62* (33), 7926-7933.

7 Summary

Within the scope of this thesis, cooperative effects on the surface of functionalised vesicles were examined and successfully applied to enhance the aqueous hydrolysis of active esters and the upconversion of light. In addition, a fast screening technique for visible light photocatalysis reactions was developed.

Chapter 1 briefly introduces into the topic of functionalised vesicles and explains the design of the projects in this thesis spanning from cooperative effects on functionalised vesicles to the development of a screening technique.

Chapter 2 presents the concept of cooperative hydrolysis on the surface of membranes. Hydrolytic activity is provided by vesicles functionalised with an amphiphilic zinc complex, which acts as a Lewis acid and is able to hydrolyse aryl esters. We showed that co-embedding of different membrane additives into the surface of the vesicles increases the hydrolytic rate up to 16-fold. We examined different lipids and observed the highest cooperative enhancement of hydrolysis in fluid DOPC membranes. Mechanistic studies suggested that in such fluid membranes the reactions follow a Michaelis-Menten saturation kinetic, while in rigid DSPC vesicles second order kinetics are observed.

Chapter 3 shows that, not only catalytic activity of functionalised vesicles can be enhanced using membrane additives, but also the selectivity. By co-embedding of an amphiphilic non-chiral hydrolysis catalyst with amphiphilic chiral additives into the membrane of a phospholipid vesicle we were able to introduce enantioselectivity to a non-chiral catalyst. This was shown for enantiomerically pure amino acid esters, which in the presence of an appropriate chiral additive show a twofold enhancement of the hydrolysis rate of one enantiomer.

In **Chapter 4** we tried to simplify the concept of functionalised vesicles for hydrolysis and instead of using custom made amphiphilic metal complexes we examined the direct adsorption of lanthanide ions onto the surface of the vesicles. We show that their interaction with vesicles prepared from zwitterionic phosphatidylcholine lipids provides soft particles with surface functionalised with lanthanide ions. This was confirmed via sensitisation of europium ions by pyrene that was co-embedded inside the phospholipid bilayer. Such

assembly provides a high density of Lewis-acidic metal centres, which hydrolyse phosphodiesteres 17 times faster compared to homogeneous aqueous lanthanide solutions.

Chapter 5 is a study on triplet-triplet annihilation upconversion process in vesicles. We show that such light upconverting soft particles can be made on the basis of fluid DOPC vesicles in aqueous media. This process consists of the interaction between two sets of dyes (sensitizer and annihilator). We studied the effect of their position in the membrane on the upconversion efficiency: High local concentration of the dyes in the membrane increases the intensity of the detected delayed fluorescence. This was observed whether the dyes were on the surface of the bilayer or inside. Crucial for the upconversion to take place in vesicles is the fluidity of the membrane. In rigid membranes no upconversion is observed.

In **Chapter 6** we developed a high throughput screening technique for photocatalytic transformations using known indicators and microtiter plate instrumentation. Photocatalytic reactions often produce beside the desired products a stoichiometric by-product, such as reactive oxygen species or acids. These can be easily detected by an indicator allowing to perform 96 reactions at once and evaluate the reaction conversion by addition of the indicator measuring its absorbance. The concept is able to reproduce reported reaction results and correlates well with GC analysis. We used this system for identifying two new catalysts for the hydroxylation of boronic acids. We successfully employed the technique for photochemical reductions, monitoring the formation of aryl radicals from aryl halides. To confirm the robustness of the method for different substrates we screened various drugs bearing an aryl halide moiety and identified two new dehalogenation reactions.

8 Zusammenfassung

Im Rahmen dieser Arbeit wurden kooperative Effekte auf der Oberfläche funktionalisierter Vesikel untersucht und erfolgreich zur Verbesserung wässriger Hydrolyse aktiver Ester und zur Aufkonversion von Licht eingesetzt. Zusätzlich wurde eine schnelle Screening-Methode für photokatalytische Reaktionen entwickelt.

Kapitel Eins gibt einen kurzen Überblick über das Thema funktionalisierter Vesikel und erläutert die Planung der einzelnen Projekte dieser Arbeit, die von kooperativen Effekten auf funktionalisierten Vesikeln bis zur Entwicklung einer neuen Testmethode für photochemische Reaktionen reichen.

Kapitel Zwei stellt das Konzept einer kooperativen Hydrolyse auf Membranoberflächen vor. Die hydrolytische Aktivität wird dabei durch Vesikel bereit gestellt, die mit einem amphiphilen Zinkkomplex funktionalisiert wurden. Dieser fungiert als Lewis-Säure und ist in der Lage Arylester zu hydrolysieren. Es wurde gezeigt, dass die gemeinsame Verankerung von verschiedenen Membranadditiven in der Vesikeloberfläche die Hydrolyserate um das 16-fache steigert. Verschiedene Lipide wurden untersucht und die größte Steigerung der kooperativen Hydrolyse konnte mit fluiden DOPC-Membranen beobachtet werden. Mechanistische Studien weisen darauf hin, dass Reaktionen in solch fluiden Membranen einer Michaelis-Menten Sättigungskinetik folgen, während in rigiden DSPC Vesikeln eine Kinetik nach zweiter Ordnung beobachtet wird.

In **Kapitel Drei** wird gezeigt, dass durch Additive in der Membran nicht nur die katalytische Aktivität von funktionalisierten Vesikeln gesteigert werden kann, sondern auch deren Selektivität. Durch gleichzeitige Einlagerung eines amphiphilen nicht chiralen Hydrolysekatalysators zusammen mit chiralen amphiphilen Additiven in die Membran eines Phospholipidvesikels, waren wir in der Lage einem nicht chiralen Katalysator Enantioselektivität zu verleihen. Dies wurde anhand der Hydrolysegeschwindigkeit enantiomerenreiner Aminosäureester gezeigt. In Anwesenheit eines geeigneten chiralen Additives verdoppelt sich die Hydrolyserate nur eines Enantiomers.

Kapitel Vier stellt einen einfachen Weg zu funktionalisierten Vesikel für die Hydrolyse vor. Anstelle von individuell synthetisierten amphiphilen Metalkomplexen, wurde eine direkte

Adsorption von Lanthanoidionen auf die Vesikeloberfläche untersucht. Wir konnten zeigen, dass deren Wechselwirkung mit Vesikeln, hergestellt aus zwitterionischem Phosphatidylcholin, zu oberflächenfunktionalisierten Partikeln führt. Durch Sensibilisierung von Europiumionen mit Pyren, das in die Phospholipiddoppelschicht eingelagert wurde, konnte dies bestätigt werden.

Diese Art der Funktionalisierung liefert eine hohe Dichte an Lewis-sauren-Metal-Zentren, welche Phosphodiester im Vergleich zu homogenen wässrigen Lanthanoidlösungen 17-fach schneller hydrolysieren.

Kapitel Fünf fasst die Ergebnisse zur Energieaufkonversion über Triplet-Triplet Annihilierungsprozesse in Vesikeln zusammen. Wir zeigen, dass diese Lichtaufkonvertierungs-Partikel auf der Basis von fluiden DOPC Vesikeln in wässrigem Medium hergestellt werden können. Dieser Prozess basiert auf der Wechselwirkung zweier Farbstoffsorten (Sensibilisator und Annihilator). Wir haben den Effekt der Positionierung der Farbstoffe in der Membran auf die Effizienz der Aufkonversion untersucht: eine hohe lokale Konzentration der Farbstoffe in der Membran erhöht die Intensität der detektierbaren verzögerten Fluoreszenz. Diese konnte beobachtet werden, wenn die Farbstoffe auf der Oberfläche oder im Inneren der Doppelschicht waren. Ausschlaggebend für das Auftreten der Aufkonversion in Vesikeln ist die Membranfluidität. In rigiden Membranen konnte keine Aufkonversion beobachtet werden.

In **Kapitel Sechs** wurde eine Hochdurchsatz-Screening-Methode für photokatalytische Transformationen mittels bekannten Indikatoren in Mikrotiterplattenentwickelt. Photokatalytische Reaktionen liefern häufig zusätzlich zum gewünschten Produkt stöchiometrischen Mengen an Nebenprodukt, wie reaktive Sauerstoff-Spezies oder Säuren. Diese können leicht mit Hilfe eines Indikators detektiert werden, der es ermöglicht 96 Reaktionen gleichzeitig durchzuführen. Der Fortschritt der Reaktion wird nach Zugabe eines Indikators durch Absorptionmessung ermittelt. Die Methode ist in der Lage die Substratbreite bereits beschriebener Reaktionen zu reproduzieren und korreliert gut mit gaschromatographischen Analysen. Zwei neuartiger Katalysatoren für die Hydroxylierung von Boronsäuren wurden mit der Methode identifiziert. Zudem wurden die photochemische Erzeugung von Arylradikalen aus Arylhalogeniden, erfolgreich verfolgt. Um die Robustheit dieser Methode im Hinblick auf verschiedene Substrate zu bestätigen, wurden verschiedene Arzneistoffe, deren Struktur ein Arylhalogenid beinhaltet, untersucht und so zwei neue Dehalogenierungsreaktionen gefunden.

9 Abbreviations

Ac	Acyl
Aq.	Aqueous
Ar	Aryl
a.u.	Arbitrary unit
BOC	<i>tert</i> -Butyloxycarbonyl
bpy	2,2'-bipyridine
BNPP	Bis(4-nitrophenyl) phosphate
CCD	Charge-coupled device
CF	Carboxyfluorescein
DCC	<i>N,N'</i> -Dicyclohexylcarbodiimide
DIPEA	<i>N,N</i> -Diisopropylethylamine
DLS	Dynamic light scattering
DNA	Deoxyribonucleic acid
DCM	Dichloromethane
DMAP	4-Dimethylaminopyridine
DMF	<i>N,N</i> -dimethylformamide
DMPC	1,2-Dimyristoyl- <i>sn</i> -glycero-3-phosphocholine
DMSO	Dimethylsulfoxide
DOPC	1,2-Dioleoyl- <i>sn</i> -glycero-3-phosphocholine
DPA	Diphenylanthracene
DPPC	1,2-Dipalmitoyl- <i>sn</i> -glycero-3-phosphocholine
DSPC	1,2-Distearoyl- <i>sn</i> -glycero-3-phosphocholine
EA	Ethyl acetate
e.e.	Enantiomeric excess

EI	Electron impact
eq.	Equivalent
Et	Ethyl
ET	Energy transfer
ESI	Electrospray ionization
FDA	Fluorescein diacetate
FRET	Förster resonance energy transfer
f.u.	fluorescence unit
GC	Gas chromatography
GC-FID	Gas chromatography coupled with flame ionization
HEPES	2-[4-(2-Hydroxyethyl)piperazin-1-yl]ethanesulfonic acid
HOBT	Hydroxybenzotriazole
HPLC	High-performance liquid chromatography
<i>i</i> Pr	<i>iso</i> -Propyl
ISC	Intersystem crossing
K_M	Michaelis constant
LCD	Liquid-crystal display
LED	Light emitting diode
Me	Methyl
MOF	Metal-organic framework
MS	Mass spectrometry
Nd:YAG	Neodymium-doped yttrium aluminium garnet
NMR	Nuclear magnetic resonance
OPO	Optical parametric oscillator
PDI	Perylene-3,4,9,10-bis(dicarboximide)
PE	Petroleum ether
PEG	Polyethylene glycol
PET	Photo-induced electron transfer

PMMA	Polymethylmethacrylat
PNPP	4-Nitrophenylphosphate
ppm	Parts per million
ppy	2-phenylpyridine
PtOEP	Platinum octaethylporphyrin
RT	Room temperature
SCE	Standard calomel electrode
SMPC	1-Stearoyl-2-myristoyl- <i>sn</i> -glycero-3-phosphocholine
TAMRA	5-Carboxytetramethylrhodamine
<i>t</i> Bu	<i>tert</i> -Butyl
TEA	Triethylamine
THF	Tetrahydrofuran
TLC	Thin layer chromatography
T_m	Melting point
TTA:	Triplet-triplet annihilation
TTET	Triplet-triplet energy transfer
UC	Up-conversion
UPLC	Ultra-performance liquid chromatography
UV	Ultraviolet radiation
VIS	Visible radiation

10 Curriculum Vitae

Michal Poznik

Nationality: Slovak • DOB: 25 July 1988 • Phone: +49 17685964468 • poznik@gmail.com

Research Experience

- OCT 2012–PRESENT** Postgraduate student (PhD), Regensburg University, Germany
Preparation and properties of functionalised membranes for catalysis
Supervisor: Prof. Burkhard König
- JAN 2015–MAR 2015** Visiting Researcher, IISC Bangalore, India
The interface makes a difference: Lanthanide ion coated vesicles hydrolyse phosphodiesterases
Supervisor: Prof. Uday Maitra
- SEP 2010–JUN 2012** Graduate student (MSc), UCT Prague, Czech Republic
Novel fluorescent dyes and their use in material chemistry
Supervisor: Prof. Jiří Svoboda
- JUN 2010–SEP 2010** Visiting Researcher, Radboud University Nijmegen, The Netherlands
Synthesis of new BODIPY dye as a peroxidase probe
Supervisor: Prof. Alan Rowan
- SEP 2007–JUN 2010** Undergraduate student (BSc), UCT Prague, Czech Republic
Synthesis and properties of dithienofurane
Supervisor: Prof. Jiří Svoboda
-

Work Experience

- OCT 2011–MAY 2012** Laboratory technician, Henkel Prague, Czech Republic
Sample preparation, calibration of analytical equipment, disposal of chemicals and maintenance of storage
Supervisor: David Jaroš MSc

JUL 2011–AUG 2011

Summer internship, INTERPHARMA PRAHA, Czech Republic
Optimization of the purification in API preparation

List of Publications

- “Enantioselective ester hydrolysis by an achiral catalyst co-embedded with chiral amphiphiles into a vesicle membrane”, Michal Poznik, Burkhard Koenig, *RSC Adv.* **2016**, 6, 44456–44458
- “Light upconverting soft particles: triplet–triplet annihilation in the phospholipid bilayer of self-assembled vesicles”, Michal Poznik, Uwe Faltermeier, Bernhard Dick, Burkhard Koenig, *RSC Adv.* **2016**, 6, 41947–41950
- “Dithieno[3,2-b:2',3'-d]furan as a new building block for fused conjugated systems”, Václav Kozmík, Michal Poznik, Jirí Svoboda, Pierre Frère, *Tetrahedron Lett.*, **2015**, 56, 6251–6253
- “The interface makes a difference: Lanthanide ion coated vesicles hydrolyse phosphodiesteres”, **Michal Poznik**, Burkhard Koenig and Uday Maitra, *Org. Biomol. Chem.* **2015**, 13, 9789–9792
- “Cooperative hydrolysis of aryl esters on functionalized membrane surfaces and in micellar solutions”, **Michal Poznik** and Burkhard Koenig, *Org. Biomol. Chem.* **2014**, 12, 3175–3180
- “Di- and tri-oxalkyl derivatives of a boron dipyrromethene (BODIPY) rotor dye in lipid bilayers”, Marie Olšinová, Piotr Jurkiewicz, **Michal Poznik**, Radek Šachl, Tereza Prausová, Martin Hof, Václav Kozmík, Filip Teplý, Jiří Svoboda and Marek Cebecauer, *Phys. Chem. Chem. Phys.*, **2014**, 16, 10688–10697

Awards and Honours

2012–2013	<u>BayHost</u> scholarship (PhD funding)
2011	3 rd place at <u>Student Science conference</u> (MSc section), UCT Prague, Czech Republic
2010	2 nd place at <u>Student Science conference</u> (MSc section), UCT Prague, Czech Republic
2010	<u>SPP Foundation</u> Scholarship, for research stay in Netherlands
2010	<u>Poster prize</u> at: Progress in Organic, Bioorganic and Pharmaceutical Chemistry - “Liblice 2010”, Czech Republic
2010	<u>Bachelor diploma with honours</u>

- 2009 2nd place at Student Science conference (BSc section), UCT Prague, Czech Republic
- 2008 Chemistry Olympiad, Successful competitor, National round, Slovakia

Meetings and Conferences

- ORAL PRESENTATIONS**
- 8th International Conference on Molecular Imprinting, Zhenjiang, China (2014)
 - 5th EuCheMS Chemistry Congress, Istanbul, Turkey (2014)
- POSTERS**
- Suprachem, Münster, Germany (2013)
 - 14th Blue Danube Symposium on Heterocyclic Chemistry, Podbanske, Slovakia (2011)
 - Progress in Organic, Bioorganic and Pharmaceutical Chemistry - "Liblice 2011", Lazne Belohrad, Czech Republic (2011)
 - Progress in Organic, Bioorganic and Pharmaceutical Chemistry - "Liblice 2010", Nymburg, Czech Republic (2010)
- PARTICIPANT**
- Roche Continents, Art and Science, Salzburg, Austria (2014)
 - COST School on Surface Analytical Techniques, Regensburg, Germany (2016)

Additional Information

- LANGUAGES** Slovak (native), English (fluent), German (fluent), Czech (fluent), Polish (fluent), Mandarin (basics)
- TEACHING** Teaching Assistant, Practical Organic Chemistry Course
Supervisor (bachelor thesis, research internship)
- GRANT** Co-author, Slovak Research and Development Agency (APVV) grant LPP-0277-09: Correspondence seminars from chemistry and biology for secondary schools
- AUTHOR** and reviewer of problems from Biochemistry for Chemistry seminar (competition for high school students)
- ORGANISATION** Founded annual university orienteering race and organised it for 5 years

SOFTWARE	MS-Office, Photoshop, Illustrator, Premiere, ChemDraw, Origin, Scifinder, Endnote, MestReNova, Hyperchem, Gaussian, Spartan
INSTRUMENTATION	Standard organic synthesis methods, NMR, IR, ATR-IR, UV-Vis, fluorescence, phosphorescence, DLS, GC, microtitreplate handling, electrophoresis
PERSONAL INTERESTS	Acrylic painting, student theatre member, passionate filmmaker, gardening, outdoor sports enthusiast

11 Acknowledgement

First, before I thank the academy, I would like to take a moment and appreciate my supervisor Prof. Burkhard König. He was a great mentor and he was able to always find a silver lining in a hopeless project, which I always admired. I learned a lot from him about how to conduct effectively a high quality research. But honestly, I want to thank, because that he was able to put up with me. I must have been a challenge and I acknowledge it and deeply appreciate. My big thanks also goes over the globe to IISC Bangalore, India to Prof. Uday Maitra, who was a great supervisor during my stay there and introduced me to the research done in India in the best way possible.

I would like to thank the examiners Dr. Rainer Müller and Prof. Dr. Olga Garcia Mancheño for being so kind to find time and help me with my final quest of my PhD studies. Same applies to Dr. Sabine Amslinger, who kindly took the role of chairman (chairwoman).

I would love to thank my dear and beloved lab mates. You were all great. I am grateful to Benno for his grumpy mornings and warnings about the project I decided to work on (and not listen). And of course the beers, oh the beers. Then, there is Stefan, who guided me (and sometimes I guided him) through most of my life in Regensburg (apart of the time he was making his nails). Damn it was a good time, even when we did not drink. And of course I look more Bavarian than you, Stefan. Now it is written in thesis so it has to be true. Melli, who showed a great deal of courage when she managed to be my lab mate and did a great job in making me a more emotional and sensitive human being. Also that time I sprayed that nasty spray all over you and you did not kill me, respect. Tonda, I would like to thank you for showing me that you can recognise a single pixel on an LCD and of course for being a great support and in general a highest quality human being (and for correcting my acknowledgments chapter, and all papers).

Two is a company, three is a party, four is a crowd. Therefore, I cannot forget all the great people of our kingdom. You were the best and I am happy that I was able to meet you all and share a coffee (or beer) with you. I hope that team Johanna will rise in numbers and get even with the team Melli. Also, I am very thankful that you survived my rubbish talk all the time, I appreciate that. Hopefully you learned something valuable on the way, I sure did (wink, wink).

The days would not be complete without our daily trip to the Kingdom of salt and its brine bowls commonly known as Mensa and soups. Thanks go to Malte, Troppi, Anna, Manuel and Andi who were the core at the beginning and were willing to listen to my lunch trash talk, afterwards of course all the other members of the ever growing lunch group.

I should not forget my fellow slaves/students who contributed to this thesis during their F-Praktikum: Franzi, Jana, Denis, Johannes, Tobi, Mustafa, Thomas and Valentin. Thank you!

Special thanks go to Malte, who I consider a good friend and fellow companion in all the movies and projects I undertook. You were my most important critic and help in my artistic development.

Andy Müller, thank you for the great time at the Uni and on our Danube trip. I am happy that you are my friend and we are both not quitters and accomplished what we initially planned.

Carina and Soraia, you were the suns on my beer sky, thank you for all the great parties (to come)!

Thanks also go to my temporary colleagues in India, especially to Bala, who was always a voice of reason, Sayantan for his company in gym and of course Raju for taking me to MG road (and whole north-east gang, Zimik, I hope you will once go to a prom).

Michal I would like to thank you for our long time together spanning over nearly a decade and three countries. It was a good time and I cherish our professional and personal friendship, which I hope will continue even when we are on different parts of the globe.

I would like to thank Viktor, the best German-speaking, Russian Kazachstani I have ever met. Pocking is the best, Ruhrsdorf second.

It would take too long to thank all the people individually and I am afraid someone would still slip so in short: Thank you all!!!

At the end, I would like to thank Shuang for mentoring me through Chinese culture and being my great support all the time. And of course my family!

Na koniec by som chcel poďakovať svojím rodičom (a samozrejeme bratovi) za ich podporu, ktorú si hlboko cením a nikdy na ňu nezabudnem! Aj keď som ďaleko, myslím na vás častejšie ako sa vám zdá. Ďakujem vám veľmi pekne za všetko!